

Measurements of Peroxy Radicals in the Regional Boundary Layer using the PERCA Technique

Thesis submitted for the degree of
Doctor of Philosophy
at the University of Leicester

by

Mark Jacob
Department of Chemistry

Supervisor: Paul Monks
Committee member: Andrew Ellis
September 2006

Acknowledgements

First and foremost I would like to thank Magdalena for sticking by me through some stressful times and also Dominic and Oliver for cheering us both up.

Thanks to the Monks group old and not so old, especially to Zoë and Alex for their PERCA expertise and help on campaign and also to Paul for being patient with me. Many thanks to the guys in the workshops, who made everything possible – especially to Gerry, Phil and Keith for their dedication and skill.

I also appreciated the help of the TORCH community while on campaign.

Abstract

The work in this thesis describes measurements of peroxy radicals from a ground-based platform using a PERCA (Peroxy Radical Chemical amplifier) at two field campaigns, TORCH I and II (Tropospheric Organic Chemistry Experiment). TORCH I took place during July and August of 2003 in Writtle, Essex, 25 miles northeast of London. TORCH II took place one year later in April and May at the Weybourne Atmospheric Observatory, 120 miles northeast of London. Originally conceived to compare relatively fresh air masses from London with more processed air masses some distance from London, the two TORCH campaigns rarely experienced wind coming from the London direction. During TORCH I record temperatures hit much of the UK and Europe with ozone mixing ratios exceeding 150 ppbv at the measurement site and peroxy radicals having average midday mixing ratios during the heatwave over three times non-heatwave averages. The relationship between the high ozone and peroxy radical mixing ratios is explored. A comparison of measured, modelled and PSS (Photostationary state) peroxy radicals for the TORCH I campaign is presented. Although during TORCH II the desired air masses from London did not come and there was no such heatwave as in TORCH I, the measurement site did experience air masses with a variety of histories. A particular event from the TORCH II field campaign involved high concentrations of propene (3 orders of magnitude higher than the previous or subsequent hourly measurements) at 20:00 hours and concomitant five-fold increase in peroxy radical mixing ratio. Radical production is attributed to ozone-alkene reactions and although the importance of such reactions for radical production is well-known, the case study presented represents a clear example occurring in the planetary boundary layer. In order to enhance the capabilities of the PERCA instrument a further inlet was added to it with a view to the separate measurement of HO₂ from SR_iO₂ (the sum of organic peroxy radicals). A calibration source for generating HO₂ radicals was built and tested. Laboratory tests showed that the system could measure either the sum of peroxy radicals or organic peroxy radicals only but results from deployment at TORCH I proved inconclusive.

1	INTRODUCTION	1
1.1	THE EARTH'S ATMOSPHERE.....	1
1.1.1	<i>Chemical composition</i>	1
1.2	CHEMISTRY OF THE TROPOSPHERE.....	2
1.2.1	<i>Ozone in the troposphere</i>	2
1.3	MEASUREMENTS OF PEROXY RADICALS IN THE TROPOSPHERE	8
1.4	THESIS PREVIEW	14
2	INSTRUMENTATION	16
2.1	MEASURING PEROXY RADICALS IN THE FIELD	16
2.1.1	<i>PerCIMS</i>	17
2.1.2	<i>MIESR</i>	18
2.1.3	<i>PERCA</i>	19
2.1.4	<i>PERCA-LIF</i>	20
2.2	THE UL/UEA PERCA 4.....	21
2.2.1	<i>Perca components</i>	24
2.2.2	<i>Detection of NO₂</i>	24
2.2.3	<i>Isothermal Unit</i>	26
2.2.4	<i>Data PC</i>	26
2.2.5	<i>Ethernet PC</i>	26
2.2.6	<i>Electrical distribution box (EDB)</i>	27
2.2.7	<i>DC power supply unit (PSU)</i>	27
2.2.8	<i>Uninterruptible power supply (UPS)</i>	27
2.3	THE DUAL INLET SYSTEM.....	28
2.4	CALIBRATIONS.....	29
2.4.1	<i>Chain length calibrations</i>	29
2.4.2	<i>NO₂ sensitivity calibrations</i>	30
2.4.3	<i>HO₂ calibration source</i>	32
3	TORCH OVERVIEW	34
3.1	GOALS OF TORCH	34
3.2	MEASUREMENT SITES	34
3.2.1	<i>Writtle</i>	34
3.2.2	<i>Weybourne</i>	36
3.3	INSTRUMENTATION	37
3.4	METEOROLOGY.....	39
3.4.1	<i>Meteorology at TORCH 1</i>	39
3.4.2	<i>Meteorology at TORCH 2</i>	41
3.5	CHEMICAL OBSERVATIONS AT TORCH 1.....	45
3.6	CHEMICAL OBSERVATIONS AT TORCH 2.....	46
4	PSS, MEASURED AND MODELLED PEROXY RADICALS AT TORCH 1	57
4.1	PSS THEORY.....	57
4.2	PSS RESULTS.....	59
4.2.1	<i>PSS O₃ production vs destruction</i>	61
4.3	MEASURED VS PSS DERIVED ROX	65

4.4	MEASURED VS MODELLED HO ₂ +SR ₁ O ₂	69
4.5	MEASURED VS MODELLED HO ₂ AND OH.....	75
4.6	THE INFLUENCE OF NO ON MEASURED:MODELLED RADICAL RATIOS.....	78
4.6.1	<i>Whole campaign</i>	78
4.6.2	<i>19th to 28th August</i>	80
4.7	CHAPTER 4 SUMMARY.....	83
5	OZONE PHOTOCHEMISTRY DURING THE U.K. HEAT WAVE OF AUGUST	
2003	84
5.1	INTRODUCTION – HIGH TEMPERATURES AND HIGH OZONE CONCENTRATIONS.....	84
5.2	HEALTH CONSEQUENCES OF AIR QUALITY IN 2003 HEAT WAVE.....	88
5.3	SUMMER 2003 IN CONTEXT – PAST AND FUTURE HEAT WAVES IN THE UK.....	88
5.4	CHEMICAL CLIMATOLOGY.....	90
5.5	MORNING OZONE ENTRAINMENT.....	95
5.5.1	<i>Boundary Layer Height Measurements</i>	95
5.5.2	<i>Precursor tracer Ratios</i>	96
5.6	PEROXY RADICALS.....	98
5.7	RATE OF OZONE PRODUCTION.....	104
5.8	BIOGENIC VOC – THE LINK BETWEEN HIGH TEMPERATURE AND OZONE?.....	106
5.9	CHAPTER 5 SUMMARY.....	108
6	OZONE ALKENE EVENT.....	109
6.1	INTRODUCTION.....	110
6.1.1	<i>Ozone-alkene reactions</i>	110
6.2	MEASUREMENT SITE.....	113
6.3	OBSERVATIONS.....	114
6.3.1	<i>Chemical Observations</i>	114
6.4	METEOROLOGICAL OBSERVATIONS.....	120
6.5	RO ₂ PRODUCTION.....	122
6.5.1	<i>OH Steady state</i>	122
6.5.2	<i>RO₂ production</i>	124
6.6	HYDROCARBONS AND THEIR SOURCES.....	127
6.6.1	<i>Plume identification</i>	127
6.6.2	<i>VOC Fingerprints</i>	131
6.7	CHAPTER 6 SUMMARY.....	135
7	SPECIATING HO₂ AND SR₁O₂ WITH PERCA.....	136
7.1	INTRODUCTION.....	136
7.1.1	<i>Why speciate HO₂ and SR₁O₂?</i>	136
7.1.2	<i>Measurements of SR₁O₂ and HO₂ – past and present</i>	137
7.1.3	<i>Separate measurement with a PERCA</i>	138
7.2	EQUIPMENT FOR DENUDING HO ₂	140
7.2.1	<i>PERCA</i>	140
7.2.2	<i>HO₂ source</i>	141
7.2.2.1	<i>HO₂ Source Construction</i>	144
7.2.2.2	<i>HO₂ source characterisation</i>	145

7.2.2.2.1	Oxygen cross section	145
7.2.2.2.2	Water cross section	146
7.2.2.2.3	O ₃ Sampling point.....	147
7.2.2.2.4	Measurement methods	149
7.2.2.2.5	Humidity generation	154
7.2.3	<i>Comparison of HO₂ source and CH₃O₂ source</i>	154
7.3	DETERMINATION OF LOSS RATES FOR HO ₂ AND CH ₃ O ₂	155
7.3.1	<i>Inlet extension</i>	155
7.3.2	<i>Loss rates through glass extensions</i>	157
7.3.3	<i>Loss rates through metal extensions</i>	157
7.3.4	<i>Modifications to extension</i>	159
7.4	AN ATTEMPT TO MEASURE BOTH HO ₂ AND RO ₂ IN AMBIENT AIR.....	160
7.4.1	<i>Calculation of HO₂</i>	160
7.5	CHAPTER 7 SUMMARY.....	162
8	CONCLUSIONS AND FURTHER RESEARCH.....	163

1 Introduction

1.1 The Earth's atmosphere

The Earth's atmosphere is essential to life, providing oxygen for us to breathe and containing the ozone layer, which protects plants and animals from harmful ultraviolet radiation. Weather only occurs in the lowest part of the atmosphere, the troposphere, and various phenomena can be observed there, such as rainbows or, higher up and closer to the poles, amazing light shows known as auroras. The atmosphere can be divided into layers delineated by the change of temperature with altitude (Figure 1.1).

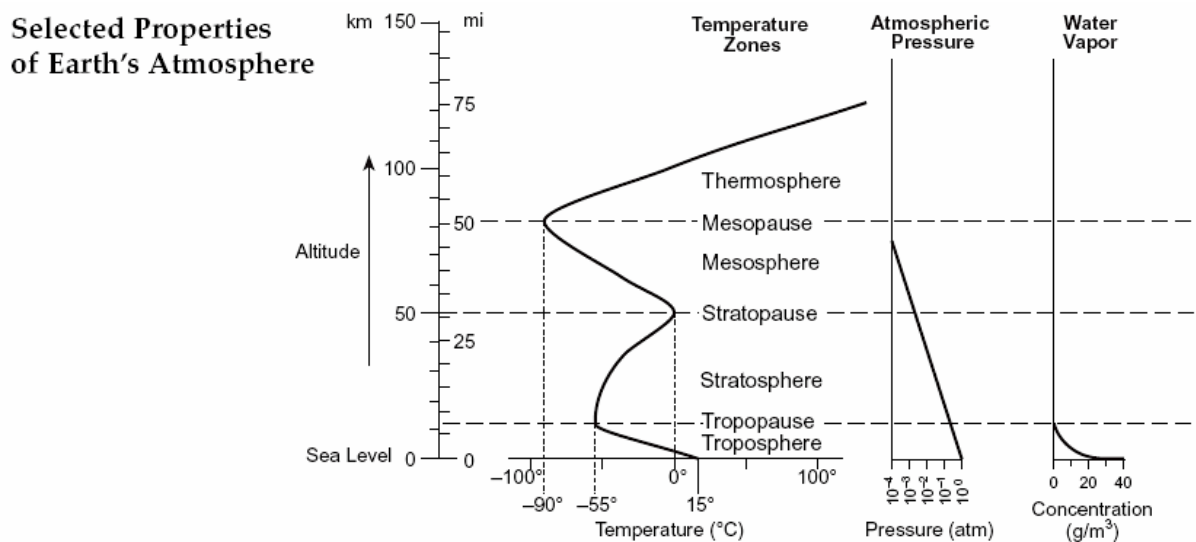


Fig 1.1 The average temperature profile, pressure and water vapour through the Earth's atmosphere, from <http://geolor.com/geoteach/images2/ESRT-atm.gif>

1.1.1 Chemical composition

The chemical composition of the atmosphere has evolved from one which mostly consisted of carbon dioxide to now containing Nitrogen (78%) and Oxygen (21%) but there are many

other gases and aerosols, which govern the composition of the atmosphere. 99% of the mass of the atmosphere is concentrated in the stratosphere and troposphere and 50% is below an altitude of 5.5km. The research in this report focuses on processes occurring in the lowest layer of the atmosphere, the troposphere.

1.2 Chemistry of the troposphere

Each year millions of tonnes of chemicals are emitted from the surface of the Earth into the troposphere, not just as a result of human activities but also by vegetation and animals as well as from geochemical processes such as volcanic eruptions. These compounds are removed from the atmosphere in various ways: deposition to the Earth's surface, either dry or wet (scavenged by precipitation or literally 'rained out'); chemical reaction with other compounds either in the gas phase, in particles (aerosols) or on their surfaces; as well as direct photolysis.

This thesis is particularly concerned with the processes involved in the chemical removal of volatile organic compounds (VOC). Atmospheric oxidation of such compounds in the presence of oxides of nitrogen and sunlight can lead to the production of smog, the main component of which being ozone.

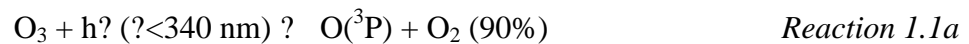
1.2.1 Ozone in the troposphere

Most atmospheric ozone is located between the altitudes of 20 to 30 km but a significant amount can also be found in the troposphere, close to the ground. The origin of this ozone is either transport across the tropopause from the stratosphere or in situ production. VOC, NO_x and sunlight are all needed if photochemical production of ozone in the Earth's troposphere is to occur. In urban centres, with concentrated emissions of vehicle exhaust fumes, high NO_x

conditions prevail, where production of ozone is sensitive to changes in VOC concentration. Rural areas have lower NO_x mixing ratios so ozone production is sensitive to NO_x.

The gas-phase chemistry of the troposphere is governed by the OH radical by day and the NO₃ radical and O₃ at night.[*Salisbury, et al., 2001*] These species initiate oxidation and chemical conversion of trace tropospheric constituents, occurring via radical chain mechanisms. The conversion of CO, H₂, CH₄, and other hydrocarbons to CO₂ and H₂O constitutes a low temperature combustion system.

The main source of tropospheric OH radicals during the day is the photolysis of O₃ and subsequent reaction of the O(¹D) atom with water although OH can also be generated by photolysis of species such as HCHO and HONO [*Harris, et al., 1982*].



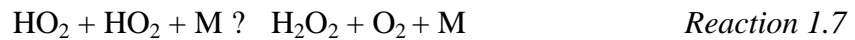
The ground state O(³P) atoms react with O₂ to reform ozone while excited state O(¹D) can either collide with an air molecule and go back to its ground state or react with water to form two OH radicals. [*Levy, 1971*]



Examples of species readily oxidised by OH are CO and CH₄. The initial steps involve formation of peroxy radicals, HO₂ and CH₃O₂.



In unpolluted, i.e. low NO_x regimes, the loss reactions of peroxy radicals are dominated by self-reaction to form peroxides



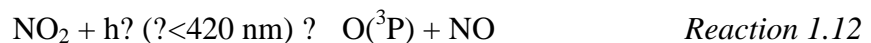
And by reaction with O₃ leading to ozone destruction



In polluted, i.e. high NO_x regimes, the peroxy radicals react with NO_x.



OH goes back into the oxidation cycle (leading to formation of more peroxy radicals) NO₂ is photolysed resulting in formation of O₃.



An important feature of a particular airmass is the net ozone productivity and is equal to production minus loss of ozone due to chemistry.

$$N(O_3) = P(O_3) - L(O_3) \quad \text{Equation 1.1}$$

$$P(O_3) = [NO](k_{HO_2+NO}[HO_2] + ? k_i[R_iO_2]) \quad \text{Equation 1.2}$$

$$L(O_3) = \{f \cdot j(O^1D) + k_{OH+O_3}[OH] + k_{HO_2+O_3}[HO_2]\}[O_3] \quad \text{Equation 1.3}$$

$$N(O_3) =$$

$$[NO](k_{HO_2+NO}[HO_2] + ? k_i[R_iO_2]) - \{f \cdot j(O^1D) + k_{OH+O_3}[OH] + k_{HO_2+O_3}[HO_2]\}[O_3]$$

$$\quad \text{Equation 1.4}$$

Where f is the fraction of $O(^1D)$ atoms that go on to react with water to form OH.

$$f = k_{O(^1D)+H_2O}[H_2O] / (k_{O(^1D)+H_2O}[H_2O] + k_{O(^1D)+M}[M]) \quad \text{Equation 1.5}$$

In the absence of fresh NO_x emissions or rapid NO_x removal, a photochemical steady state between NO and NO_2 is rapidly established. The sum total peroxy radical concentration can be inferred using the following steady state equation, [Penkett, *et al.*, 1997]

$$k_{eff} [HO_2 + RO_2]_{pss}[NO] + k_{NO+O_3}[NO][O_3] = j(NO_2)[NO_2] \quad \text{Equation 1.6}$$

the terms on each side of the equation being equal to ozone production

This process can be summarised in Figure 1.3:

aerosol formation. (Figure 1.4) This organic complexity represents a considerable challenge for the understanding and quantification of ozone photochemistry.

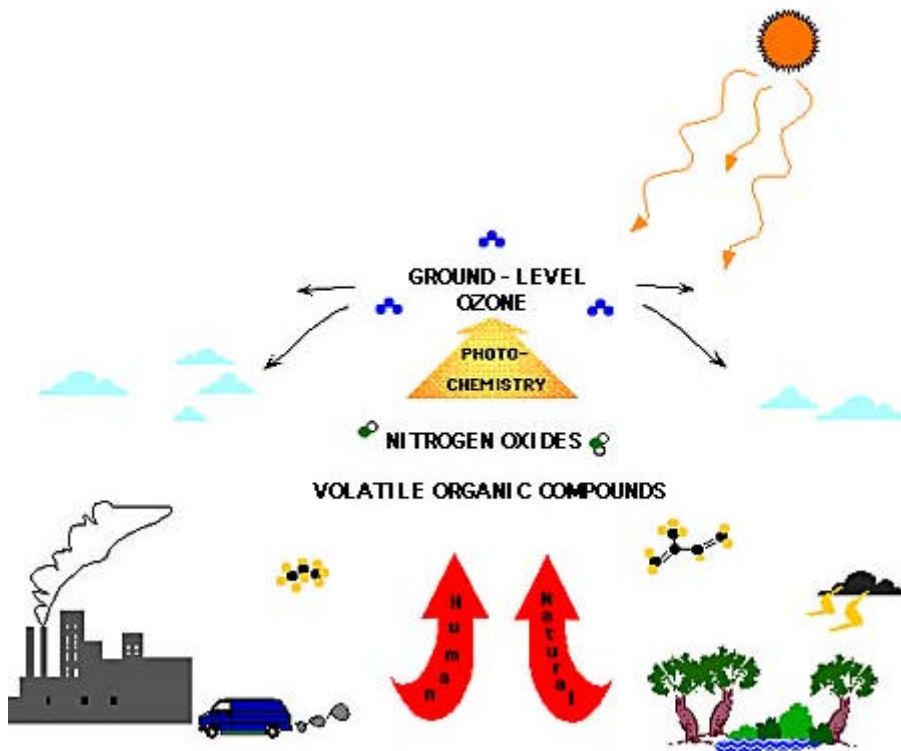


Figure 1.3 shows biogenic as well as anthropogenic compounds contributing to formation of ground level ozone

1.3 Measurements of Peroxy radicals in the troposphere

In the last fifteen or so years there have been a number of reported measurements of peroxy radicals, over thirty of which are listed in Table 1.1. The highest concentrations of measured peroxy radicals, $\text{HO}_2 + \text{RO}_2$, are 200 pptv, at the ROSE and ESCOMPTE campaigns. The ROSE campaign took place at canopy height in a forest in Alabama. Isoprene, which is highly reactive towards OH, NO_3 and O_3 , was the most significant hydrocarbon in terms of peroxy radical production. Large concentrations of formaldehyde of around 7 ppbv were measured and in early morning and late afternoon photolysis of formaldehyde was responsible for over half of all HOx ($\text{HO}_2 + \text{OH}$) production. The ESCOMPTE campaign took place in the region around Marseille in the summer of 2001. The high mixing ratios of peroxy radicals measured by PERCA were highly influenced by the urban and industrial plume.

Measurements of peroxy radicals have been carried out in a variety of environments: forests, marine boundary layer, remote locations, rural, urban, Southern hemisphere, Antarctica, upper troposphere and so on (Table 1.1). Over the years it has become increasingly apparent that a great number of supporting measurements are needed to properly evaluate the peroxy radical budget. This is especially true in environments with relatively high loadings of VOC, either from local emissions or from atmospheric transport.

<i>Experiment (Acronym)</i>	<i>Location, Year</i>	<i>Technique(s)</i>	<i>Midday max. [HO₂] or [HO₂ +SRO₂] /pptv</i>	<i>Comments</i>	<i>Reference(s)</i>
-	Oregon, 1986-7	FAGE (HO ₂)	8	One coastal site, one urban site; similar maxima at both sites for clear-sky conditions	[Hard, et al., 1992]
-	Schauinsland, 1990	MIESR	40	Forested location; anti-correlation between RO ₂ and NO ₃ at night	[Mihelcic, et al., 1993]
ROSE 1	Alabama, 1990	PERCA	200	Forested location; measured levels compared well with PSS calculations	[Cantrell, et al., 1992], [Cantrell, et al., 1993a], [Cantrell, et al., 1995]
MLOPEX 2	Mauna Loa, 1991-2	PERCA	25	Free troposphere; upslope/downslope effects; measurements low compared with PSS calculations; peroxy radicals observed at night	[Cantrell, et al., 1995], [Cantrell, et al., 1996c], [Cantrell, et al., 1996d]; [Cantrell, et al., 1997a]; [Hauglustaine, et al., 1999]
SONTOS	Ontario, 1992	PERCA	23	Rural site	[Arias and Hastie, 1996]
OCTA	Izaña, Tenerife, 1993	3 PERCA instruments and 1 MIESR instrument	80-100	2 PERCA instruments within 25% of MIESR instrument, 1 systematically low	[Zenker, et al., 1998]
-	Denver, Colorado, 1993	PERCA	20-80	Urban site; reactions of O ₃ with alkenes claimed as important source of peroxy radicals at night	[Hu and Stedman, 1995]
FIELDVOC	Brittany, 1993	PERCA	60	Measurements much lower than PSS calculations; low night-time levels	[Cantrell, et al., 1996a]

Table 1.1 Summary of peroxy-radical measurements in the troposphere (extended from [Salisbury, 2001])

<i>Experiment (Acronym)</i>	<i>Location, Year</i>	<i>Technique(s)</i>	<i>Midday max. [HO₂] or [HO₂ +SRO₂] /pptv</i>	<i>Comments</i>	<i>Reference(s)</i>
LAFRE	Los Angeles, 1993	FAGE (HO ₂)	8	Measurements in smog; poor agreement with simple model at midday	[George, <i>et al.</i> , 1999]
TOHPE	Idaho Hill, Colorado, 1993	FAGE(HO ₂), PERCA	6 (HO ₂), 60	RO ₂ /HO ₂ ratio 4-15 times larger than predicted; HO ₂ /OH ratio in range 15-80: agreed well with theory for [NO] > 100 pptv; factor of 3-4 too low under clean conditions	[Cantrell, <i>et al.</i> , 1995], [Cantrell, <i>et al.</i> , 1997b]; [Mather, <i>et al.</i> , 1997]; [Stevens, <i>et al.</i> , 1997]
PRICE I	Schauinsland, 1994	4 PERCA instruments and 1 MIESR instrument	25 (PERCA) , 50 (MIESR)	No systematic difference between PERCA instruments; MIESR instrument measured systematically higher	[Carpenter, 1996]
WAO- TIGER	Weybourne, Norfolk, 1993-5	PERCA	12	Positive correlation of peroxy radicals and NO ₃ observed at night	[Carpenter, 1996]; [Clemishaw, <i>et al.</i> , 1997]; [Carshaw, <i>et al.</i> , 1997]; [Carpenter, <i>et al.</i> , 1998]
BESSE	Bush Estate, Edinburgh, 1994	PERCA	15	Measurements systematically low compared with PSS Calculations	[Carpenter, 1996]
SOAPEX I	Cape Grim, Tasmania, 1995	PERCA	11	Relationships of peroxy radicals with j(O ¹ D) in clean and polluted air; O ₃ compensation point ca. 25 pptv NO; CH ₃ O ₂ at night; winter / summer comparison; measurements systematically low by factor of 2-3	[Monks, <i>et al.</i> , 1996], [Monks, <i>et al.</i> , 1998], [Monks, <i>et al.</i> , 2000]; [Carpenter, <i>et al.</i> , 1997]; [Penkett, <i>et al.</i> , 1997]

Table 1.1(continued) Summary of peroxy-radical measurements in the troposphere

<i>Experiment (Acronym)</i>	<i>Location, Year</i>	<i>Technique(s)</i>	<i>Midday max. [HO₂] or [HO₂ SRO₂] /pptv</i>	<i>Comments</i>	<i>Reference(s)</i>
ATAPEX	Mace Head, Ireland, 1995	PERCA	5	Compensation point ca 50 pptv NO	[Carpenter, <i>et al.</i> , 1997]
STRAT	Aircraft, 1995-6	FAGE (HO ₂)	N/A	Measurements in upper troposphere; acetone photolysis as major HO _x source in dry upper troposphere / lower stratosphere	[Jaegle, <i>et al.</i> , 1997]; [McKeen, <i>et al.</i> , 1997]; [Wennberg, <i>et al.</i> , 1998]
SUCCESS	Aircraft, 1996	FAGE (HO ₂)	N/A	HO ₂ /OH ratios 30 % higher than modeled	[Brune, <i>et al.</i> , 1998]; [Jaegle, <i>et al.</i> , 1998]
-	Aircraft, 1996	IM-RMS	N/A	4-8 km altitude; good agreement between measurements and steady-state calculations for clear skies	[Reiner, <i>et al.</i> , 1997], [Reiner, <i>et al.</i> , 1999]
ACSOE- EASE	Mace Head, Ireland, 1996-7	FAGE (HO ₂), PERCA	8 (HO ₂), 25	No correlation between NO ₃ and peroxy radicals at night PSS derived peroxy radicals correlate with measured values but are factor of 2	[Creasey, <i>et al.</i> , 1997]; [Carslaw, <i>et al.</i> , 1999a], [Carslaw, <i>et al.</i> , 1999b], [Carslaw, <i>et al.</i> , 2000]; [Carslaw, <i>et al.</i> , 2002]; [Savage, <i>et al.</i> , 2001]; [Salisbury, <i>et al.</i> , 2001], [Salisbury, <i>et al.</i> , 2002]
SONEX	Aircraft, 1997	FAGE (HO ₂)	N/A	Effect of aircraft emissions in troposphere	[Brune, <i>et al.</i> , 1999]; [Jaegle, <i>et al.</i> , 1999], [Jaegle, <i>et al.</i> , 2000]; [Faloona, <i>et al.</i> , 2000]

Table 1.1(continued) Summary of peroxy-radical measurements in the troposphere

<i>Experiment (Acronym)</i>	<i>Location, Year</i>	<i>Technique(s)</i>	<i>Midday max. [HO₂] or [HO₂ +SRO₂] /pptv</i>	<i>Comments</i>	<i>Reference(s)</i>
FREETEX	Jungfrauoch, Switzerland, 1996, 1998	PERCA	18	Radicals shown to be dependent on $v(j(O^1D))$ in low-NO _x ozone-production regime; seasonal comparison; photochemical control of diurnal ozone variation	[Zanis, <i>et al.</i> , 1999], [Zanis, <i>et al.</i> , 2000a], [Zanis, <i>et al.</i> , 2000b], [Zanis, <i>et al.</i> , 2003]
-	Oki Island, Japan, 1998	FAGE (HO ₂)	14	HO ₂ observed at night	[Kanaya, <i>et al.</i> , 1999]
BERLIOZ	Berlin, 1998	MIESR (HO ₂) MIESR (? RO ₂) FAGE (HO ₂)	15-20 15-20 15-30	Importance of RO ₂ recycling in the chemical mechanism Missing OH sink responsible for over estimation of peroxy radicals	[Mihelcic, <i>et al.</i> , 2003]
PROPHET	Michigan, 1998	FAGE (HO ₂)	70	isoprene has an impact on both radical production and loss	[Mihele and Hastie, 2003]
SOAPEX 2	Cape Grim, Tasmania, 1999	FAGE (HO ₂), PERCA	8 (HO ₂); 20	peroxy radical mixing ratios a factor of <i>ca</i> 1.6 lower in winter than in summer	[Salisbury, <i>et al.</i> , 2001]
PUMA	Birmingham, 1999, 2000	FAGE (HO ₂)	0.6 – 4 Summer and winter	Similar HO ₂ mixing ratios in summer and winter despite factor of 15 lower $j(O^1D)$ in winter	[Emmerson, <i>et al.</i> , 2005a], [Emmerson, <i>et al.</i> , 2005b]
PRIME	Ascot, 1999	FAGE (HO ₂), PERCA	Not given	Measurements during solar eclipse; response of [HO ₂] to falling $j(O^1D)$	[Abram, <i>et al.</i> , 2000]
TOPSE	Aircraft, 2000	CIMS	N/A	evolution of photochemical activity as time progresses through the study period due to increases in free radical source rates	[Cantrell, <i>et al.</i> , 2003]

Table 1.1(continued) Summary of peroxy-radical measurements in the troposphere

<i>Experiment (Acronym)</i>	<i>Location, Year</i>	<i>Technique(s)</i>	<i>Midday max. [HO₂] or [HO₂ +SRO₂] /pptv</i>	<i>Comments</i>	<i>Reference(s)</i>
ESCOMPTE	Marseille, 2001	PERCA	200	high concentrations of RO ₂ +HO ₂ at ground level under the influence of the urban and industrial plume	[Coll, et al., 2005]
WAOWEX	Weybourne, 2002	PERCA	25	Winter/summer comparison (comparison with INSPECTRO)	[Fleming, 2005]
ECHO	Jülich 2002	FAGE(HO ₂)	-	Concentration profiles in forest canopy	[Koppmann, 2004]
NAMBLEX	Mace Head, 2002	PERCA	10-40	Strong NO _x dependence on peroxy radicals	[Fleming, et al., 2006]
		FAGE (HO ₂)	3.5-8.2	Including reaction with BrO and IO as well as aerosol uptake improves model agreement	[Smith, et al., 2006]
INSPECTRO	Weybourne, 2002	PERCA	10	Winter/summer comparison (comparison with WAOWEX)	[Green, et al., 2006] [Fleming, 2005]
TORCH 1	Writtle, 2003	PERCA FAGE (HO ₂)		PERCA results presented in this thesis	[Lee, et al., 2006] [Emmerson, et al., 2006]
TORCH 2	Weybourne, 2004	PERCA FAGE (HO ₂)		PERCA results presented in this thesis	-
ITOP	Aircraft, 2004	PERCA FAGE (HO ₂)	N/A	No results yet published	-
CHABLIS	Antarctica, 2005	PERCA FAGE (HO ₂)	N/A	No results yet published	-
AMMA	Aircraft, 2006	PERCA FAGE (HO ₂)	N/A	No results yet published	-

Table 1.1(continued) Summary of peroxy-radical measurements in the troposphere

1.4 Thesis Preview

Chapter two of this thesis describes briefly the PERCA instrument and how it is calibrated. The instrument belongs jointly to the universities of Leicester and East Anglia, and was until November 2002 based at UEA in Norwich. It was subsequently transferred to Leicester along with some spares and peripheral items owing to the departure from UEA of its creator, Tim Green. Much time and effort was spent by technicians and members of the Monks Group getting the instrument ready for the TORCH campaigns and working out the exact details of how the instrument functioned. An extra inlet was added and a new calibration source was designed and constructed (more in Chapter 7). The TORCH II campaign clashed with onboard testing for the ITOP aircraft campaign and so everything other than the inlet box had to be reconstructed from spares and new parts in order to have two working instruments.

An overview of the two TORCH campaigns is given in Chapter 3, with case studies from TORCH I and TORCH II in Chapters 5 and 6 respectively. A comparison of measured, modelled and PSS (Photostationary state) peroxy radicals is presented in Chapter 4. Originally conceived to compare relatively fresh air masses from London with more processed air masses some distance from London, the two TORCH campaigns rarely experienced wind coming from the London direction. Much excitement did arise from the fact record temperatures hit much of the UK and Europe during the TORCH I campaign with ozone mixing ratios exceeding 150 ppbv at the measurement site and peroxy radicals having average midday mixing ratios during the heatwave over three times non-heatwave averages. The relationship between the high ozone and peroxy radical mixing ratios is explored in Chapter 5.

Although during TORCH II the desired air masses from London did not come and there was no such heatwave excitement as in TORCH I, the measurement site did experience air masses with a variety of histories and these are examined in Chapter 3. A particular event involving high concentrations of propene at 20:00 hours (3 orders of magnitude higher than the previous or subsequent hourly measurement) and concomitant five-fold increase in peroxy radical mixing ratio. Radical production is attributed to ozone-alkene reactions and although the importance of such reactions for radical production is well-known, the case study in Chapter 5 represents a well-defined example occurring in the planetary boundary layer.

In order to enhance the capabilities of the PERCA instrument a further inlet was added to it with a view to the speciation of HO₂ from SRO₂ and this is described in Chapter 7. A calibration source for generating HO₂ radicals was built and tested. Laboratory tests showed that the system could speciate but results from deployment at TORCH I proved inconclusive.

Further ideas concerning instrument development and other deployments are given in Chapter 8 as well as a summary of the work in this thesis.

2 Instrumentation

2.1 Measuring Peroxy Radicals in the Field

Although measurements of peroxy radicals are extremely important in deducing and quantifying various chemical processes in the atmosphere, there is no public or commercial interest in measuring them. Unlike ozone there are no reported health issues involving gas phase peroxy radicals and no known detrimental effects on buildings or crop yields. Coupled with the fact that they are extremely short lived, typically in the order of minutes, it is not possible to buy an instrument to measure them.

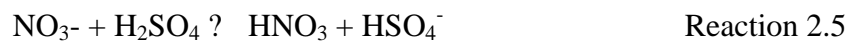
Many spectroscopic and chemical conversion techniques have been used to measure HO₂ and RO₂ in the gas phase. Peroxy radicals have characteristic absorptions due to various molecular processes[*Cantrell, et al., 1993b*]. However, these cannot be exploited for measurements in the troposphere owing to high detection limits of the techniques and interferences from absorption of other atmospheric constituents. Over the past thirty years, four techniques have been developed and implemented to make measurements of peroxy radicals in the troposphere and these are briefly described in the following sections.

2.1.1 PerCIMS

This is the latest instrument developed to make field measurements of peroxy radicals [Edwards, *et al.*, 2003]. The peroxy radical chemical ionisation mass spectrometer instrument draws ambient air through a orifice 50 μm in diameter into a low-pressure inlet. Peroxy radicals are converted into H_2SO_4 by addition of NO and SO_2 to the inlet.



HNO_3 is chemically ionised using a radioactive americium²⁴¹ source and a proton is transferred from H_2SO_4 to NO_3^- .



The resulting HSO_4^- ion is then measured by a quadrupole mass spectrometer.

PerCIMS is capable of differentiating between HO_2 and RO_2 and does so by operating in two modes; HOxROx mode, where it measures the sum of all peroxy radicals, and HO_2 mode, where concentrations of inlet reagents are increased (dramatically) to disfavour the RO_2 to HSO_4^- conversion. Measurements have been made both on the ground and on an aircraft platform with a lower detection limit of 1×10^7 radicals cm^{-3} for 15s averaging times.

2.1.2 MIESR

Matrix Isolation and Electron Spin Resonance has been used to measure NO_3 , NO_2 , $\text{CH}_3(\text{O})\text{O}_2$, HO_2 and the sum of the remaining peroxy radicals from ground based and airborne platforms [Mihelcic, et al., 1985],[Geyer, et al., 1999], [Mihelcic, et al., 1993]. There are two stages to this technique: sampling and analysis. A sample is taken up to every half hour and trapped cryogenically in a D_2O matrix at -77°C . This is then transported from the field to the laboratory for analysis and can be stored for up to two weeks with no degradation. Analysis is done by Electron spin resonance, ESR (also known as electron paramagnetic resonance), which is based on the splitting of magnetic energy levels caused by the action of a magnetic field on an unpaired electron in the molecule. It is not carried out in the field owing to the impracticalities of deploying the large magnet. The lower detection limit is 20 pptv and although MIESR cannot distinguish between different RO_2 it can separate RO_2 from HO_2 with some loss in spectral resolution.

2.1.3 PERCA

Developed in the early 1980s as a single channel instrument [Cantrell, *et al.*, 1984], and improved during the 1990s as a dual channel instrument for measurements in polluted environments [Cantrell, *et al.*, 1996b], PERCA measures HO_2 and the sum of organic peroxy radicals, $\text{HO}_2 + \sum \text{R}_i\text{O}_2$. Briefly, NO and CO are added to the incoming sample gas and a chain reaction occurs leading to amplified conversion of peroxy radicals into NO_2 (fig 2.1).

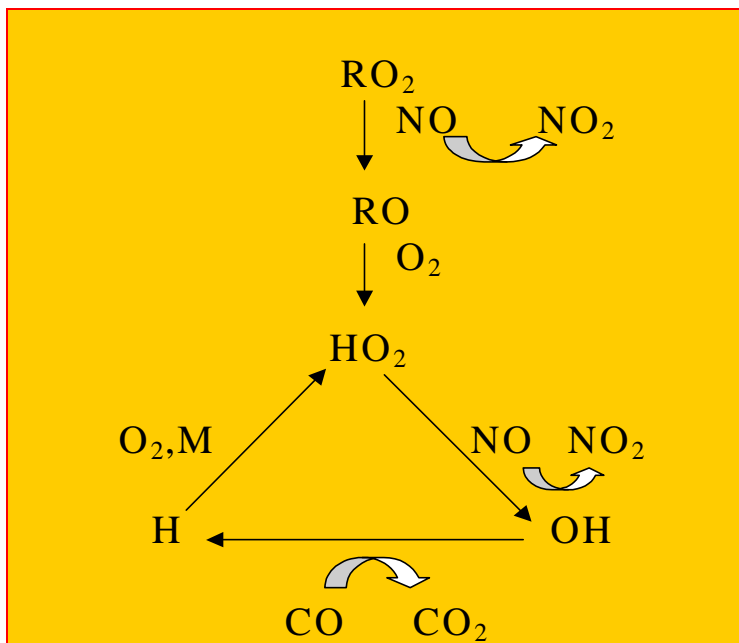


Fig.2.1 PERCA chain chemistry – Peroxy radicals are converted to NO_2

The number of cycles occurring before termination, or chain length, is typically 150 to 250 although this is significantly lower with increasing relative humidity ([Salisbury, *et al.*, 2002], [Mihele and Hastie, 1998]). Thus a radical mixing ratio of 5pptv is converted to 1ppbv of NO_2 which is readily detected by chemiluminescence with luminol solution (5-Amino-2,3-Dihydro-1,4-Phthalazinedione). More details of the technique are given in Section 2.2.

2.1.4 PERCA-LIF

This is similar to the PERCA but with NO₂ detection by laser induced fluorescence instead of luminol chemiluminescence [Sadanaga, *et al.*, 2004]. The main advantage of this is the high sensitivity and fast response time. The calculated detection limit for the only reported system is 2.7 and 3.6 pptv at ambient relative humidities of 50 and 80% respectively [Sadanaga, *et al.*, 2004]. Another advantage of this system is that it can simultaneously measure NO₂ by utilizing a second fluorescence cell.

2.2 The UL/UEA PERCA 4

The instrument described here, PERCA 4, is the one used in the TORCH 1 campaign (chapter 3). Owing to a clash in aircraft fitting, ie the PERCA instrument had to be elsewhere, the majority of the instrument minus the inlet box had to be rebuilt and thus there may be some slight differences in the specifications of the instrument used at TORCH 2. However, these differences are not fundamental and so only a description of the instrument set up used in TORCH 1 is given.

PERCA 4, as its name suggests, is the fourth generation instrument and represents a significant improvement on its predecessors. PERCAs 1 and 2 were single-inlet ground-based systems [Clemishaw, *et al.*, 1997], which performed well in clean atmospheric environments, i.e. with slowly changing ambient ozone levels and low NO_x and VOCs. PERCA 3 was also a single inlet instrument but used on an aircraft platform [Green, *et al.*, 2003]. PERCA 4 [Green, *et al.*, 2006] was initially constructed with two inlets but with inbuilt redundancy giving the possibility of adding a further two. The dual-inlet configuration has been deployed in four ground-based field campaigns in the past two years, NAMBLEX at Mace Head, Ireland [Fleming, *et al.*, 2006] the most recent of which, TORCH I (see chapter 3), a third inlet was added to attempt a separate measurement of HO₂.

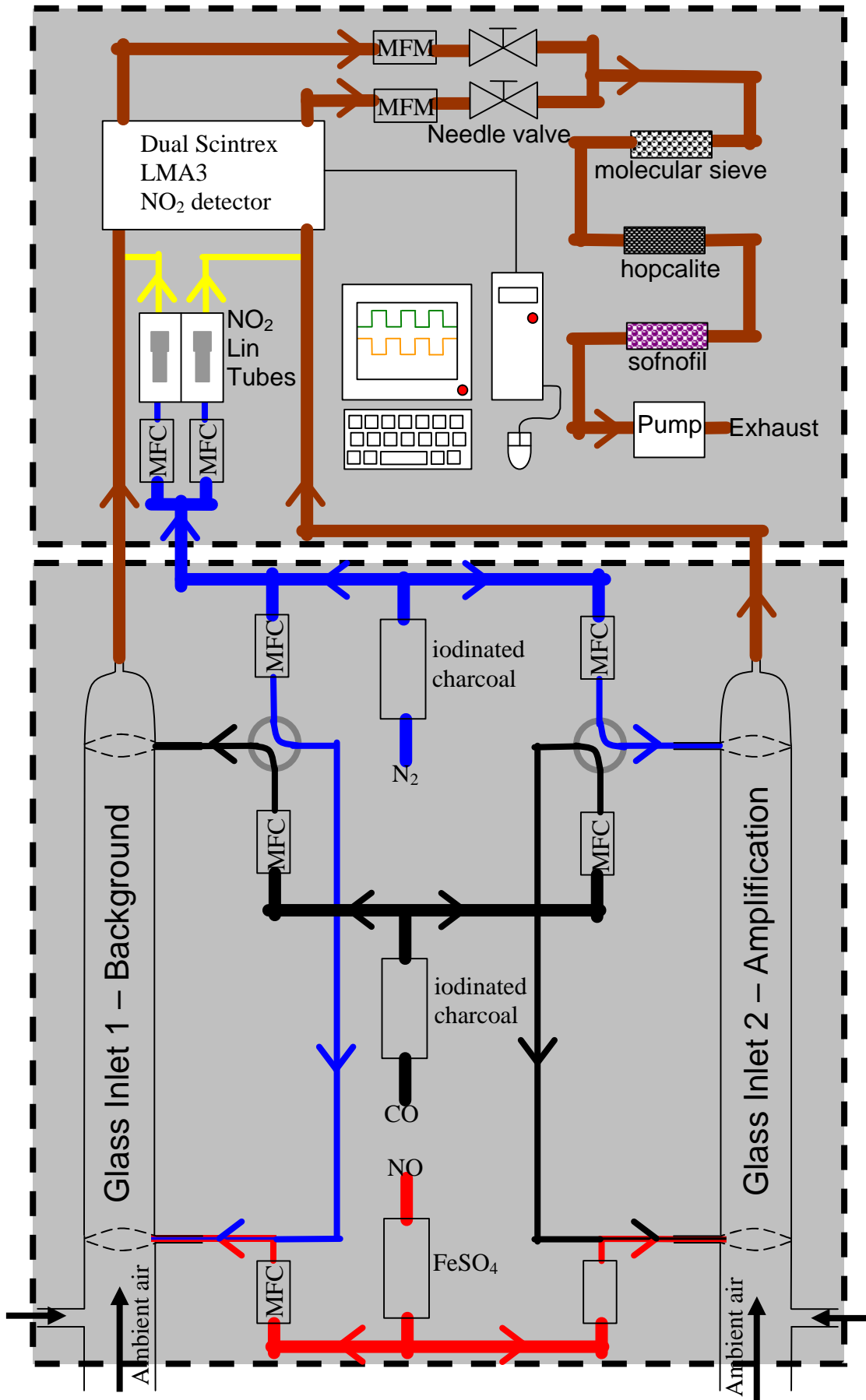


Figure 2.2 Block diagram of PERCA



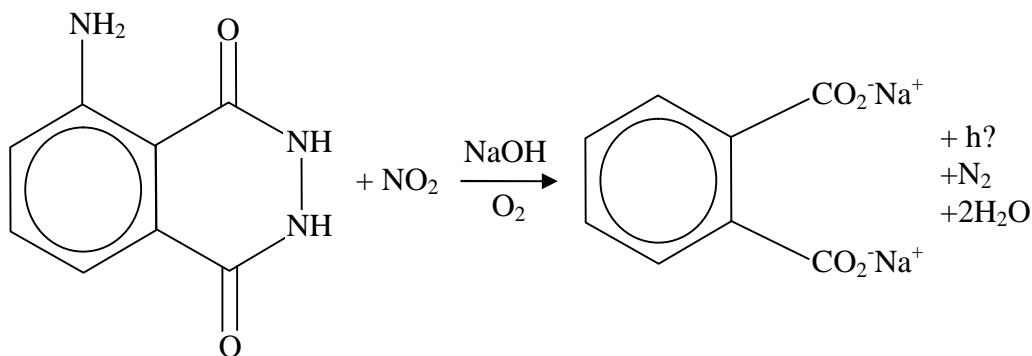
Figure 2.3 PERCA rack in foreground with inlet box on stand in background, linked by green umbilical

2.2.1 Perca components

Physically, the two main parts of the instrument are the inlet box and the rack. In the inlet box the peroxy radicals are converted into NO₂ and it is usually positioned approximately 10m up a tower. The NO₂ travels down a length of ¼” OD PFA (perfluoroalkoxy) tubing tube to the NO₂ detectors, which are housed in the rack. The rack also houses the control PC, an Ethernet PC, power supplies of various voltages, a pump and flow control system for the inlet flows and these are described in the following sections.

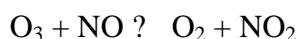
2.2.2 Detection of NO₂

There are three Scintrex LMA-3 NO₂ chemiluminescence detectors, one for each channel. The sample gas is drawn down ¼” OD tubing into a cell where it passes over a wick saturated in luminol II solution (5-amino-2,3-dihydro-1,4-phthalazineinedione). The reaction of NO₂ with luminol produces chemiluminescence at 424 nm which is detected by an adjacent photomultiplier converting this signal to a voltage. Luminol is kept in a reservoir and a constant flow of luminol is achieved by pressurising the reservoir with nitrogen. The luminol is pulled from the wick by a pump so that the luminol solution does not dry out on the wick causing a blockage. The flow of luminol to the wick can be regulated with stainless steel needle valves and is kept roughly at 0.05 mL min⁻¹.



Reaction 2.6 Chemiluminescence of luminol (5-amino-2,3-dihydro-1,4-phthalazine-1,4-dione)

The reaction of luminol and NO_2 is thought to involve two NO_2 molecules and thus the response of the detectors is quadratic at low NO_2 but linear above a few ppbv. At concentrations of NO typical for PERCA operation the detector response is linear above 20ppbv. Both ambient NO_2 and O_3 (titrated with NO – reaction 2.) contribute to detector signal and thus in a rural UK location it is highly unlikely that the Ox (sum of NO_2 and O_3) will be below 20 ppbv and thus the signal will be in the linear region.



Reaction 2.7

For clean conditions eg in remote locations or in the upper troposphere when the instrument is in its flying configuration an additional source of NO_2 is required to ensure that the detector response is linear. This is an NO_2 permeation wafer device (VICI Metronics, estimated leak rate approximately 200 ng min^{-1} at 35°C). The permeation devices are kept at 35°C in a heated aluminium block with 50 sccm N_2 running over them constantly. During the campaigns described in this thesis (TORCH 1 and 2 – see chapter 3) the linearization flows were only added during chain length calibrations (see section 2.4.1).

2.2.3 Isothermal Unit

The sample flows are maintained in this unit. A mass flow meter (Mykrolis FC360) is coupled to a needle valve and stepper motor arrangement. This was designed for use at reduced pressure ie for airborne measurements whereas on the ground a mass flow controller (MFC) would be sufficient. It also contains the chilled luminol reservoir and waste luminol vessel, which are used on the aircraft platform.

2.2.4 Data PC

This is a single board computer (Wordsworth ROCKY-3702EV) housed in an industrial chassis (Wordsworth Rack 360). It is equipped with a 64 channel A/D, analogue to digital, data card (Measurement Computing Corp. PCI-DAS64), a 16 channel D/A, digital to analogue, card (Measurement Computing Corp. CIO-DAC16) and a 16 channel thermocouple input card (Measurement Computing Corp. CIO-DAS-THERM). The control program is written in visual basic and data is written to text files with a new file starting each day midnight. To derive a peroxy radical mixing ratio the only data necessary to log are the detector signals. However, the fact that PERCA 4 logs a number of other quantities, such as sample flows, inlet temperatures and reagent gas flows has often proved invaluable when trying to interpret detector signal anomalies.

2.2.5 Ethernet PC

The Ethernet PC (PCISA single board computer, Wordsworth Juki 760E) and data PC are networked such that data can be transferred to the Ethernet PC and burnt onto CDs or manipulated directly. It is useful to work up the data in situ to see what's going on without worrying about disrupting the control and data capture on the Data PC. On an airborne

platform the Ethernet PC can be connected to the aeroplane's Ethernet and information such as altitude and concentrations of trace gases can be viewed in real time.

2.2.6 Electrical distribution box (EDB)

Mains power (240V ac, 5A) comes in and is distributed to various in the boxes and rack. Each unit can be switched on and off from this box and circuit breakers protect the equipment.

2.2.7 DC power supply unit (PSU)

This converts mains voltage (from EDB) to 5V, 12V, +15V, -15V and 24V DC for various uses around the instrument. 5V powers the stepper motors for the needle valves controlling the sample flow. And is also needed for the MFCs and MFMs. +15 and -15V power the MFCs and MFMs. 24V powers the fan cooling the inlet box and is also used for an actuator valve and solenoid valves in the aircraft inlet system thus avoiding the use of 240V AC.

2.2.8 Uninterruptible power supply (UPS)

If there is a power cut or from changing from aircraft to ground power the UPS will power the data PC for approximately 20 minutes. It is essential that the data PC does not shut down as when it powers up again the control program will not automatically start. A prolonged power cut did occur during the TORCH 1 campaign although it began at night and therefore no one was there to power down the instrument. Nothing untoward happened to the PERCA and it was started up again once power was restored.

2.3 The Dual Inlet System

The current PERCA, which is the fourth generation to be built by UEA, has a dual inlet system. When one of the inlets is converting peroxy radicals to NO_2 (amplification) the other is simply measuring ambient ozone converted to NO_2 by reaction with NO (background) along with ambient NO_2 as well as PAN. The inlets are switched every minute. The background signal is much greater than that of the amplification signal so that the signal due to peroxy radicals appears as small modulations on top of a larger signal (fig 2.3).

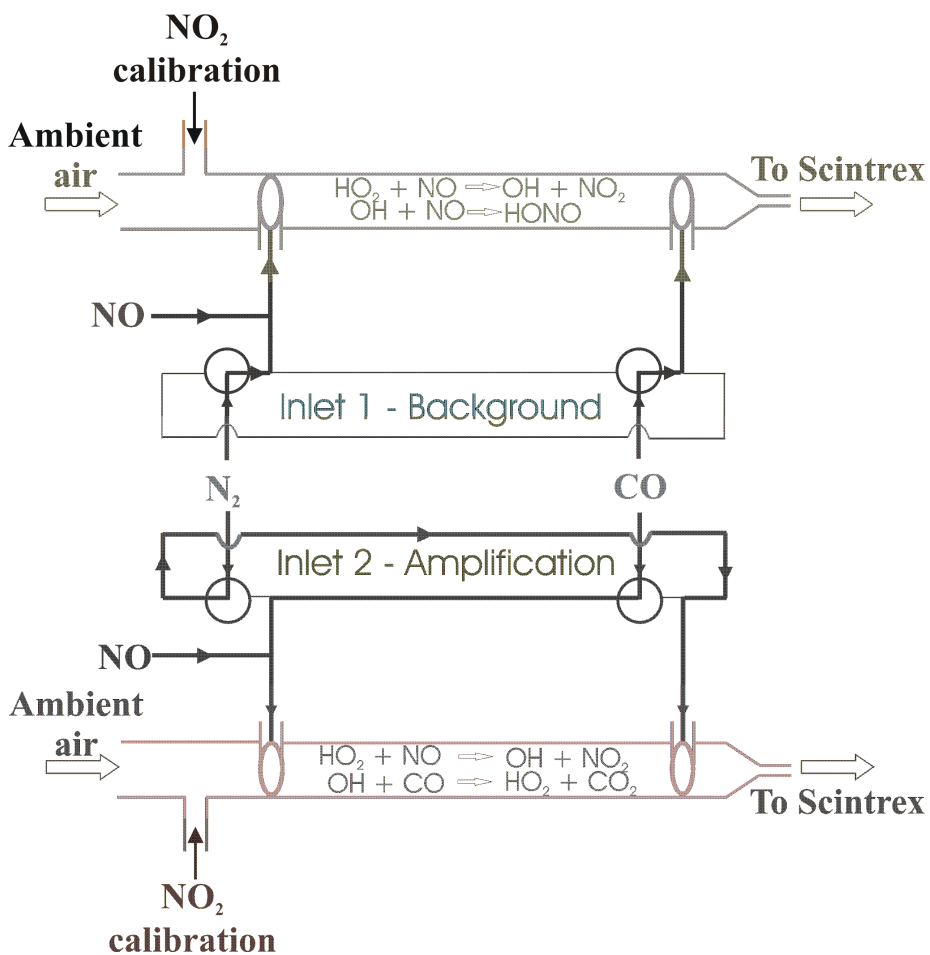


Figure 2.4 PERCA dual inlet scheme

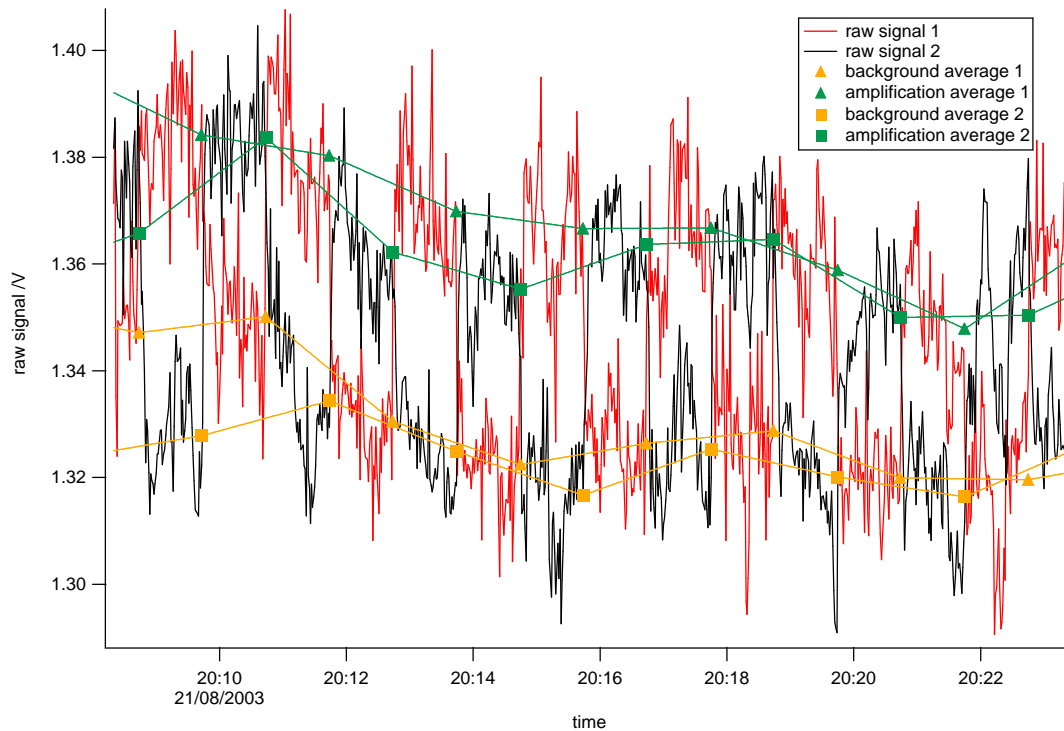


Fig 2.5 PERCA modulations,. The background signal = 1.33 V., signal due to peroxy radicals = $1.37 - 1.33 = 0.04$ V

Ozone mixing ratios at ground level vary strongly in urban and polluted environments and therefore a dual channel instrument is a great improvement on a single channel instrument as it is constantly measuring the background signal.

2.4 Calibrations

2.4.1 Chain length calibrations

Chain length is equivalent to the number of NO_2 molecules produced from the intake of one peroxy radical. This is calculated by adding varying known concentrations of CH_3O_2 to the inlet and comparing this to the response of the detector. A graph of ?NO_2 to calculated CH_3O_2 gives a gradient of chain length.

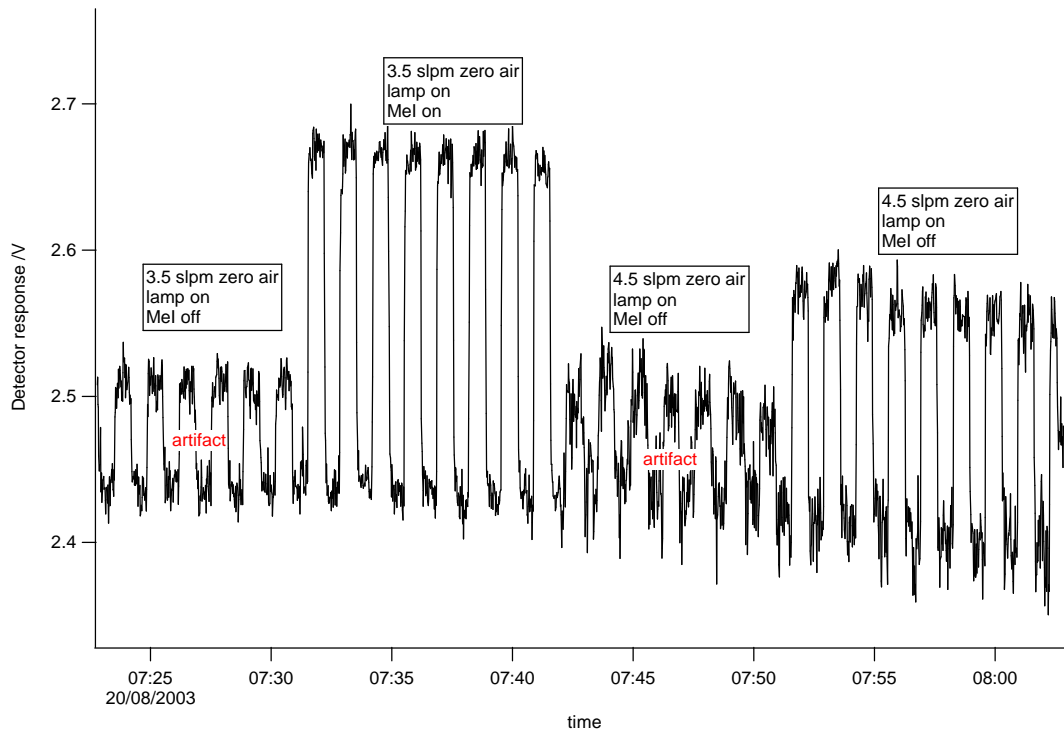


Fig 2.6 a typical chain length calibration

2.4.2 NO₂ sensitivity calibrations

The Scintrex LMA-3 NO₂ detectors are calibrated using an NO₂ permeation device certified at a release rate of 215 ngmin⁻¹ (at 40°C) but subsequently measured after 3 weighings over a period of two months to have a release rate of 176 ngmin⁻¹ (at 35°C).

A flow of 50 sccm of N₂ (zero grade) flows across the permeation device and this is incorporated into a flow of 3, 4, and 5 slpm of zero air. A plot of detector response, in volts, against calculated NO₂, in ppbv, is produced (fig 2.4).

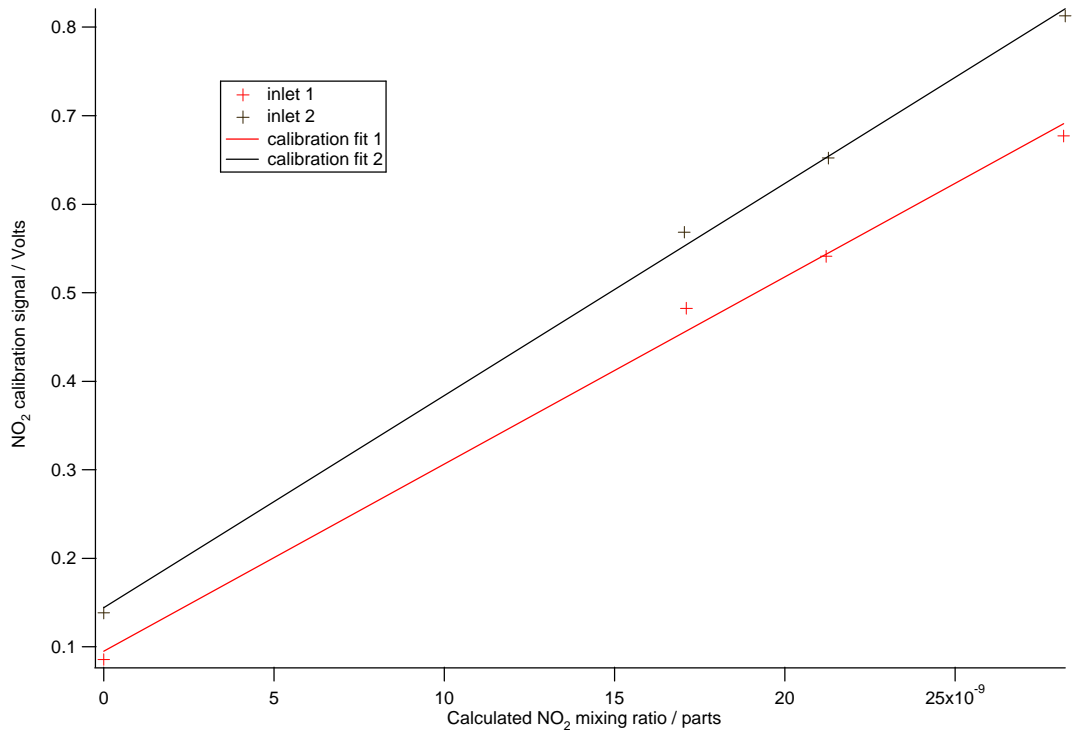


Figure 2.7 NO₂ calibrations

The detectors have been shown to have a linear response to NO₂ above 25 ppbv. Unfortunately, an earlier an earlier NO₂ permeation device with a greater release rate of 672 ngmin⁻¹ had to be replaced by the current weaker one during the TORCH field campaign and work is ongoing to verify TORCH NO₂ sensitivities.

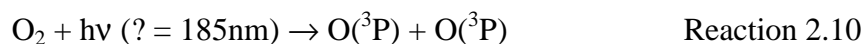
2.4.3 HO₂ calibration source

This is used to calculate chain length and produces HO₂ by the photolysis of water followed by the subsequent reaction of the H atoms with O₂ to produce HO₂ [Schultz, *et al.*, 1995]. This is the method used by several research groups to calibrate not only PERCA instruments but also FAGE and PerCIMS. Leicester currently uses a methylperoxy radical calibration source [Clemittshaw, *et al.*, 1997] but the quest to separate HO₂ from RO₂ necessitates the building of an HO₂ source.



A mercury penray lamp is used to photolyse the water. Water concentration is measured with a General Eastern 1311DR dewpoint hygrometer.

HO₂ concentration is deduced *via* chemical actinometry. Ozone is also produced *via* photolysis of O₂ at 185 nm and can be measured using a commercial ozone instrument. In producing very low concentrations of peroxy radicals suitable for calibration (<100pptv) ozone concentrations are below the detection limit of the ozone instrument. In this case,



With the addition of CO, the photolysis of water leads to the formation of two molecules of HO₂ and two of O₃.

$$P_{HO_2} = s_{H_2O}^{185} \cdot q_1^{185} \cdot \Theta^{185} \quad \text{Equation 2.1}$$

$$P_{O_3} = s_{H_2O}^{185} \cdot q_4^{185} \cdot \Theta^{185} \quad \text{Equation 2.2}$$

P = production

s^{185} = absorption cross section at 185 nm

q^{185} = quantum yield at 185 nm

Θ^{185} = photon flux at 185 nm

The mixing ratios of OH and HO₂ can be determined from the following equation:

$$[OH] = [HO_2] = \frac{[O_3][HO_2]s_{185nm(H_2O)}f_{HO_x}}{[O_2]s_{185nm(O_2)}f_{O_3}} \quad \text{Equation 2.3}$$

3 TORCH overview

3.1 Goals of TORCH

Organic compounds are found throughout the atmosphere and contribute to the generation of both fine aerosol and photochemical oxidants such as ozone. TORCH is a comprehensive and integrated programme of modelling and measurements to address three inter-linked areas of current uncertainty:

- (i) To increase understanding of the role played by primary and partially oxidised organics in gas phase photochemistry.
- (ii) To develop thermodynamic and microphysical descriptions of organic aerosol and use them in improved models of behaviour in the atmosphere.
- (iii) To investigate the production, composition and evolution of organic aerosol and its links with gas phase organic oxidation.

The goals are to provide both a detailed data set on organic composition in the polluted atmosphere, and to develop theoretical and modelling tools, which may be used in defining future air quality policy. The Tropospheric Organic Chemistry experiment forms a multi-institution consortium project within the Polluted Troposphere programme.

3.2 Measurement sites

3.2.1 Writtle

Measurements at TORCH 1 were made at Writtle College, Writtle, Essex (51°:44':12''N; 0°:25':28''E), a location approximately 25 miles North East of central London. The site comprised several shipping container laboratories and temporary buildings located in a grass field situated to the South East of the main college buildings, which was little influenced by

local road sources of pollutants. The site was over 2 miles from the nearest busy road (to the South), with the prevailing wind direction (South Westerly) coming from an area of flat arable farmland with scattered agricultural buildings for a distance of ~ 2 miles. Electricity for the measurement instruments was provided by a diesel powered generator situated ~ 200 metres to the East of the sampling location. The location of the site had been chosen as a typical rural location in the South East of England, relatively close to London, which would allow for the study of freshly polluted air masses that had passed over densely populated areas of London and the South East of England.



Figure 3.1 Field site for TORCH 1, Writtle

3.2.2 Weybourne

TORCH 2 took place at Weybourne Atmospheric Observatory, Weybourne, on the north Norfolk coast of England ($52^{\circ} 57'23''\text{N}$, $1^{\circ}7'40''\text{E}$). It is situated at an altitude of 16m above sea level, on land which slopes gently down to a pebble beach [Clemmitshaw, 1994]. The WAO has an open seaward fetch of some 30 degrees, bounded by the east coasts of England and Scotland and the west coast of Norway, with a clear view across the North Sea to the Arctic Ocean and Bering Sea beyond [Penkett, *et al.*, 1999]. The location experiences clean arctic air masses as well as air masses having passed over polluted regions of the UK and Europe. The county of Norfolk comprises primarily flat, arable farm land with several small coniferous and deciduous forests and pockets of light industry [Penkett, *et al.*, 1999]. This location was chosen to experience processed air masses having passed over London, which is located 120 miles (roughly 200km) from the observatory.



Figure 3.2 Field site for TORCH 2, Weybourne

3.3 Instrumentation

<i>Parameter</i>	<i>Technique</i>	<i>DL</i>	<i>F</i>	<i>Institute</i>
Temperature	AWS	0.1 °C	1 s	UFAM
Local wind	AWS		1 s	UFAM
<i>Gas Phase Species</i>				
Ozone	UV photometric	1 ppbv	10s	UEA, Leeds
Water vapour H ₂ O		±1 °C		Leeds
Peroxyacetylnitrate	Gas Chromatography GC	20 pptv	5 min	Leeds
NMHCs	GC-FID	0.1 – 5 pptv	1 hour	Leeds
Aromatics, alcohols, ketones, aldehydes, ethers	Dual Channel GC-FID-HID, Also 2D GC with 2D-GC-TOF confirmation	0.1 – 5 pptv	1 hour	York
Carbon monoxide	VUV fluorescence	1 ppbv	1 s	UEA
Organic nitrates	NICI-GC-MS	Sub pptv	1 hour	UEA
Semivolatike VOCs	Canister samples with 2D-GC	0.1 – 5 pptv	2 hour	York
Fast VOCs	ORAC in flight GC	5 pptv	4 min	Leeds
Oxygenates	PTR-MS	10 pptv	10 s	UEA
Oxygenates	PTR-TOF	10 pptv	10 s	York, Leic
PAN, MPAN, PPN	PTR-MS	70 pptv	15 s	UEA
Nitric oxide	Chemiluminescence	10 pptv	1 min	UEA
Nitrogen dioxide	Photolysis + chemiluminescence	10 pptv	1 min	UEA
Nitric acid	Tunable diode laser	100 pptv	1 s	Manc
Ammonia	Tunable diode laser	100 pptv	1 s	Manc
NO ₂ photolysis, <i>j</i> (NO ₂)	Photometer		1 s	Leic
O ₃ photolysis, <i>j</i> (O ₃)	Fixed bandwidth radiometry		1 s	Leic
Photolysis rates	Spectral radiometry		1 min	Leic
Speciated peroxides	Enzyme fluorimetry	20 pptv	10 s	UEA

(organic and inorganic)				
Formaldehyde	Hantsch reaction	50 pptv	10 s	UEA
SO ₂	Pulsed fluorescence	1 ppbv	1 min	UEA
Peroxy radicals (HO ₂ + ? RiO ₂)	Chemical amplifier – PERCA	1 pptv	1 min	Leic/UEA
Aerosols				
Number and size distribution	SMPS (3 – 500 nm), optical particle counters (0.1 – 300 µm)		10 min	Manc
CN	Light scattering (TSI)	7 nm	10 s	UEA, Manc
Total/ultrafine particles	> 3nm TSI 3025, < 10 nm TSI 310		1 s	Manc
Chemical composition	Aerosol mass spectrometer for nitrate, sulphate, ammonium and organic (Aerodyne), Impactors (NH ₄ ⁺ , Na ⁺ , Cl ⁻ , SO ₄ ²⁻), water soluble organics, incl. functionality as a function of molecular weight Impactors for EC/OC commercial lab analysis	0.25 µg m ⁻³ (100 particles/s)	3 min 3-12 hours	Manc Manc/ISAO Manc
Hygroscopic growth factor	Hygroscopicity Tandem DMA (H- TDMA) Mode (1) several dry sizes (10%) grown in 90% humidity Mode (2) 2 dry sizes grown in a range of humidities		1 hour	Manc

Table 3.1 Instrumentation at the TORCH campaigns. Manc is Manchester, Leic is Leicester, UEA is University of East Anglia, UFAM is Universities Facility for Atmospheric measurements, ISAO is the Institute of Atmospheric and Oceanic Sciences, Bologna

3.4 Meteorology

3.4.1 Meteorology at TORCH 1

The 5 day back trajectory calculations revealed a range of air mass types. From 1st–3rd August, the air was Atlantic in origin, passing subsequently over the Southern U.K and London before arriving at the site from a southerly/south-westerly direction. On 4th and 5th August the air was also Atlantic in origin, but passed over northern France and the North Sea before arriving at the site from an easterly direction. For these 5 days, wind speeds at the site ranged between 5–8 ms⁻¹ and peak daytime temperatures ranged from 19–25°C. From the 6th–10th August, a high pressure weather system presided over the U.K. and much of Western Europe. Very low wind speeds, ranging from 0.5–5 ms⁻¹ were experienced, with a typically westerly local wind direction and maximum daily temperatures of 26–37°C. Temperatures exceeded 35°C on 6th, 9th and 10th August, and the highest ever recorded U.K. air temperature was observed during this period at Faversham, Kent (around 30 miles from the site) at 38.5°C. During the period from 13th–24th August, the air was again Atlantic in origin, passing over the U.K. and arriving at the site in a westerly/north-westerly direction. Wind speed was generally higher during this period, ranging from 7–15 ms⁻¹, with temperatures between 20 and 25°C. From 25th–30th August, the air originated in the Arctic, travelling over the North Sea before arriving at Writtle from a northerly/north-easterly direction. Wind speeds ranged from 5–8 ms⁻¹ during this period, with maximum temperatures between 17–20°C

The most interesting period from the point of view of air pollution is from 5th – 11th August and will be described as the ‘heatwave period’. Although back trajectories under these conditions are less reliable than under cyclonic flow, they demonstrate that air arriving at the Writtle site at midday on all days from 6th – 10th August had been slow moving over the U.K. or Europe for at least the previous 5 days, providing an unusually long period for the

accumulation of photochemical pollutants. This stagnation of air over areas of elevated emissions allowed both primary and secondary pollutants to reach significant concentrations.

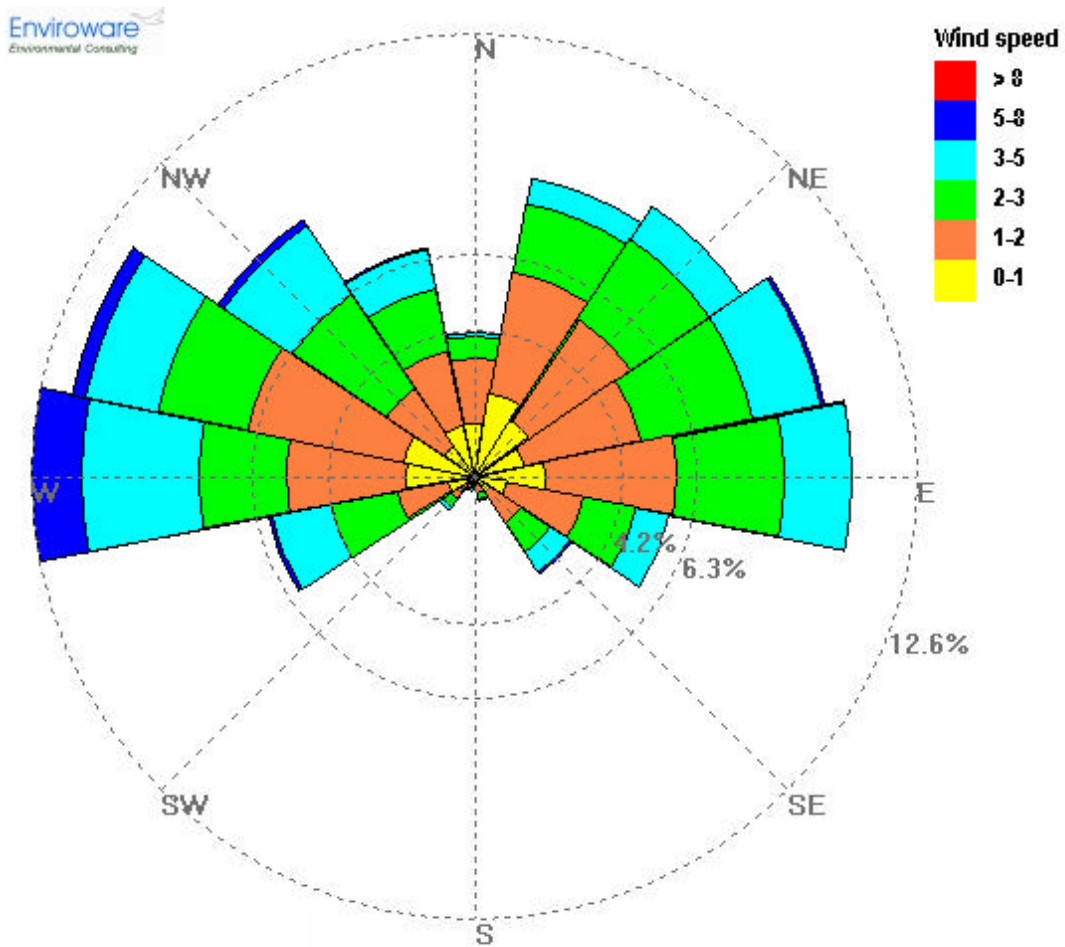


Figure 3.3 Wind speed and direction at TORCH 1

3.4.2 Meteorology at TORCH 2

Similarly to the TORCH 1 campaign, five day back trajectories show airmasses arriving at the Weybourne site having passed over a range of locations.

From 4th – 6th May, airmasses cross the Atlantic before passing over Ireland and heading along the South Coast of England, arriving at Weybourne from the South/South East. Temperatures are between 6 and 16°C. On May 7th the trajectories swing round to arrive at Weybourne from the North West, having looped over the North Sea. From 8th – 10th May, the airmasses are polar continental, coming from Eastern Europe and passing over the Baltic States and Denmark, later Scandinavia, crossing the North Sea and arriving at Weybourne from Northerly directions. From the morning of the May 11th to the evening of May 13th, airmasses have not passed over any land on their way to Weybourne from North of Greenland arriving at Weybourne from the North. Temperatures from May 7th to 13th are between 8 and 12°C. May 14th – 20th are characterised by polar maritime airmasses, generally having passed over the North of England or the English Midlands. A number of trajectories loop round before reaching Weybourne and thus arrive at the site from various directions. Three trajectories at 10:00, 12:00 and 14:00 on May 17th appear to have passed over London. This is significant as one aim of the campaign was to sample processed air influenced by emissions from London. May 14th – 20th was the warmest period of the campaign, experiencing temperatures between 11 and 24°C, with the highest temperature being on the 17th. Local wind direction is complicated somewhat by sea breeze effects evident throughout this warm period, i.e. during the night there is breeze out to sea (local southerly wind) and during the day there is a breeze from the sea (local Northerly wind). Temperatures of 8 - 12°C occur on May 21st and 22nd with airmasses arriving at Weybourne from Northerly directions, not having passed over land until late on the 22nd when the trajectories just clip the North of

Scotland. This continues into the 23rd and on May 24th airmasses pass over the North of England reaching Weybourne from the North/North West. On the 25th trajectories swing round so that on May 26th trajectories do not pass over any land whereas on May 27th morning trajectories clip the North East corner of Scotland. Temperatures were 8 - 16°C from May 23rd – 25th and 8 - 12°C on May 26th – 27th. On May 28th and 29th, the last two days of the campaign, airmasses travel South across the North Sea missing Great Britain. They then turn West across Benelux and then head back North across South East England, reaching Weybourne from the South and South East. Temperatures for May 28th – 29th were between 7 and 19°C (temperature data for May 28th and 29th from University of Leicester met sensor, positioned slightly higher than Leeds sensor). Sea breeze effects were also noted on May 24th, 25th and 27th (no wind data available for May 28th and 29th).

A wind rose using all available minute data for local wind speed and direction for May 4th – 27th shows the predominance of North and North Westerly directions with a significant fraction of South Westerlies (Figure 3.2, 31080 data points, from met station operated by University of Leeds). Wind speeds are generally greater than for TORCH 1 (for the met station positioned at an equivalent height above the ground).

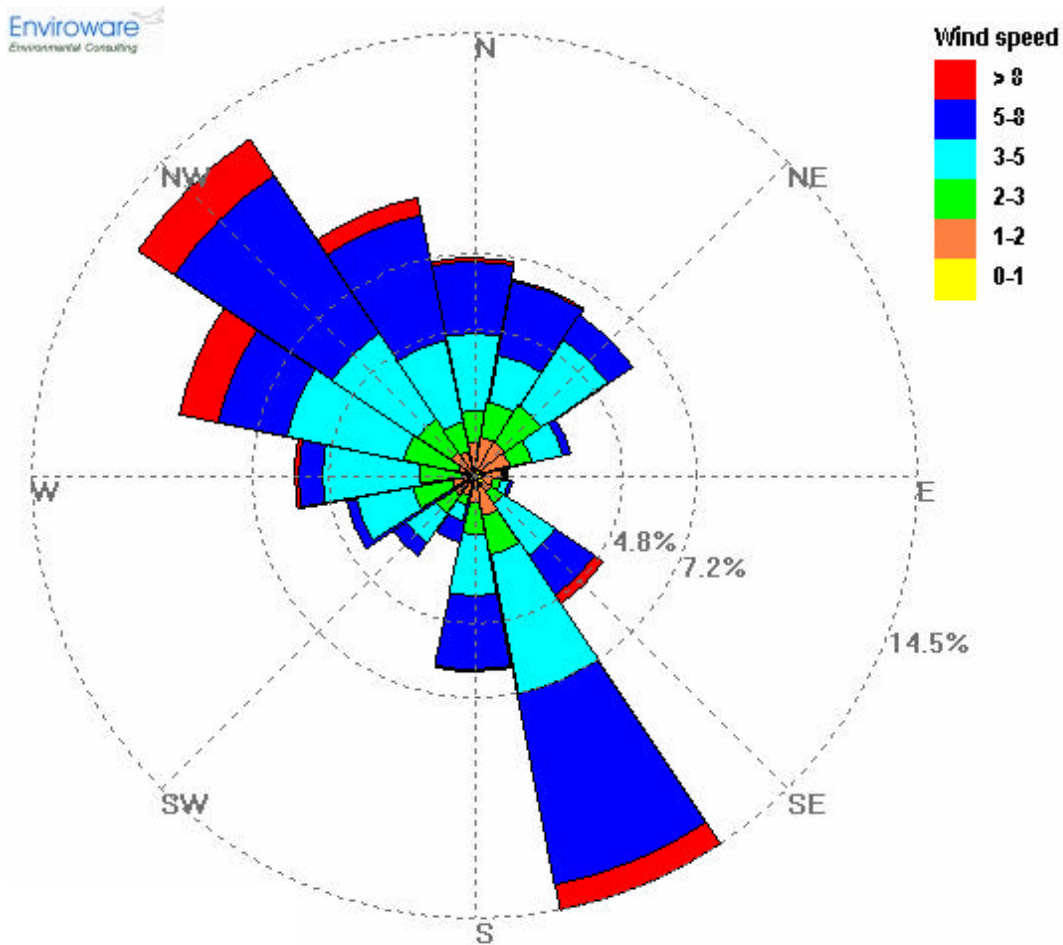


Figure 3.4 Wind speed and direction at TORCH 2.

For the purposes of analysis, the section of the campaign for during which the PERCA instrument was operating (May 4th – 29th 2004) has been divided into 7 periods (Tables 3.2 and 3.3). These are based on five day back trajectories calculated in a similar manner to those for the TORCH 1 campaign.

<i>Period</i>	<i>Dates (all May 2004)</i>	<i>Temp range /°C</i>	<i>Wind speed/ ms⁻¹</i>	<i>Relative humidity /%</i>	<i>Pressure /hPa</i>
1	4 th – 6 th	6 – 16	4.9	80.6	983
2	8 th – 10 th	9 – 11	5.0	98.0	1003
3	11 th – 13 th	8 – 12	5.0	81.4	1020
4	14 th -19 th	11 – 24	3.3	74.1	1023
5	21 st – 22 nd	8 – 12	6.6	71.2	1024
6	26 th – 27 th	4 – 12 ^a	3.1	67.4	1020
7	28 th – 29 th	7 – 19 ^b	na	66.7 ^b	na

Table 3.2 Basic meteorological data from TORCH 2 divided by time period

S

<i>Period</i>	<i>Air mass classification</i>	<i>Influences</i>
1	Returning polar maritime	Southern England
2	Polar continental	Eastern Europe
3	Polar Maritime	North Sea (no land passed over)
4	Polar Maritime	Northern England
5	Polar Maritime	North Sea (no land passed over)
6	Polar Maritime	North Sea (little land passed over)
7	Polar Maritime	Benelux

Table 3.3 History of airmasses from TORCH 2 periods

3.5 Chemical Observations at TORCH 1

Period	O ₃ /ppbv	CO /ppbv	NO /ppbv	NO ₂ /ppbv	b:t ratio
1	37.26	234.28	8.47	21.58	0.57
	<i>21.66</i>	<i>48.22</i>	<i>8.41</i>	<i>11.78</i>	
2	59.92	280.91	1.06	13.30	0.63
	<i>36.48</i>	<i>41.65</i>	<i>1.67</i>	<i>6.30</i>	
3	30.65	186.48	3.56	9.38	0.65
	<i>11.14</i>	<i>22.07</i>	<i>4.11</i>	<i>5.24</i>	
4	24.78	175.31	1.01	7.89	0.50
	<i>13.16</i>	<i>44.08</i>	<i>1.50</i>	<i>4.71</i>	
5	29.07	155.05	4.58	9.85	0.70
	<i>7.22</i>	<i>31.90</i>	<i>4.35</i>	<i>6.64</i>	
Campaign	34.27	203.98	2.76	11.01	0.64

Table 3.4 Chemical observations divided by period of TORCH 1 campaign (numbers in italics are standard deviations)

3.6 Chemical Observations at TORCH 2

Inorganic chemical observations and benzene:toluene ratios (Table 3.4) are generally consistent with air mass classification by five-day back trajectory. Trajectories for periods 1, 4 and 7 show that land has been passed over immediately prior to air mass arrival in Weybourne (Southern England, Northern England and Benelux/Southern England respectively). These periods have the highest difference in O₃ (difference between peak ozone and period average), CO, NO, NO₂ and NO_y mixing ratios. They also have low benzene:toluene ratios indicating less-well processed air masses relative to the other periods. Trajectories for periods 3, 5 and 6, on the other hand, show little or no passing over land in the previous five days. These three periods have the lowest O₃ differences, CO, NO, NO₂ and NO_y mixing ratios. They have the highest benzene:toluene ratios indicating a long time since these air masses experienced pollution emissions. The trajectory for period 2 is interesting because, although it spent the day or so prior to arriving in Weybourne travelling across the North Sea, it originates in Eastern Europe, where it was potentially injected with polluted air. This is evident in a higher than average CO mixing with a relatively low standard deviation. It is NO_x depleted but has significantly more NO_y than periods 3, 5 and 6, indicating an air mass that has undergone a great deal of chemical processing.

Periods 1, 2, 4 and 5 have all passed over land and this shows in their higher than campaign average for CO. The trajectory for period 2, however, starts over Eastern Europe and the air mass spends the day before arriving at Weybourne travelling over the North Sea.

Period	O ₃ /ppbv	CO /ppbv	SO ₂ /ppbv	NO /ppbv	NO ₂ /ppbv	NO _y /ppbv	b:t ratio
1	33.52	128.82	2.99	1.53	4.63	4.04	0.80
	<i>7.52</i>	<i>12.42</i>	<i>0.90</i>	<i>0.55</i>	<i>1.95</i>	<i>4.53</i>	
2	49.07	121.81	5.73	0.19	0.67	2.91	4.92
	<i>6.59</i>	<i>4.01</i>	<i>1.05</i>	<i>1.02</i>	<i>1.30</i>	<i>2.59</i>	
3	48.44	103.62	5.93	0.22	0.71	1.12	10.46
	<i>4.97</i>	<i>4.24</i>	<i>0.55</i>	<i>1.16</i>	<i>1.44</i>	<i>2.10</i>	
4	34.74	112.64	7.09	0.79	3.36	6.88	0.91
	<i>10.79</i>	<i>18.52</i>	<i>1.40</i>	<i>1.10</i>	<i>1.79</i>	<i>3.85</i>	
5	42.92	98.70	5.08	0.10	0.45	0.48	10.21
	<i>2.69</i>	<i>4.68</i>	<i>0.97</i>	<i>0.11</i>	<i>0.98</i>	<i>1.03</i>	
6	46.95	93.53	4.40	0.26	0.65	0.97	6.09
	<i>4.70</i>	<i>3.46</i>	<i>1.06</i>	<i>1.34</i>	<i>0.99</i>	<i>2.30</i>	
7	39.00	125.82	5.93	0.72	4.24	9.65	1.12
	<i>9.45</i>	<i>15.45</i>	<i>1.20</i>	<i>0.83</i>	<i>2.26</i>	<i>4.94</i>	
Campaign	40.52	110.52	5.53	0.50	2.30	4.21	4.14

Table 3.4 Chemical observations divided by period of TORCH 2 campaign (numbers in italics are standard deviations)

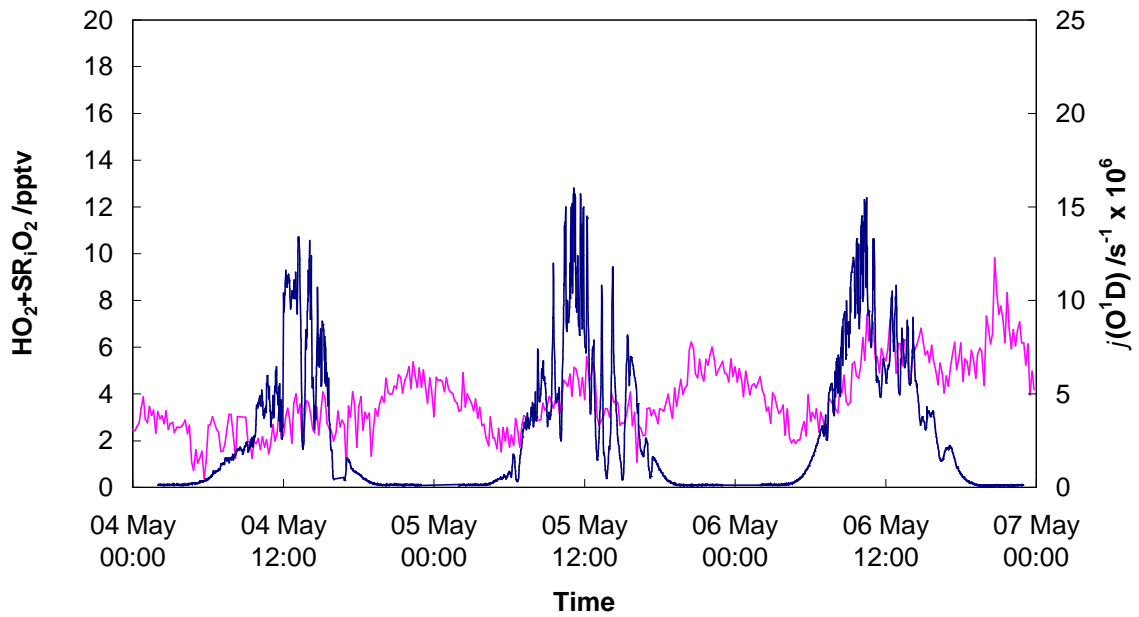


Figure 3.5a Peroxy radical mixing ratios (ten-minute averages, pink line) and $j(O^1D)$ (one-minute averages, blue line) for Period 1 of TORCH 2

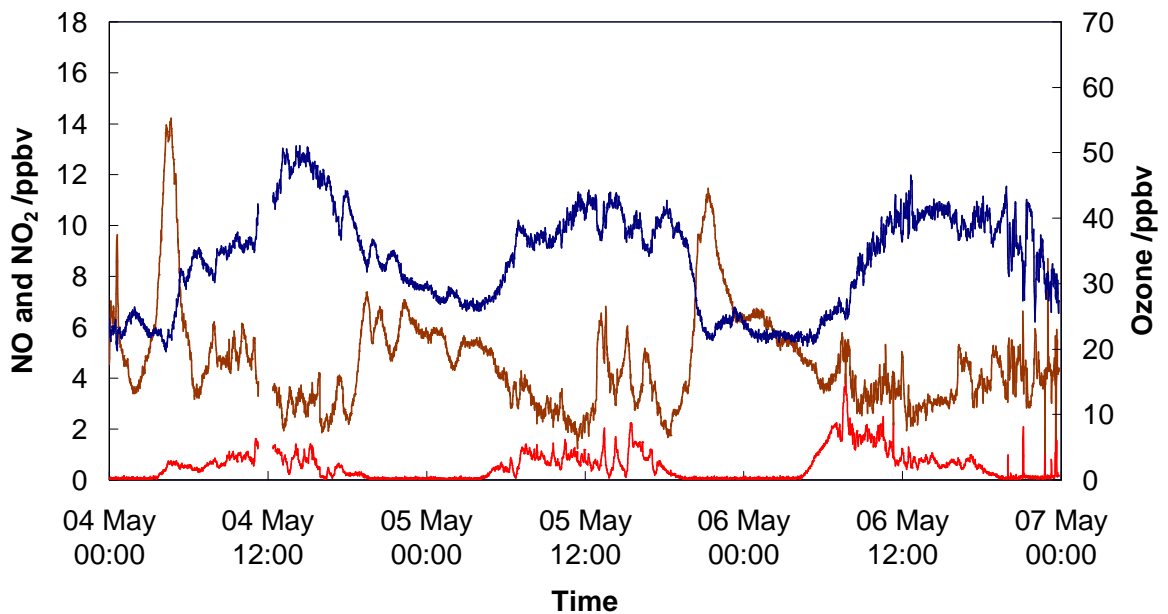


Figure 3.5b Ozone (blue line), NO (red line) and NO₂ (brown line) mixing ratios for Period 1 of TORCH 2 (all one-minute averages)

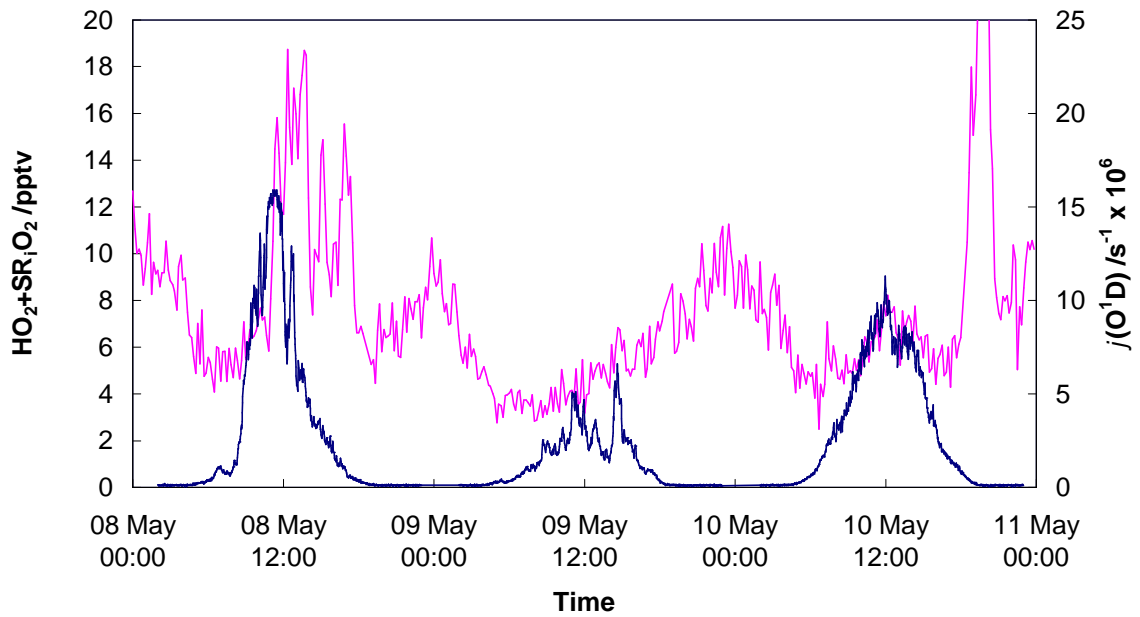


Figure 3.6a Peroxy radical mixing ratios (ten-minute averages, pink line) and $j(O^1D)$ (one-minute averages, blue line) for Period 2 of TORCH 2

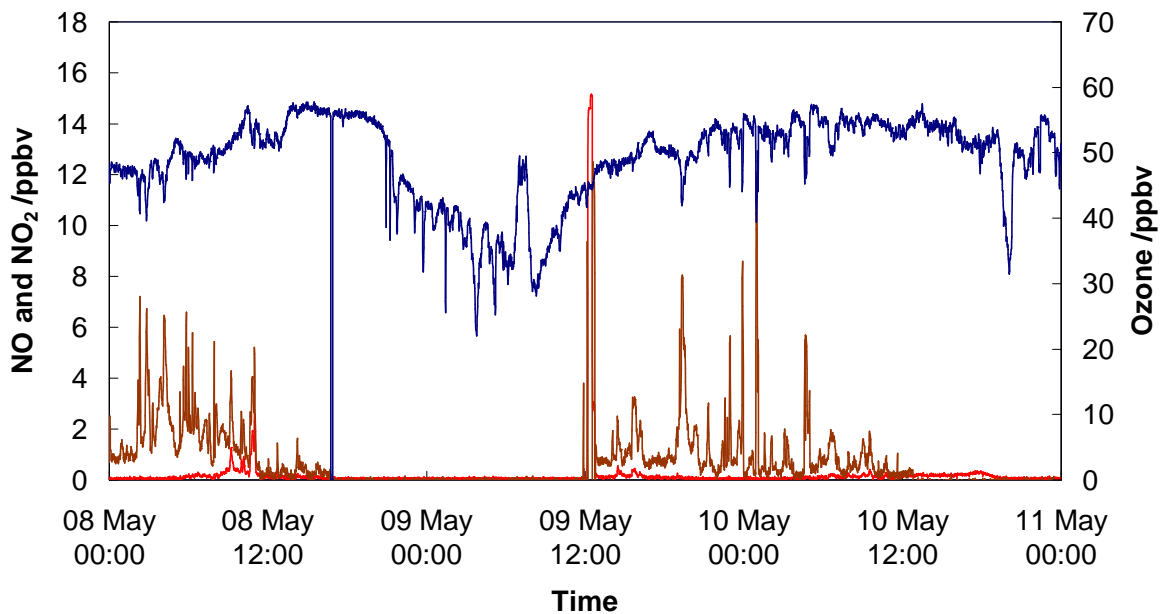


Figure 3.6b Ozone (blue line), NO (red line) and NO₂ (brown line) mixing ratios for Period 2 of TORCH 2 (all one-minute averages)

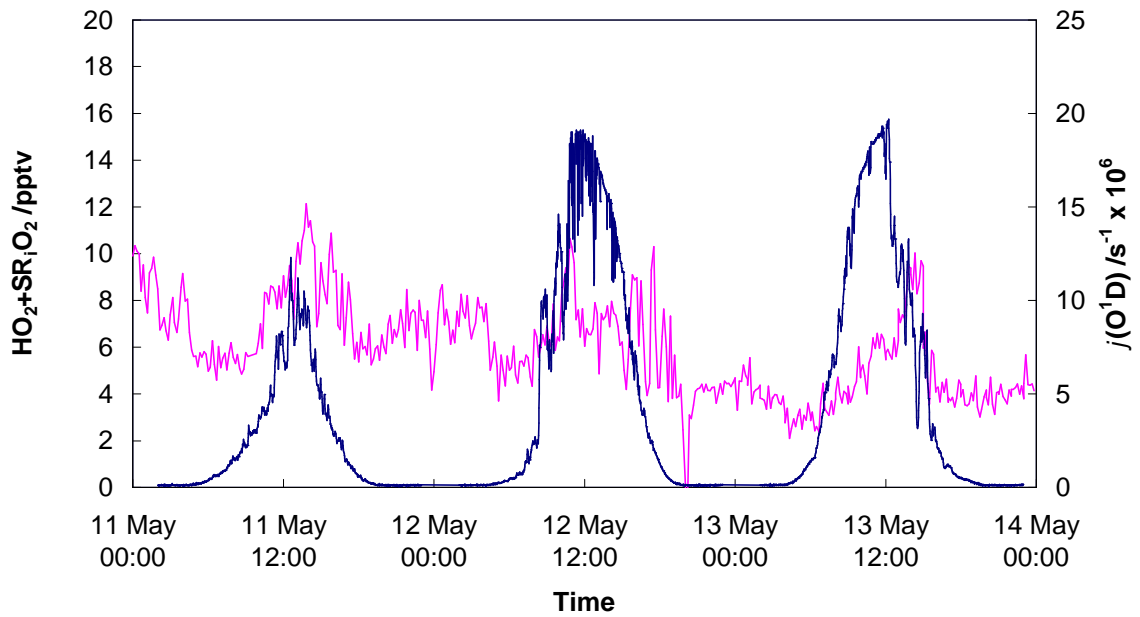


Figure 3.7a Peroxy radical mixing ratios (ten-minute averages, pink line) and $j(O^1D)$ (one-minute averages, blue line) for Period 3 of TORCH 2

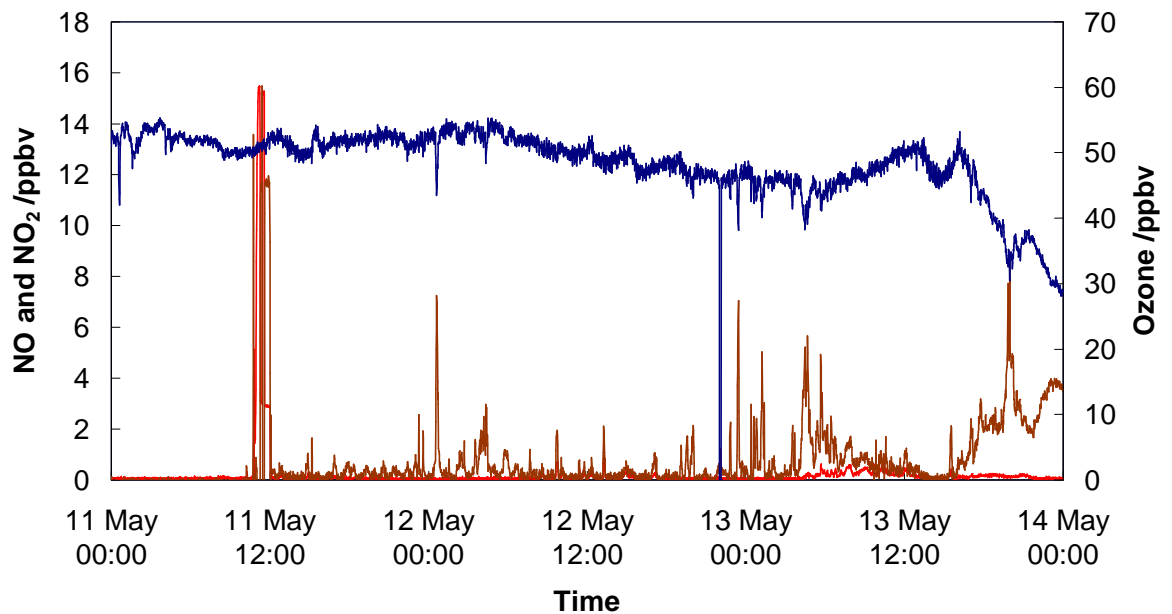


Figure 3.7b Ozone (blue line), NO (red line) and NO₂ (brown line) mixing ratios for Period 3 of TORCH 2 (all one-minute averages)

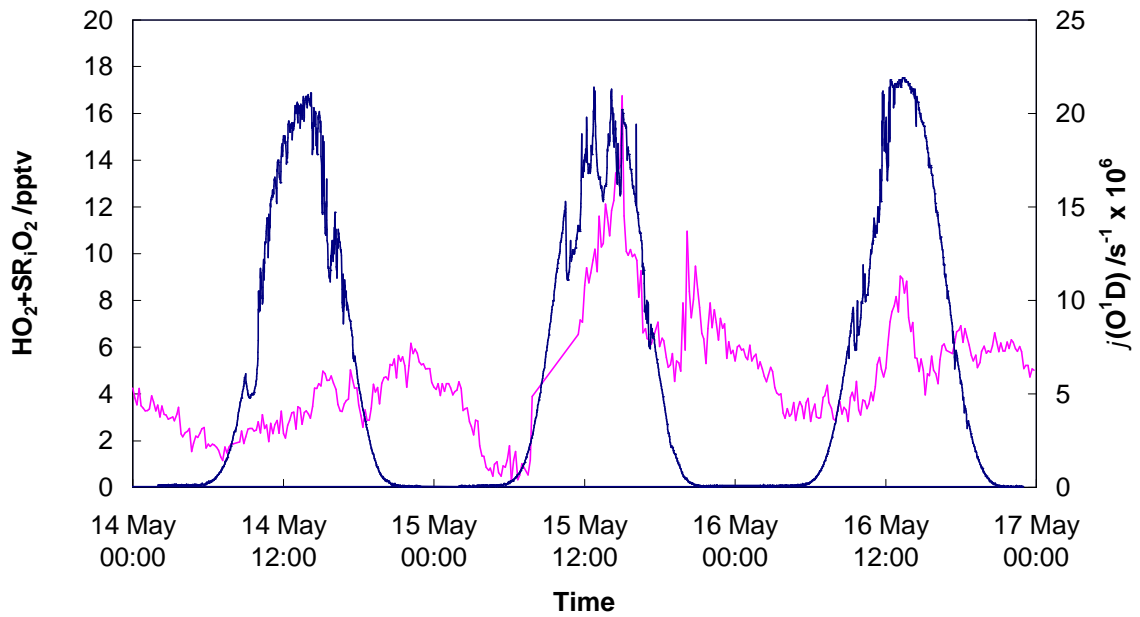


Figure 3.8a Peroxy radical mixing ratios (ten-minute averages, pink line) and $j(O^1D)$ (one-minute averages, blue line) for Period 4a of TORCH 2

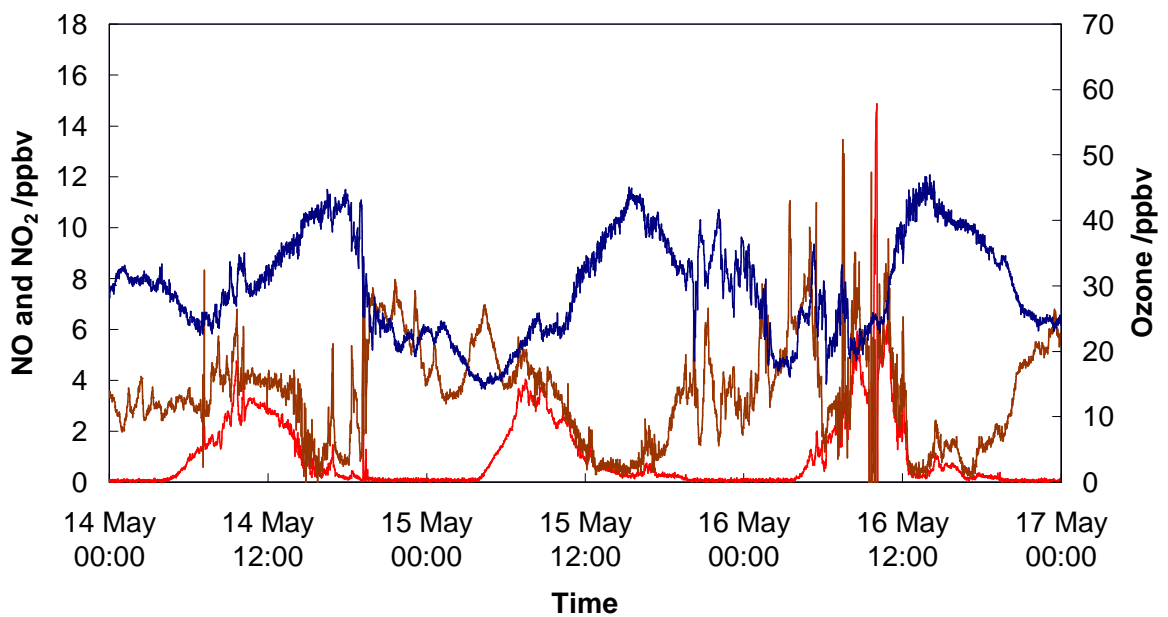


Figure 3.8b Ozone (blue line), NO (red line) and NO₂ (brown line) mixing ratios for Period 4a of TORCH 2 (all one-minute averages)

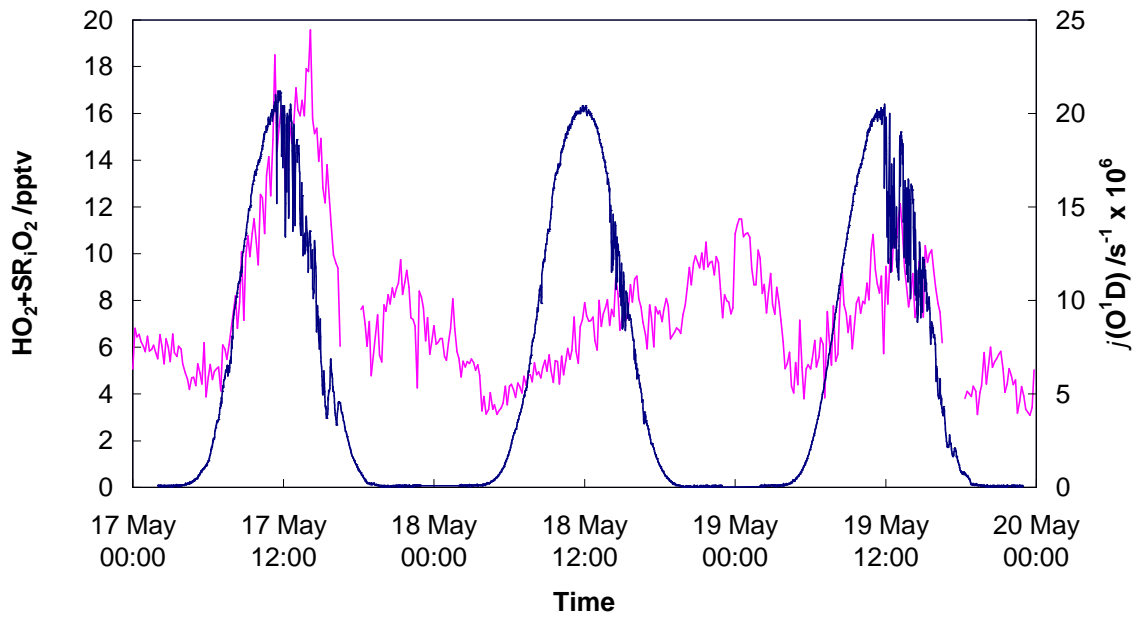


Figure 3.9a Peroxy radical mixing ratios (ten-minute averages, pink line) and $j(O^1D)$ (one-minute averages, blue line) for Period 4b of TORCH 2

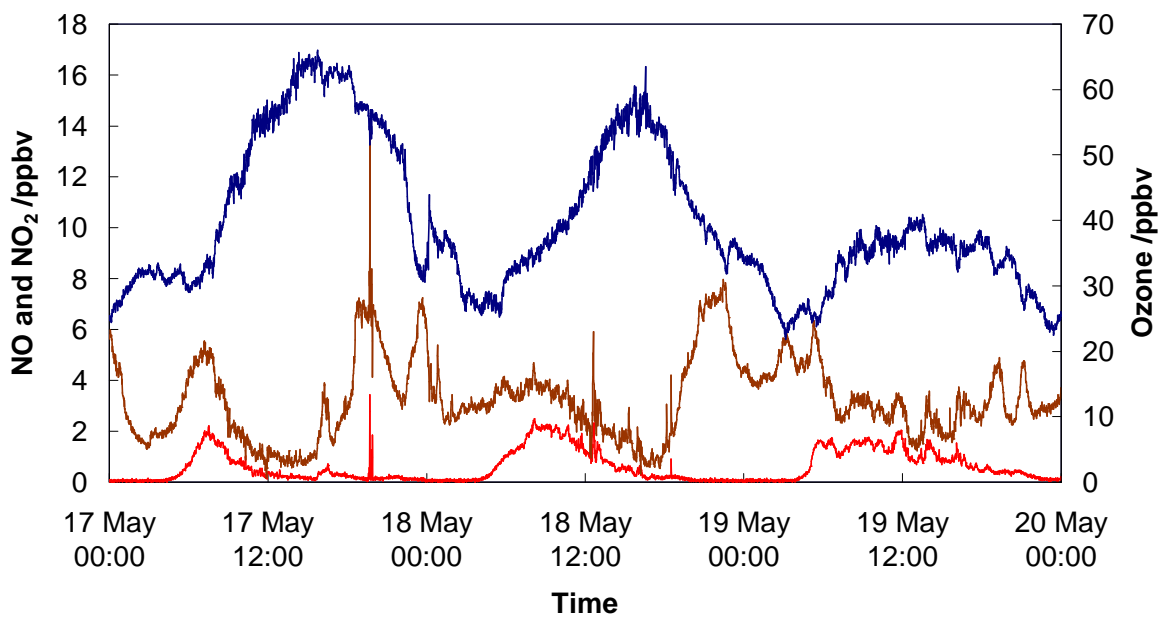


Figure 3.9b Ozone (blue line), NO (red line) and NO₂ (brown line) mixing ratios for Period 4b of TORCH 2 (all one-minute averages)

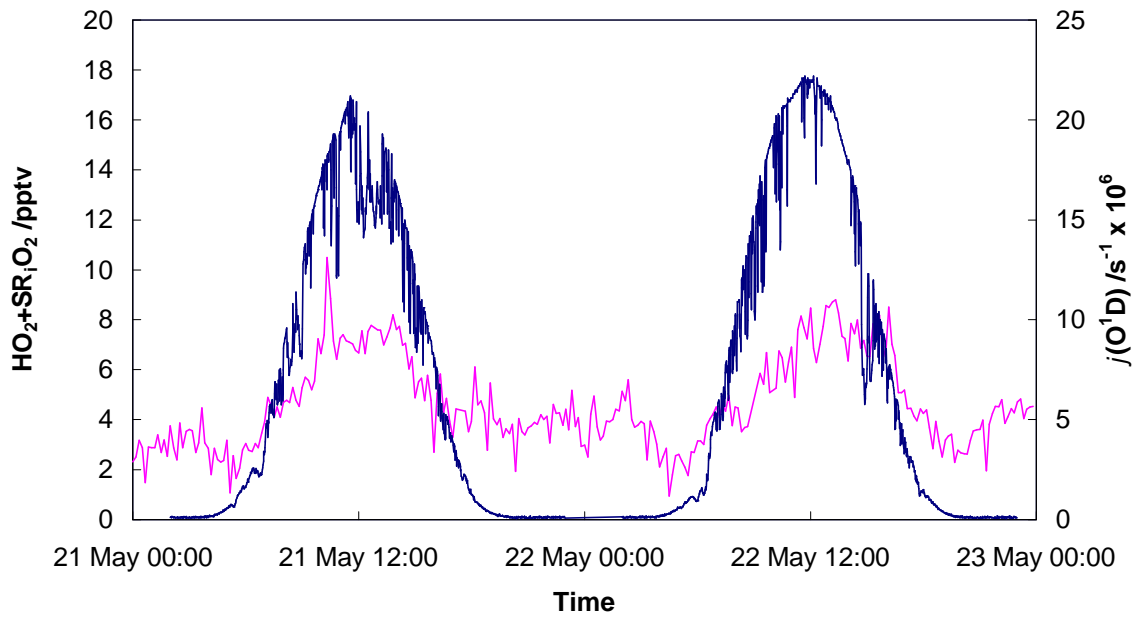


Figure 3.10a Peroxy radical mixing ratios (ten-minute averages, pink line) and $j(O^1D)$ (one-minute averages, blue line) for Period 5 of TORCH 2

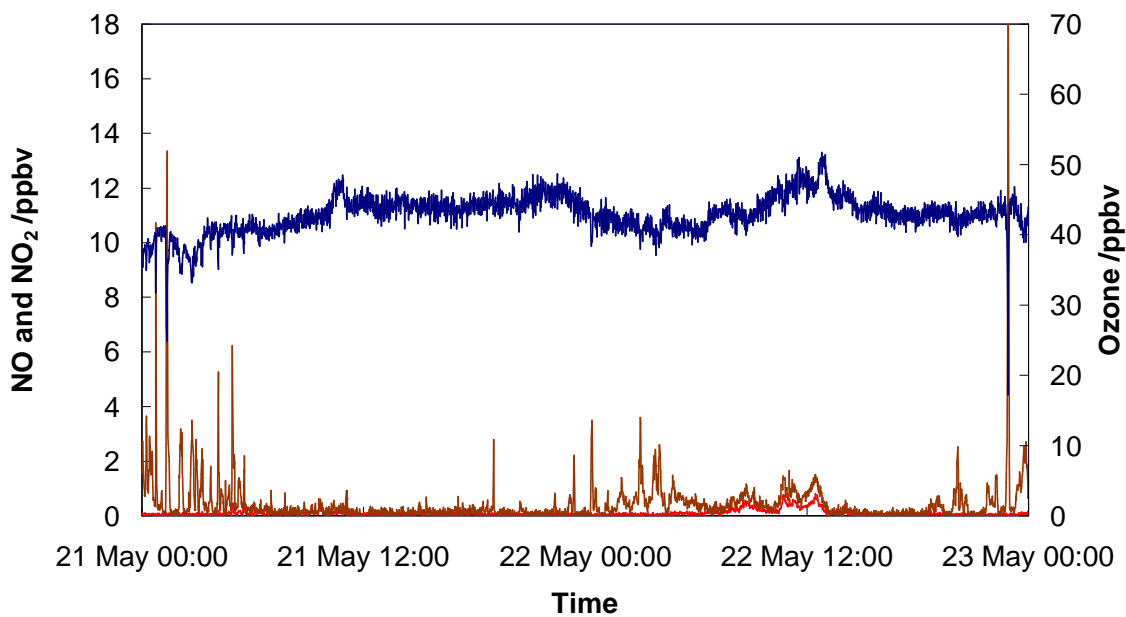


Figure 3.10b Ozone (blue line), NO (red line) and NO₂ (brown line) mixing ratios for Period 5 of TORCH 2 (all one-minute averages)

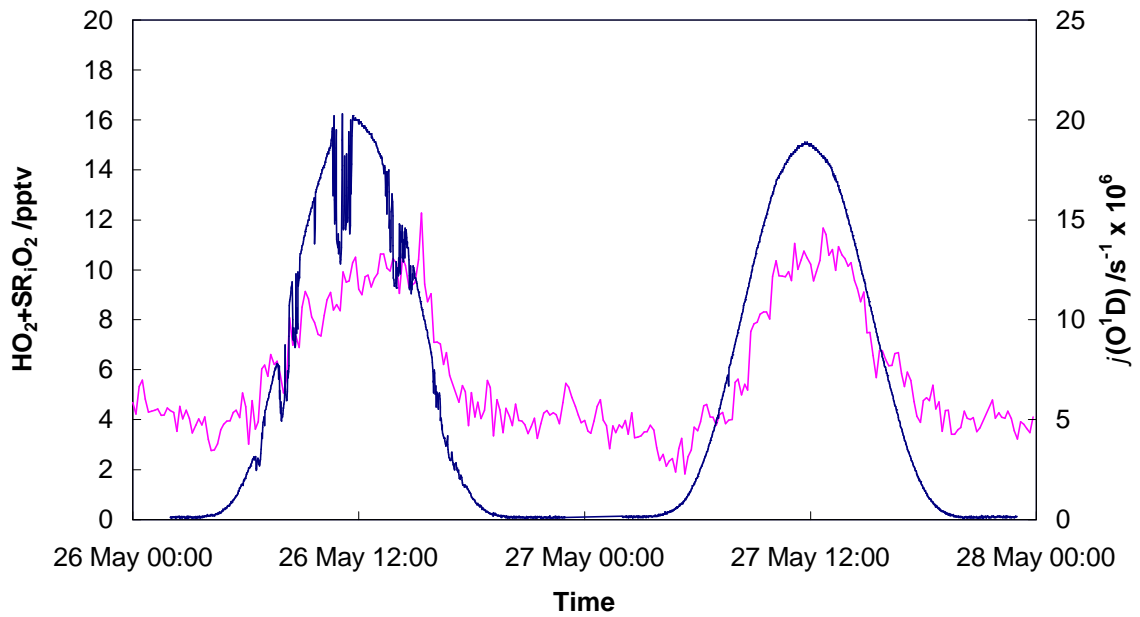


Figure 3.11a Peroxy radical mixing ratios (ten-minute averages, pink line) and $j(O^1D)$ (one-minute averages, blue line) for Period 6 of TORCH 2

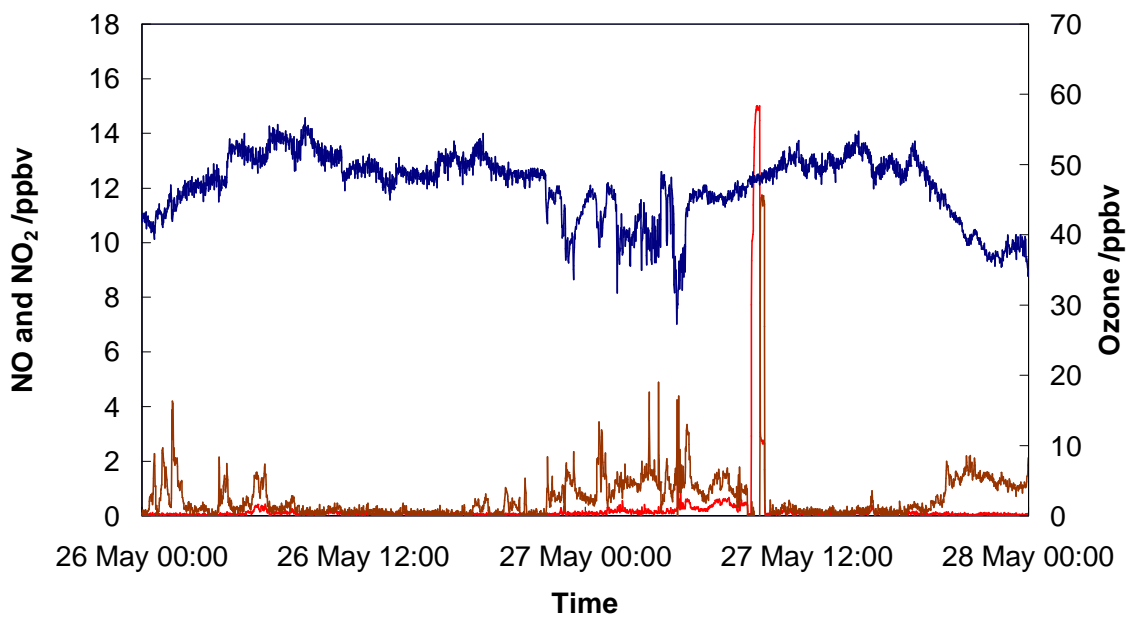


Figure 3.11b Ozone (blue line), NO (red line) and NO₂ (brown line) mixing ratios for Period 6 of TORCH 2 (all one-minute averages)

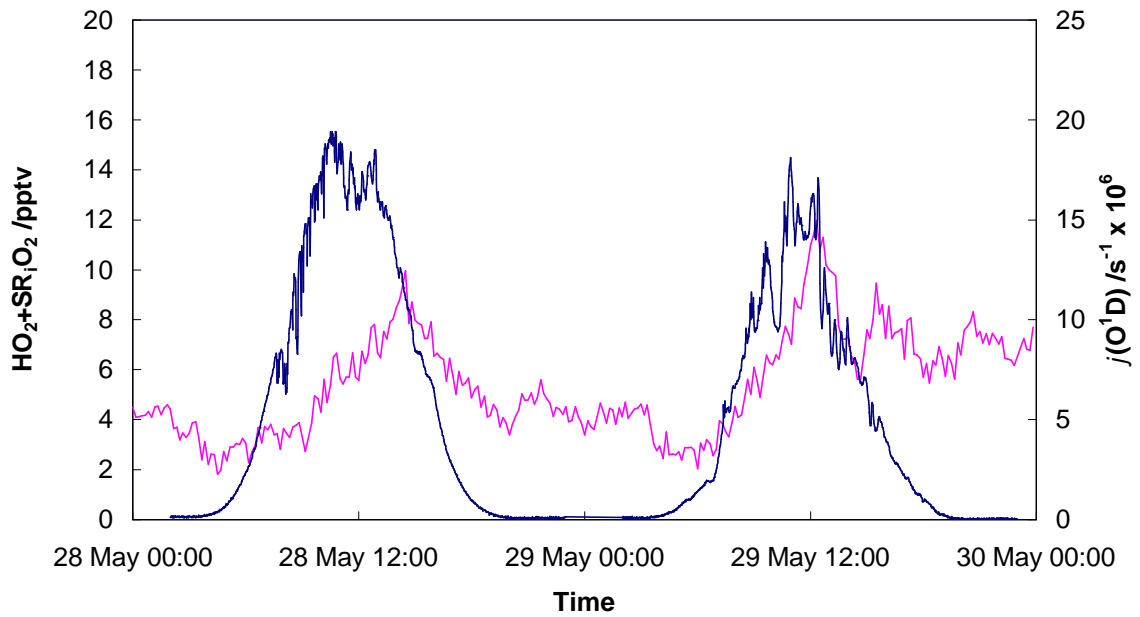


Figure 3.12a Peroxy radical mixing ratios (ten-minute averages, pink line) and $j(O^1D)$ (one-minute averages, blue line) for Period 7 of TORCH 2

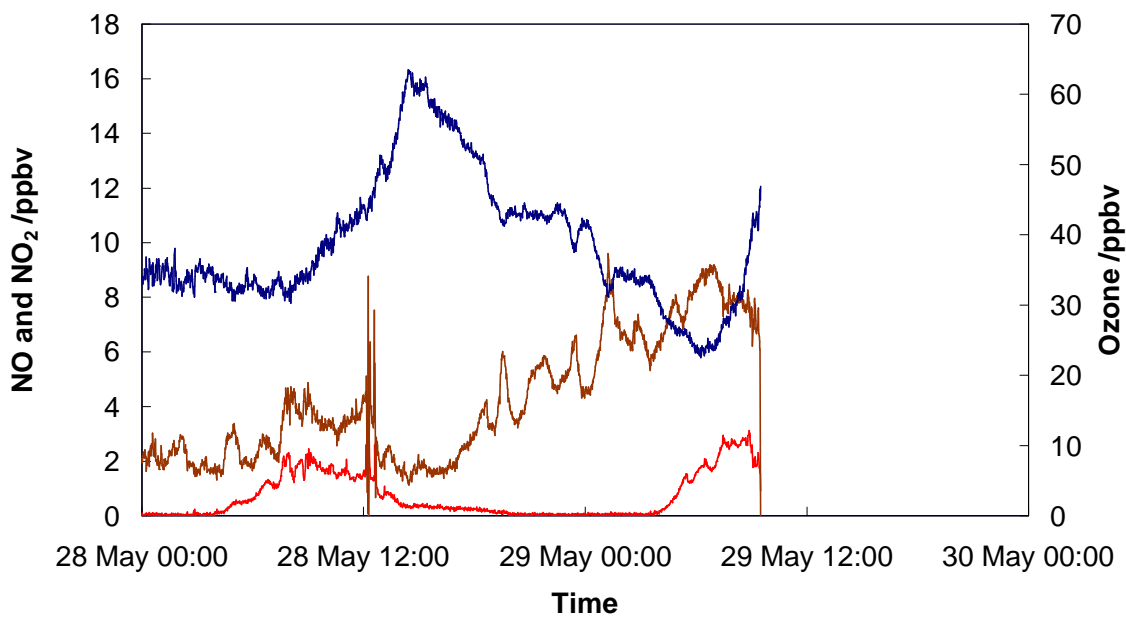


Figure 3.12b Ozone (blue line), NO (red line) and NO₂ (brown line) mixing ratios for Period 7 of TORCH 2 (all one-minute averages)

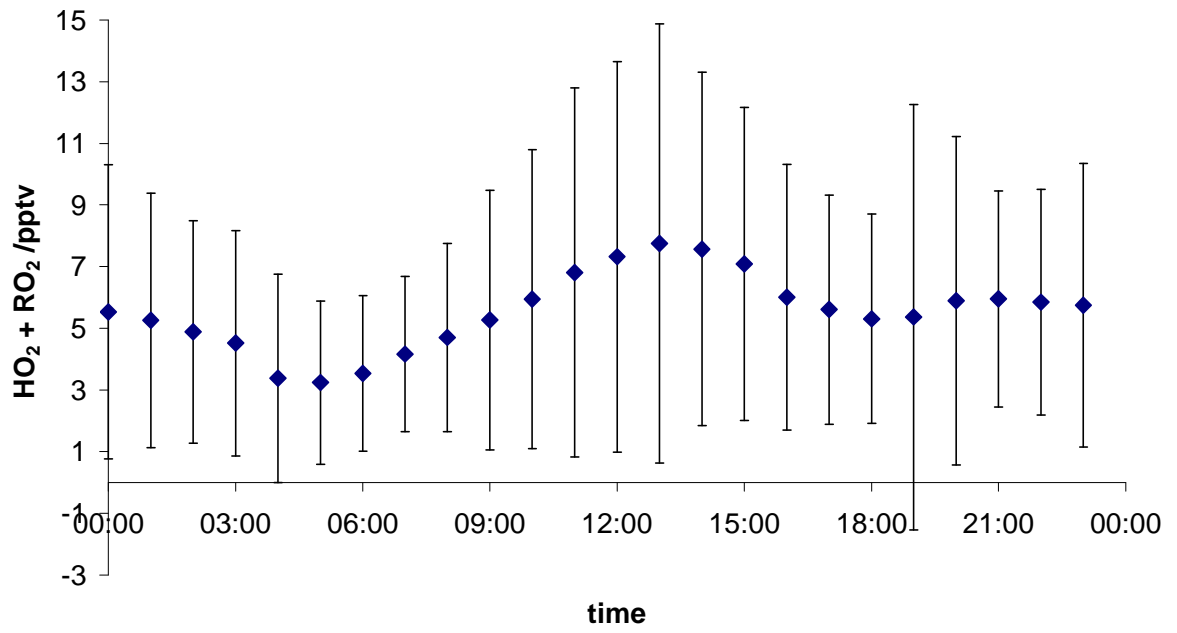


Figure 3.13 TORCH 2 PERCA peroxy radical average diurnal.

4 PSS, Measured and Modelled Peroxy Radicals at TORCH 1

4.1 PSS Theory

As described in Chapter 1, the only known process for the chemical production of O₃ in the troposphere is reaction of NO with a peroxy radical followed by photolysis of the resulting NO₂ to form a ground-state oxygen radical which reacts with a molecule of oxygen to form ozone (Reactions 4.1 – 4.4)



O₃ is also destroyed by reaction with NO



When enough radiation is available for Reaction 4.3, a photostationary state [Leighton, 1961] is achieved when the destruction and the production of ozone are equal:

$$j\text{NO}_2[\text{NO}_2] = k_{\text{NO}+\text{O}_3}[\text{O}_3][\text{NO}] \quad \text{Equation 4.1}$$

For daytime cloud-free values of $j\text{NO}_2$ during the summer, steady state is reached within minutes. This steady state can be perturbed by peroxy radicals and in the marine boundary layer by halogen containing compounds.

When steady state is not perturbed ozone production divided by destruction, denoted by f , is equal to one (Equation 4.2):

$$f = \frac{j\text{NO}_2[\text{NO}_2]}{k_{\text{NO}+\text{O}_3}[\text{O}_3][\text{NO}] + k_{\text{HO}_2+\text{NO}}[\text{NO}][\text{HO}_2] + k_{\text{RiO}_2+\text{NO}}[\text{NO}][\text{R}_i\text{O}_2]} \quad \text{Equation 4.2}$$

If peroxy radicals are present then f will be greater than 1 as peroxy radicals are competing with ozone for NO. In polluted urban environments f is expected to be 1 as high NO₂ concentrations remove peroxy radicals via reaction with OH [Matsumoto, *et al.*, 2006], [Calvert, 1976] and [Shetter, *et al.*, 1983]. In rural and remote environments, NO_x concentrations are low enough for peroxy radicals to have a significant impact on the steady state [Parrish, *et al.*, 1986], [Chameides, *et al.*, 1990], [Cantrell, *et al.*, 1997b] and [Hauglustaine, *et al.*, 1996].

Assuming that the rate constants for reaction of NO with the various peroxy radicals (RO_x) are similar, PSS can be used to calculate peroxy radical concentration.

$$[\text{RO}_x] = \frac{j\text{NO}_2[\text{NO}_2] - k_{\text{NO}+\text{O}_3}[\text{O}_3][\text{NO}]}{k_{\text{RO}_x+\text{NO}}[\text{NO}]} \quad \text{Equation 4.3}$$

A number of other factors can lead to a shift in the system away from steady state, including the presence of something destroying ozone or local sources of NO.

4.2 PSS Results

Where f deviates from 1 the system is not in steady state. Above 1 indicates potentially the presence of peroxy radicals. Less than 1 indicates for example a local source of NO. There are a number of days in which f is less than 1 (Table 4.1): from the afternoon of the 3rd to the 6th, 15th to 17th inclusive, and the 24th onwards. From the 7th to the 10th f is consistently higher than 1, often over 2 and reaching 4.13 on the 9th. From the 12th to the afternoon of the 14th f is over 1 but never reaches 2, similarly to the 18th to the 22nd. Values of f up to 3.43 occur on 23rd.

The periods of $f < 1$ relate to periods of high NO mixing ratios. During these periods local wind direction is from the East, where the generator powering all the instrumentation is located and the high NO mixing ratios are probably heavily influenced by the exhaust from the diesel powered generator. This was situated 250m from the instrument inlets so at windspeeds of 5 ms^{-1} the air would take less than a minute to reach them and thus the system would not have reached steady state.

The period 7th to 10th August had the highest values of f , which is consistent with the observation that peroxy radical mixing ratios were highest at this time.

<i>August day</i>	<i>09:00</i>	<i>10:00</i>	<i>11:00</i>	<i>12:00</i>	<i>13:00</i>	<i>14:00</i>	<i>15:00</i>	<i>16:00</i>	<i>17:00</i>
2	1.29	0.96	1.51	0.92	1.46	1.68	1.62	1.31	1.21
3	0.99	1.25	1.05	1.28	0.73	0.60	0.63	0.58	0.47
4	0.84	0.61	0.58	0.54	0.54	0.58	0.52	0.33	0.21
5	0.93	0.74	0.51	0.49	0.49	0.27	0.25	0.16	0.19
6	0.83	0.57	0.58	0.01	0.00	0.23	0.17	0.09	
7	1.27	1.38	1.73	2.60	2.34	3.98	3.68	2.82	2.36
8	1.61	2.08	2.75	3.39	3.96	2.72	1.79	2.65	2.36
9	1.78	2.58	3.90	4.13	3.54	3.37	2.95	2.69	2.61
10	1.41	3.88	2.87	1.60	3.25	2.17	3.32	3.03	3.59
11					1.34	1.36	1.15	0.64	0.47
12	1.31	1.37	1.36	1.97	1.12	1.22	0.98	1.28	1.06
13	1.33	1.63	1.93	1.70	1.54	1.63	1.98	1.68	1.53
14	1.21	1.28	1.49	1.45	1.39	1.24	0.97	1.00	0.29
15	0.65	0.56	0.66	0.54	0.57	0.59	0.42	0.38	0.20
16	0.58	0.69	0.60	0.64	0.49	0.52	0.34	0.37	0.24
17	0.62	0.65	0.65	0.68	0.70	0.58	0.48	0.42	0.30
18	1.67	1.73	1.79	1.90	1.80	1.74	1.58	1.44	1.40
19	1.25	1.42	1.50	1.59	1.58	1.49	1.12	1.31	1.25
20	1.33	1.33	1.40	1.50	1.54	1.80	1.42	1.49	1.40
21	1.24	1.24	1.34	1.48	1.48	1.55	1.87	2.28	2.39
22	1.40	1.42	1.39	1.52	1.66	1.68	1.51	1.49	1.96
23	2.07	3.05	3.03	2.43	3.43	2.38	2.29	2.17	1.59
24	0.43	0.44	0.50	0.67	0.18	0.47	0.34	0.32	0.16
25	0.45	0.50	0.36	0.34	0.25	0.22	0.18	0.23	0.18
26	0.42	0.38	0.46	0.57	0.61	1.12	0.34	0.34	0.13
27	0.49	0.58	1.03	0.69	0.37	0.38	0.36	0.29	0.19
28	0.54	0.47	0.35	0.44	0.30	0.22	0.08	0.17	0.13
29	1.11	0.17	0.78	0.22	0.40	1.25	0.90	1.06	0.85

Table 4.1 PSS *f* for TORCH 1

4.2.1 PSS O₃ production vs destruction

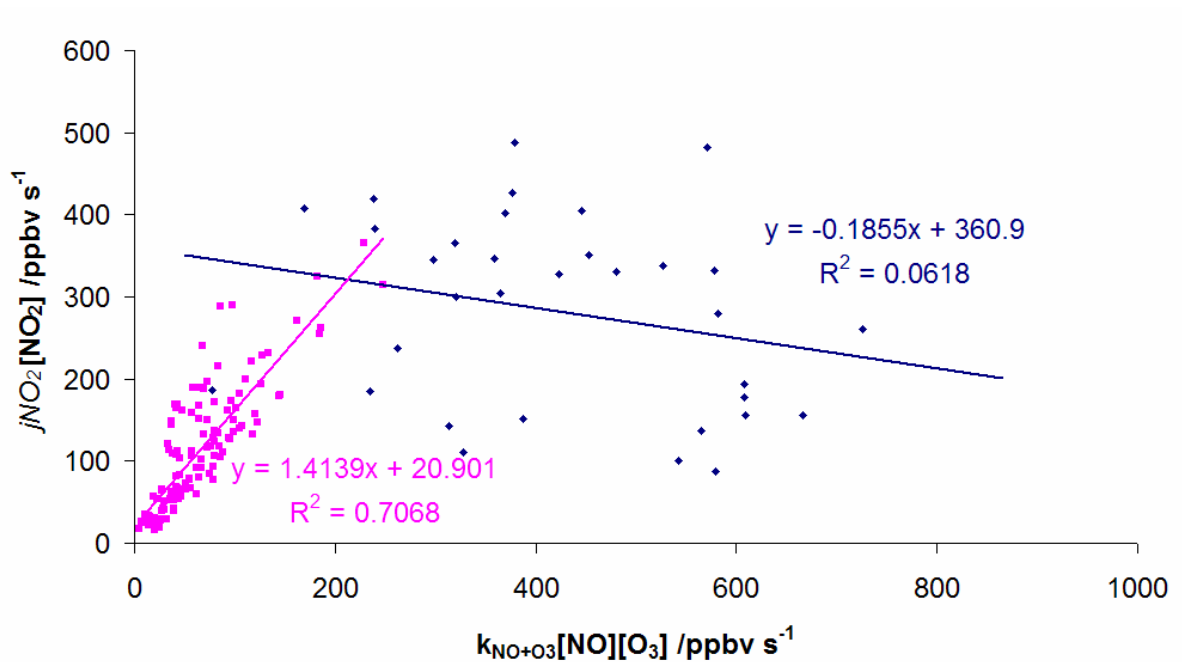


Figure 4.1 PSS ozone production vs destruction for the whole TORCH 1 campaign. (See text for key)

Figure 4.1 shows ozone production, $j\text{NO}_2[\text{NO}_2]$, plotted against $k_{\text{NO}+\text{O}_3}[\text{NO}][\text{O}_3]$ for the whole TORCH 1 campaign. The campaign is divided into two sets of data: those where the site experiences local winds from East Northeast to East ($60 - 90^\circ$) and hourly averages of NO are generally above 5 ppbv (blue data points), and those where the site experiences local wind directions other than from the East Northeast to East and hourly averages of NO are generally below 1 ppbv (pink data points). Good correlation ($R^2=0.71$) exists for the low NO period with ozone destruction generally below 200 ppbv s^{-1} whereas during the high NO period there is no correlation and ozone destruction is generally above 200 ppbv s^{-1} . This is probably due to the elevated NO mixing ratios coming from a local source and thus the system has not had time to reach a steady state.

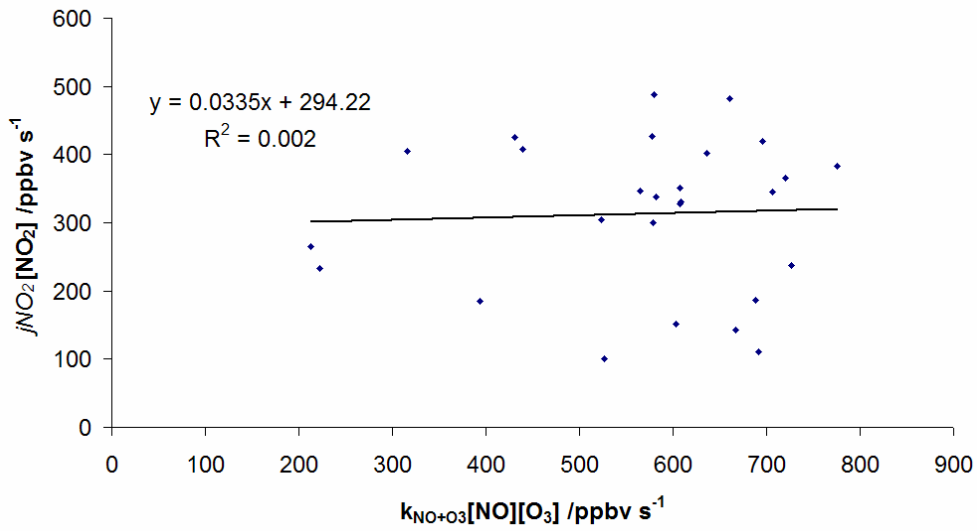


Figure 4.2a PSS ozone production vs destruction for August 3rd – 5th

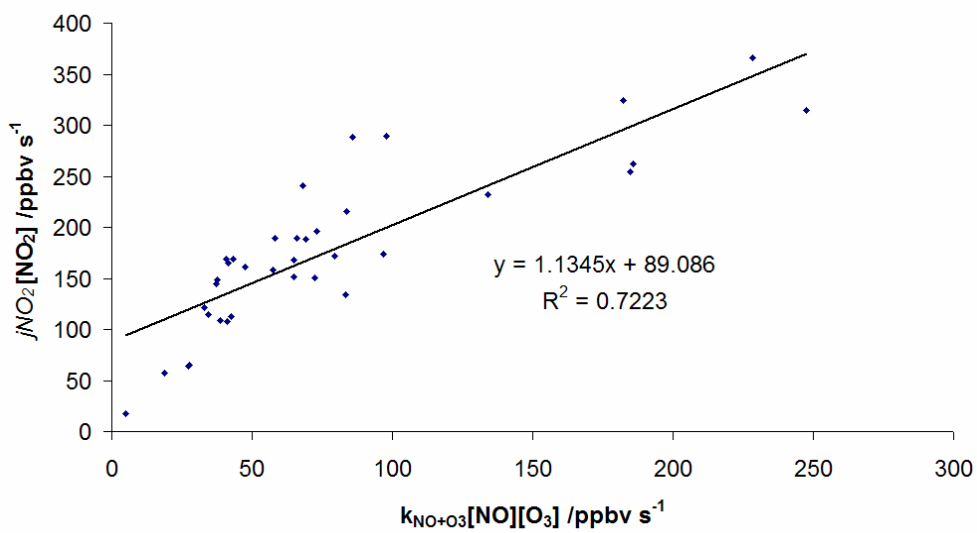


Figure 4.2b PSS ozone production vs destruction for August 7th – 10th

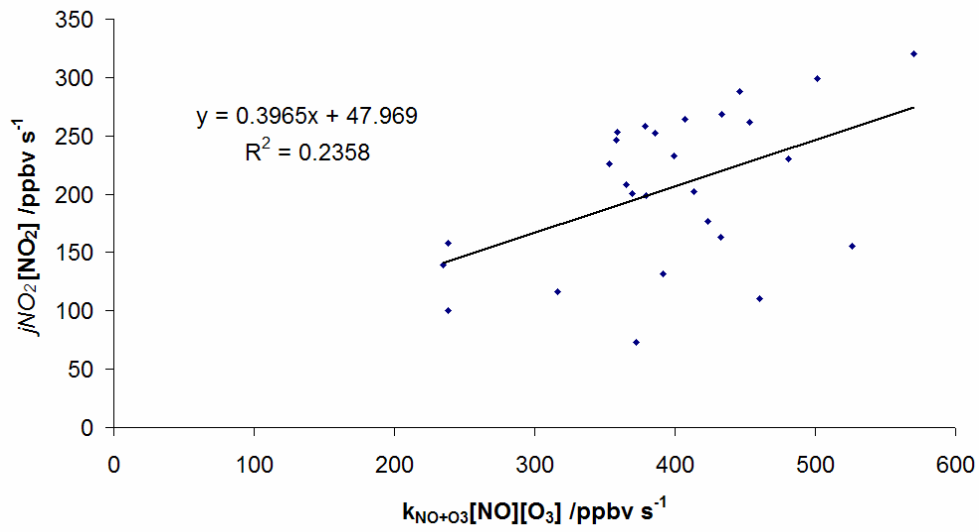


Figure 4.2c PSS ozone production vs destruction for August 15th – 17th

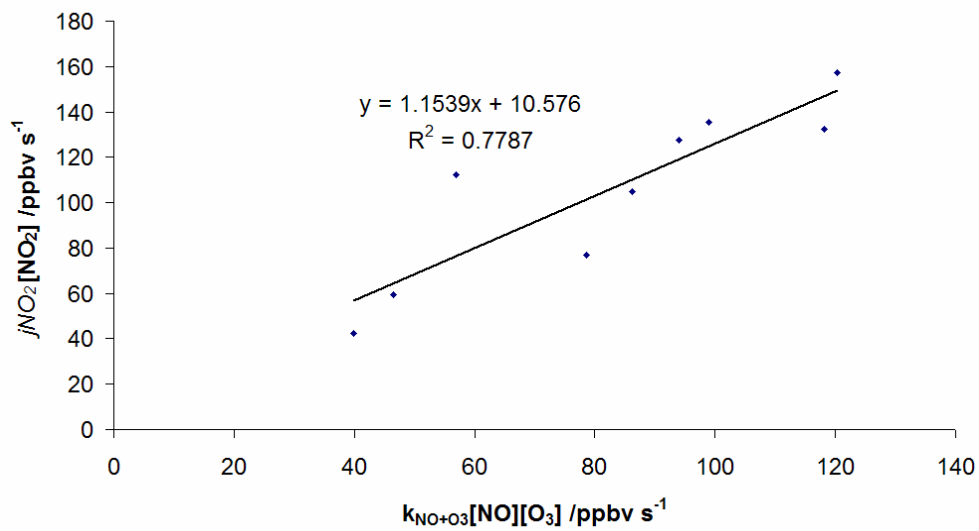


Figure 4.2d PSS ozone production vs destruction for August 12th

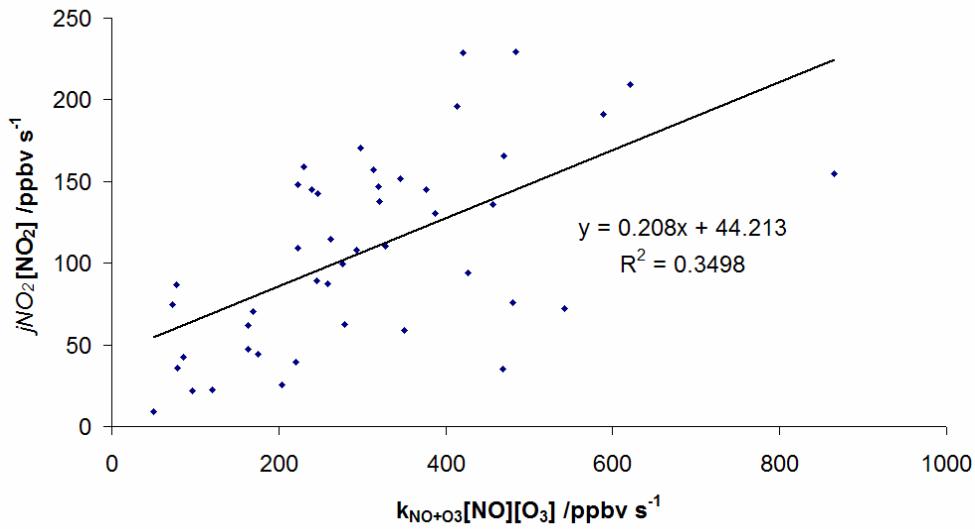


Figure 4.2e PSS ozone production vs destruction for August 24th – 28th

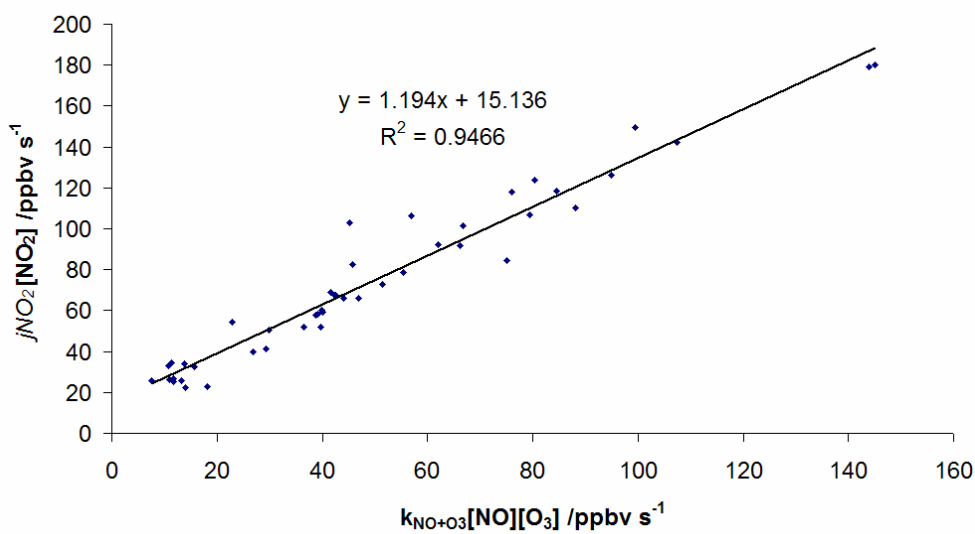


Figure 4.2f PSS ozone production vs destruction for August 19th – 23rd

Figure 4.2 a-f Ozone production vs destruction for six periods during the TORCH 1 campaign. Figures a, c and e are from days with elevated NO (hourly averages generally above 5 ppbv). Figures b, d and f are from days with lower NO mixing ratios (hourly averages generally below 1 ppbv).

Figures 4.2 a-f break down the campaign into 6 periods, three of which had high NO and three of which low NO mixing ratios. As was seen in Figure 4.1 for the whole campaign, where NO mixing ratios are not affected by immediately local sources a good correlation between ozone production and destruction exists. In all three cases (Figures b, d and f) the gradient of the regression line is above 1 indicating the potential presence of peroxy radicals. Where NO mixing ratios are affected by local sources (Figures a, c and e) there is not good correlation between ozone production and destruction.

4.3 Measured vs PSS derived RO_x

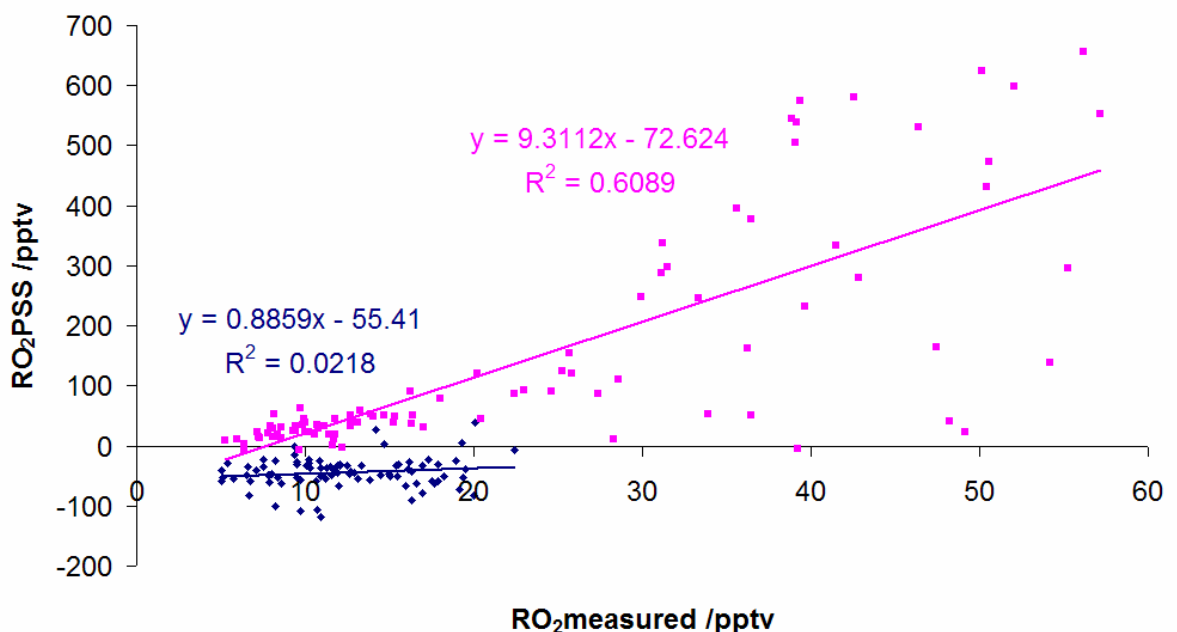


Figure 4.3 Measured vs PSS derived peroxy radical mixing ratio for TORCH 1. Pink squares are for NO < 5ppbv, blue diamonds for NO > 5 ppbv.

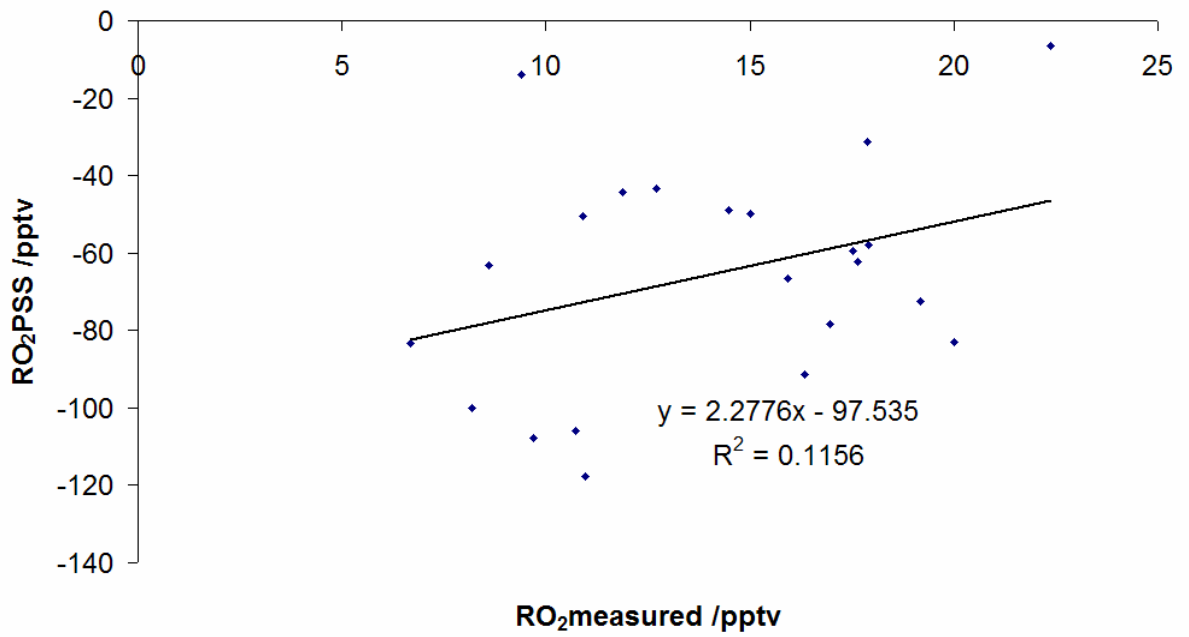


Figure 4.4a Measured vs PSS derived peroxy radical mixing ratio for August 3rd – 5th

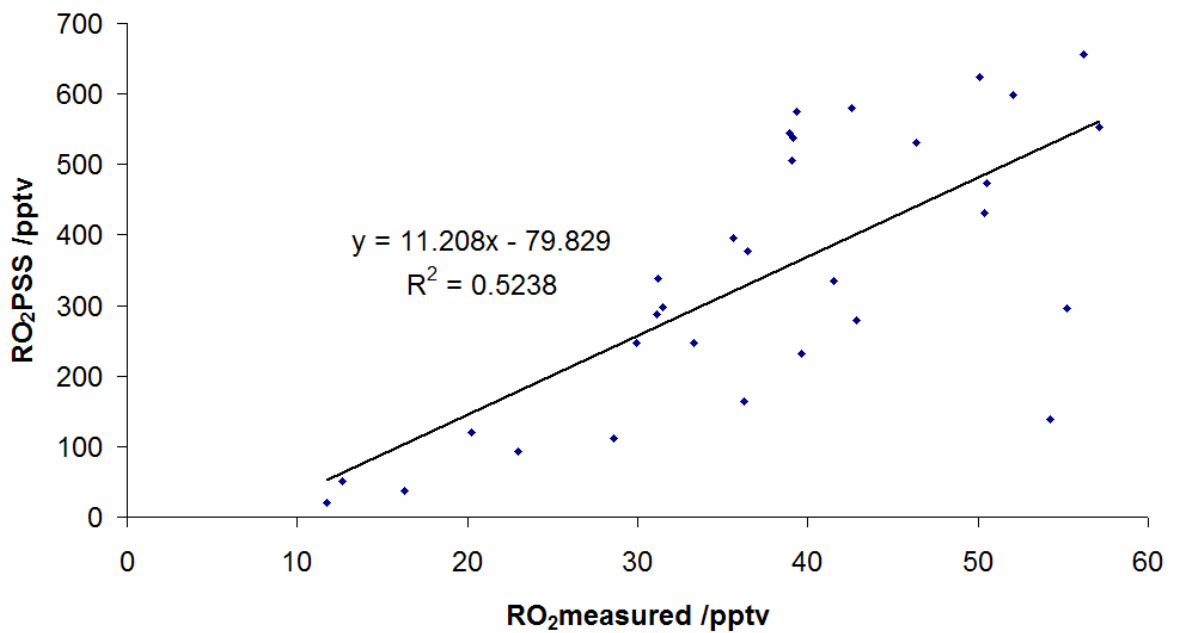


Figure 4.4b Measured vs PSS derived peroxy radical mixing ratio for August 7th – 10th

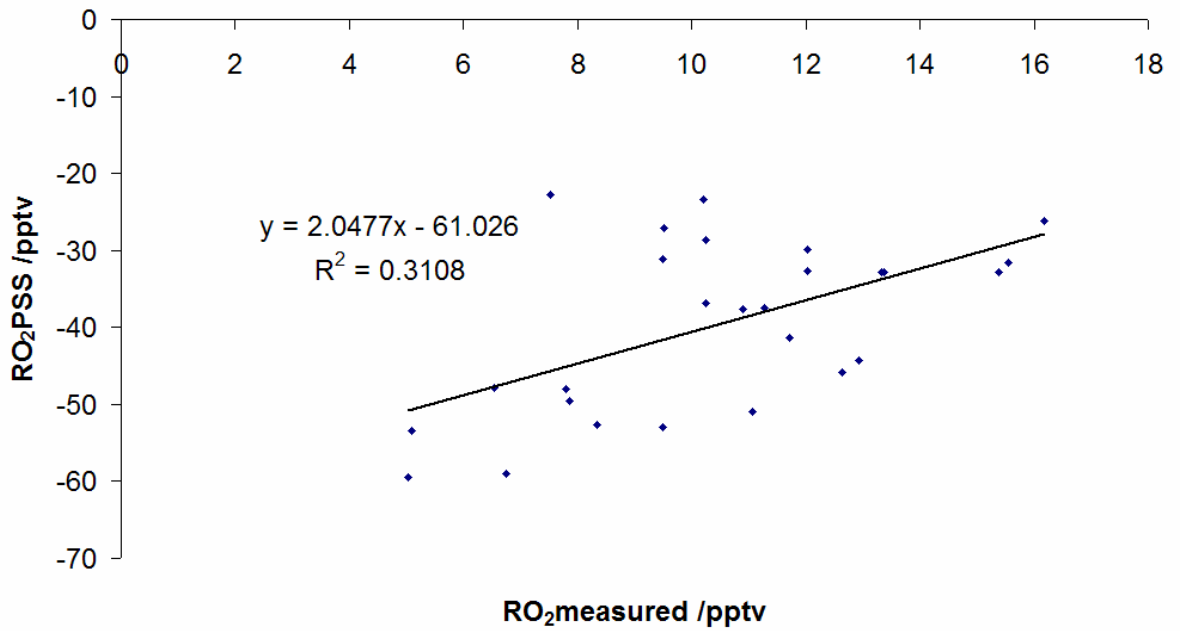


Figure 4.4c Measured vs PSS derived peroxy radical mixing ratio for August 15th – 17th

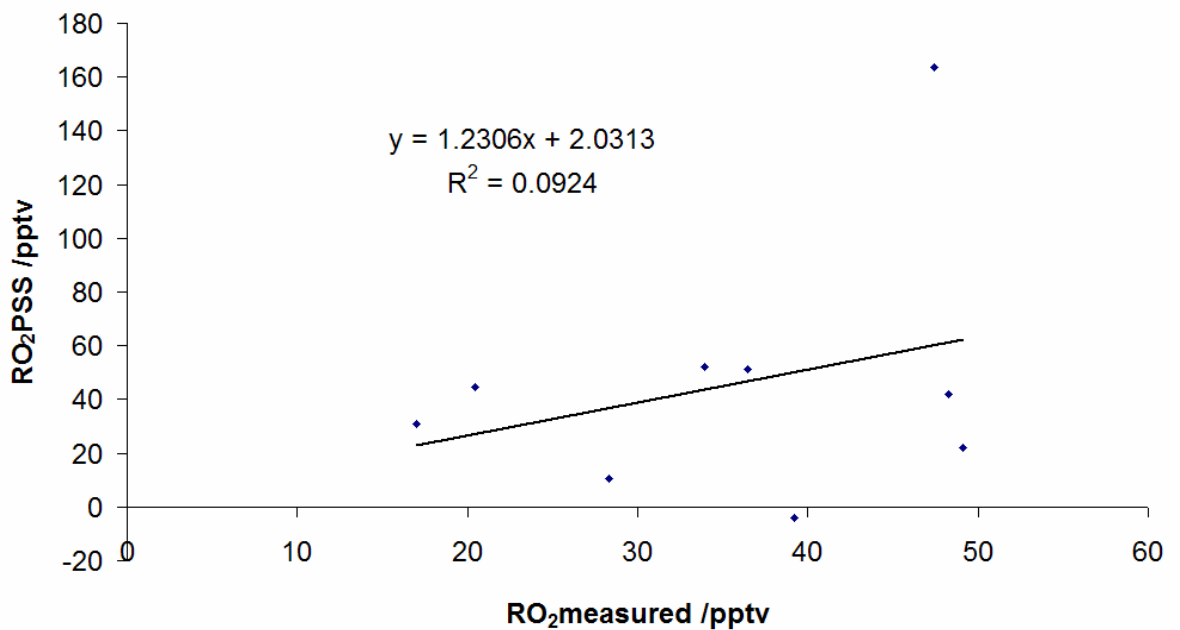


Figure 4.4d Measured vs PSS derived peroxy radical mixing ratio for August 12th

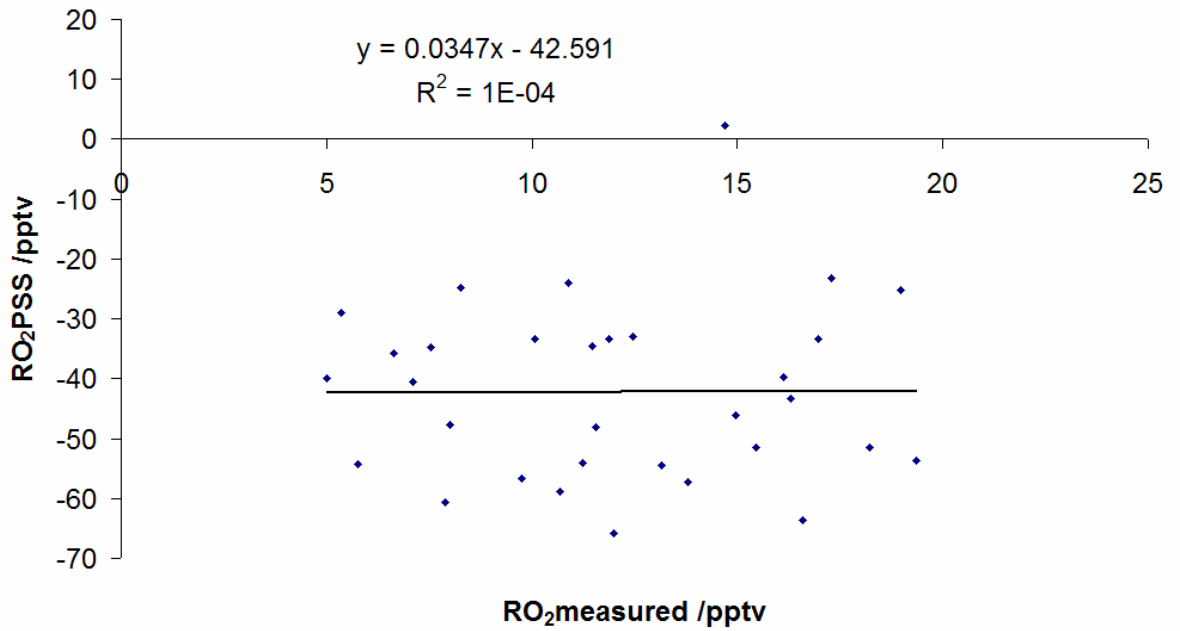


Figure 4.4e Measured vs PSS derived peroxy radical mixing ratio for August 24th – 28th

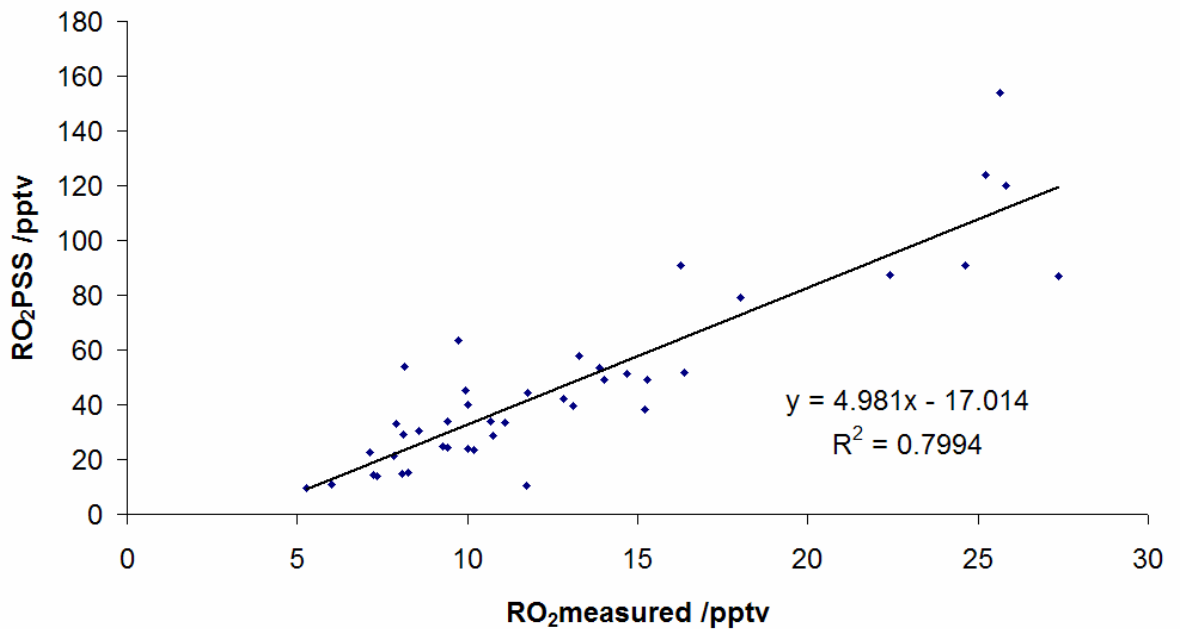


Figure 4.4f Measured vs PSS derived peroxy radical mixing ratio for August 19th – 23rd

4.4 Measured vs Modelled HO₂+SR_iO₂

The Master Chemical Mechanism version 3.1 (MCM, available online at <http://www.chem.leeds.ac.uk/Atmospheric/MCM/mcmproj.html>) contains near-explicit chemical degradation schemes for 135 primary emitted VOCs, based on the most important species in the UK National Atmospheric Emissions Inventory ([*Jenkin, et al.*, 2003], [*Saunders, et al.*, 2003]), resulting in ~14000 reactions involving ~5000 molecular and free radical species. The MCM is a comprehensive mechanism treating each degradation step explicitly and as such, makes no simplifications through the use of lumping techniques or the adoption of surrogate species.

A detailed description of the model as used for TORCH 1 is given in [*Emmerson, et al.*, 2006]. Interestingly for this campaign a loss route of HO₂ onto aerosol surfaces has been calculated using measurements of aerosol size and number distributions (following [*Haggerstone, et al.*, 2005]), and takes into account diffusion of HO₂ to the particle surface and interfacial mass transport. Using the appropriate aerosol measurements, heterogeneous loss of HO₂ was treated using a rate coefficient, k_t , integrated over all bin sizes of particles up to 768 nm (Equation 4.4):

$$k_t = \int_0^\infty \frac{dV(r)}{dr} \left(\frac{r^2}{3D_g} + \frac{4r}{3\bar{v}} \right)^{-1} dr \quad \text{Equation 4.4}$$

where k_t is the rate of loss of HO₂ to the aerosol surface, V is the volume of aerosol, r is the particle radius (in a particular size bin), D_g is the gas diffusivity constant, \bar{v} is the mean molecular velocity and γ is the accommodation coefficient for uptake of HO₂ onto the aerosols. In the atmosphere, γ is a function of the aerosol composition and radius: the composition of the aerosol surface is assumed to be homogeneous for the purposes of this parameterisation.

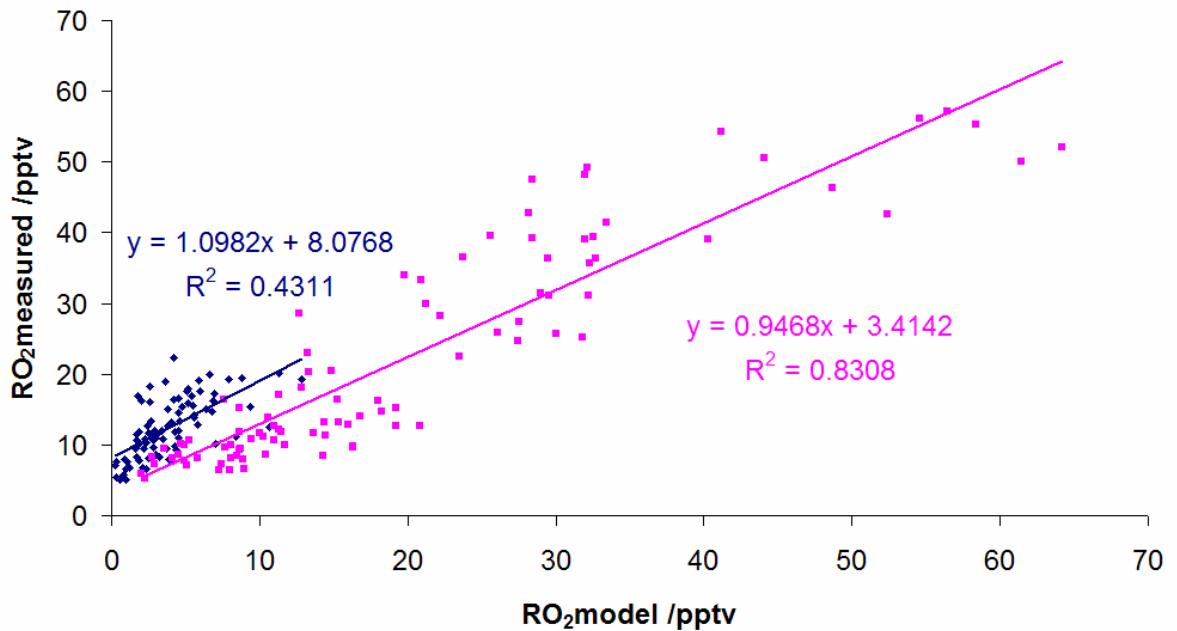


Figure 4.5 Measured vs modelled peroxy radicals split into days with high NO (blue points) and low NO (pink points)

The gradient of the low NO data (pink points in figure 4.5) is very close to 1 (0.95) with good correlation ($R^2=0.83$) which shows that the model is good at simulating the measurements at low NO over a wide range of peroxy radical mixing ratios. The positive intercept reflects the fact that hourly averaged measured peroxy radicals generally never dip below 5 pptv. Mixing ratios of peroxy radicals could really be like this or there could be an offset caused by the way the data is reduced.

For the high NO data the correlation between measured and modelled peroxy radical mixing ratio is not as good ($R^2=0.43$) although interestingly at 1.10 the gradient is very close to 1.

Taking a closer look at the six periods of the campaign (Figures 4.6a-f) correlation between measured and modelled is excellent for the three low NO periods ($R^2=0.82 - 0.93$), although the gradients are much different to 1. For 7th to 10th (Figure 4.6b) and 19th to 23rd (Figure 4.6f) it is roughly 0.7, which is still within instrument error of 35%. For the 12th the gradient is 1.55

outside experimental error. Correlation is very good ($R^2=0.93$) and part of the difference at least could be due to the particular NO_2 and CH_3O_2 sensitivities used that day. For the periods of high ambient NO mixing ratio (Figures 4.6 a, c and e) correlation is less good for 3rd to 5th and not significant for the other two periods. For 3rd to 5th (Figure 4.6a) measured peroxy radicals are 2.4 times greater than modelled. This is due to the peroxy radicals being ‘killed’ by NO in the model.

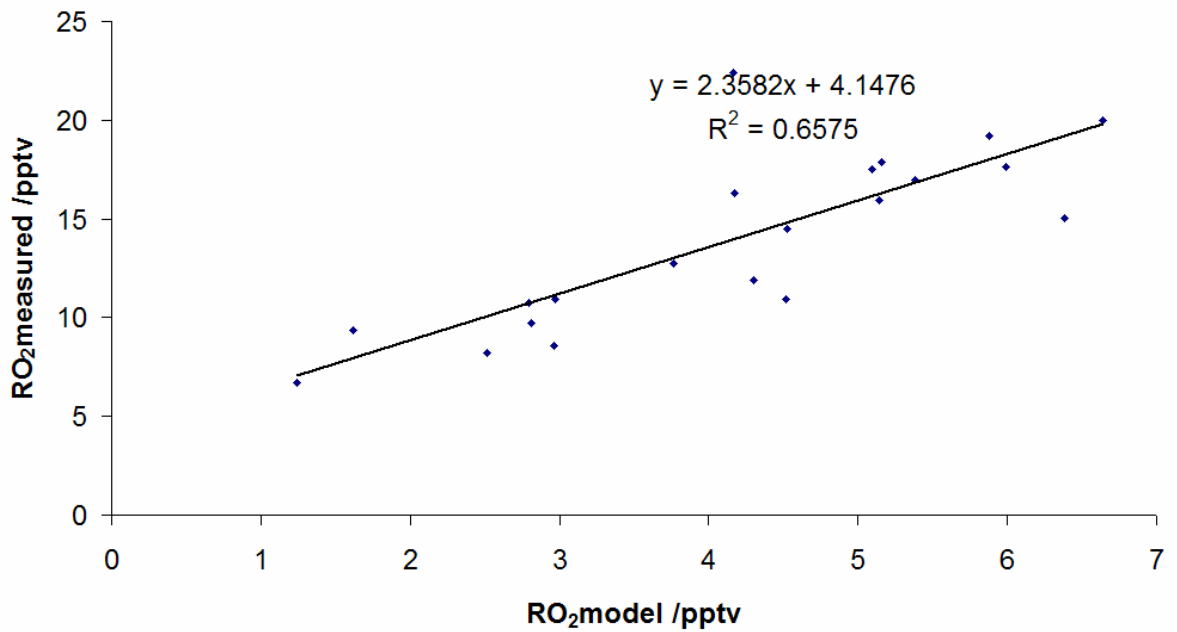


Figure 4.6a Measured vs modelled peroxy radicals for August 3rd – 5th

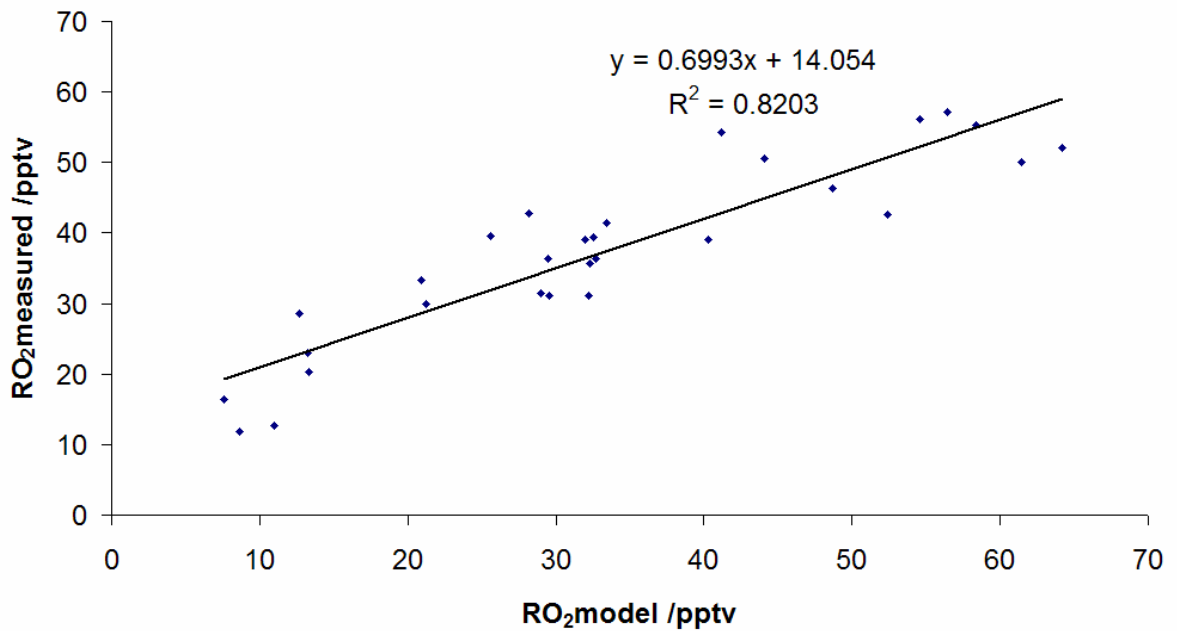


Figure 4.6b Measured vs modelled peroxy radicals for August 7th – 10th

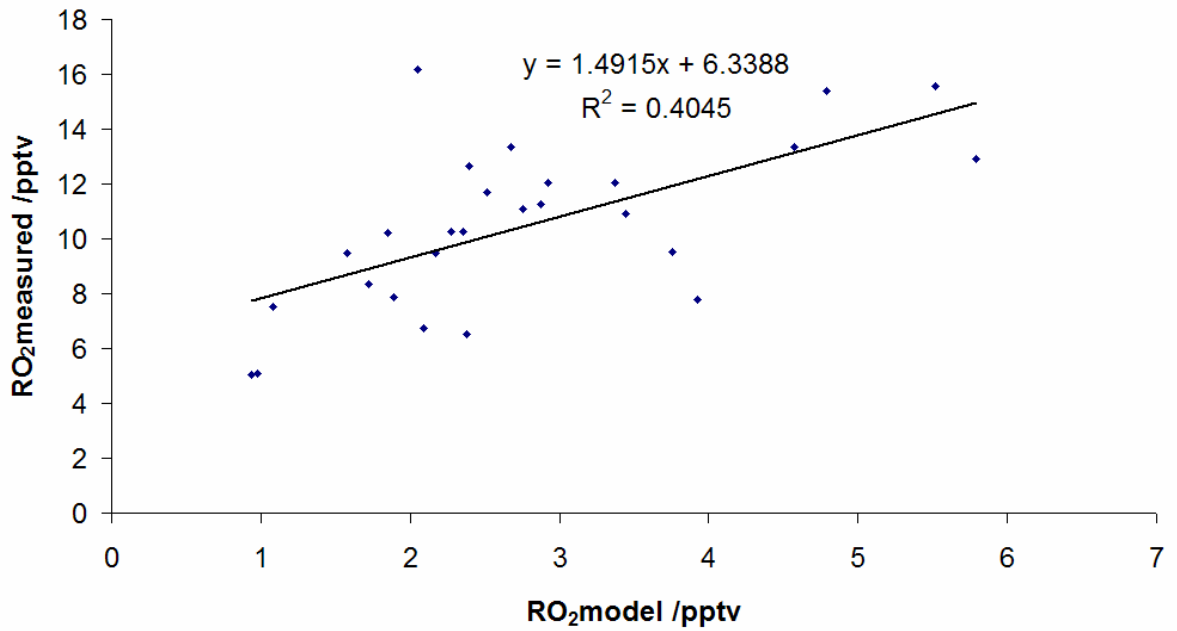


Figure 4.6c Measured vs modelled peroxy radicals for August 15th – 17th

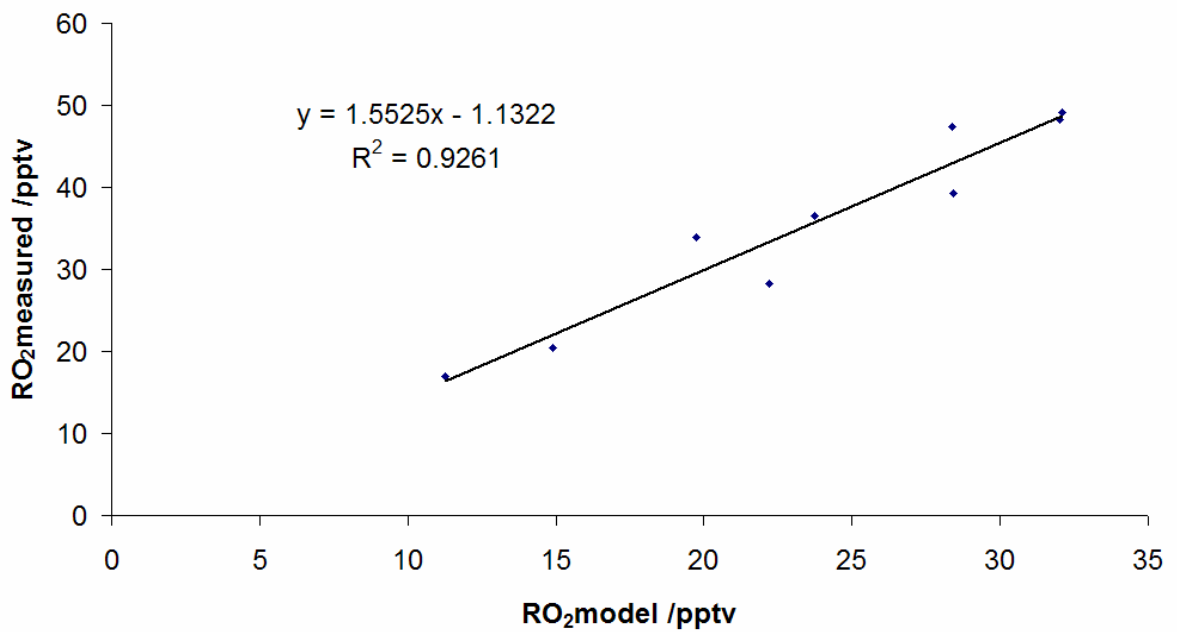


Figure 4.6d Measured vs modelled peroxy radicals for August 12th

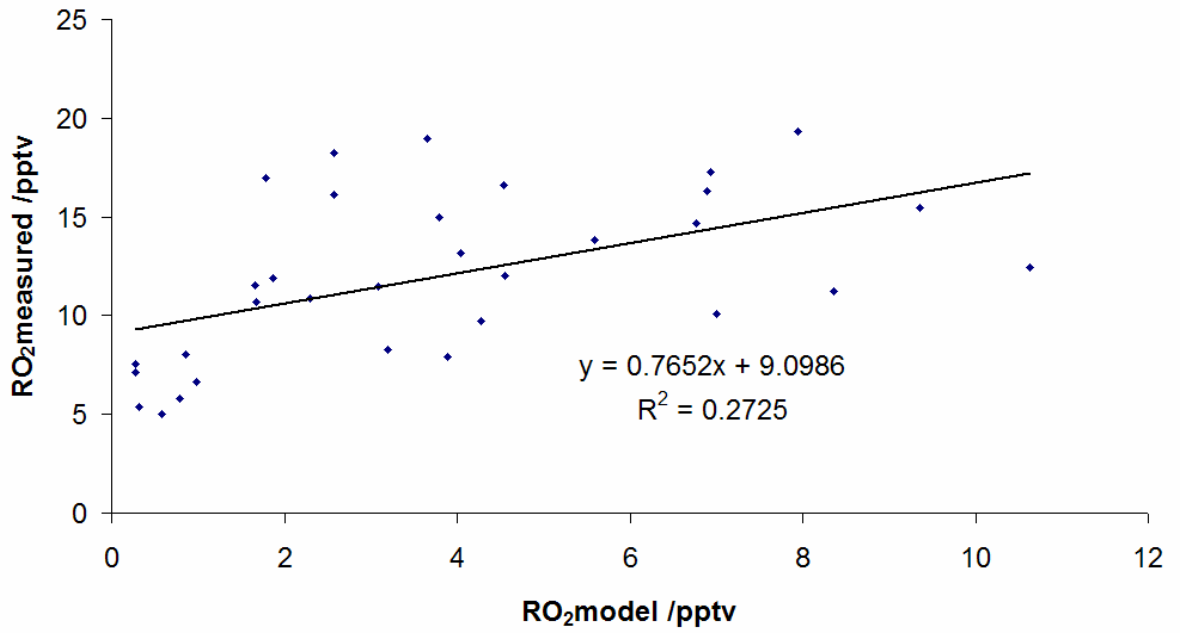


Figure 4.6e Measured vs modelled peroxy radicals for August 24th – 28th

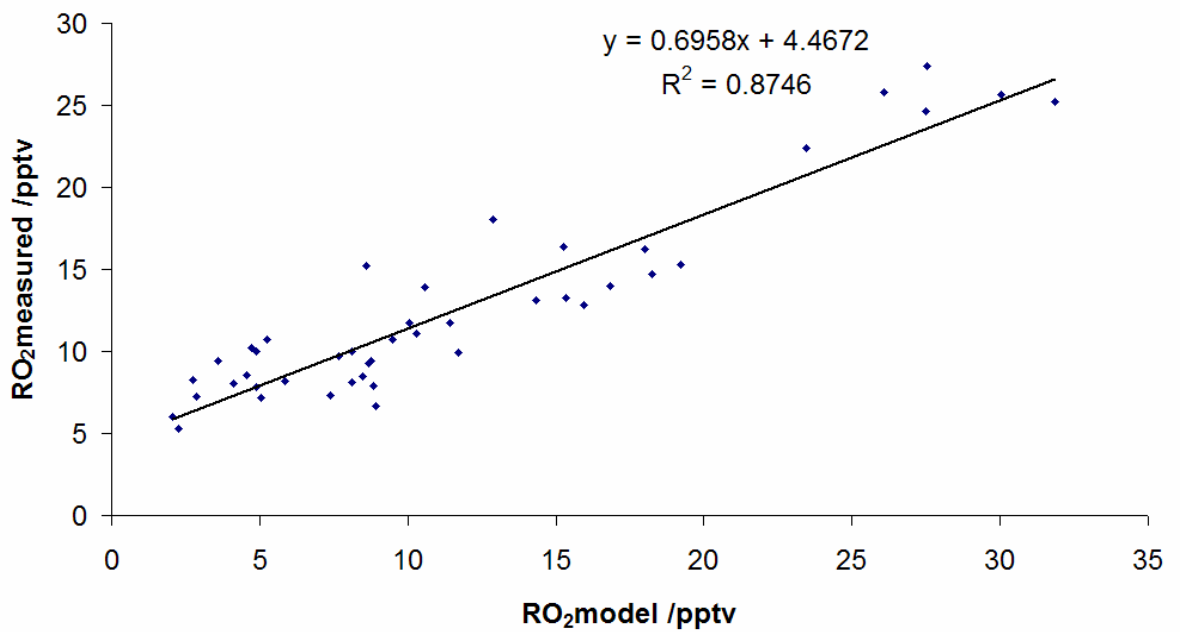


Figure 4.6f Measured vs modelled peroxy radicals for August 19th – 23rd

4.5 Measured vs Modelled HO₂ and OH

HO₂ as well as OH measurements were carried out (see Chapter 4, Table 4.1) by the Heard group from the University of Leeds using a FAGE LIF instrument. OH and HO₂ data is available for three of the periods so it is useful to compare the performance of the model for OH and HO₂ with that for total peroxy radicals.

The period of 19th to 28th August was chosen to assess the measured: modelled ratios of HO₂ and OH as the FAGE instrument was running reliably during this period. The first half of this period (19th – 23rd August) was characterised by low NO mixing ratios (<5ppbv) whereas the second half (24th – 28th) had high NO mixing ratios (>5ppbv).

For the period 19th to 23rd August correlation between measured and modelled HO₂ (R²=0.83) and OH (R²=0.71) is good although the model significantly overestimates absolute values of both HO₂ and OH (Figures 4.7a and b and 4.8a and b).

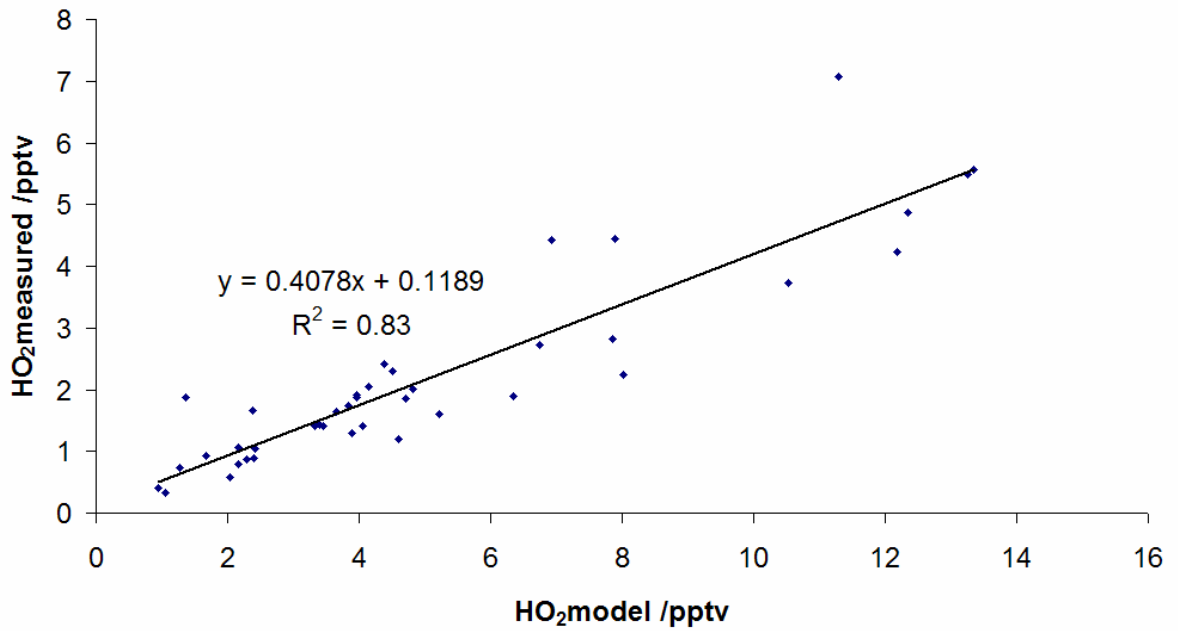


Figure 4.7a Measured vs Modelled HO₂ mixing ratio for 19th to 23rd August (hourly averages)

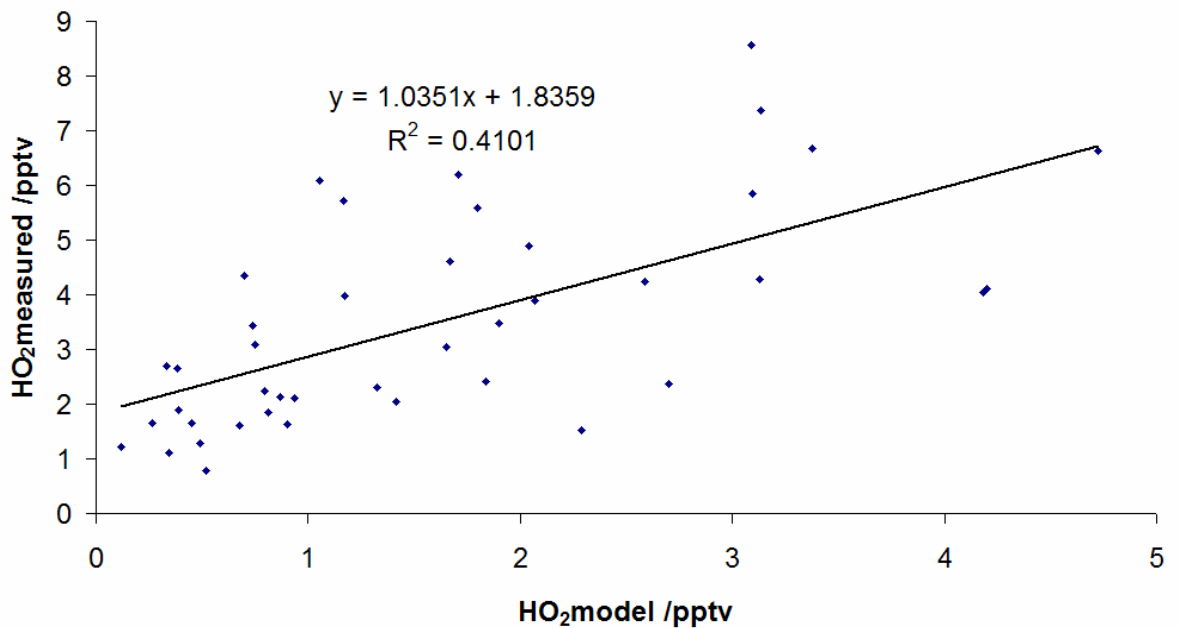


Figure 4.7b Measured vs Modelled HO₂ mixing ratio for 24th to 28th August (hourly averages)

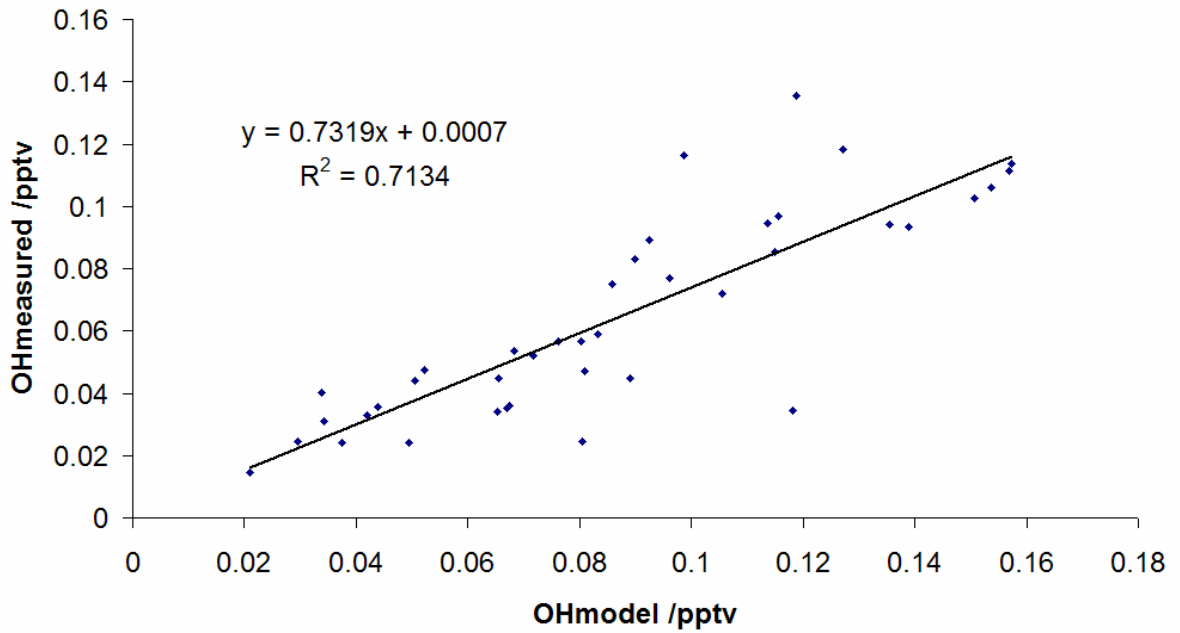


Figure 4.8a Measured vs Modelled OH mixing ratio for 19th to 23rd August (hourly averages)

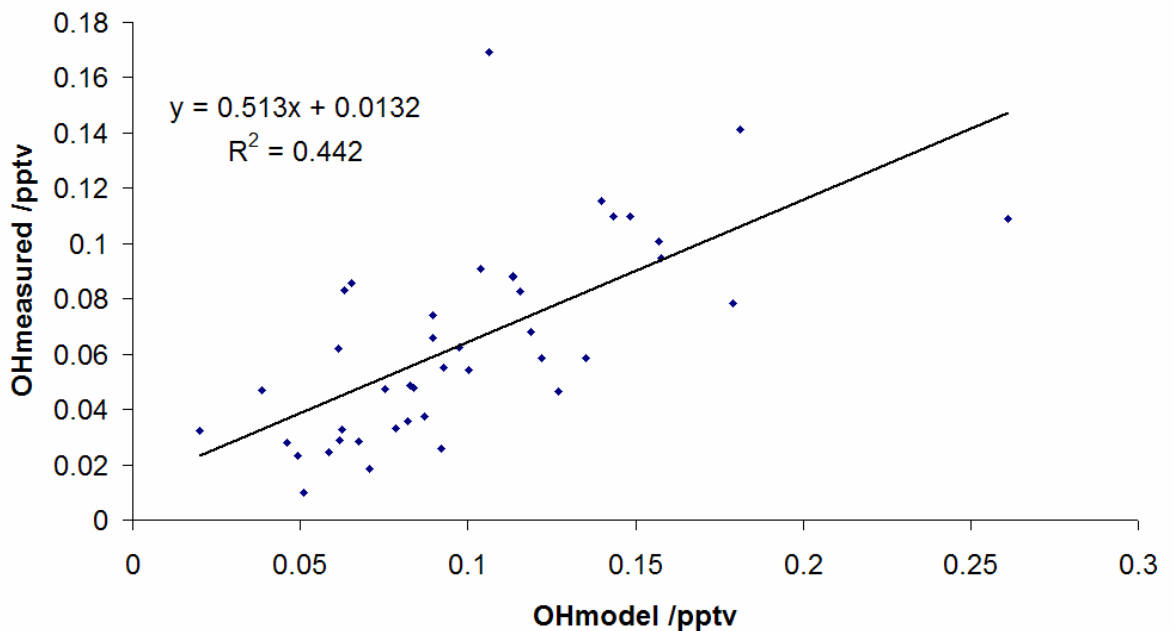


Figure 4.8b Measured vs Modelled OH mixing ratio for 24th to 28th August (hourly averages)

4.6 The Influence of NO on Measured:Modelled Radical Ratios

4.6.1 Whole campaign

For $\text{HO}_2 + ? \text{R}_i\text{O}_2$ (Figure 4.9) measured:modelled ratio is close to 1 at NO mixing ratios at around 1 and less than 1 ppbv. At NO mixing ratios of greater than 1 ppbv measured:modelled ratios increase, i.e. the model becomes worse at simulating peroxy radicals. A similar relationship occurs for HO_2 (Figure 4.10) suggesting that NO is more important in the model for reducing peroxy radical mixing ratios than it is in the measured data.

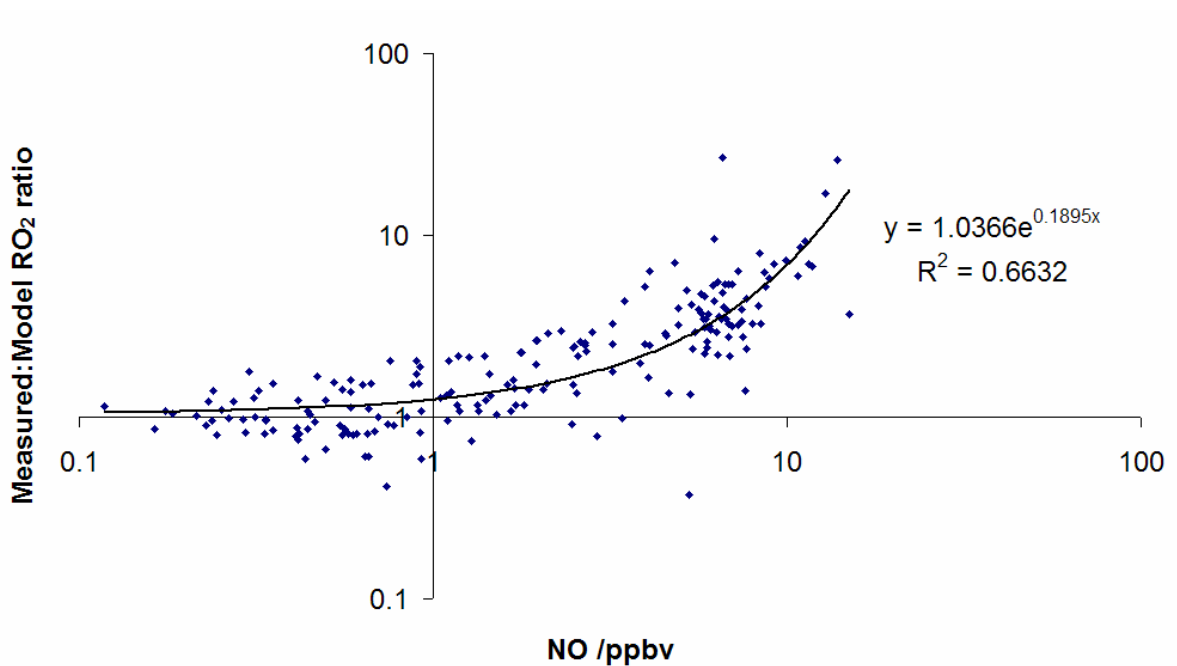


Figure 4.9 Dependence of measured:modelled ratio on NO for the whole campaign (hour-averaged data).

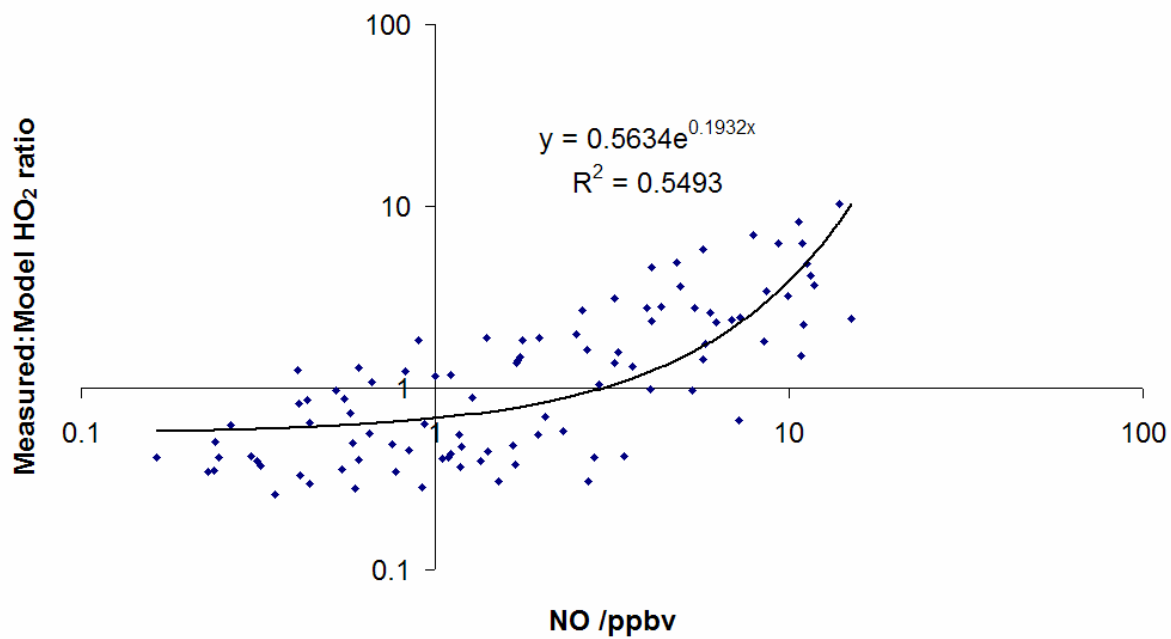


Figure 4.10 Dependence of measured: modelled ratio of HO₂ on NO for 19th to 29th August (hour-averaged data).

4.6.2 19th to 28th August

The period of 19th to 28th August was also chosen to assess the influence of NO on measured to model ratios of HO₂ as measured by FAGE and HO₂ + ? R₁O₂ as measured by PERCA. The reason for this was that data was available for both instruments for the majority of the period. The first half of this period (19th – 23rd August) was characterised by low NO mixing ratios (<5ppbv) whereas the second half (24th – 28th) had high NO mixing ratios (>5ppbv). (Figure 4.11)

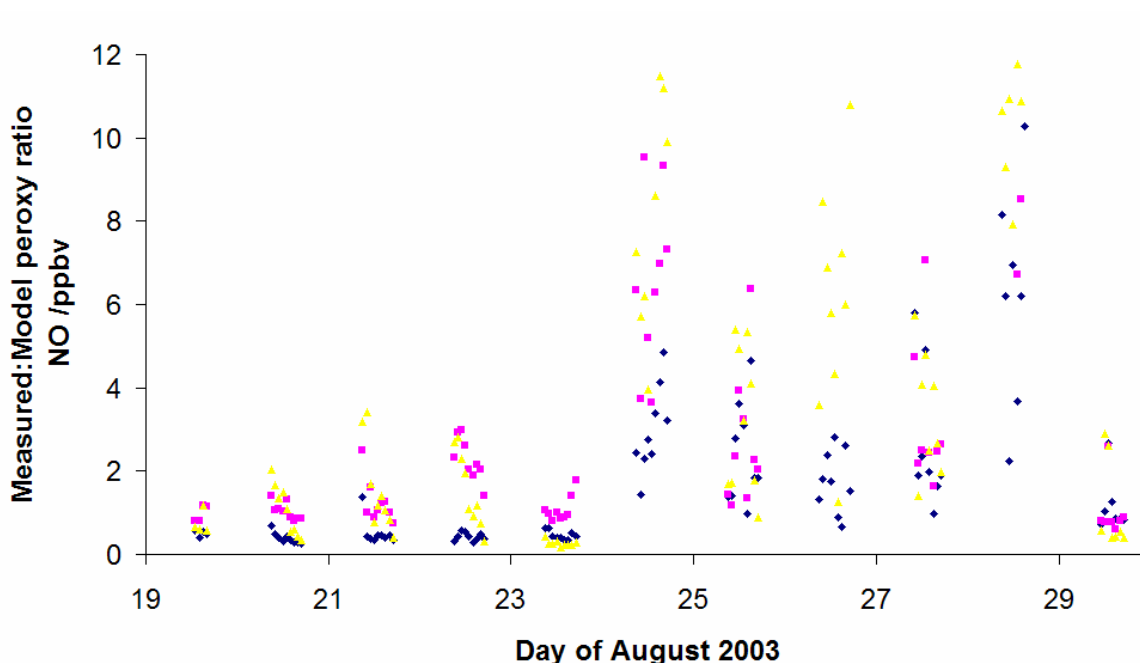


Figure 4.11 Yellow triangles are NO mixing ratio, blue diamonds are measured:modeled HO₂ ratio and pink squares are RO_x measured:modelled ratios.

Measured to modelled ratios for HO₂ + ? R₁O₂ (Figure 4.12) are around 1 for NO up to 1 ppbv (similar to hourly data for the whole campaign, see Figure 4.9). Above 1 ppbv the ratio increases to 10 for 10 ppbv NO. For HO₂ (and also for ? R₁O₂,) the relationship is similar, up to 2ppbv NO, measured:modelled ratios are around 0.5.

A different relationship is observed for OH – decreasing measured:modelled ratio as NO mixing ratio increases.

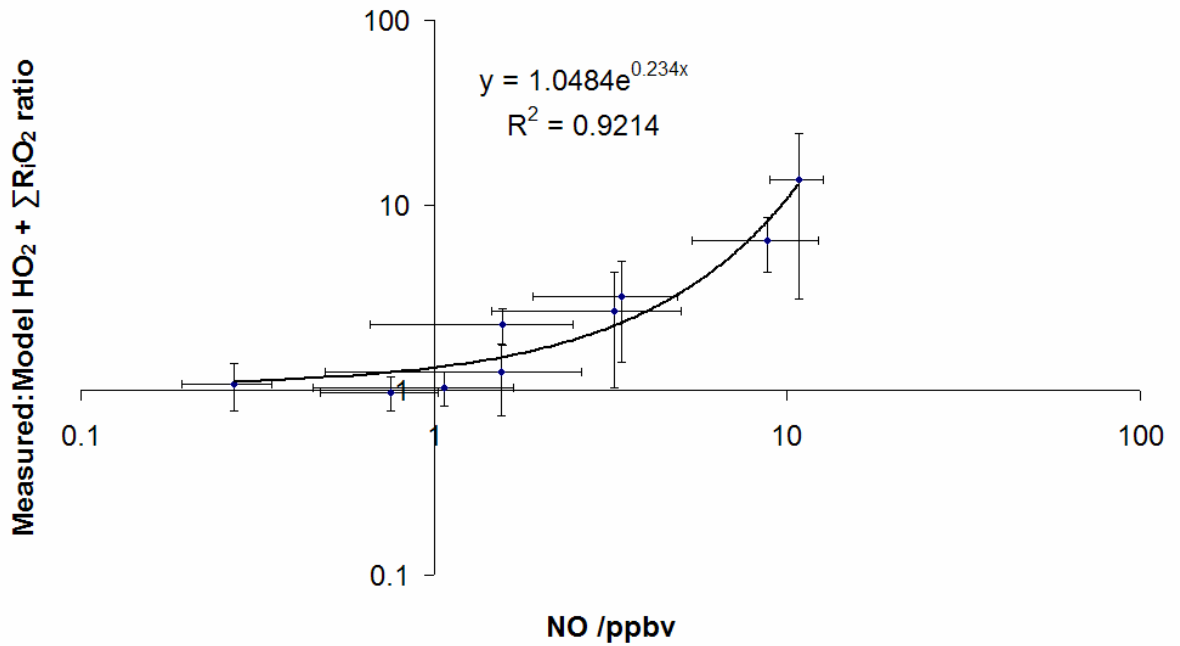


Figure 4.12 Measured: modelled $\text{HO}_2 + \sum \text{R}_i\text{O}_2$ ratio vs NO, daily averages for 19th to 28th August (not including 26th August)

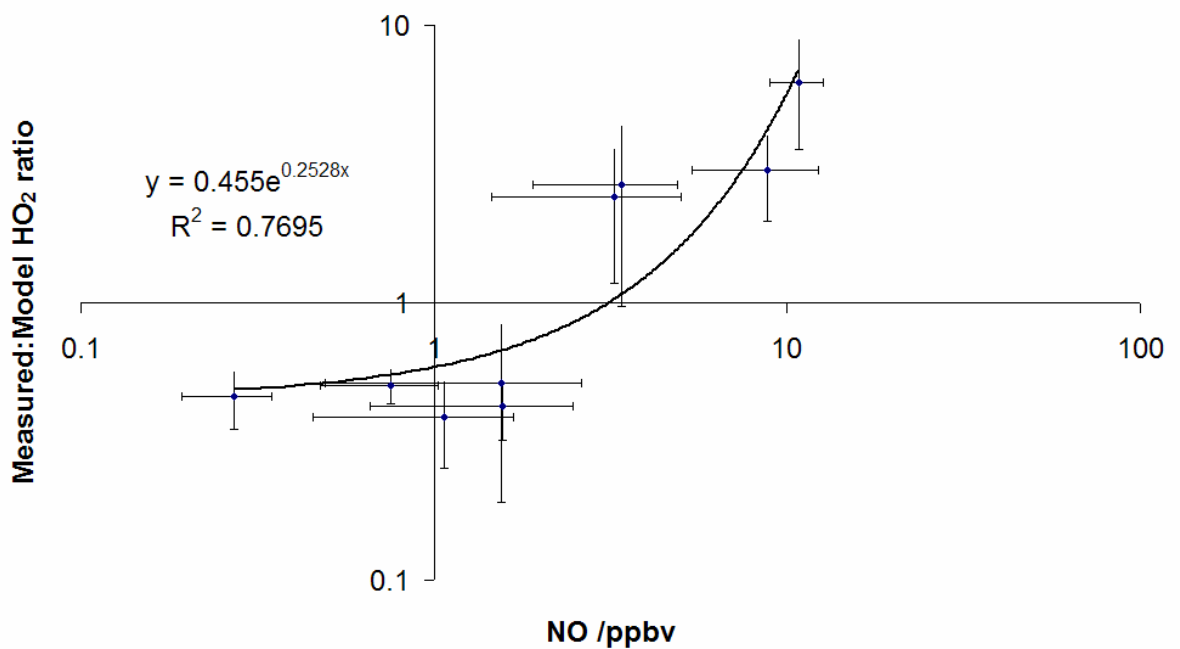


Figure 4.13 Measured: modelled HO_2 ratio vs NO, daily averages for 19th to 28th August (not including 26th August)

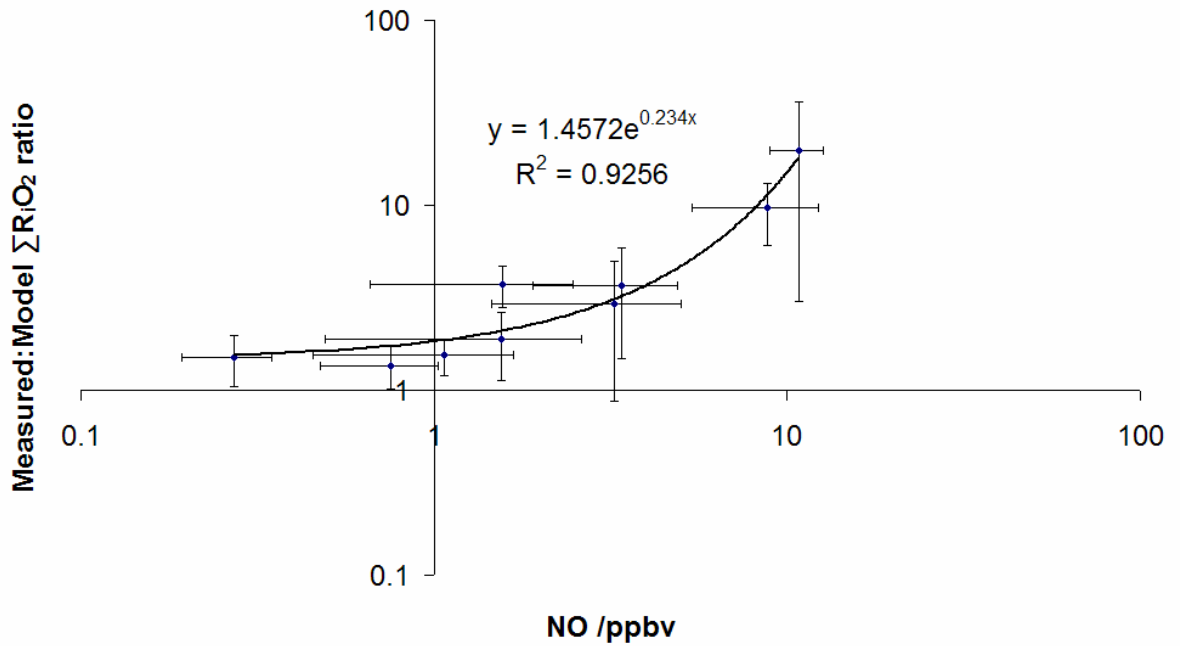


Figure 4.14 Measured: modelled $\Sigma R_i O_2$ ratio vs NO, daily averages for 19th to 28th August (not including 26th August)

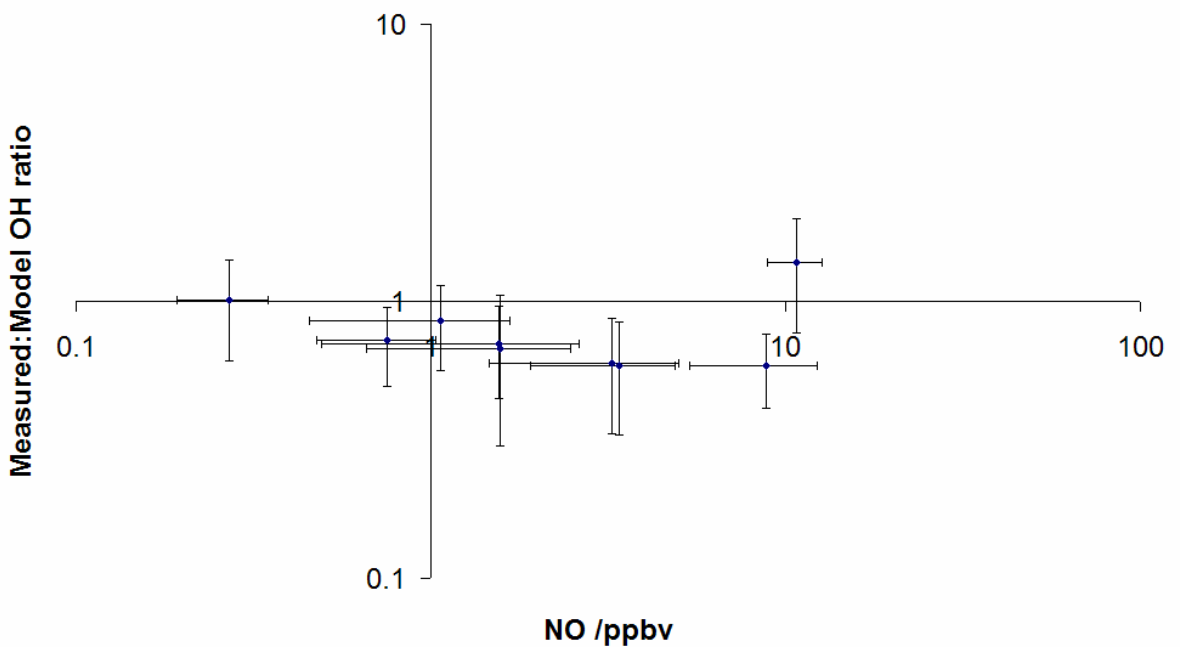


Figure 4.15 Measured: modelled OH ratio vs NO, daily averages for 19th to 28th August (not including 26th August)

4.7 Chapter 4 Summary

5 Ozone photochemistry during the U.K. heat wave of August 2003

5.1 Introduction – high temperatures and high ozone concentrations

During a 10-day period, a blocking anticyclone persisted over Western Europe, with air temperatures of up to 40°C [Black, 2004]. The UK also experienced this heat wave with temperatures reaching 38.5°C at Faversham, Kent, approximately 60 km to the south west of the measurement site, the highest since records began in 1875.

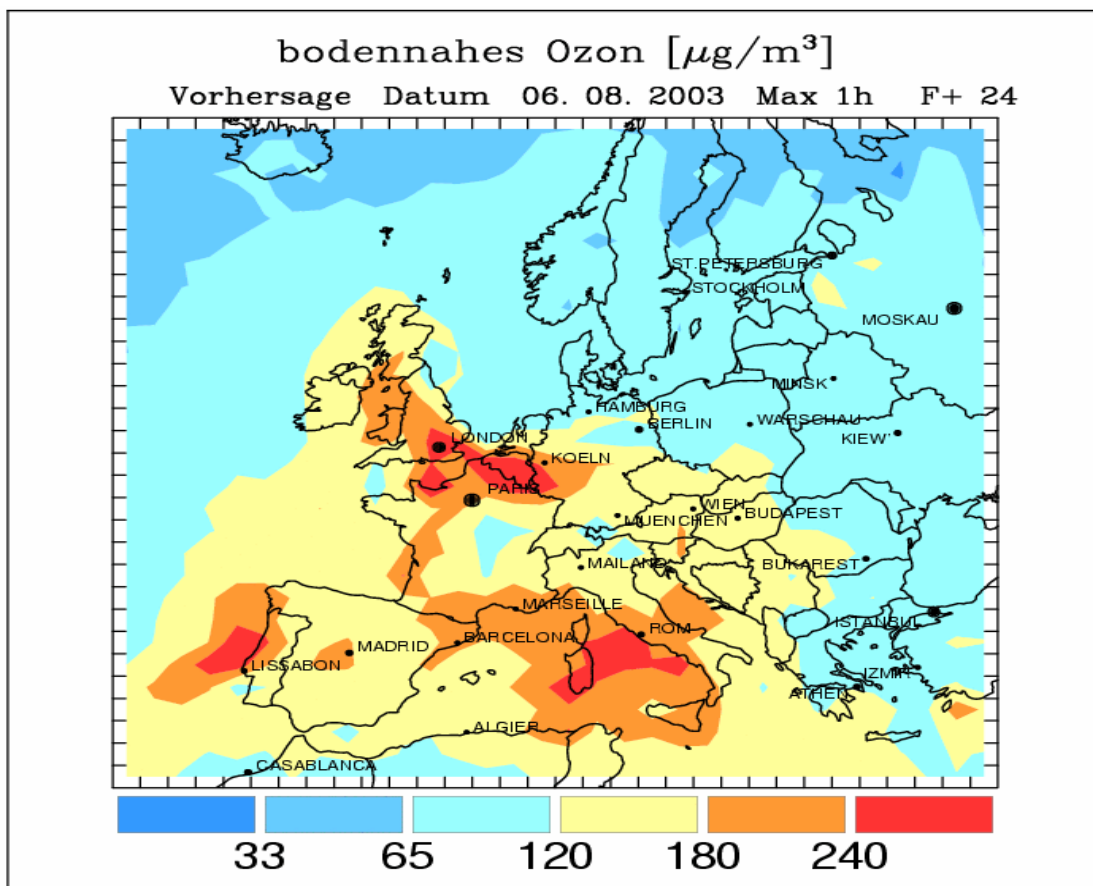


Figure 5.1 Ozone forecast showing the extent of the enhanced ground level ozone concentrations across Western and southern Europe for 6th August. Units are $\mu\text{g}/\text{m}^3$ which

correspond to 0.51 ppbv at 298 K and 1 atmosphere pressure – from the EURAD European Acid Deposition) model, available online at http://www.uni-koeln.de/math-nat-fak/geom/eurad/index_e.html.

Hourly average ozone mixing ratios of approximately 120 ppbv were recorded at Brent and North Kensington both in London at 15:00 on August 6th. This is reflected in the forecast in figure 4.1 with London being in a patch of red denoting concentrations above $240 \mu\text{g m}^{-3}$ (120 ppbv) This was not only an urban phenomenon, however, with 115 ppbv measured at Wicken Fen, at a rural location in Cambridgeshire, England. On 6th August, fifteen of the sixty sites of the UK air quality network exceeded hourly ozone mixing ratios of 90 ppbv, the information threshold. According to EU council directive 92/72/EEC on air pollution by ozone, EU Member States have to inform the public when hourly average ozone concentrations exceed the information threshold of 90 ppbv. The warning threshold of 180 ppbv, set by the same directive, was not exceeded in 2003 at any UK measurement stations. A number of locations did exceed this warning level, the highest value in Europe for ozone reaching 210ppbv at Sausset les Pins, France, on 3rd August 2003.

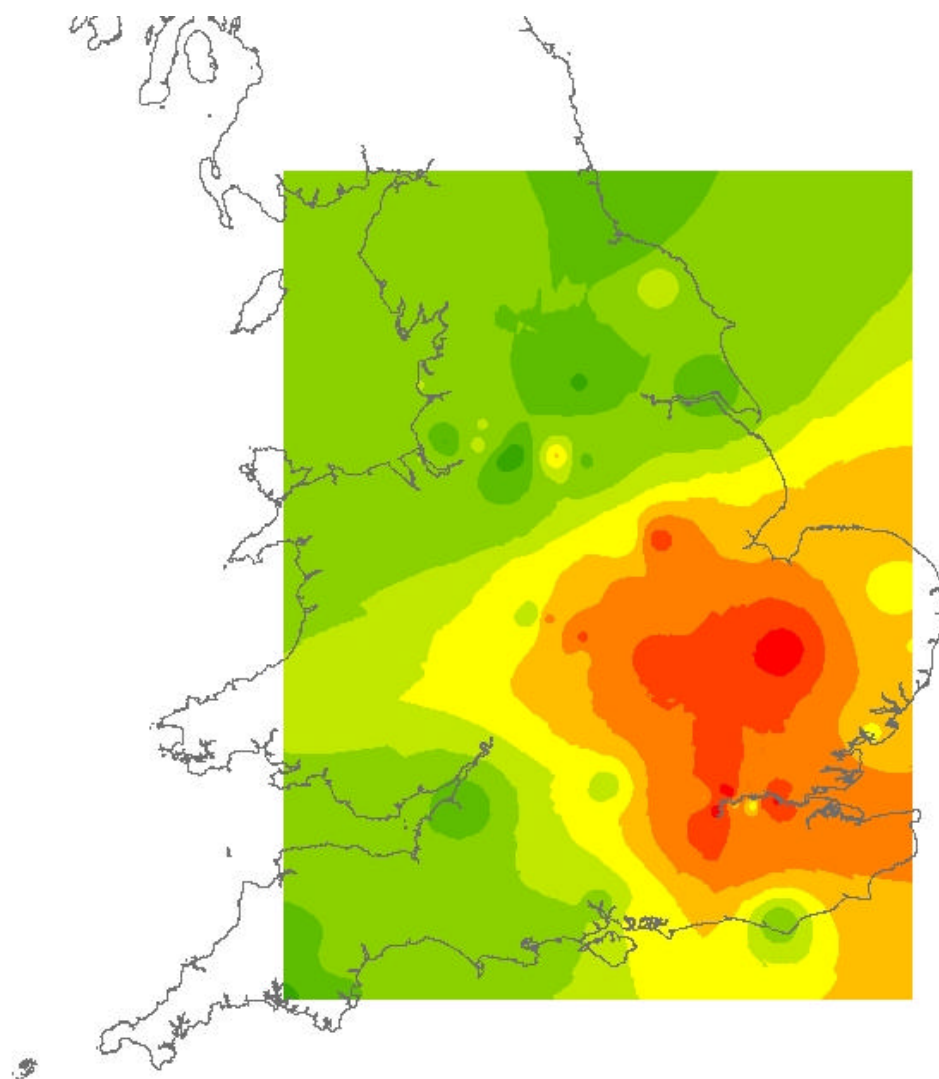


Figure 5.2 Ozone contour plot generated using ARC GIS software. Data from fifty-eight monitoring stations in England (<http://www.airquality.co.uk/archive/index.php>) were combined to give a rough idea of the spatial extent of the high ozone mixing ratios. This figure shows 14:00 on August 6th, 2003.

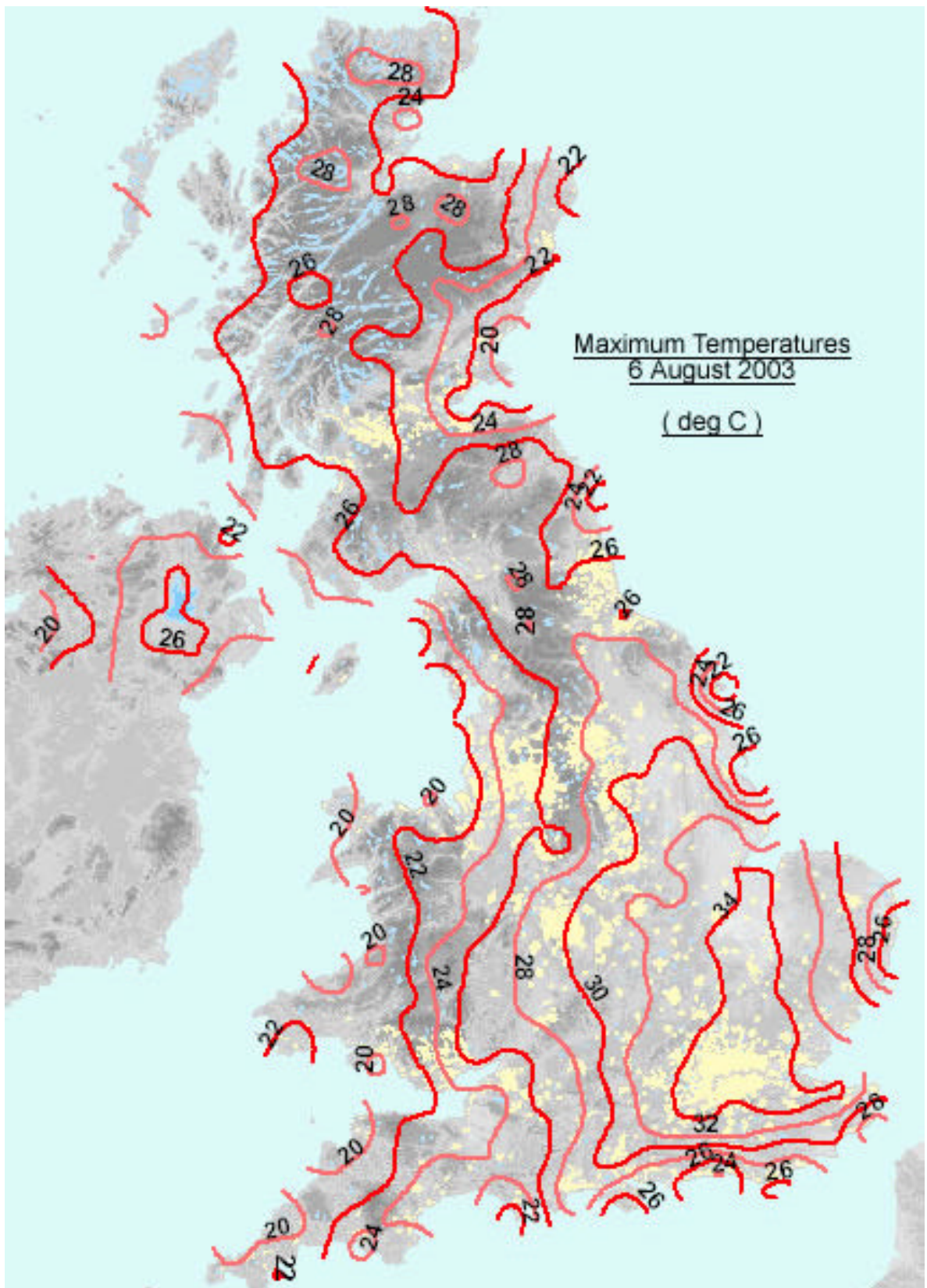


Figure 5.3 Maximum temperatures for 6th August 2003 in the UK from: <http://www.met-office.gov.uk/climate/uk/interesting/aug03maxtemps.html>

Similarly to the ozone mixing ratios, maximum temperatures occurred in London and the South East of England.

5.2 Health Consequences of Air Quality in 2003 Heat wave

The human consequences of this were excess deaths owing to both heat and reduced air quality. The UK office for national statistics reported an excess of 2045 deaths in England and Wales for the period 4th – 13th August 2003, above the average for the period 1998 – 2002. [Stedman, 2004] analysed data from Sites around the UK monitoring ozone and particulate matter, PM10 and concluded that between 225 and 593 deaths were due to ozone and 207 due to PM10. The range in number of deaths caused by enhanced ozone levels appears because it is unclear whether or not there is a threshold for the health effects of ozone (for particulate matter it is clear that there is not [COMEAP, 1998]. The lower number is for analysis including a threshold of 0 $\mu\text{g m}^{-3}$ and the higher number for a threshold of 100 $\mu\text{g m}^{-3}$. Together they account for 21 – 38% of all deaths brought forward for the heat wave period. It is therefore of utmost importance to policy as well as simple scientific curiosity to investigate the causes of such ozone episodes.

5.3 Summer 2003 in context – Past and future heat waves in the UK

High ozone concentrations during heat waves have been experienced in the UK before [PORG, 1997]. The summers of 1976 and 1995 were particularly hot and dry with ozone mixing ratios reaching 254 ppbv at Harwell, Oxfordshire in July 1976. The highest mixing ratio of the heat wave of 1995 was 130 ppbv, recorded at Yarnier Wood in early August. Both years experienced anticyclonic conditions although 1976 air masses had passed over polluted

regions of mainland Europe and wind speeds were low, whilst in 1995 brisk wind speeds brought air masses from Northern Europe. In 2003, a blocking high prevailed over much of Central and Western Europe for a number of days at the beginning of August. This resulted in stagnant conditions with relatively low wind speeds (typically $< 5\text{ms}^{-1}$) and potential for a build up of ozone and other photochemical pollutants. Ozone mixing ratios did not reach 1976 levels (120 ppbv compared to over 250 in 1976) but the question arises why did the UK experience mixing ratios above 100 ppbv when when emissions of ozone precursors, ie NO_x and VOC, have been falling leading to a decline in peak concentrations of ozone [Derwent, *et al.*, 2003].

Climate models suggest that the occurrence of extreme high temperature periods are likely to significantly increase over the period to 2080 [Schar, *et al.*, 2004],[Stott, *et al.*, 2004]. The current probability in the U.K. of exceeding 35°C is 0.6 %, however by 2080 it is estimated to become 6 %, (e.g. temperatures in excess of 35°C currently occur roughly one day every two years whereas in 2080 we may expect 5 days yr⁻¹, or once every 2.5 weeks during summer. This underlines the importance of studying the photochemistry of events in the UK with temperatures above 35°C as they are likely to occur more often in the future.

5.4 Chemical Climatology

The bottom panel of figure 5.4 shows the data series obtained for the reactive peroxy radical intermediates $\text{HO}_2 + \Sigma\text{RO}_2$.

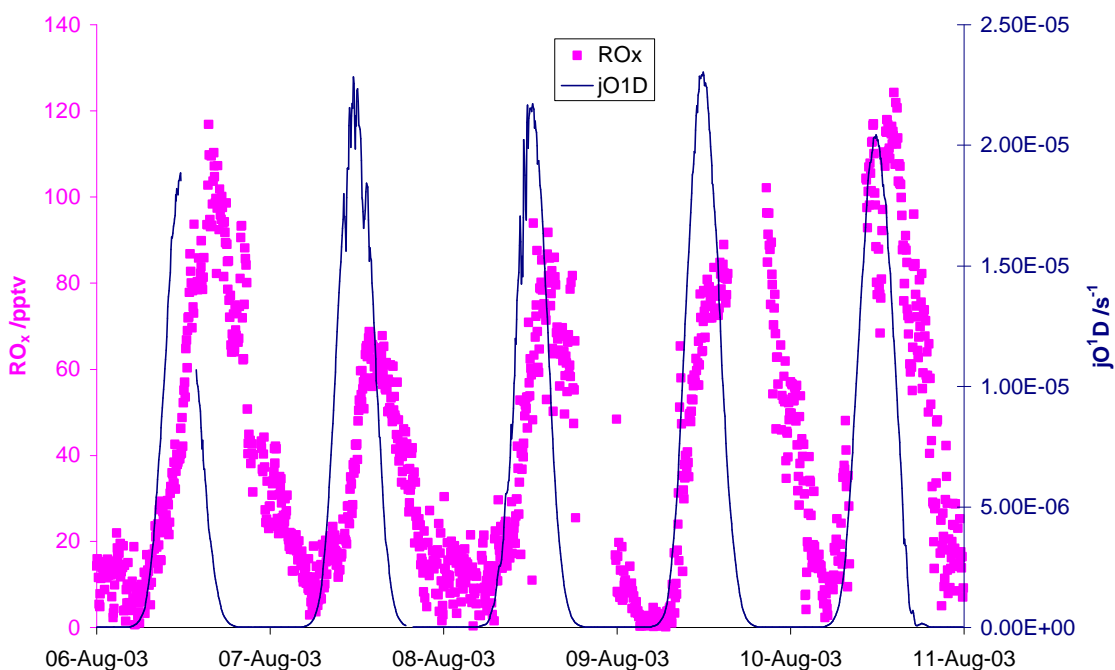


Figure 5.4 Peroxy radical mixing ratios and $j\text{O}^1\text{D}$

From Figure 5.4 we can see the difference in photolysis strength is not reflected in peak concentration of ROx . Indeed outside the heat wave photolysis rates were not much different and radical mixing ratios were much lower.

Overlaid on this plot is a measure of photolysis frequency for generation of O^1D from ozone— $j(\text{O}^1\text{D})$. During the heat wave period mixing ratios of peroxy radicals reached 60 pptV during mid-afternoon. The peroxy radicals had an average mixing ratio of 45 pptV at 15:00 GMT over the 5 days of the heat wave over twice that of the average for the rest of the campaign,

which peaked at 13:00 GMT. These levels are lower than values recorded during the ESCOMPTE campaign of summer 2001 in Southern France where mixing ratios of up to 200 pptV were observed [Coll, *et al.*, 2005]. During the heat wave period, peroxy radicals were strongly correlated to ozone, PAN and peroxides, i.e. secondary products of photochemical oxidation. The average peroxy radical diurnal profile over the whole TORCH campaign is similar in shape and magnitude to that from the suburban Berlioz campaign that took place outside Berlin in 1998 [Mihelcic, *et al.*, 2003] As with BERLIOZ, the peroxy radical mixing ratios increase with $j(\text{O}^1\text{D})$ to a maximum shortly after solar noon. They also show a nighttime phase with radical mixing ratios rising from a minimum at approximately 18:00 GMT when the main source of peroxy radicals switches from photochemical to so called 'dark reactions' i.e., oxidation of VOCs *via* oxidation by NO_3 and ozone (see for example [Salisbury, *et al.*, 2001]).

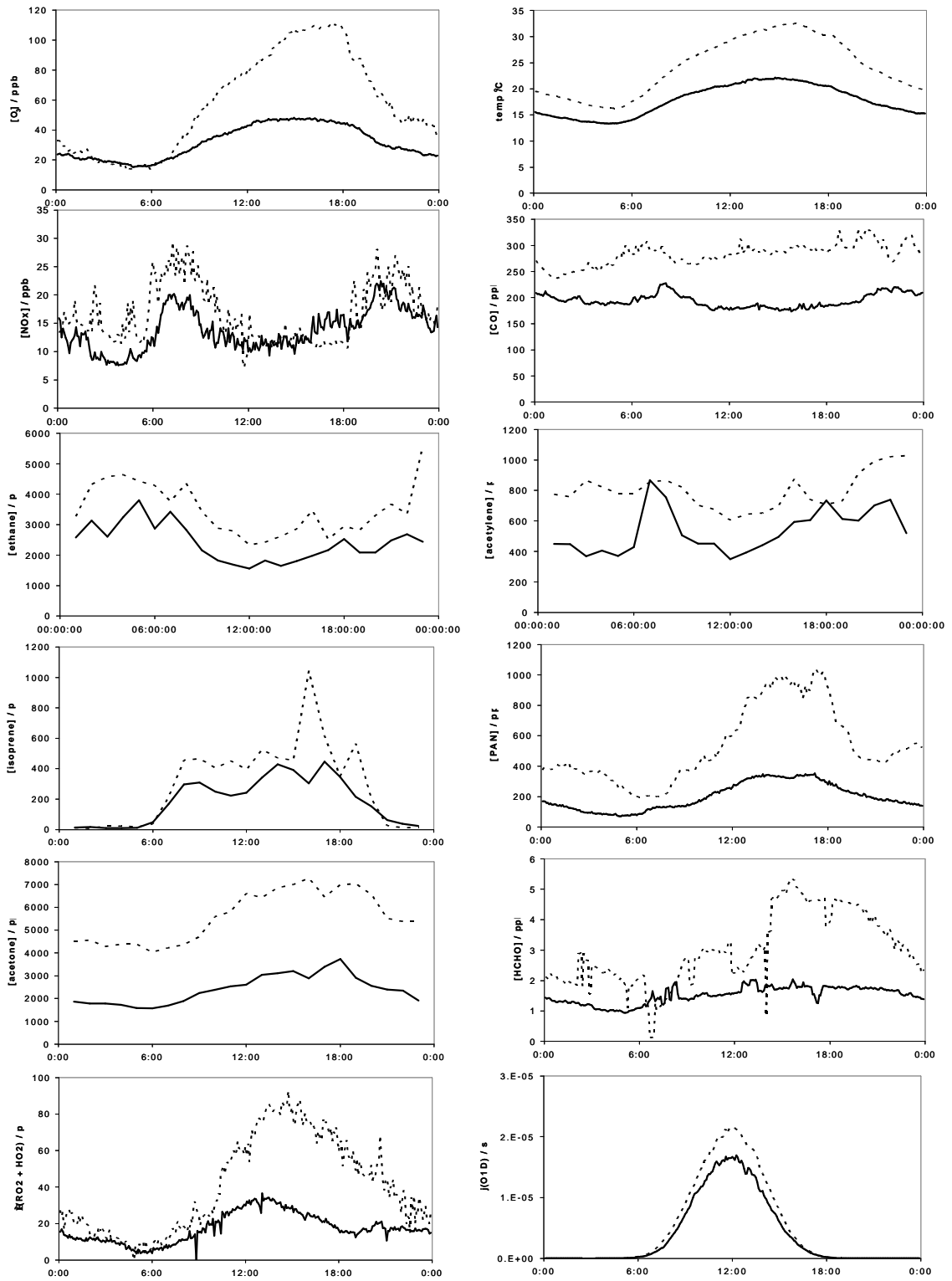


Figure 5.4 The five days of the heat wave starting on the 6th August and finishing on the 10th August are considered.

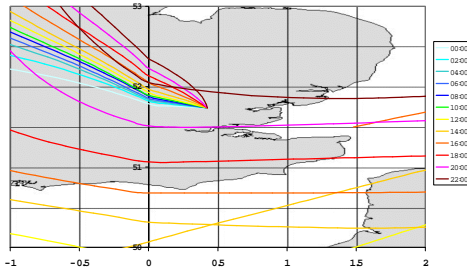


Figure 5.6 a(i) 6th August 2003

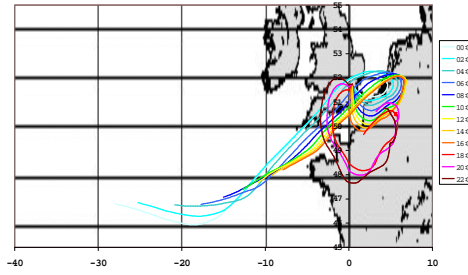


Figure 5.6 a(ii) 6th August 2003

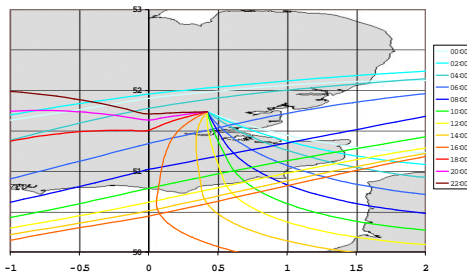


Figure 5.6 b(i) 7th August 2003

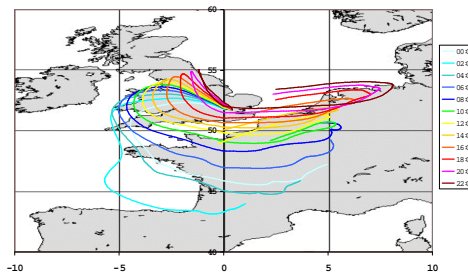


Figure 5.6 b(ii) 7th August 2003

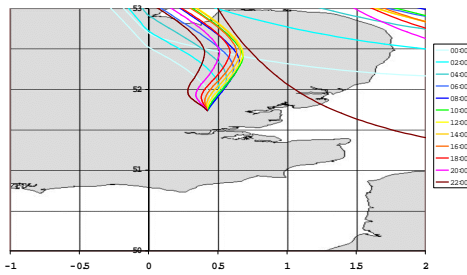


Figure 5.6 c(i) 8th August 2003

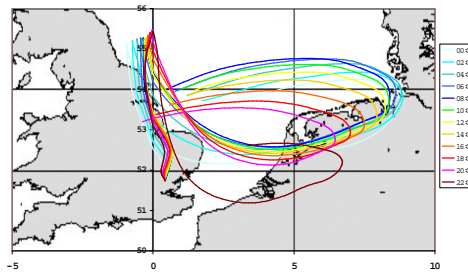


Figure 5.6 c(ii) 8th August 2003

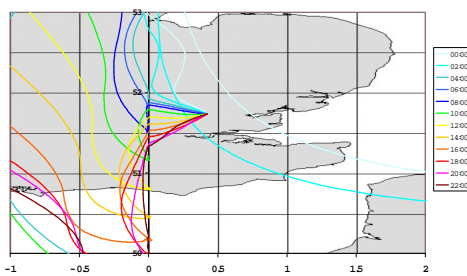


Figure 5.6 d(i) 9th August 2003

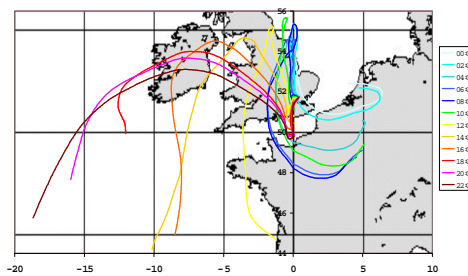


Figure 5.6 d(ii) 9th August 2003

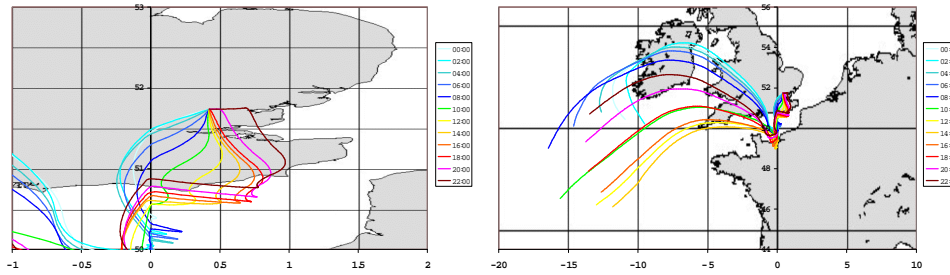


Figure 5.6 e(i) 10th August 2003

Figure 5.6 e(ii) 10th August 2003

The trajectories in figure 5.6 (a) – (e) show the path of an air mass five days up to arrival at the site. (i) shows the South East corner of England while (ii) zooms out to look at the whole trajectory. The trajectories were run to finish 500m above the site in Writtle. They are done in two hourly intervals from ECMWF analyses carried out by James Lee.

The trajectories provide evidence that air arriving at the site in Writtle had spent the previous five days over polluted regions of Europe.

5.5 Morning Ozone Entrainment

5.5.1 Boundary Layer Height Measurements

As noted in chapter 1, the lowest layer of the troposphere is known as the planetary boundary layer. Over time periods of about one day the physical influence of the Earth's surface is restricted to this layer [Oke, 1987]. However, it is not a simple homogeneous structure but consists of several layers that can change in height, temperature and composition throughout the day and night [Oke, 1987]. By day, the Earth's surface is heated by the sun and vigorous thermal mixing enables the boundary layer to extend to about 1 – 2 km. In the evening the process is reversed and the planetary boundary layer shrinks to as low as 100m creating a nocturnal boundary layer decoupled from a weak mixed layer. Pollutants in the nocturnal boundary layer are thus susceptible to dry deposition. This is the case for ozone the concentration of which can decrease at night time as it is a secondary pollutant with no known nocturnal sources. On all five days of the heat wave ozone concentrations increased from about 6am and reached a maximum late in the afternoon. Mixing ratios then dropped rapidly at about 6pm just at the time of the evening boundary layer collapse. Approximate boundary layer heights for the 6th – 10th of August (Figure 5.7) show a typical pattern for clear skies over a simple flat surface. Unfortunately it is not possible to differentiate morning entrainment of ozone from the weak mixed layer from in situ ozone production from oxidation of NO and subsequent photolysis of NO₂ as no measurements of ozone were carried out in the weak mixed layer.

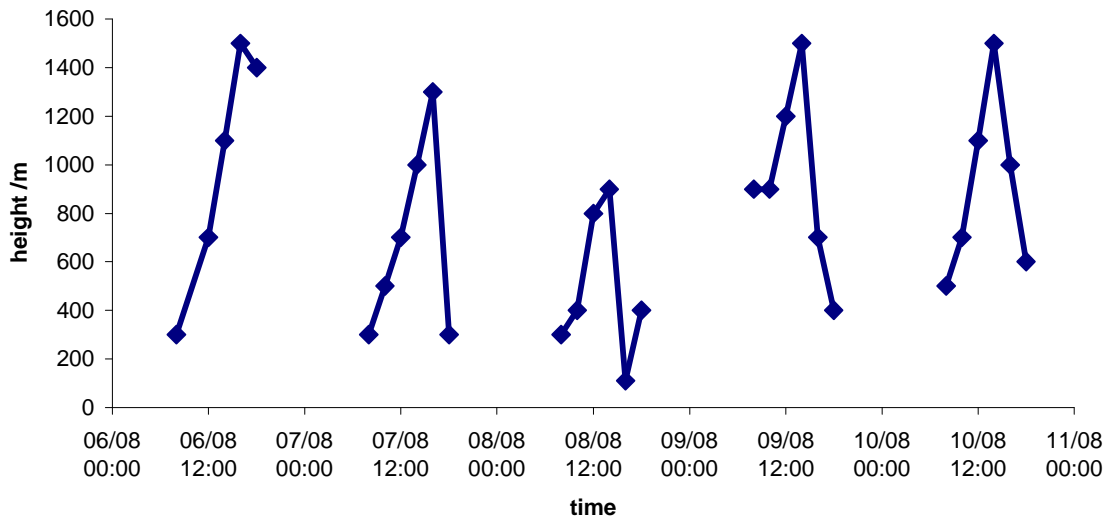


Figure 5.7 Approximate boundary layer heights for the heat wave period. Data courtesy of Emily Norton, University of Aberystwyth.

5.5.2 Precursor tracer Ratios

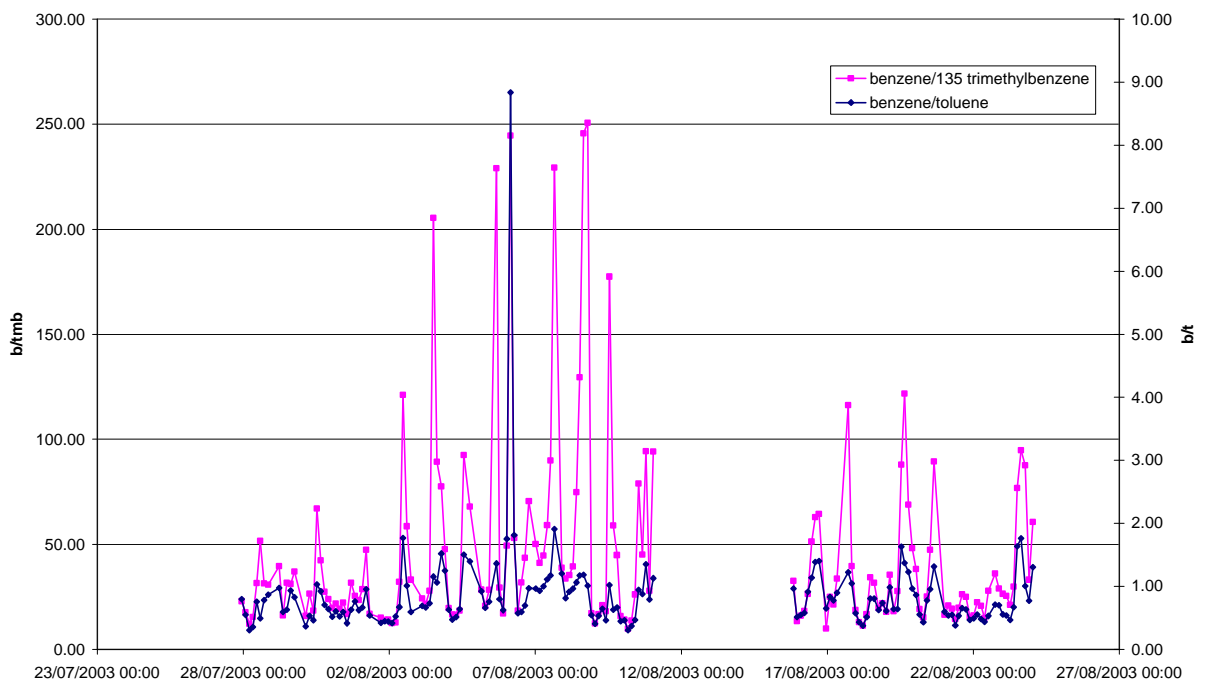


Figure 5.8 Tracer ratios

Tracer ratios of aromatics have been used in Lee et al (manuscript in preparation). More substituted benzene rings are more reactive with respect to OH and are thus the ratio of two different species (assuming known emission ratios which are well known and generally from exhaust fumes) will increase (or decrease) as an airmass moves away from sources of pollution. Benzene:toluene (b:t) ratios were not significantly different in the heat wave than in the period of Westerlies immediately preceding it. Choosing a more reactive tracer, ie 1,3,5 trimethylbenzene (tmb) gives a different picture. The ratio b:tmb shows a diurnal cycle during the heat wave suggesting morning entrainment of tmb depleted, ie more processed air from the residual layer as the daytime boundary layer evolves. [Lee, et al., 2006] put forward two explanations for this ratio:

1. TMB was emitted and depleted in a two hour period.
2. TMB depleted air was mixed down from the residual layer as the nocturnal inversion is dispersed and the daytime boundary layer evolves.

The first hypothesis was rejected as it would mean OH concentrations of the order of 1×10^8 molecules cm^{-3} , well above concentrations reasonable for the site. The second is in agreement with mixing ratios of other anthropogenic tracers.

5.6 Peroxy radicals

Peroxy radicals are key intermediates and chain carriers in the gas phase oxidation of volatile organic compounds, and owing to their short lifetime can give an indication of *in situ* photochemical ozone production [Monks, 2005]. In this section, the chemistry of the peroxy radicals will be explored as an indicator of the local photochemical environment.

In order to delineate the different contributions to the peroxy radical chemistry, a steady state analysis of RO_x production/loss, in which intraconversions among RO_x radicals are not considered, was carried out [Mihele and Hastie, 2003], [Penkett, et al., 1997]. In steady-state, the change in peroxy radical concentration can be represented as,

$$\frac{d[RO_x]}{dt} = P_{RO_x} - L_{SR} - L_{NO_2} = 0 \quad \text{Equation 5.1}$$

the term RO_x includes organic peroxy radicals as well as HO_x, P_{RO_x} is the total RO_x production, L_{SR} the losses owing to self reactions and L_{NO_2} the losses owing to reactions with NO_x. The peroxy-radical production term can be written as

$$P_{RO_x} = 2fj(O^1D)[O_3](1+\gamma) \quad \text{Equation 5.2}$$

essentially comprising RO_x production from O₃ photolysis (primary production) and a term γ representing production of RO_x from other sources related as a function of primary production, where f is the fraction of O¹D atoms that react with water to form OH (equation 4.3)

$$f = \frac{k_{H_{20+O^1D}}[H_2O]}{k_{H_{20+O^1D}}[H_2O] + k_{M+O^1D}[M]} \quad \text{Equation 5.3}$$

The losses owing to self reactions can be simplified assuming that the reaction coefficient for the HO₂ self reaction is to that of the reaction of HO₂ and organic peroxy radicals (Equation 5.4).

$$L_{SR} = 2k_{HO_2+HO_2}[HO_2][HO_2] + 2k_{HO_2+RO_2}[HO_2][RO_2] \approx 2k_{HO_2+RO_2}[HO_2]([RO_x]) \quad \text{Equation 5.4}$$

Using $\mathbf{a} = \frac{HO_2}{RO_2}$ from [Penkett, et al., 1997] gives

$$L_{SR} = 2k_{HO_2+HO_2}\mathbf{a}[RO_x]^2 \quad \text{Equation 5.5}$$

Introducing $\mathbf{b} = \frac{L_{NO_2}}{L_{SR}}$ which is an indicator of the dominant radical loss mechanism one

arrives at:

$$\frac{d[RO_x]}{dt} = 2f \cdot j(O^1D)[O_3](1+\mathbf{g}) - 2k\mathbf{a}[RO_x]^2 - \mathbf{b}2k_{HO_2+HO_2}\mathbf{a}[RO_x]^2 = 0$$

$$[RO_x] = \sqrt{\frac{f \cdot j(O^1D)[O_3]}{k_{HO_2+HO_2}}} \sqrt{\frac{1}{\mathbf{a}}} \sqrt{\frac{1}{(1+\mathbf{b})}} \sqrt{(1+\mathbf{g})}$$

Equations 5.6 and 5.7

The equation can also be rearranged to find ?

$$g = \frac{(1 + b)k_{HO_2+HO_2}a[RO_x]^2}{f \cdot j(O^1D)[O_3]} - 1 \quad \text{Equation 5.8}$$

For the PROPHET site three possible influences on g in the afternoon were suggested:

- (i) formaldehyde photolysis – formaldehyde has a strong diurnal cycle with a maximum concentration in the afternoon
- (ii) ozonolysis of biogenic VOCs – VOCs emitted by plants and trees increase with temperature, which is at a maximum in the afternoon
- (iii) thermolysis of PAN and other peroxyacyl nitrates – augmented by afternoon temperatures

Table 5.1 shows the relative significance of four of these sources for which data are available. Whilst HONO was not measured, its contribution to RO_x production in a semi-rural location such as Writtle is considered more significant in the early morning hours as it builds up overnight and is therefore present in lower concentrations in the afternoon [Alicke, *et al.*, 2003]. Average radical production rates for the heat wave period from ozone photolysis, formaldehyde photolysis, ozonolysis of alkenes and thermolysis of PAN for the afternoon period (12:00 – 18:00) are shown in Table 5.1. Thermolysis of PAN is the largest source of RO_x production at this time (1.85×10^7 radicals $cm^{-3} s^{-1}$) with 67% of radical production attributed to it, with ozone photolysis (5.22×10^6 radicals $cm^{-3} s^{-1}$) accounting for 24%. Formaldehyde photolysis and ozonolysis of alkenes make up 3.4 and 5.3% of RO_x production respectively. The magnitude of RO_x production from PAN is much greater than that of maximum ozone photolysis for the 6th, 9th, and 10th of August, coinciding with the days when ozone mixing ratios were at their highest. PAN as an afternoon source of RO_x is not surprising considering its extremely short lifetime at temperatures experienced during this

heat wave period; the PAN lifetime being as short as 7.5 minutes for temperatures of 36°C (figure 5.9) with average PAN lifetime with respect to decomposition of 18.3 minutes (12:00 – 18:00, 6th – 10th August). The thermolysis of PAN produces a peroxy acetyl radical (PA) and NO₂:



The PA radical can then undergo reformation with NO₂ to reform PAN, or react with NO



with resulting NO to NO₂ oxidation. Therefore, the fractional reformation of PAN can be expressed as:

$$\frac{k_8[\text{CH}_3\text{CO}_3][\text{NO}_2]}{k_8[\text{CH}_3\text{CO}_3][\text{NO}_2] + k_9[\text{CH}_3\text{CO}_3][\text{NO}]} \quad \text{Equation 5.8}$$

k_8 and k_9 are 1.2×10^{-11} and 2.1×10^{-12} molecule cm³ s⁻¹ respectively, hence the reformation of PAN is largely controlled by the ratio of NO₂ / NO. During the heat wave period, daytime NO₂ / NO ranged from 10 - 60, hence the fractional PAN reformation can be calculated to range from 0.85 – 0.95. This analysis shows that although PA radicals are formed from thermolysis of PAN (and will be measured as radicals by the PERCA instrument), a large fraction of them will reform to PAN *via* reaction with NO₂. Depending on prevailing NOx distribution however the steady-state concentration of PA radicals may be higher in episodic conditions over cyclonic, due to the higher temperatures and shifting of the equilibrium from

PAN to PA, in conjunction with higher quantities of the initial feedstock in the form of reactive carbon. PA itself is important as an intermediate and precursor to the formation of other peroxy radicals and as a result, more detailed modeling studies would be required to ascertain whether PAN is a net source or sink of radicals. A further radical source could also come from other PAN species, such as PPN and mPAN, which were not measured in this study. A full analysis of the radical chemistry in polluted environments would need measurements of these species, so future work in similar environments should include their measurement.

When $\gamma = 1$, additional sources of RO_x are equal to those from O_3 photolysis. As can be seen from Tables 5.1 and 5.2, for the heat wave period, γ values were greater than one for the afternoon period indicating that other sources beyond primary production are necessary to account for the measured peroxy radical mixing ratios and are indeed much more significant than ozone photolysis.

As discussed in section 1, the main photochemical sources of HO_x in a polluted environment are photolysis of ozone, HCHO and HONO [Monks, 2005]. Additional sources of RO_x are photolysis of higher aldehydes and thermolysis of PAN and PAN analogues. Table 5.3 shows the relative significance of four of these sources for which data is available. While HONO was not measured, its contribution to RO_x production in a semi-rural location such as Writtle is considered more significant in the early morning hours as it builds up overnight and is therefore present in lower concentrations in the afternoon [Alicke, *et al.*, 2003]. Average radical production rates for the heat wave period from ozone photolysis, formaldehyde photolysis, ozonolysis of alkenes and thermolysis of PAN for the afternoon period (12:00 – 18:00) are shown in Table 4. Thermolysis of PAN is the largest source of RO_x production at this time (1.85×10^7 radicals $\text{cm}^{-3} \text{ s}^{-1}$) with 67% of radical production attributed to it with

ozone photolysis (5.22×10^6 radicals $\text{cm}^{-3} \text{s}^{-1}$) accounting for 24%. Formaldehyde photolysis and ozonolysis of alkenes make up 3.4 and 5.3% of RO_x production respectively. The magnitude of RO_x production from PAN is much greater than that of maximum ozone photolysis for the 6th, 9th, and 10th of August, coinciding with the days when ozone mixing ratios were at their highest.

The dominance of PAN as an afternoon source of RO_x is not surprising considering its extremely short lifetime at temperatures experienced during this heat wave period, the PAN lifetime being as low as 7.5 minutes for temperatures of 36°C. In order to sustain such high mixing ratios of a relatively local source is necessary as the average wind speed was 5.5 ms^{-1} and average PAN lifetime 18.3 minutes (12:00 – 18:00, 6th – 10th August). Therefore, PAN would need to be produced within a small footprint of around 6km around the observing location, rather than being a species transporting in from regional sources. Figure 5.10 shows the correlation between PAN production (calculated assuming PAN is in steady state) and isoprene mixing ratios for the 6th – 9th August although the 10th does not seem to fit this pattern. The average values for PAN production and isoprene for the afternoon period (12:00 – 18:00) display a striking correlation of $R^2 = 0.99$ (not including the 10th) although the relationship is not necessarily causative. A direct chemical link between isoprene and PAN exist through the formation of the CH_3CO_3 radical formed through both methacrolein and methyl vinyl ketone channel in isoprene degradation which can subsequently react with NO_2 .

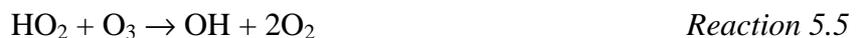
5.7 Rate of Ozone production

Peroxy radical mixing ratios can be used to investigate the *in situ* production rate of ozone, and by extension estimate O₃ formation which may have occurred on that day of observation. The ozone tendency or net photochemical *in situ* production rate of ozone (N(O₃)) is a measure of the ozone productivity of an air mass and neglects transport and deposition processes [Monks, *et al.*, 2000]. N(O₃) is made up of a production term, P(O₃) minus the loss term, L(O₃):

$$N(O_3) = k_p[NO][HO_2 + \sum RO_2] - \{f_j(O^1D) + k_x[OH] + k_x[HO_2]\}[O_3]$$

Equation 5.9

Where k_p is a combined rate coefficient for the oxidation of NO to NO₂ by all peroxy radicals and $f_j(O^1D)[O_3]$ represents the fraction of ozone photolysed to yield O(¹D) atoms and then OH (with f being the proportion of O(¹D) atoms which react with H₂O to give OH rather than being collisionally deactivated). The rate constants k_x and k_x are from the ozone loss reactions:



The average P(O₃) for 07:00 to 16:00 for the heat wave period is 42 ppbv h⁻¹ compared to 21 ppbv h⁻¹ for Westerly conditions of 19th –23rd August. [Kleinman, *et al.*, 2005], sampled plumes from five American cities and found that in an urban plume under conditions where P(O₃) > 25ppb h⁻¹ there is a potential to transform a typical regional background into a severe ozone episode. Average O₃ mixing ratios for the same section of day for the heat wave and Westerly periods are 72 ppbv and 30 ppbv respectively implying that radical chemistry within the boundary layer is more active during the heat wave than during the cooler period.

As well as being characteristically different from the rest of August, the values of $P(O_3)$ during the heat wave exhibit some variability. Values of $P(O_3)$ of over 100 ppbv h^{-1} occur on three of the mornings: 08:00 and 11:00 on the 6th, 08:00 on the 9th and 07:00 on the 10th. On these three days the maximum O_3 mixing ratio exceeded 100 ppbv in the afternoon possibly suggesting that an early morning boost plays a role in determining peak ozone concentrations. The close correlation ($R^2 = 0.93$) of average $P(O_3)$ and peak O_3 value for each day of the heat wave are indicative of a link between *in situ* (day of observation) chemistry and O_3 concentrations and that this is effectively additive to that via regional entrainment.

5.8 Biogenic VOC – the link between high temperature and ozone?

As explained in chapter 1, VOC are a necessary ingredient for photochemical production of ozone. A wide variety of VOC have been detected in the atmosphere (reference and how many); some biogenic, some anthropogenic and others both. Globally VOC emissions are greater than anthropogenic although in the UK the reverse is true (biogenics account for roughly 3% of total VOC averaged from 1970 – 1995 [*PORG*, 1997]). The contribution of biogenic VOC to urban ozone production has been discussed by [*Chameides, et al.*, 1988], [*Roselle, et al.*, 1991] and [*Pierce, et al.*, 1998]. In the UK heat wave of 2003 isoprene, C_5H_8 , Figure 5.11, had the highest reactivity with respect to oxidation by OH of all the measured VOC (number and explanation as to how it was calculated). It is emitted by certain species of trees and vegetation and to a much lesser extent in car exhausts (reference).

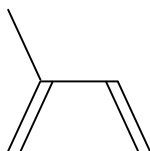


Figure 5.11: isoprene, C_5H_8

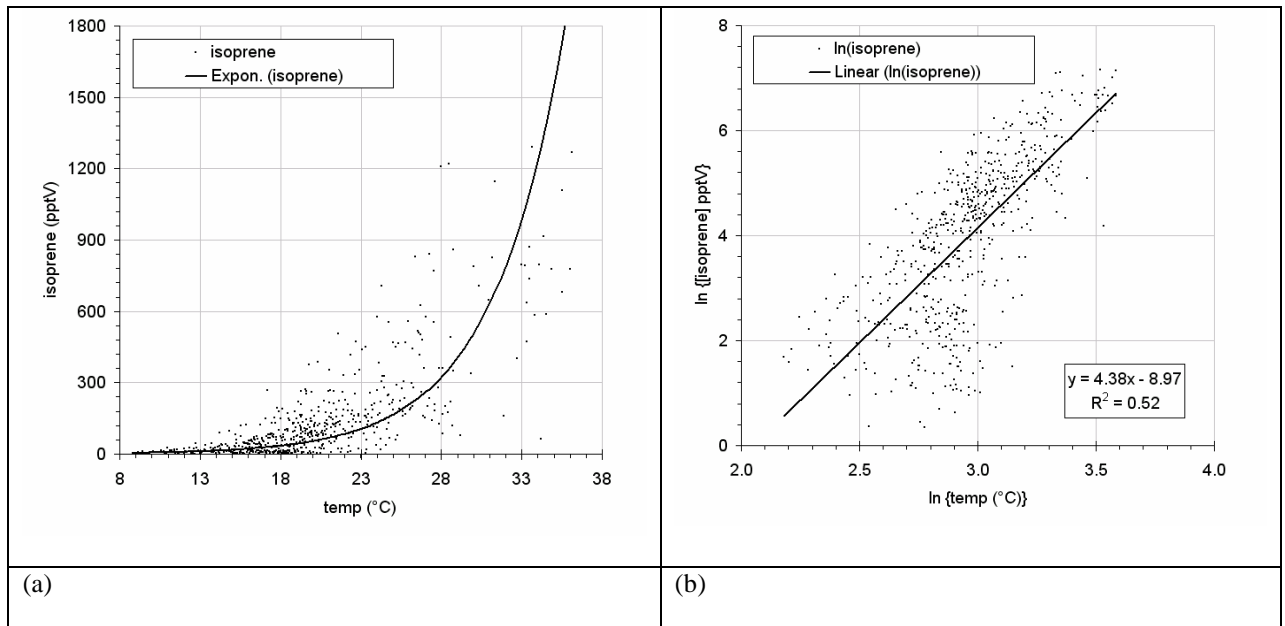


Figure 5.12 Isoprene vs temperature for the whole TORCH 1 campaign. (a) Measured mixing ratios of isoprene increase exponentially with temperature. (b) linear relationship between $\ln(\text{temp})$ and $\ln(\text{isoprene})$ for TORCH 1 campaign.

Biogenic emissions of isoprene are light as well as temperature sensitive, increasing as the plant is stressed. Emissions increase exponentially as temperature increases (see the algorithm in [Guenther, *et al.*, 1995]) and this becomes dramatic as temperatures exceed 35°C . During the UK heat wave temperatures did exceed 35°C and enhanced concentrations of isoprene were measured. Although they are still low compared to the Southern United States they are still high for the UK and indeed local sources of isoprene that could lead to such concentrations are not present in the emissions inventory for the area. Also, with climate change predicted to increase the frequency of high temperature events in the UK (reference) could potentially lead to more high ozone events with consequences for human health as well as economic losses (lower crop yields and material damage).

5.9 Chapter 5 Summary

Measurements of a peroxy radicals and a range of other compounds and meteorological parameters were made in a semi-rural location in the vicinity of London in August 2003. This coincided with a heat wave across much of Europe including the UK with temperatures exceeding 38°C in the South of England. Average afternoon peroxy radical mixing ratios during the period of high temperatures were 80 pptv, a factor of two greater than outside it. The highest value recorded was 120 pptv on the afternoon of August 6th. Concentrations of ozone as well as of other secondary photochemical products were also higher during the heat wave. The significance of the peroxy radical mixing ratios with respect to high ozone levels will be discussed as will the context and consequences of the high ozone levels.

A photostationary steady state analysis was carried out also predicting enhanced peroxy radical mixing ratios during the heat wave.

An investigation of the sources and sinks of RO_x was carried out and suggested that during the heat wave PAN thermolysis was a greater source of RO_x than primary production via photolysis of ozone and subsequent reaction with water. A correlation of isoprene and PAN production suggests isoprene as a source for PAN and therefore also for peroxy radicals and ultimately ozone.

A comparison of P(O₃) with hour on hour actual change in ozone mixing ratio also seems to correlate rather well for the heat wave period.

6 Ozone alkene event

During the TORCH II campaign at Weybourne, on the Norfolk coast of the East of England in the evening of the 10th May there was an unusual event during which peroxy radical concentration suddenly rose to values in excess of 25 pptv. At about 20:00 GMT, with photochemical radical production negligible, this amounted to four times the midday maximum. The event was correlated with enhanced CO, acetaldehyde and HCHO (increases of 5.8, 14.6, and 7.1 ppbv respectively) and a drop in ozone of 13.52 ppbv (all values are hourly averages). At the same time the alkene loading rose to 144 ppbv, mostly owing to propene exceeding values of 143 ppbv. The rise in propene is indicative of Weybourne being influenced by emissions from the oil and natural gas industries in the North Sea. The increase in CO and carbonyl compounds and the decrease in ozone provides dramatic evidence for the potential of ozone-alkene reactions to produce peroxy radicals and initiate oxidation in the atmosphere.

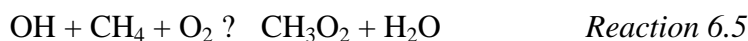
6.1 Introduction

6.1.1 Ozone-alkene reactions

Production of peroxy radicals in the atmosphere can be initiated by photolysis of ozone, followed by reaction with water and subsequent reaction with, for example, carbon monoxide or ozone (Reactions 6.1 to 6.4) [Monks, 2005].



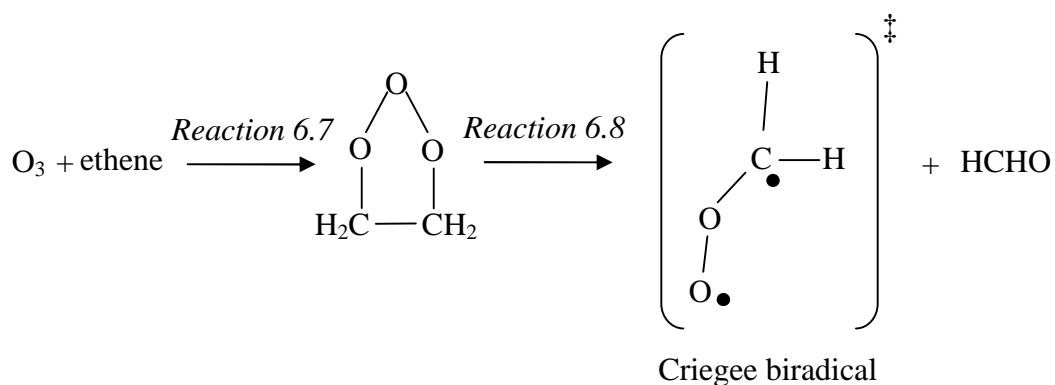
The hydroxyl radical can also react with methane or another hydrocarbon to produce organic peroxy radicals (reactions 6.5 – 6.6) [Monks, 2005].



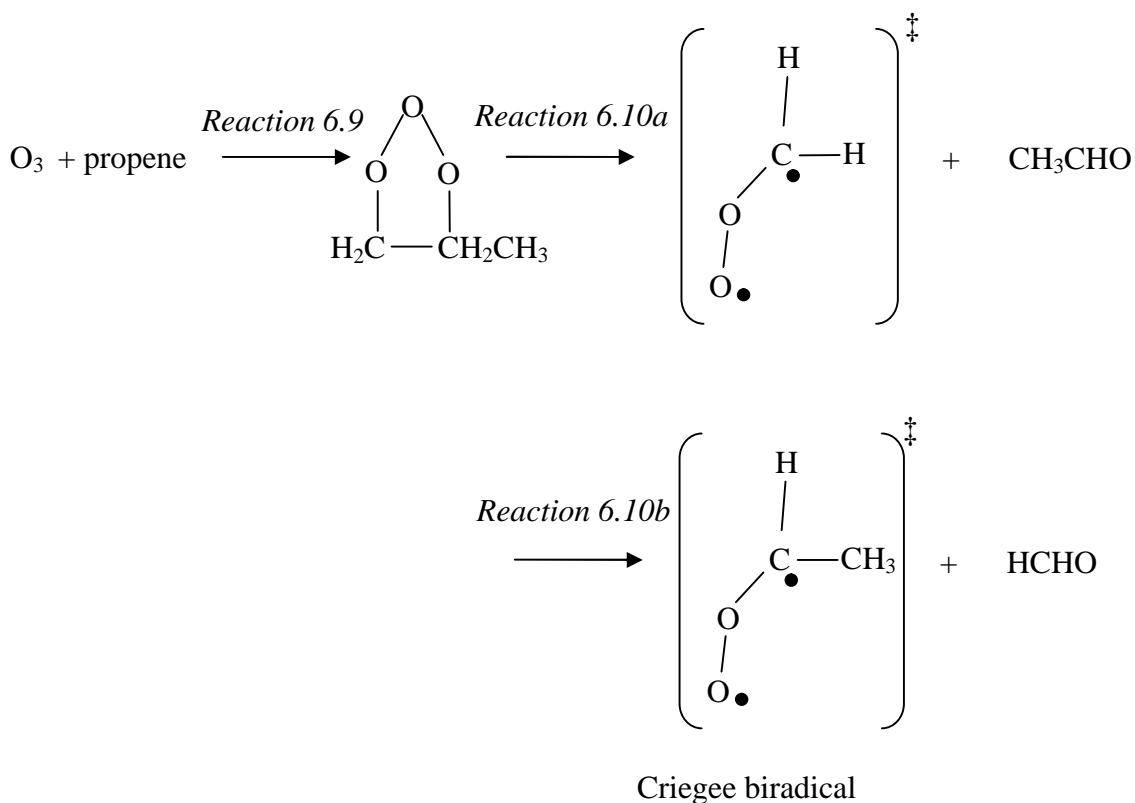
Photochemical production of peroxy radicals is not, however, their only source. OH and peroxy radicals have been observed at night and in winter. It is now established that ozonolysis of alkenes and reaction of the nitrate radical, NO_3 , with a number of VOC can lead to the production of substantial concentrations of hydroxy and peroxy radicals, (RO_x) [Monks, 2005]. Non-photolytic peroxy radical production routes are potentially important for the oxidation of VOCs and other trace gases especially at night, in wintertime and in overcast conditions [Monks, 2005].

In the UK, ozone initiated reactions of alkenes make an important contribution to oxidation of VOC. For example, 2-butene and 2-methyl-2-butene both have shorter chemical lifetimes with respect to O_3 than with respect to OH (for typical O_3 mixing ratios of 30 ppbv and OH concentrations of 1.6×10^6 molecule cm^{-3}) [Fowler, 1997].

Ozonolysis of alkenes begins with addition of ozone to the double bond forming an ozonide (eg for ozonolysis of ethene, Reaction 6.7). This then falls apart to form a biradical (Criegee intermediate) and a carbonyl compound (Reaction 6.8).



For ozonolysis of ethene the carbonyl is formaldehyde while propene ozonolysis leads to the formation of formaldehyde and acetaldehyde (Reactions 6.9 and 6.10).



The Criegee biradical can either fall apart leading to among other things the formation of OH, HO₂ and other peroxy radicals (Reaction 6.11).



Alternatively the Criegee biradical can be stabilised (Reaction 6.12) and go on to react with water to form carboxylic acids, hydroxyalkyl hydroperoxides and H₂O₂. (Reaction 6.13)





The OH and peroxy radicals formed in the ozonolysis of alkenes can go on to oxidise other compounds in the same way as occurs during the daytime (see Chapter 1).

6.2 Measurement Site

TORCH II took place at Weybourne Atmospheric Observatory, Weybourne, on the north Norfolk coast of England ($52^\circ 57'23''\text{N}$, $1^\circ 7'40''\text{E}$). It is situated at an altitude of 16m above sea level, on land which slopes gently down to a pebble beach [Clemishaw, 1994]. The WAO has an open seaward fetch of some 30 degrees, bounded by the east coasts of England and Scotland and the west coast of Norway, with a clear view across the North Sea to the Arctic Ocean and Bering Sea beyond [Penkett, *et al.*, 1999]. The location experiences clean arctic air masses as well as air masses having passed over polluted regions of the UK and Europe. The county of Norfolk comprises primarily flat, arable farm land with several small coniferous and deciduous forests and pockets of light industry [Penkett, *et al.*, 1999]. This location was chosen to experience processed air masses having passed over London, which is located 120 miles (roughly 200km) from the observatory.

6.3 Observations

6.3.1 Chemical Observations

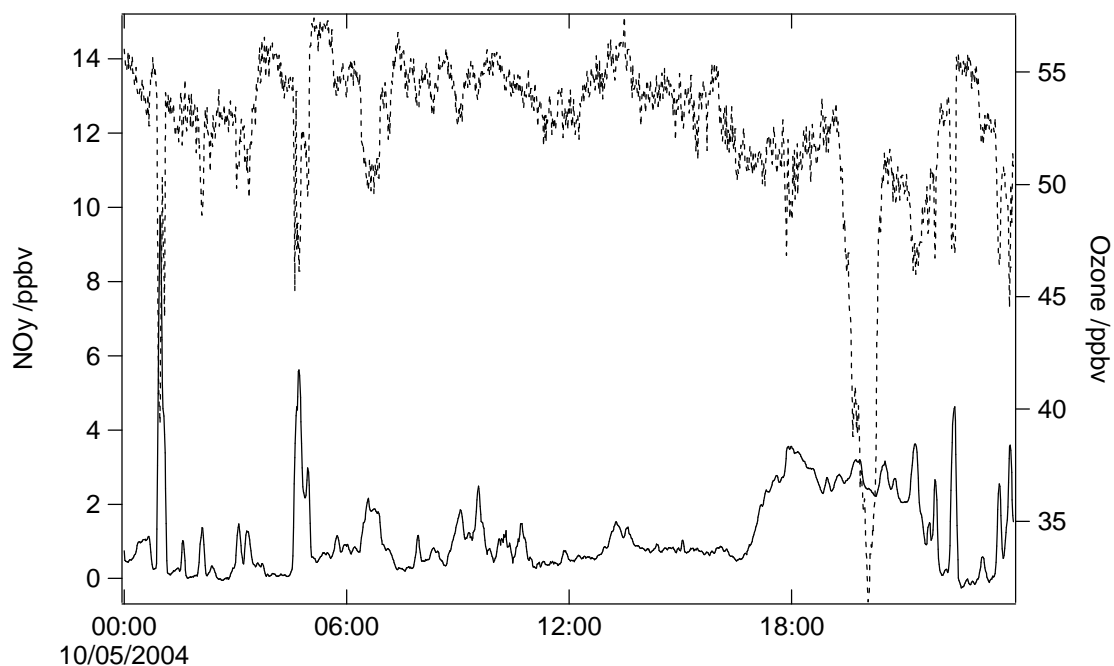


Figure 6.1 *NO_y (left-hand x axis) and ozone (right-hand x axis)*

As can be seen in Figure 6.2, when peaks occur in NO_y, ozone decreases. This is evident, for example, at around 01:00 and 04:40. This is explained by the reaction of NO with ozone, from which NO₂, a major component of NO_y, is formed (Reaction 5.14).



However, around 20:00 hours there is a sharp dip in ozone concentration not reflected in NO_y. At 19:12 the ozone mixing ratio is 53 ppbv falling to 31 ppbv at 20:05 and recovering again to 51 ppbv at 20:41.

Conversely to the behaviour of ozone, peroxy radical mixing ratio peaks dramatically at around 20:00, rising from 3.4 pptv at 18:00 to 25.6 pptv at 19:50 before falling back to 3.7 pptv at 21:00 (Figure 6.2). During the middle of the day peroxy radicals follow roughly jO^1D (Figure 5.3 inset). The peak in peroxy radicals at 20:00 is approximately five times the midday maximum. At 20:00 jO^1D is essentially 0, i.e. photolysis of O_3 leading to production of OH and subsequent oxidation of VOC to form peroxy radicals does not occur (Figure 6.3).

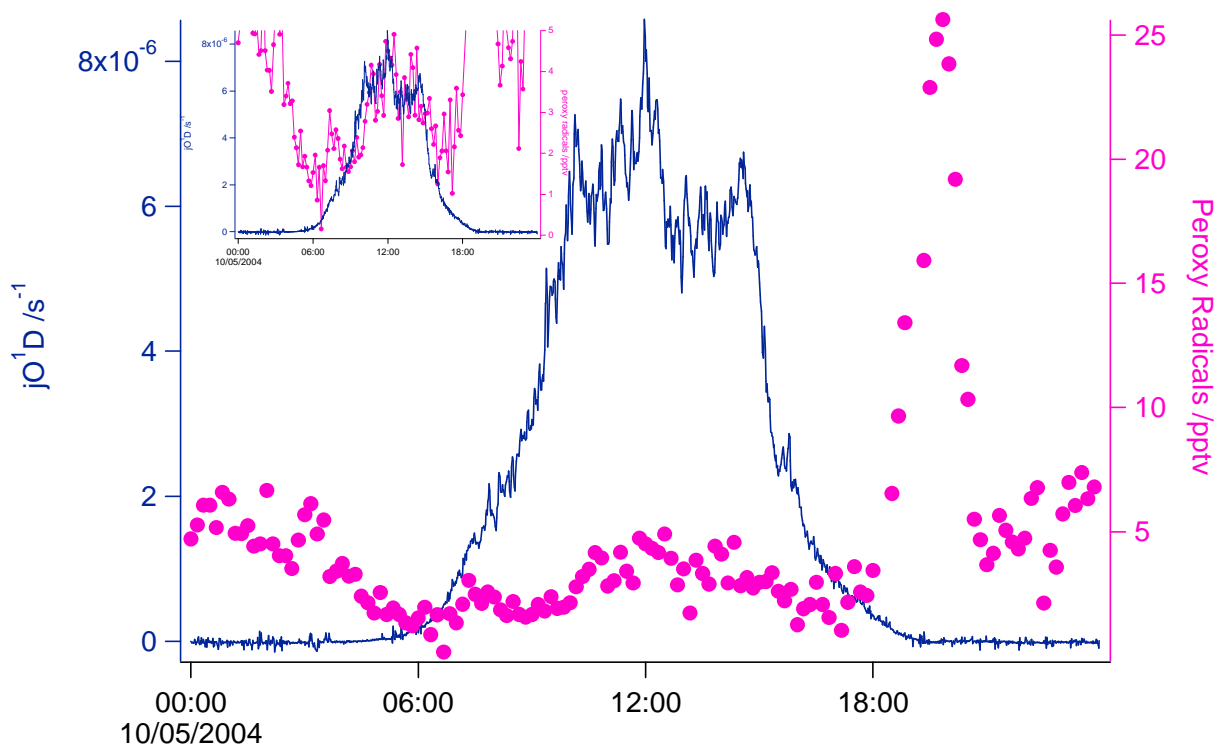


Figure 6.2 Ten-minute averaged peroxy radical mixing ratio (pink dots) and jO^1D (blue line). Inset with peroxy radical axis scale multiplied by a factor of five to show detail during the middle of the day.

During the campaign, HO_2 as well as OH measurements were carried out by the University of Leeds, using a FAGE LIF instrument. As can be seen (Figure 6.3) for the middle section of the day, HO_2 and $HO_2 + SR_1O_2$ show a similar pattern, with mixing ratios rising in the morning and falling in the afternoon. Unfortunately the instrument was offline during the

period of interest in the evening, although just before 18:00 the concentration of HO₂ does appear to be increasing.

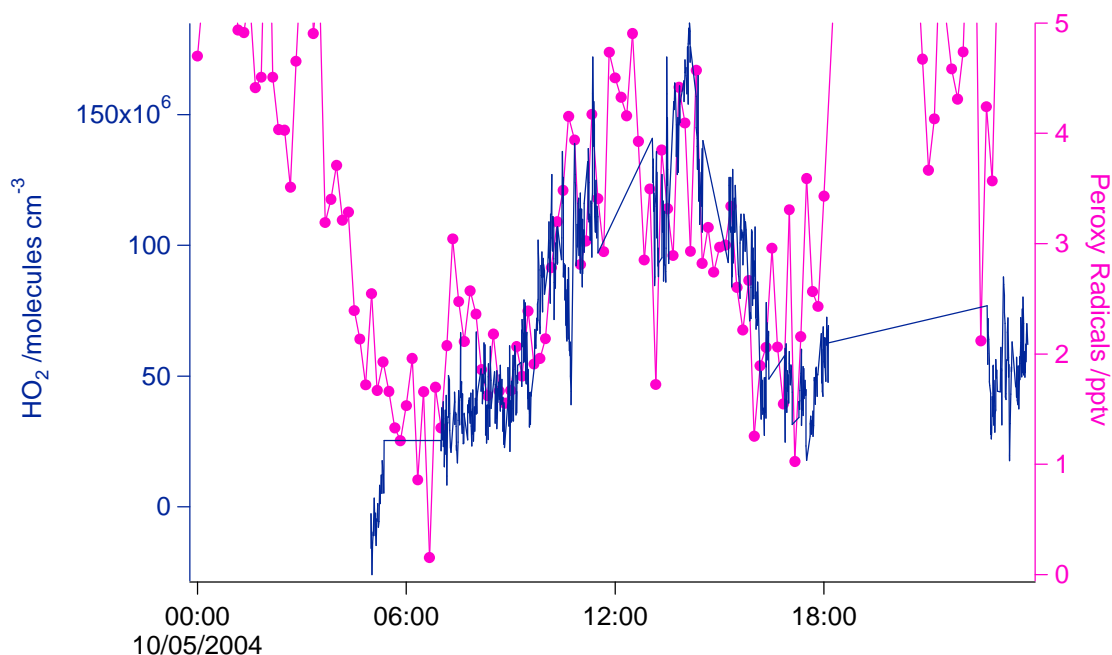


Figure 6.3 Concentration of HO₂ as measured by FAGE (blue line, left-hand x axis) and total peroxy radical mixing ratio (pink dots and line, right-hand x axis)

Many VOC also exhibited peaks at 20:00, around the time of the maximum peroxy radical mixing ratio. The most significant VOC rise is from propene which peaks at 143000 pptv. Mixing ratios of propene are in the 10s of pptv range for the rest of the 10th of May, thus the peak value represents an increase of three to four orders of magnitude (Table 6.1). As well as significant increases in alkanes and alkenes, acetaldehyde mixing ratio was an order of magnitude higher than the rest of the day and methanol was also higher.

Between 16:00 and 20:00 CO increased by approximately 5 ppbv. This is a small increase and could be due to from other VOC present in the plume for OH, i.e.,

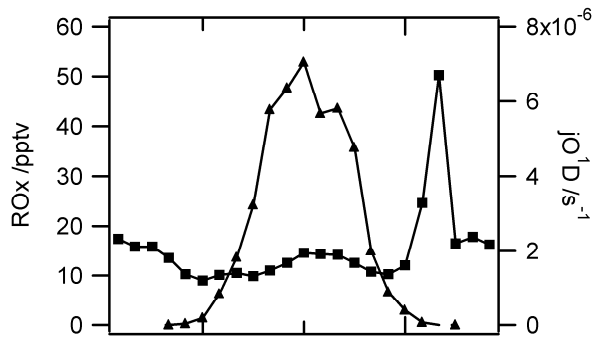


Figure 6.4a

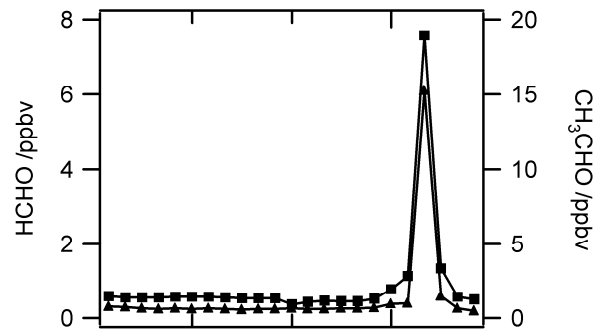


Figure 6.4b

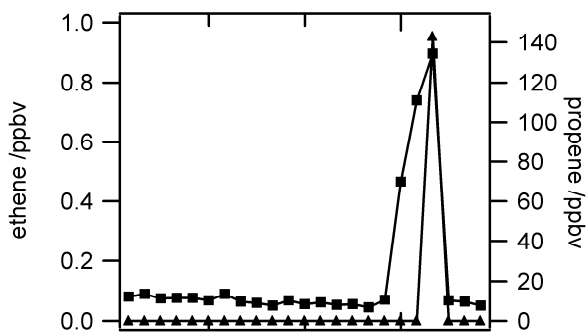


Figure 6.4c

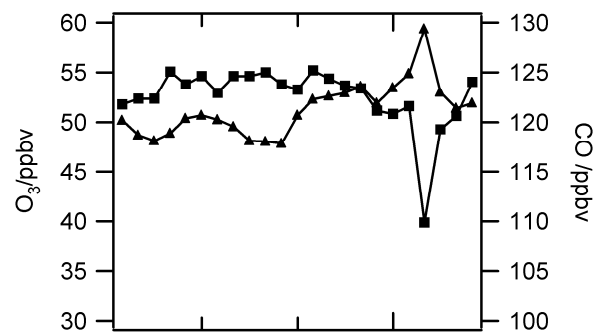


Figure 6.4d

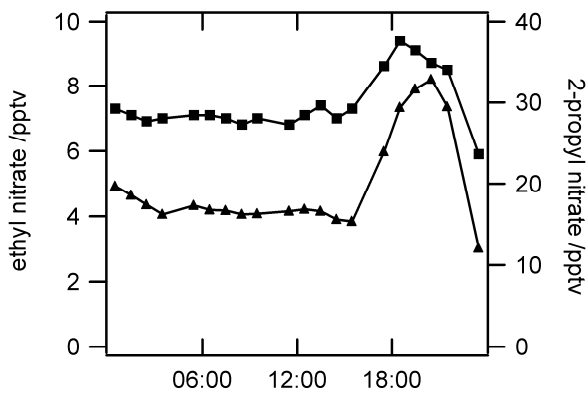


Figure 6.4e

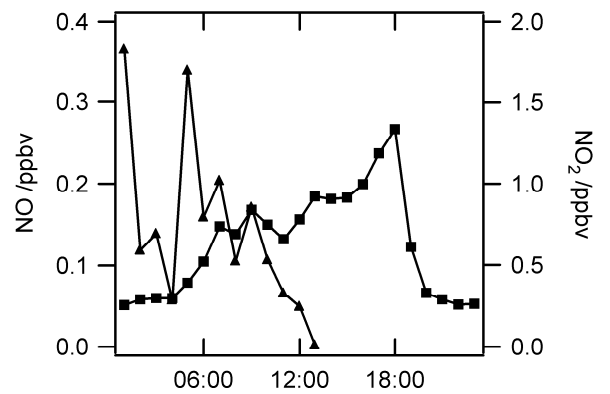


Figure 6.4f

Figure 6.2 Hourly data from 10th May 2004, TORCH II campaign. In each panel the square data points correspond to the left-hand x axis and the triangular data points correspond to the right-hand x axis.

<i>Species</i>	<i>Mixing ratio at 16:00</i>	<i>Mixing ratio at 20:00</i>	<i>Change in mixing ratio</i>	<i>Ratio of 20:00 to 16:00</i>	<i>Ratio of Campaign to average</i>	<i>Ratio of 20:00 to campaign average</i>
<i>Alkanes</i>						
ethane	2311.21	3926.48	1615.27	1.70	2328.67	1.69
propane	838.37	7357.42	6519.05	8.78	882.22	8.34
isobutane	127.26	456.39	329.13	3.59	195.67	2.33
n-butane	250.06	925.45	675.39	3.70	335.83	2.76
cyclopentane	13.73	24.17	10.44	1.76	20.61	1.17
isopentane	65.62	189.94	124.32	2.89	172.17	1.10
n-pentane	62.66	187.98	125.32	3.00	105.79	1.78
2,2-dimethylbutane	4.89	18.89	14	3.86	34.2	0.55
2+3-methylpentane	14.35	39.13	24.78	2.73	53.42	0.73
n-hexane	11.75	36.36	24.61	3.09	33.36	1.09
n-heptane	4.84	7.85	3.01	1.62	17.24	0.46
<i>Alkenes</i>						
ethene	44.49	896.08	851.59	20.14	296.48	3.02
propene	18.64	143095.91	143077.27	7676.82	80.27	1782.68
trans-2-butene	4.06	7.67	3.61	1.89	6.28	1.22
1-butene	5.3	5.7	0.4	1.08	13.03	0.44
isobutene	8.94	19.9	10.96	2.23	15.95	1.25
cis-2-butene	2.41	4.62	2.21	1.92	3.92	1.18
1,2-butadiene		1.36			3.43	0.40
trans-2-pentene	2.17	8.85	6.68	4.08	6.89	1.28
1-pentene		5.7			4.71	1.21
2-methyl-1-butene		2.46			6.07	0.41
2-methyl-2-butene		1.02			3.98	0.26
cis-2-pentene		2.82			3.11	0.91
<i>Alkynes</i>						
acetylene	345.32	360.48	15.16	1.04	415.45	0.87
propyne	19.59	13.73	-5.86	0.70	17.91	0.77
<i>Aromatics</i>						
benzene	121.7	162.79	41.09	1.34	131.96	1.23
toluene	13.72	29.74	16.02	2.17	114.85	0.26
<i>Oxygenates</i>						
formaldehyde	438.67	7580.74	7142.07	17.28	1510	5.02
acetaldehyde	622.88	15241.53	14618.65	24.47	1312.69	11.61
methanol	3015.38	3123.08	107.7	1.04	4639.03	0.67
acetone	1175.95	957.68	-218.27	0.81	999.14	0.96

Table 6.1 Mixing ratios of 11 alkanes, 12 alkenes, 3 alkynes, 2 aromatics and 4 oxygenates measured at TORCH II

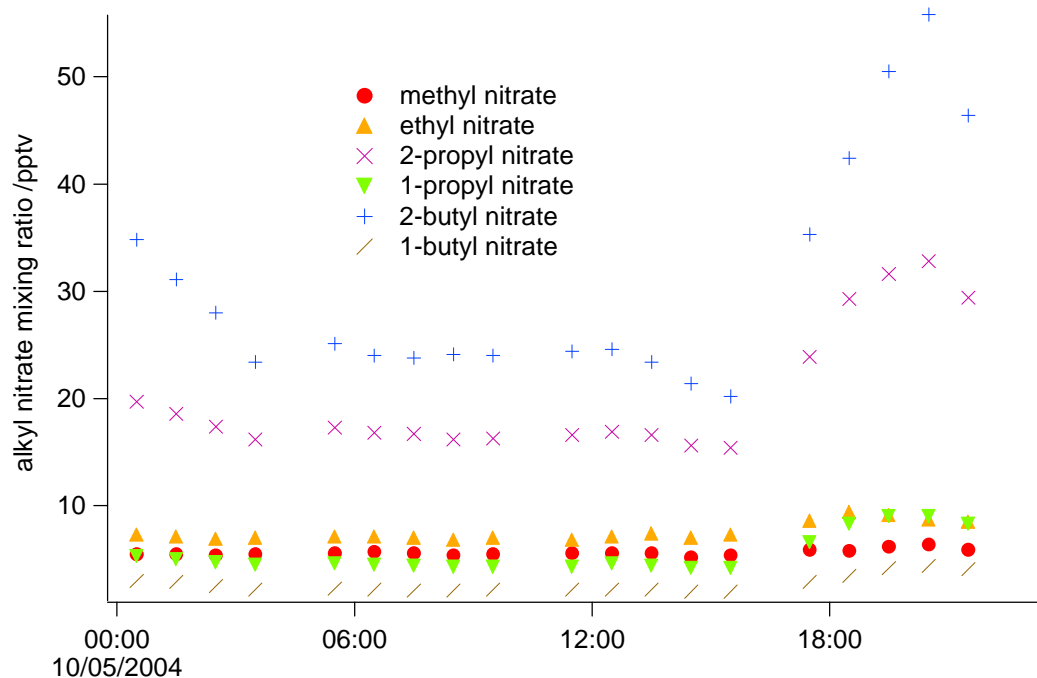


Figure 6.5 Mixing ratios of six alkyl nitrates for 10th May 2004

Six different alkyl nitrates were measured using GC-NICI (Figure 6.5). Five of them had a maximum, not just for May 10th but for the whole campaign at 20:30. The sixth, ethyl nitrate, reached its campaign maximum at 18:30 on May 10th. Since alkyl nitrates are formed from the reaction of a peroxy radical with NO (Reaction 6.6) increased concentration of alkyl nitrates implies the presence of peroxy radicals.



Alkyl nitrates have a relatively long chemical lifetime (approximately one week for 2-butyl nitrate, assuming OH concentration of 1.7×10^6 molecule cm^{-3} and rate coefficient with respect to reaction with OH of 9.2×10^{-13} cm^3 molecule s^{-1} at 298K). Therefore it is not easy

to determine whether the high concentrations of alkyl nitrates observed were due to in situ production or transport.

6.4 Meteorological Observations

Local wind direction for the evening of the 10th May was Westerly to North Westerly (Figure 5.6). Wind speed was around 3ms^{-1} in the afternoon/evening until 21:00 when it rose to a peak of 6ms^{-1} at 21:30 dropping back to between 3 and 5ms^{-1} (Figure 6.6).

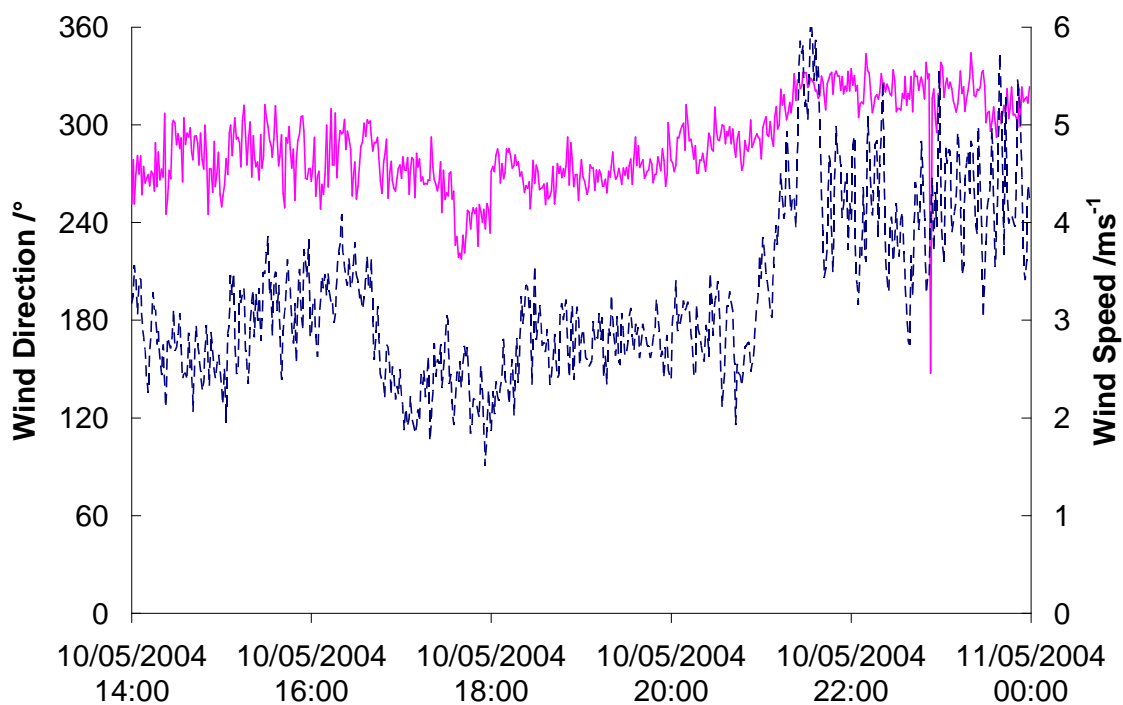


Figure 6.6 Wind direction, North = 360° , (pink solid line) and wind speed (dashed blue line) for the afternoon/evening of 10th May.

Temperatures were mild at between 9 and 10°C (Figure 6.7) and conditions throughout the day had been somewhat overcast. Relative humidity was around 100% for the whole afternoon/evening of 10th May (Figure 6.7)

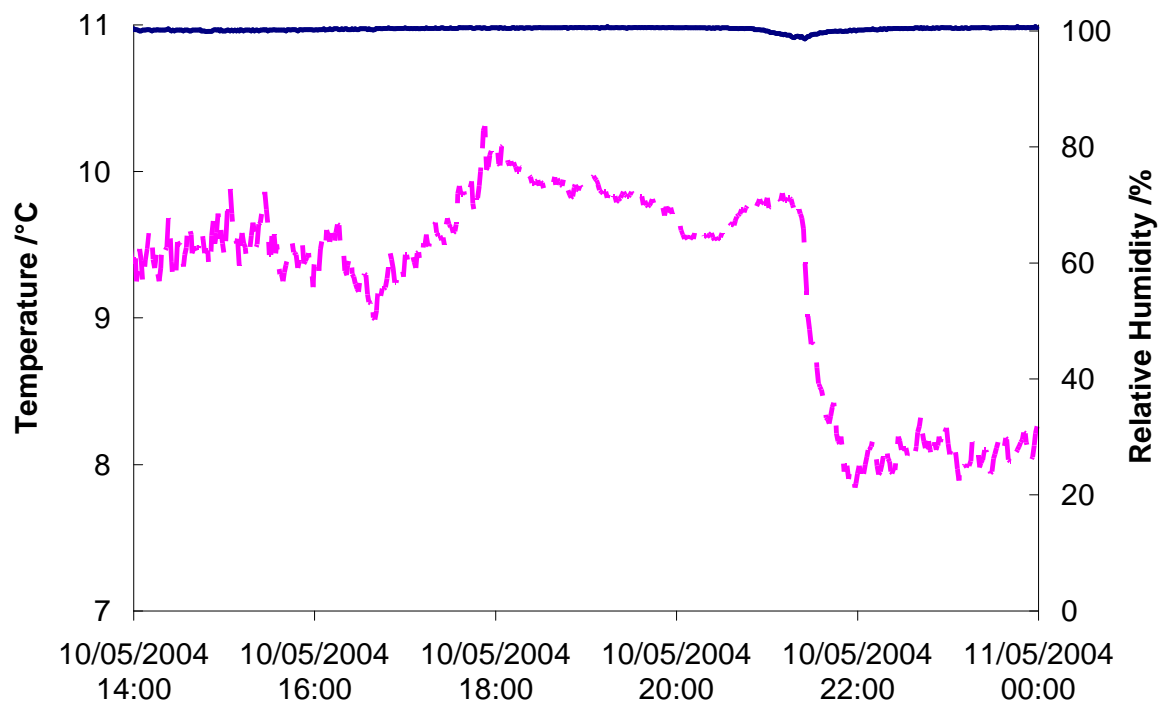
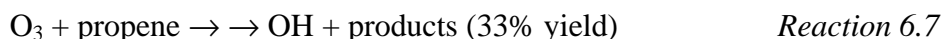


Figure 6.7 Temperature (pink dashed line) and relative humidity (solid blue line) for the afternoon/evening of 10th May

6.5 RO₂ production

6.5.1 OH Steady state

In order to estimate RO₂ mixing ratios from the organic and inorganic species measured at the site it is also necessary to know the OH concentration. Unfortunately, no measurements of OH were made during the event of the evening of 10th May. However, owing to the fact that the propene mixing ratio was orders of magnitude higher than other VOC, we can assume the only source of OH is the ozonolysis of propene (Reaction 6.7) and thus calculate a steady state OH concentration.



$$k_{(\text{O}_3+\text{propene})} = 7.18 \times 10^{-18} \text{ cm}^3 \text{ molecule}^{-1} \text{ s}^{-1}$$

Assuming four loss routes for OH (Reactions 6.8 – 6.11) it is possible to calculate OH concentrations assuming it is in a steady state (Equation 6.1).



$$[\text{OH}] = \frac{k_{5.7}[\text{O}_3][\text{C}_3\text{H}_6] \times \text{OH yield}}{k_{5.8}[\text{CO}] + k_{5.9}[\text{VOC}] + k_{5.10}[\text{NO}_2] + k_{5.11}[\text{O}_3]} \quad \text{Equation 6.1}$$

In the afternoon and evening of May 10th NO₂ mixing ratios as measured by the Cranox instrument were below zero. Thus, NO_y measured by the TECO instrument was used instead with the assumption that most of the NO_y was NO₂. The four loss terms from 6.8 to 6.11 were 0.56, 6.32, 0.92 and 0.09 s⁻¹ respectively giving a total of 7.89 s⁻¹. The main contribution to OH destruction are from VOC so even if accepting that NO₂ mixing ratios were effectively zero would not make a great difference to the calculated OH concentration.

The OH yield for the ozone propene reaction is around 0.33. This gives an OH concentration of 1.2×10^6 molecule cm⁻³ at 20:00, 40% of the measured value during the middle of the same day (3×10^6 molecules cm⁻³). Recycling reactions of OH (Reactions 6.12 to 6.14) have not been included in the calculation of OH concentration. Assuming that HO₂ accounted for half the peroxy radicals measured by PERCA, recycling would increase the OH concentration to 1.8×10^6 molecule cm⁻³.



The most significant contribution to OH reactivity at 20:00 comes from acetaldehyde (Table 6.2). At 19:00 it is less than half the magnitude of CO whereas at 20:00 it is an order of magnitude greater. Formaldehyde is also has a higher OH reactivity than CO at 20:00 whereas at 19:00 it was insignificant. It is interesting to note that while propene dominates reactivity with respect to ozone, it has little impact on OH destruction, being under 1% of the OH reactivity.

<i>Species</i>	<i>[X] at 19:00</i>	<i>[X] at 20:00</i>	<i>OH reactivity*</i>	<i>OH reactivity**</i>
	<i>/pptv</i>	<i>/pptv</i>	<i>relative to CO at 19:00</i>	<i>relative to CO at 20:00</i>
CO	124895.00	129370.00	1.00	1.00
CH ₄ ***	1800000.00	1800000.00	0.39	0.38
Propane	1471.48	7357.42	0.07	0.33
Isobutane	219.42	456.39	0.05	0.11
Propene	35.43	143095.91	0.00	0.15
Formaldehyde	438.67	7580.74	0.20	3.35
Acetaldehyde	622.88	15241.53	0.43	10.25
Methanol	3015.38	3123.08	0.13	0.13

Table 6.2 *at 19:00 CO reactivity = 0.540 s^{-1} , at 20:00 CO reactivity = 0.557 s^{-1} ,
*** CH₄ mixing ratio estimated at 1800 ppbv.

6.5.2 RO₂ production

A steady state calculation was performed to quantitatively link the high propene mixing ratio at 20:00 (143 ppbv) and the peak in peroxy radicals (five times the midday concentration). At 20:00, production of RO_x (defined as the sum of all peroxy radicals plus HO_x) via ozone photolysis is insignificant so it is assumed that the only source of RO_x is from the ozonolysis of propene (Reaction 6.7). Ozonolysis of alkenes produce OH as well as other radicals such as peroxy radicals [Monks, 2005]. Ozonolysis of different alkenes produce varying yields of OH and peroxy radicals but for this analysis it assumed that the yield of RO_x is one. Losses of RO_x are taken as the reaction of OH with NO₂ (Reaction 6.10) and the RO_x self-reaction (Reaction 6.15), using the rate constant for the self-reaction of HO₂. Reactions to form reservoir species such as PAN were not considered as no data was available for PAN. VOC reactions with NO₃ could also provide a source of radicals. However, concentrations of the

precursors of NO₃, O₃ and NO₂, are not particularly high, coupled with the fact that propene is relatively unreactive with respect to NO₃.



Equation 6.2 was used to calculate RO_x at 20:00.

$$[\text{RO}_x] = v \frac{k_{5.7}[\text{O}_3][\text{C}_3\text{H}_6] - k_{5.10}[\text{NO}_2][\text{OH}]}{2k_{5.15}} \quad \text{Equation 6.2}$$

For comparison RO_x was also calculated for the middle period of the day (Equation 6.3). It was assumed that RO_x production occurred only via photolysis of ozone (Reactions 6.1 and 6.2).

$$[\text{RO}_x] = v \frac{2Fj\text{O}^1\text{D}[\text{O}_3] - k_{5.10}[\text{NO}_2][\text{OH}]}{2k_{5.15}} \quad \text{Equation 6.3}$$

where F = fraction of O(¹D) that go on to form OH (see Chapter 1).

In Equation 6.2, [OH] was calculated in section 6.4.1. In Equation 6.3, [OH] was measured by the University of Leeds FAGE instrument.

RO_x production at 20:00 is an order of magnitude higher than at midday ($2.86 \times 10^7 \text{ cm}^3 \text{ molecule}^{-1} \text{ s}^{-1}$ compared to $1.48 \times 10^6 \text{ cm}^3 \text{ molecule}^{-1} \text{ s}^{-1}$). This leads to steady state calculated RO_x at 20:00 to be roughly five times the concentration of that calculated for the middle of the day (Figure 6.8). The evening:midday ratio of PERCA measured RO_x is also around five.

Of the alkenes only propene has a mixing ratio high enough to produce enough RO_x to account for the observations.

While the evening:midday ratios agree very well for steady state calculations and PERCA measurements, steady state mixing ratios are four times those measured. This could be because of the assumption that $k_{5,15}$

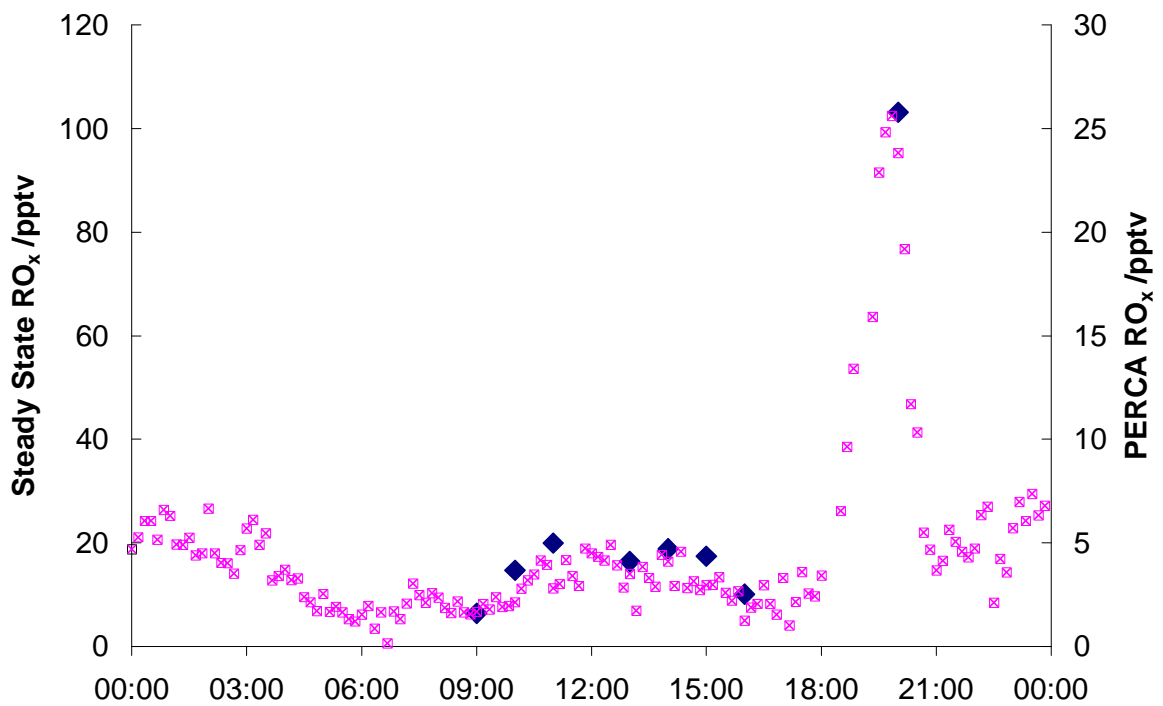


Figure 6.8 RO_x mixing ratio calculated by a steady state relationship (large blue diamonds) and RO_x measured by PERCA (pink crosses).

6.6 Hydrocarbons and their Sources

6.6.1 Plume identification

Two five-day periods from the TORCH II campaign were chosen to investigate the influence of VOC emissions on chemical composition at Weybourne in order to link peaks in hydrocarbon concentrations with emission source regions, the ultimate aim being to understand the origins of the high VOC mixing ratios and thus the peak in radical concentrations on the evening of 10th May. The first period, 7th to 11th May 2004 inclusive, chosen to include 10th May, is characterised by lower temperature (9.3°C), high relative humidity (96%) and airmasses arriving at Weybourne from the North, from across the North Sea. The second period is characterised by higher temperature (14.8°C), lower relative humidity (74%) and airmasses arriving at Weybourne from across the North of England. For each period, four hydrocarbon peaks (plumes) were identified (Figures 6.9 and 6.10).

For each plume, one-day back trajectories were calculated using the HYSPLIT model from NOAA (Figures 6.11 and 6.12). For Period 1, it was established that the four cases of elevated hydrocarbons had not encountered land in the previous 24 hours and came from the North Sea (Figures 6.12a-d). For Period 2, the four airmasses associated with elevated hydrocarbons all passed over the North of England.

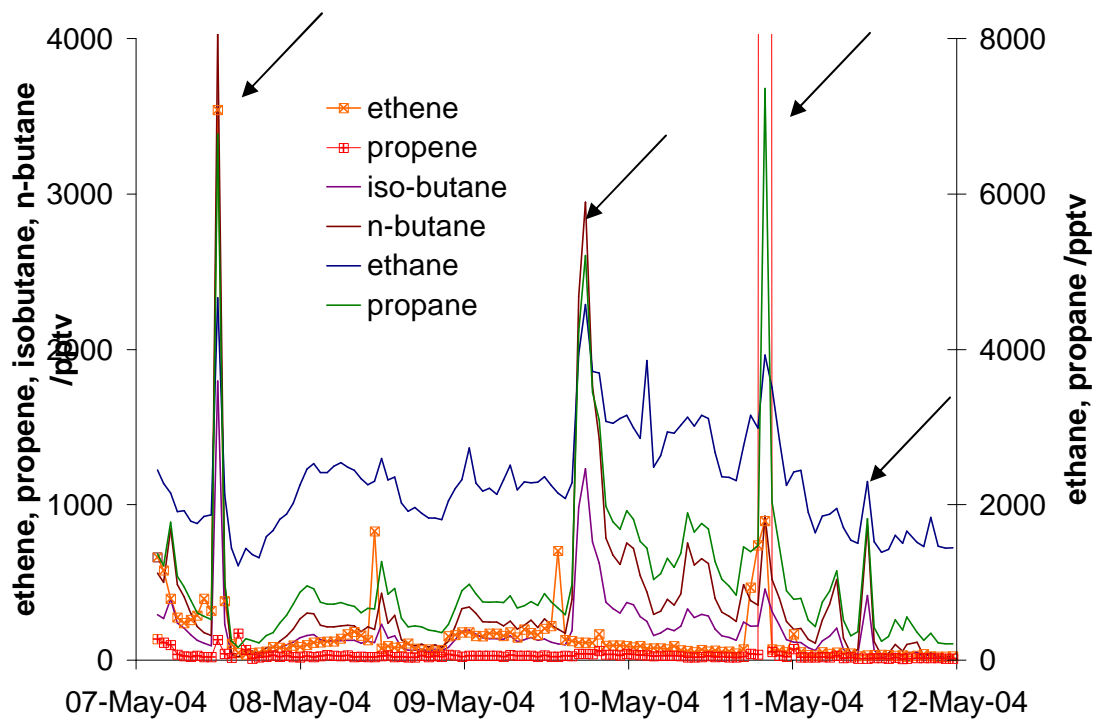


Figure 6.9 Mixing ratios for four non-methane alkanes and two alkenes for 7th – 11th May 2004 inclusive. Propene in the third peak towards the end of May 10th goes off the scale as it reached 143000 pptv.

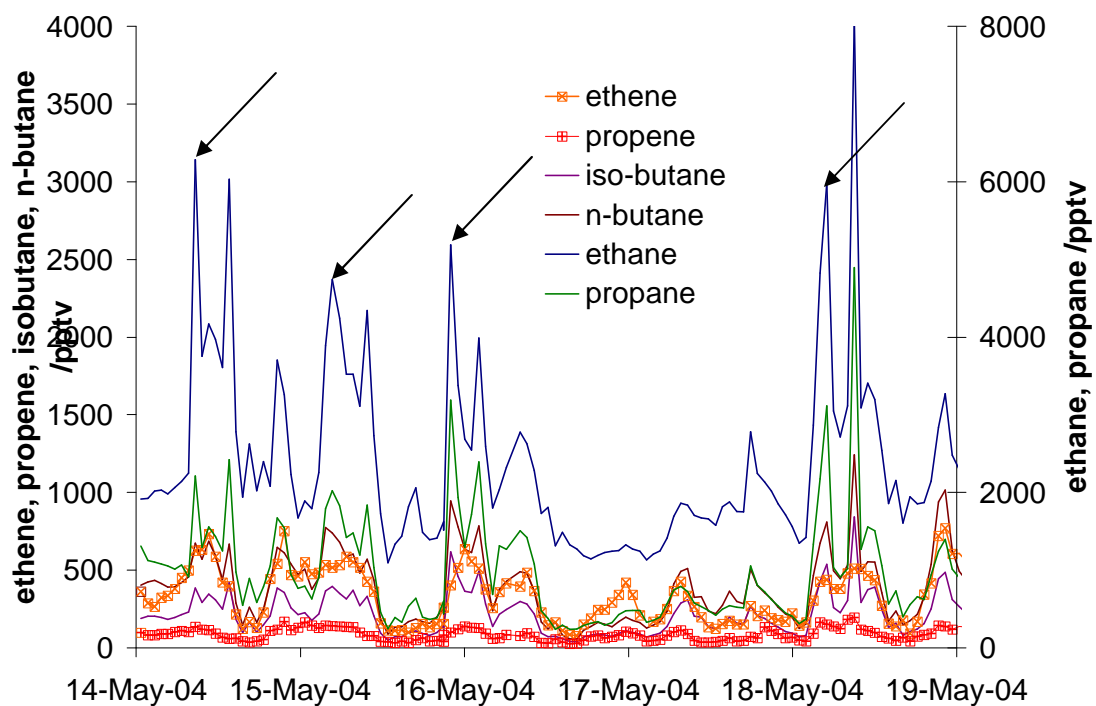
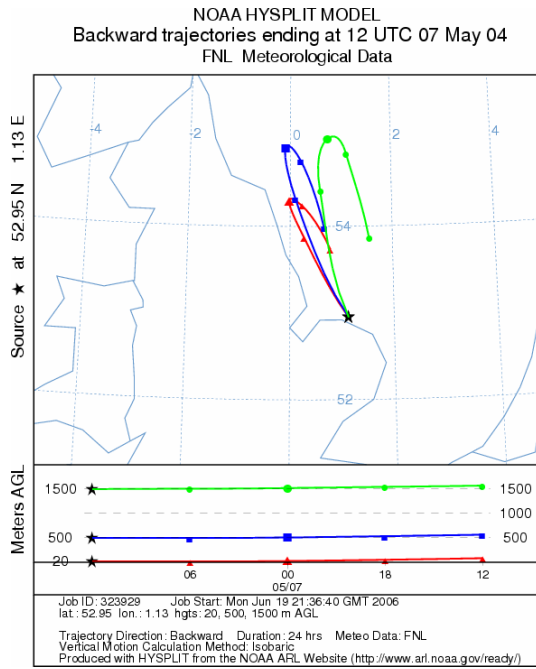
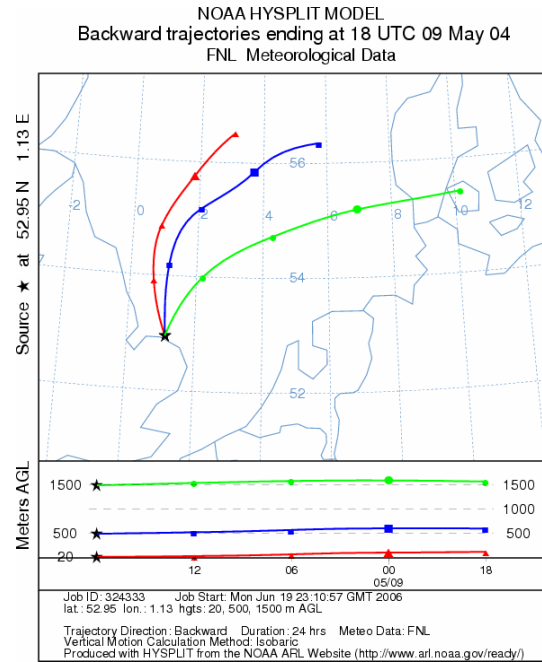


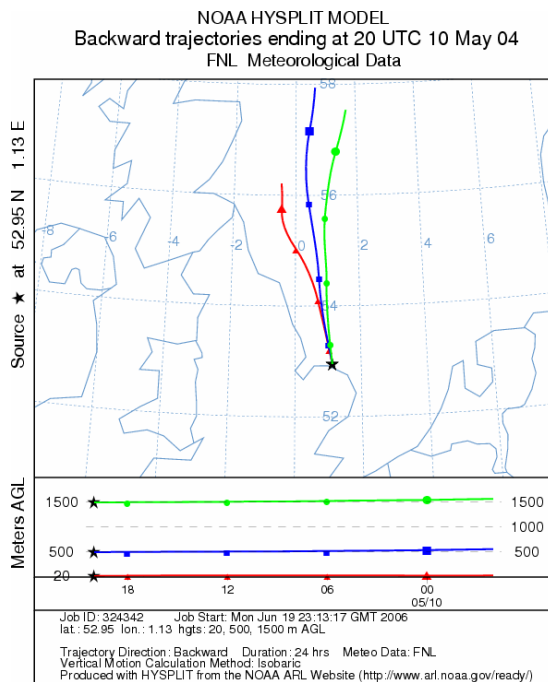
Figure 6.10 Mixing ratios for four non-methane alkanes and two alkenes for Period 1, 7th – 11th May 2004 inclusive.



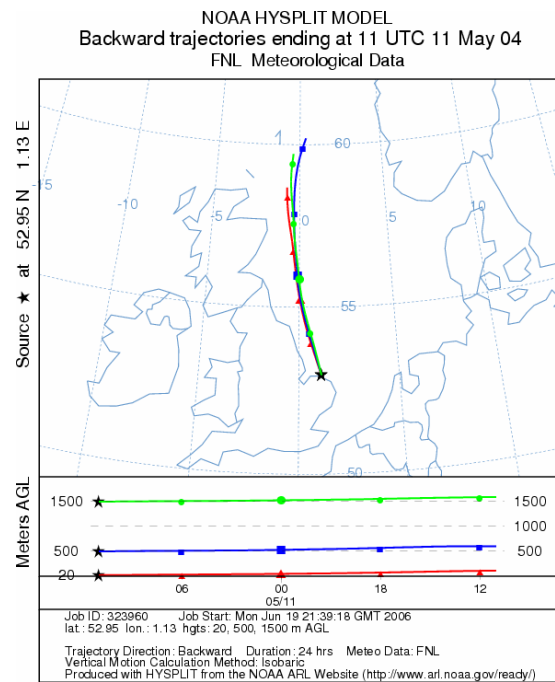
6.11a



6.11b

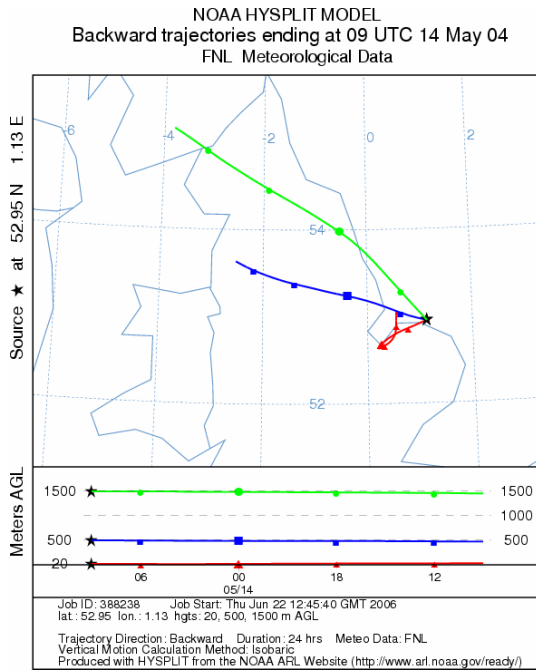


6.11c

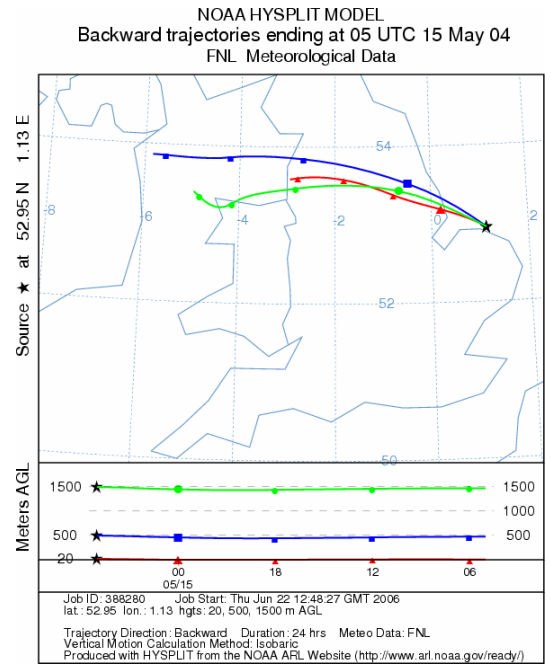


6.11d

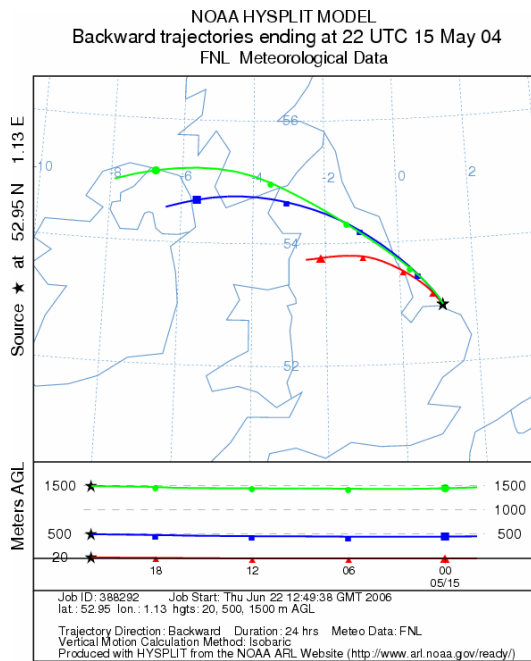
Figure 6.11 One-day back trajectories for the four plumes in Period 1



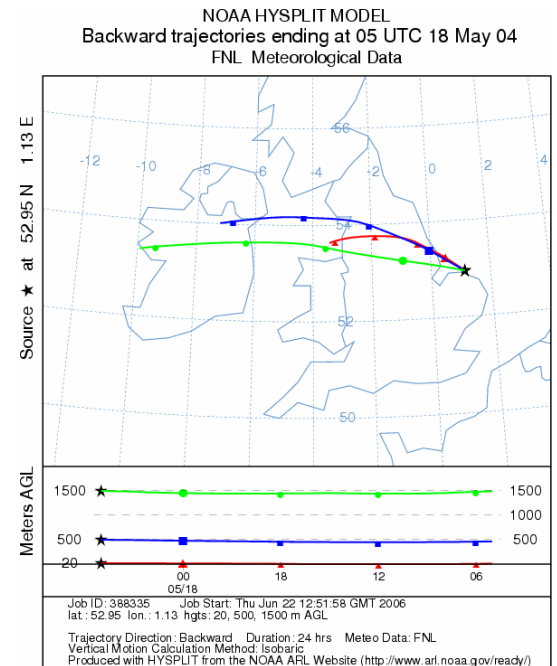
6.12a



6.12b



6.12c

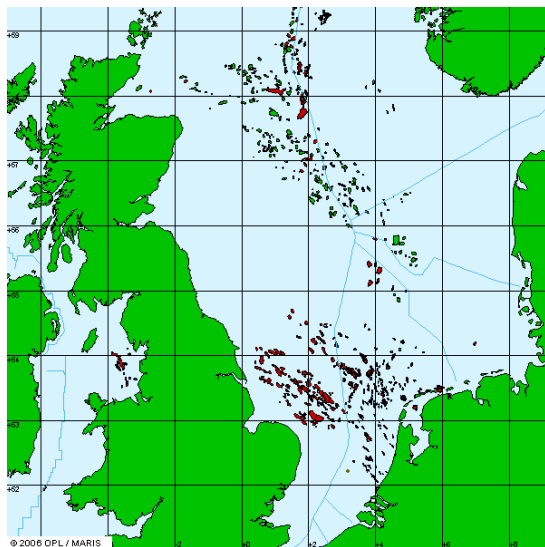


6.12c

Figure 6.12 One-day back trajectories for the four plumes in Period 2

6.6.2 VOC Fingerprints

6.13a



6.13b

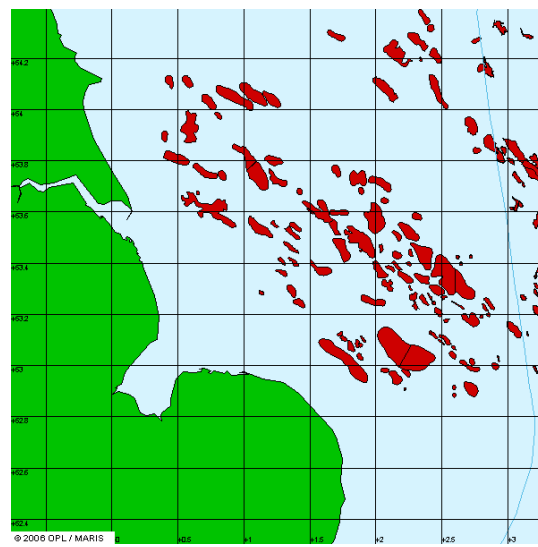


Figure 6.13 the oil and gas fields of the North Sea (Oil fields – red, gas fields – green), 6.13b shows a close up view of the oil fields of the coast of Eastern England.

Having established the immediate history of the airmasses one possibility is that the plume comes from activities relating to the oil and gas industry in the North Sea. The site at Weybourne, North Norfolk can be influenced by airmasses coming across the North Sea, potentially having passed over oil and gas fields. Such operations can emit large quantities of VOC, which can impact the chemical composition of the atmosphere and thus the radical chemistry taking place at coastal sites such as Weybourne. In Norway, which also has extensive oil and gas fields in the North Sea, an estimated 45-50% of national VOC emissions have been attributed to offshore loading of crude oil [Skjølsvik, 2001]. In the UK, 28% of estimated VOC emissions in 2003 were related to the oil and gas industries, although not all emissions were directly from the North Sea (NAEI emissions data, www.naei.org.uk/emissions/emissions.php).

Figure 6.13 shows the location of the oil fields to the North and West of Weybourne, precisely the area over which the polluted airmasses traversed before being measured. The biggest releases of VOC from this industry come from the loading of oil tankers at sea, as well as unloading in ports. Transported to the mainline these emissions can have an impact on ozone formation once they come into contact with NO_x rich air. A speciation of the VOCs from such Crude oil gathering tanks [Viswanath, 1989] were analysed using GC FID with crude oil from US wells (Table 6.3).

<i>Compound</i>	<i>Percent of total (including minor constituents not shown in this table)</i>	<i>Percent of selection (only including those compounds listed in this table)</i>
Propane	25.84	31.63
n-Butane	20.03	24.52
Ethane	9.28	11.26
n-pentane	7.3	8.93
Isobutane	7.14	8.74
Isopentane	6.29	7.70
n-hexane	2.20	2.69
2- and 3-methylpentane	2.83	3.46
cyclopentane	0.51	0.62
Toluene	0.23	0.28
bezene	0.12	0.15
TOTAL	81.65	99.98

Table 6.3 Speciation of VOC from crude oil tanks. Roughly half of the remaining VOC not listed here are unidentified, the other half are divided among 18 VOC with low contribution to the concentration.

A comparison was made between the ratios of concentrations of the 12 compounds in Table 6.3 as measured by [Viswanath, 1989] and the ambient measurements made at Weybourne.

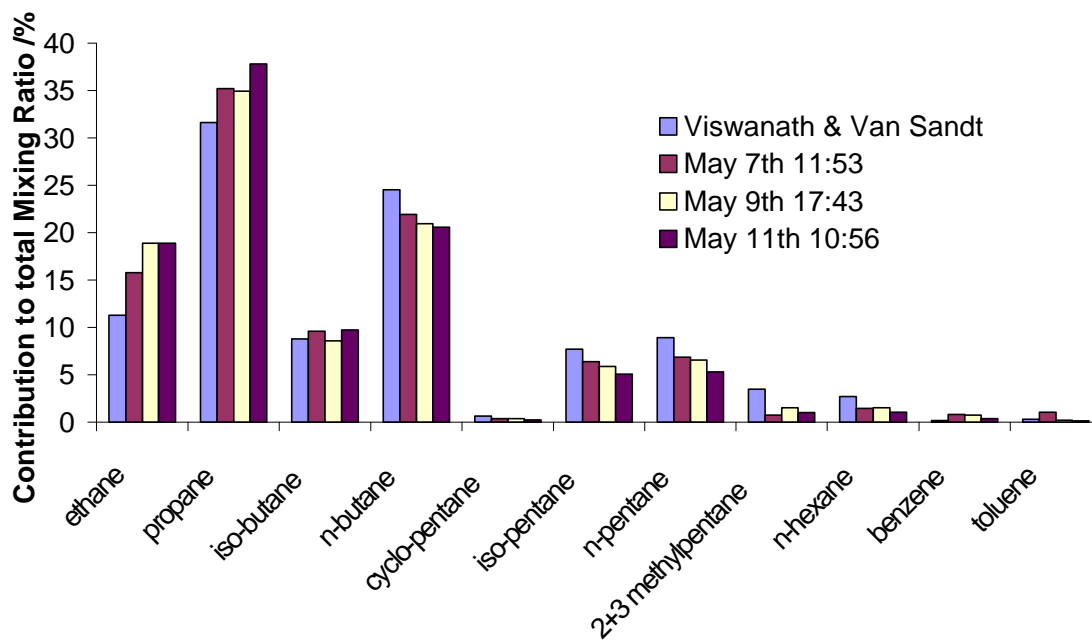


Figure 6.14 “Fingerprints” of the four selected plumes for 12 VOC from Period 1 measured at Weybourne, May 2004.

Plume concentrations were obtained by subtracting the last trough concentration from the peak concentration. For May 7th, these were the values recorded one hour before the peak, for May 9th 3 hours, May 11th 3 and 2 hours before for the peaks at 06:26 and 10:56 respectively. Although this is a seemingly rough method of calculating the excess concentrations of VOC it yields fingerprints for these plumes very similar to the literature fingerprint indicating that the composition of these plumes with respect to the VOC above is highly influenced by crude oil tank loading activity. It is interesting to note that the percentage contribution from ethane and propane, which are relatively unreactive with respect to OH oxidation, are higher than the literature value, whereas the percentage contributions for the more reactive compounds are lower than the literature value. This could be explained by the effect of transport, i.e. Ethane

and propane have longer lifetimes than longer alkanes and so are less favourably oxidised on their way from the point of emission to the sampling point.

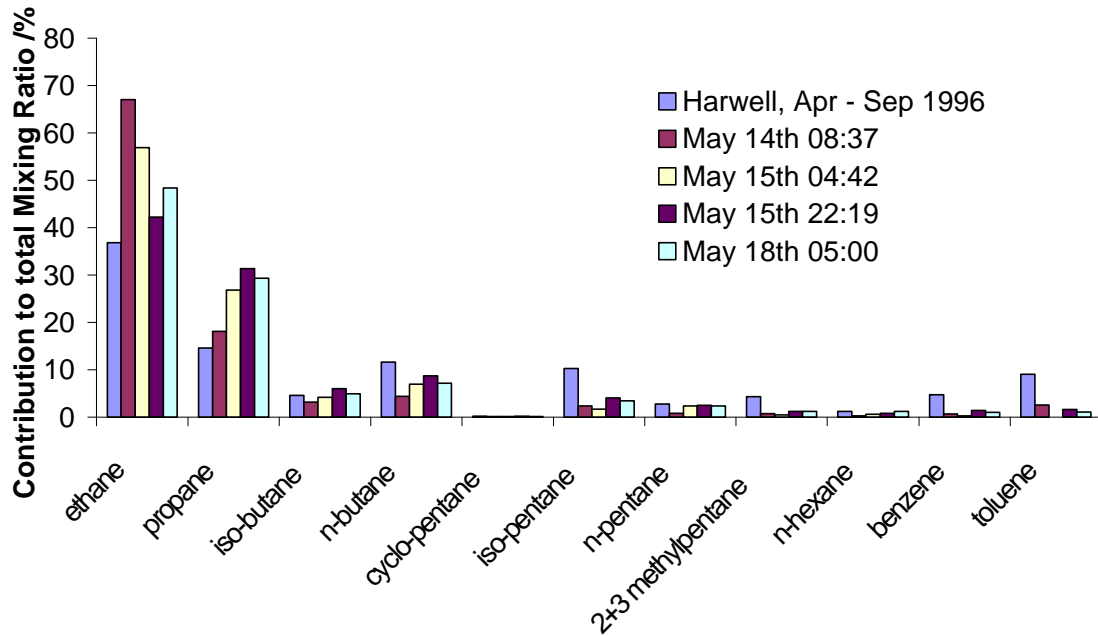


Figure 6.15 “Fingerprints” of the four selected plumes for 12 VOC from Period 2 measured at Weybourne, May 2004.

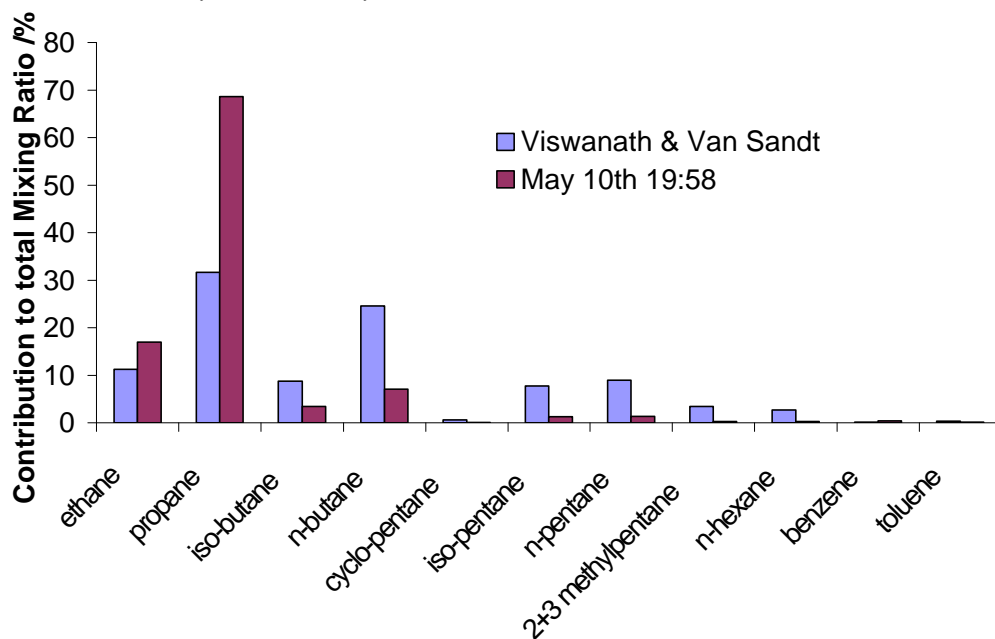


Figure 6.16 VOC contributions to mixing ratio at 20:00 on 10th May.

6.7 Chapter 6 Summary

The unusual event of high mixing ratios of peroxy radical mixing ratios is probably linked to a one off emission of propene from activities related to the crude oil or gas industry off the East Coast of England in the North Sea. This led to ozone alkene reactions producing peroxy radicals and secondary species such as alkyl nitrates.

The analysis in this chapter indicated that airmasses passing over the North Sea exhibited fingerprints consistent with those from crude oil storage tanks. Air masses having passed over mainland Britain had fingerprints consistent with those of average concentration at Harwell Oxfordshire.

Although there are frequent peaks of hydrocarbon mixing ratios observed daily coming from the North Sea, the event in the evening of 10th May was the only one of such magnitude of propene mixing ratio. This particular event was not relevant for ozone production at the measurement site as it occurred in the evening when photolysis rates were negligible. It would be interesting to carry out long term measurements of VOC to determine how rare such events are and what sort of impact they could have on photochemical ozone production were they to occur during the daytime.

7 Speciating HO₂ and SR_iO₂ with PERCA

7.1 Introduction

7.1.1 Why speciate HO₂ and SR_iO₂?

Peroxy radicals are intermediates in the photochemical oxidation of organic species in the atmosphere and in the production and loss of ozone (Chapter 1, this work and e.g. [Monks, 2005]). Knowledge of the ratio of HO₂ to SR_iO₂, along with concentrations of other gaseous species as well as photolysis frequencies and temperature, can allow a calculation of radical budgets, providing a link between O₃ precursor VOCs and *in situ* O₃ production (see Chapter X, this work).

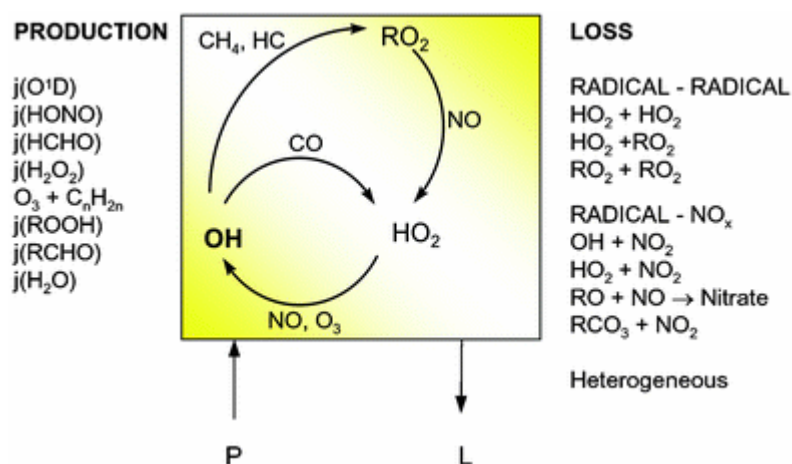


Figure 7.1 Schematic representation of radical cycling (from [Monks, 2005])

An increase in the complexity of non-methane VOCs leads to an increase in complexity of organic peroxy radicals. The fate of many RO₂ is conversion to HO₂ [Monks, 2005] so an increase in SR_iO₂ mixing ratio does not necessarily lead to an increase in the SR_iO₂:HO₂ ratio.

7.1.2 Measurements of ΣR_iO₂ and HO₂ – past and present

At present, the UK has no single instrument capable of measuring HO₂ and ΣR_iO₂ separately. The sum of the two can be measured with a PERCA and HO₂ individually by the FAGE technique [Creasey, *et al.*, 1997]. Simply taking measured PERCA minus measured FAGE should result in a number for ΣR_iO₂. This involves taking the difference of two numbers that have systematic errors of 35%. This, however, has proved difficult in the past. The two instruments have been deployed on field campaigns together on several occasions (NAMBLEX, Ireland [Fleming, *et al.*, 2006]; PUMA, Birmingham [Emmerson, *et al.*, 2005a]; TORCH 1, Writtle; TORCH 2, Weybourne; SOAPEX, Cape Grim [Monks, *et al.*, 1998],[Sommariva, *et al.*, 2004]). Several factors have led to the measurements from the two instruments to be incomparable. Firstly, it is not always possible to locate the instruments suitably close to each other thus measurements can be affected by small scale turbulence. Also, distance of the inlets above the ground can be significant as modelling studies have shown that chemistry in the stable nocturnal boundary layer is height dependent [Geyer and Stutz, 2004]. Secondly, PERCA chain lengths decrease with increasing relative humidity, causing measured radical mixing ratios to be lower than real values and this has only been recently quantified [Salisbury, *et al.*, 2002]. Thirdly, the instruments are calibrated using different techniques and different peroxy radicals: PERCA with CH₃O₂ generated by photolysis of CH₃I and FAGE with HO₂ generated by photolysis of water. The sensitivity of PERCA to a number of different peroxy radicals was investigated by [Ashbourn, *et al.*, 1998] and they found PERCA to be more sensitive to CH₃O₂ than HO₂ because of heterogeneous losses of HO₂ in the pre-inlet region ($\gamma_{\text{CH}_3\text{O}_2} = 1.1\gamma_{\text{HO}_2}$, where γ is yield of HO₂). Therefore the chainlength could be affected differently at night when the ratio of HO₂ to organic peroxy radicals is lower than in the daytime.

Another instrument that has been deployed successfully in field experiments for the measurement of speciated peroxy radicals is MIESR, (Matrix Ionisation Electron Spin Resonance, *c.f.* section 2.12), which measures CH₃O₂, HO₂ and CH₃C(O)O₂ separately [Mihelcic, *et al.*, 1985], as well as measuring NO₃ and NO₂. The main advantage, apart from its specificity, is that it is a direct technique and has small systematic errors of 5%. The main disadvantages of this method are that one sample takes 30 minutes to collect and then one day to run one spectrum, i.e., work up one data point. More crucially, however, at the time of writing this thesis the only operator of the only field MIESR is now in retirement along with the instrument. A further field instrument that can differentiate between HO₂ and ΣR_iO₂ is PerCIMS (Peroxy radical chemical ionisation mass spectrometer, *cf* section 2.x) also known as RoxMas (RO_x measurement by mass spectrometry) in Germany. PerCIMS can be run in HO₂ only mode or in total peroxy radical mode. By increasing substantially the concentration of reagent gases (SO₂ and NO) added to the sampled air, the RO₂ to HSO₄⁻ conversion (equation 2.x) is disfavoured leading to measurement of HO₂ only.

7.1.3 Separate measurement with a PERCA

One advantage of having one instrument for the separate measurement of HO₂ and organic peroxy radicals is the comparability of the measurements i.e., the data points occur at exactly the same time, the same detection method is used so systematic errors will be in the same direction and magnitude for both measurements. The same volume of air will be sampled.

There are several possibilities for using PERCA to make such measurements:

- (i) denuding the HO₂ before it gets to the reaction zone, thus only ΣR_iO₂ is converted to NO₂ and subsequently measured,
- (ii) denuding the ΣR_iO₂ in a similar fashion,

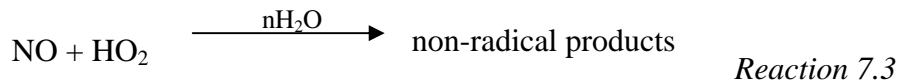
- (iii) changing the concentration of inlet reagents (as is the method for PerCIMS, see Section 2.1.1) so that conditions disfavour the conversion of RO₂ to HO₂.
- (iv) Lastly, either the organic or inorganic radicals could be removed by chemical reaction with a species added in a pre-inlet.

Option (iv) would be difficult owing to the similar chemistry displayed by both organic and inorganic peroxy radicals [Lightfoot, *et al.*, 1992]. Option (iii) is a possibility although the inlet reagents have been optimised to maximise the chain length so any change is likely to reduce the instrument sensitivity. It has been shown [Carpenter, *et al.*, 1997] that CH₃O₂ can be passed down a piece of ¼" OD PFA tubing with virtually no losses and also that HO₂ is preferentially lost (over ΣR_iO₂) in the pre-inlet, i.e. in the section of the inlet that leads to the reaction zone. [Mihele and Hastie, 1998], report a loss rate of 2.8 s⁻¹ for HO₂ and 0.8 s⁻¹ for CH₃O₂, also for ¼" OD PFA tubing. The factor of three in loss rate is attributed to the lower polarity of CH₃O₂. Also, HO₂ is preferentially lost on the walls of the inlet as humidity increases [Mihele and Hastie, 1998]. HO₂ loss increases by a factor of 2 from dry air to a relative humidity of 40%. In contrast, the organic peroxy radicals showed almost no sensitivity to water up to 70% relative humidity. Initial work done on a chemical amplifier [Cantrell, *et al.*, 1984] calculated an HO₂ wall loss of 0.35 s⁻¹ for glass (dimensions not stated) increasing to 0.85 s⁻¹ for glass coated with NaOH.

Several studies, however, concluded that wall losses were not the only reason for the water effect. [Mihele, *et al.*, 1999] proposed a termolecular reaction (Reaction 7.1) after modelling of the amplification chemistry including calculated wall losses under predicted the effect of humidity on chain length from measurements.



[Reichert, *et al.*, 2003] proposed gas phase reactions involving water dimers to explain the reduced chain length at water (Reactions 7.2 and 7.3).



This was because of the observed quadratic dependence of the loss rate on the relative humidity for a linear increase in [H₂O].

Therefore a pre-inlet of a certain length could be used to denude HO₂ preferentially over ΣR_iO₂. The dimensions and form of the pre-inlet extension are discussed in section 7.2.3.

7.2 Equipment for Denuding HO₂

7.2.1 PERCA

The ULeic/UEA Perca 4 (described in Chapter 2) was used for the HO₂ denuding experiments and deployed in the field in an attempt to measure HO₂ and ΣR_iO₂ separately. To measure the concentration of the sum of peroxy radicals, the instrument runs in dual channel mode. The instrument had built in redundancy for a further two inlets, and was modified to fit an extra inlet so that operation in the field as a dual channel instrument could continue whilst being able to measure ΣR_iO₂ with the third inlet. For the laboratory experiments only one inlet was used.

7.2.2 HO₂ source

At present, the Leicester-UEA PERCA chain length is calibrated with a source of CH₃O₂ produced by the photolysis of CH₃I and subsequent reaction of the CH₃ radical with O₂ [Clemishaw, *et al.*, 1997]. In order to determine the rate of denuding, a method of generating HO₂ radicals was required. A number of ways of producing HO₂ have been and are being used to calibrate various radical detectors (see chapter 2, section x). These include:

- (i) water photolysis at 184.9 nm [Schultz, *et al.*, 1995],
- (ii) ozonolysis of alkenes [Hard, *et al.*, 2002],
- (iii) photolysis of a mixture of H₂, Cl₂ and O₂, [Hastie, *et al.*, 1991],
- (iv) photolysis of O₃ in the presence of water [Eisele and Tanner, 1991],
- (v) thermolysis of H₂O₂ on a hot wire [Cantrell, *et al.*, 1993b].

For this work it was decided to build a HO₂ source based on the photolysis of water at $\lambda = 184.9$ nm (the emission line of mercury from a mercury argon penray lamp) as first described by [Schultz, *et al.*, 1995] (Figure 7.2).

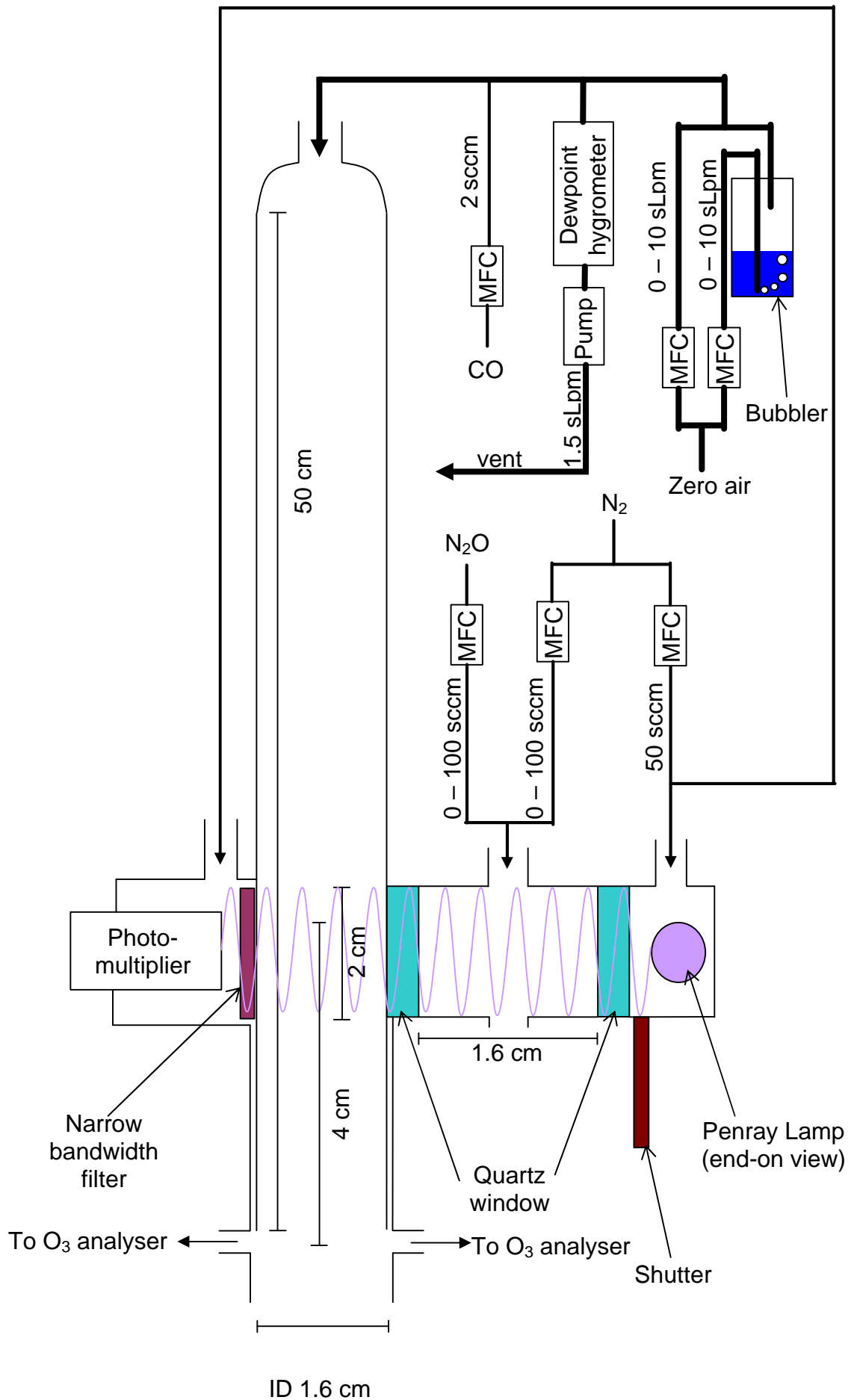
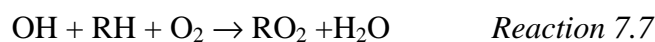


Figure 7.2 A schematic representation of the HO_2 source used in this work

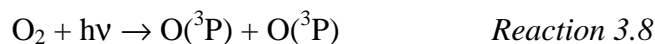
The source produces HO₂ by photolysing water (Reaction 7.4), quickly followed by addition of O₂ (Reaction 3.5) to form HO₂.



CO can also be added to convert OH to H (Reaction 7.6), followed by conversion to HO₂ (Reaction 7.5). Alternatively, a hydrocarbon can be added to create an organic peroxy radical (Reaction 7.7).



At the same time O₂ is photolysed and ozone produced (Reaction 7.8)



Thus, two HO₂ radicals are formed for every H₂O molecule photolysed and two molecules of ozone are formed for every O₂ photolysed. The system works as a chemical actinometer such that [O₃] produced is proportional to [HO₂].

$$P_{HO_2} = \mathbf{s}_{H_2O}^{185} \cdot q_1^{185} \cdot \Theta^{185} \quad \text{Equation 7.1}$$

$$P_{O_3} = \mathbf{s}_{H_2O}^{185} \cdot q_4^{185} \cdot \Theta^{185} \quad \text{Equation 7.2}$$

P = production

\mathbf{s}^{185} = absorption cross section at 185 nm

q^{185} = quantum yield at 185 nm

Θ^{185} = photon flux at 185 nm

As the photon flux for the production of ozone is equal to that for HO₂, these terms cancel out and so the mixing ratios of OH and HO₂ can be determined from the measurements of ozone, water and molecular oxygen and absorption cross sections and quantum yields for ozone and HO₂ (Equation 7.3).

$$[OH] = [HO_2] = \frac{[O_3][H_2O]\mathbf{s}_{185nm(H_2O)}\mathbf{f}_{HO_2}}{[O_2]\mathbf{s}_{185nm(O_2)}\mathbf{f}_{O_3}} \quad \text{Equation 7.3}$$

7.2.2.1 HO₂ Source Construction

Zero air of varying humidities is flowed at typically 4.5 sLpm down a quartz tube of inner diameter 16 mm (Figure 7.1) and length 50cm. The length of the tube is important in determining whether the flow is laminar (smooth) or turbulent.

$$R = \rho \cdot V \cdot D / \mu \quad \text{Equation 7.4}$$

Where ρ = density of air = 1.229 kg m⁻³, V = velocity of flow = 0.37 m s⁻¹, D = diameter of tube = 0.016 m, μ = 1.73 × 10⁻⁵ kg m⁻¹ s⁻¹, $R = (1.229 \times 0.37 \times 0.016) / 1.73 \times 10^{-5} = 421$

$$U = 0.035 \cdot D \cdot R \text{ (e.g. [Bird, 1960])} \quad \text{Equation 7.5}$$

Where U = length above which flow changes from turbulent to laminar, D = diameter of tube, R = Reynolds number. Solving Equation 3.5 for the tube used in this work gives a U of 24 cm, which is well below the length of the flow tube, i.e., laminar flow conditions prevail.

7.2.2.2 HO₂ source characterisation

7.2.2.2.1 Oxygen cross section

The O₂ absorption spectrum is highly structured near 184.9 nm, band (8,0) of the Schumann-Runge bands [Yoshino, *et al.*, 1983](Figure 7.3). Thus, the O₂ cross-section can be significantly affected by variation in lamp envelope emission spectrum, which is a function of O₂ column, lamp current and temperature [Creasey, *et al.*, 2002]. The power supply for the lamp was non-variable AC so the current is fixed for all calibrations and temperature is held roughly constant (but not measured) by flowing 50 sccm N₂ over the lamp. O₂ column is assumed to be the distance between the edge and the centre of the field calibration flow tube (i.e. the radius), which is 0.8cm, giving a column of 3.95 × 10¹⁸ molecule cm⁻².

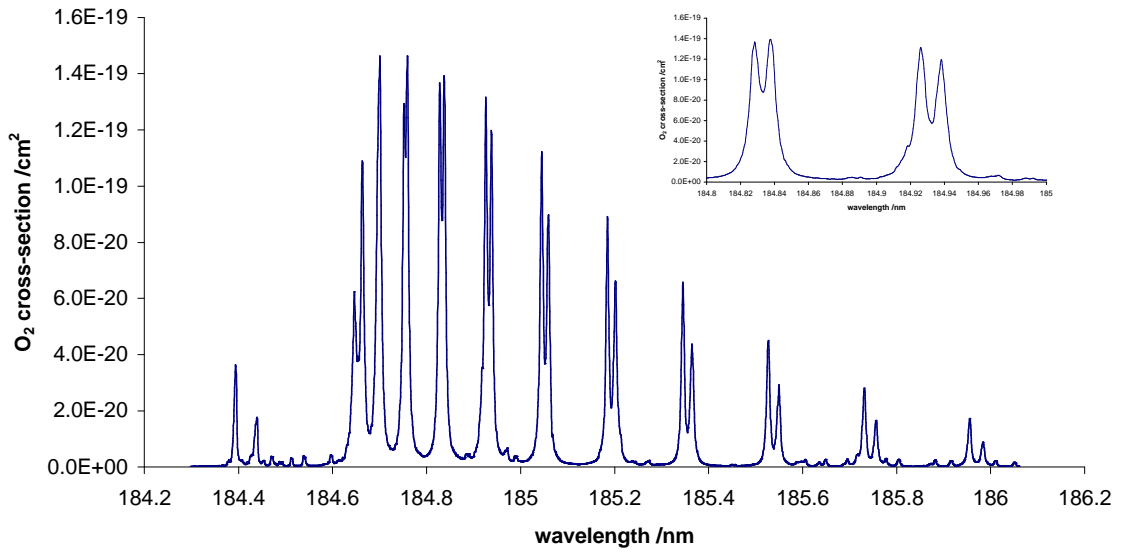


Figure 7.3 The O₂ absorption spectrum centred at 185 nm (Data from[Yoshino, et al., 1983])

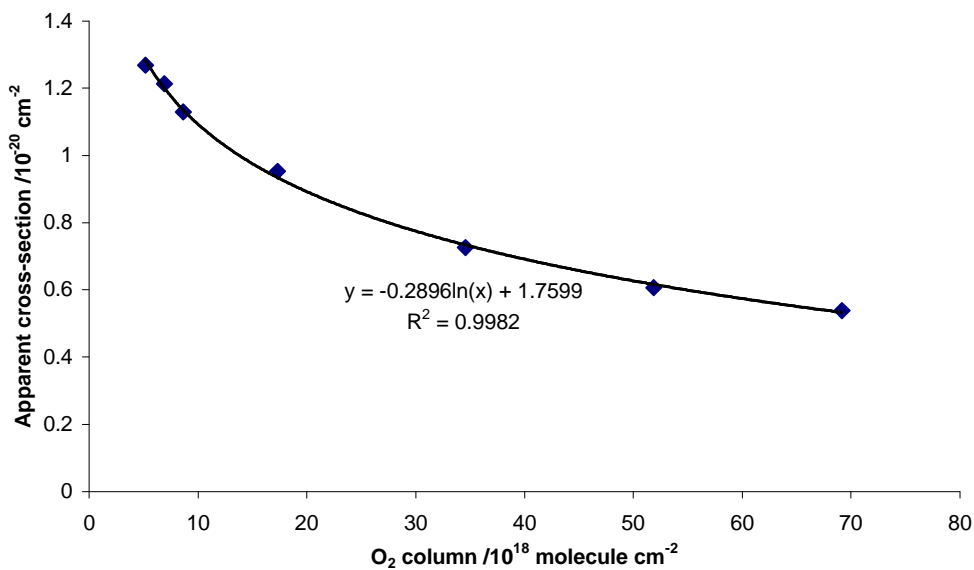


Figure 7.4 Apparent cross section

7.2.2.2.2 Water cross section

The absorption cross section of water vapour at 184.9 nm is part of a broad peak at 165 nm which has no structure but decreases logarithmically above 180 nm at about 5% per 0.1 nm [Cantrell, et al., 1997c], [Watanabe and Zelikoff, 1953]). The value used in this work, $(7.14 \pm 0.2) \times 10^{-20} \text{ cm}^2 \text{ molecule}^{-1}$ at 25°C at 184.9 nm, is that of [Cantrell, et al., 1997c]. Other

recent measurements are within experimental error of the selected value: [Hofzumahaus, *et al.*, 1997], $7 \times 10^{-20} \text{ cm}^{-2} \text{ molecule}^{-1}$; [Creasey, *et al.*, 2000], $(7.22 \pm 0.22) \times 10^{-20} \text{ cm}^{-2} \text{ molecule}^{-1}$.

7.2.2.2.3 O₃ Sampling point

Ozone was measured through the overflow (see Figure 7.1), consisting of 4 holes each of diameter 3 mm spaced evenly around the end of the flow tube and also at the centre of the flow using tubing of 1/8" internal diameter, i.e., the central 3 mm of the flow was sampled. O₃ at the edge was found to be 1.4 times that of O₃ sampled at the centre. There are several reasons for this: first under conditions of laminar flow, air at the centre of the tube is moving faster than air at the edge, thus time exposed to lamp radiation is less, therefore less O₂ is photolysed leading to smaller O₃ production. Another factor is the inhomogeneity of the lamp flux, which is greater on the side of the tube where the lamp is than in the middle or on the other side. A further factor is that the overflow does not come out evenly through the four holes, (Wilkinson, personal communication, 2005) The ozone profile of a flow tube of similar internal diameter (1.5 cm as opposed to 1.6 cm as used in this work) was determined by [Stöbener, 1999]. He measured a difference of 9.6 ppbv between maximum and minimum ozone concentrations in a cross section of the flow tube by sampling in millimetre steps through a glass tube of 4 mm internal diameter.

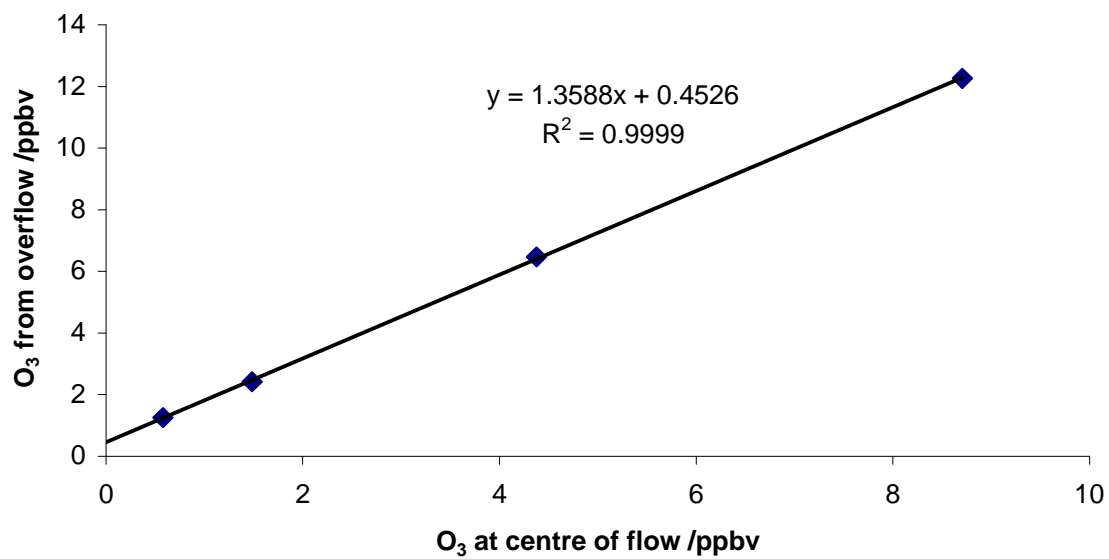


Figure 7.5 Comparison of O₃ at centre of flow versus overflow, both measured with a TECO 49C ozone analyser

7.2.2.2.4 Measurement methods

Three methods of measuring O₃ were considered, one direct (commercial ozone analyser) and two indirect (photomultiplier tube and PERCA background signal). The first method involves sampling an overflow from the HO₂ source (see Figure 3.2).

Method	Advantages	Disadvantages
Commercial O ₃ analyser TECO 49C, Environmental instruments	Direct spectroscopic measurement	Detection limit 1 ppbv Resolution 1 ppbv Max frequency 10 s
Photomultiplier tube (Hamamatsu R374)	Fast response	Not absolute (unless calibrated)
PERCA	Samples whole cross section of flow tube 1 Hz frequency	Indirect method

Table 7.1 O₃ measurement methods

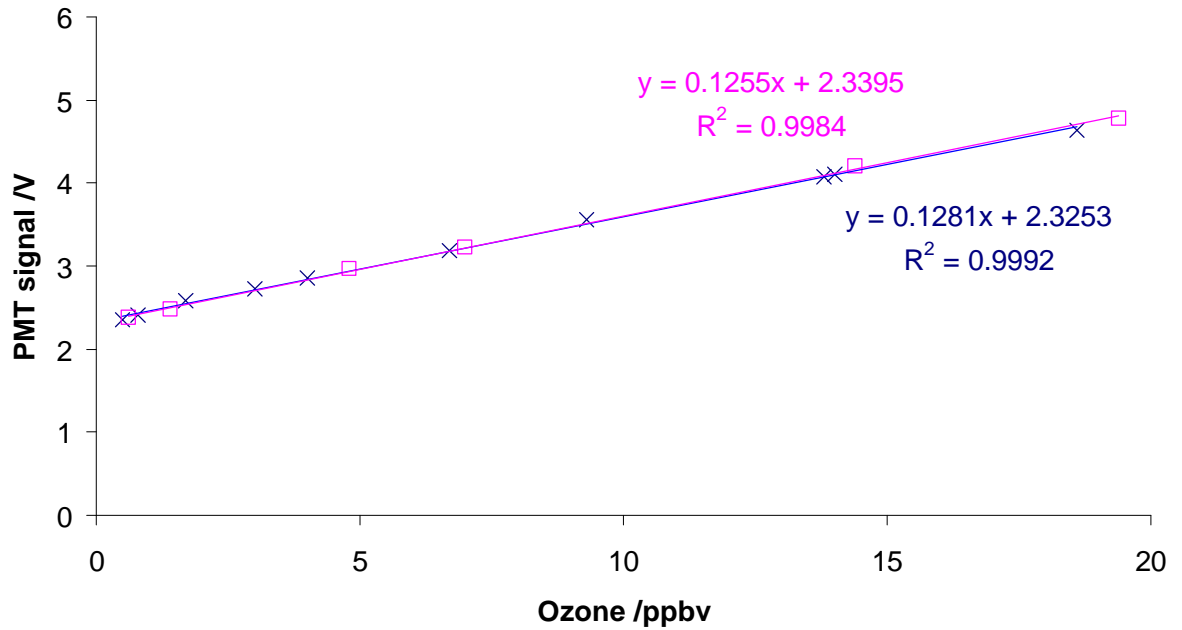


Figure 7.6 Comparison of ozone mixing ratio as measured through side arm overflow and PMT signal, a measure of lamp flux at a wavelength of 185 nm. The pink squares are points where the humidity of the air flow was -17.5°C (1290ppmv). The blue crosses are points where the humidity of the air flow was -0.4°C (5830ppmv).

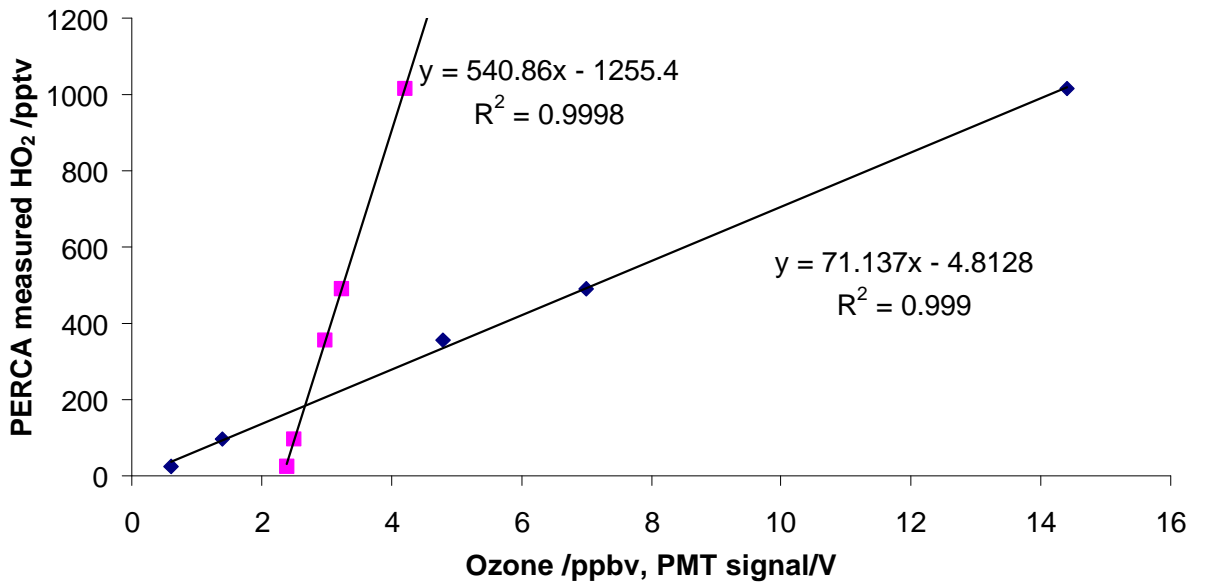


Figure 7.7 Measured HO₂ vs ozone and PMT signal

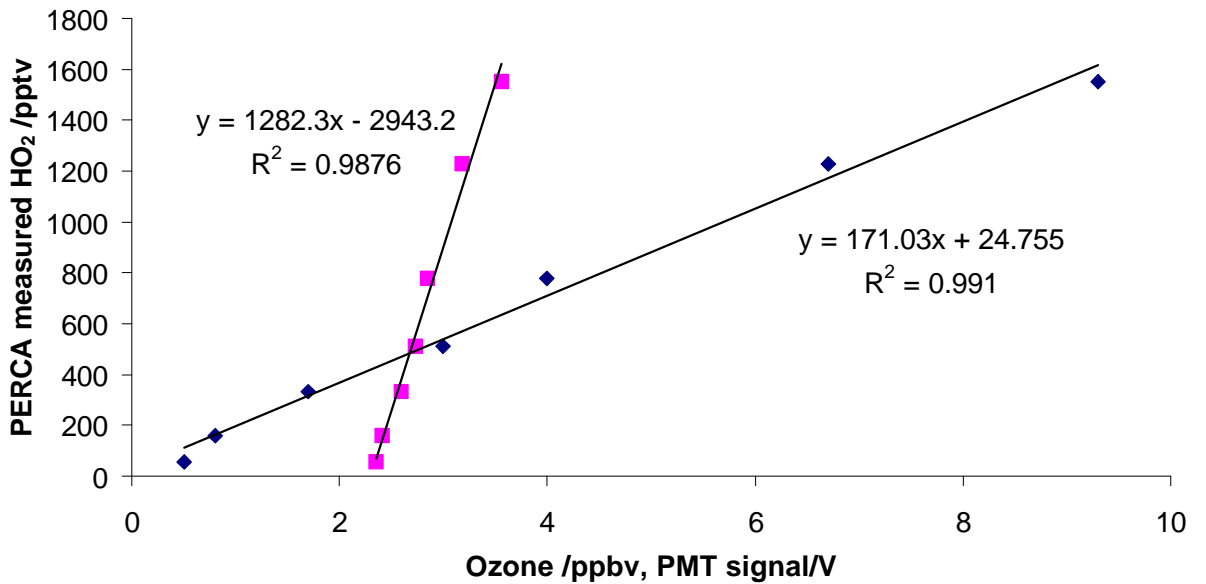


Figure 7.8 Measured HO₂ vs ozone and PMT signal

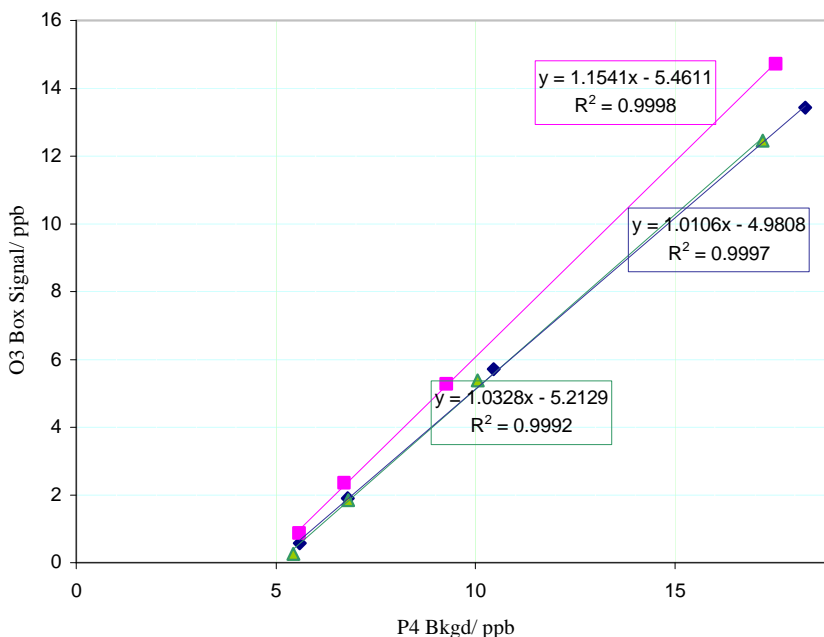


Figure 7.9 Comparison of O₃ measured by TECO 49 (y axis) and calculated from the PERCA background signal (x axis). Green triangles are for air flow of dew point = -10°C, blue diamonds for dew point = -20°C and pink squares for dew point = -30°C.

Good agreement was obtained between O₃ calculated from PERCA background signal – assuming O₃ reacts totally with NO to give NO₂ – with a small offset of around 5 ppbv representing the detector offset. The agreement between the two methods for -30°C dew point is not so good, with the ozone box reading 15% higher than PERCA background. Further experiments would need to be carried out at more humidities to establish whether this is a real effect or if the result of a slight shift in detector sensitivity owing to, for example, a slight change in luminol flow rate.

The photomultiplier tube (PMT) shows good agreement with both the commercial O₃ analyser and the PERCA background signal. It could be especially useful at low O₃ concentrations (i.e. mixing ratio of ozone < 1 ppbv) where the commercial analyser displays a negative value. The problem experienced with the PMT was that plotting data against the O₃ analyser gives a

different slope each time it was used even though none of the settings, such as voltage from the high voltage power supply, were changed. It was also not possible to log the PMT output signal on the PERCA analogue input card as the signal did not change when lamp flux was changed. The PMT output, monitored with an oscilloscope, was found to be wavelike, i.e. not constant (see Figure 7.10) and this is due to the lamp being powered by an AC supply.

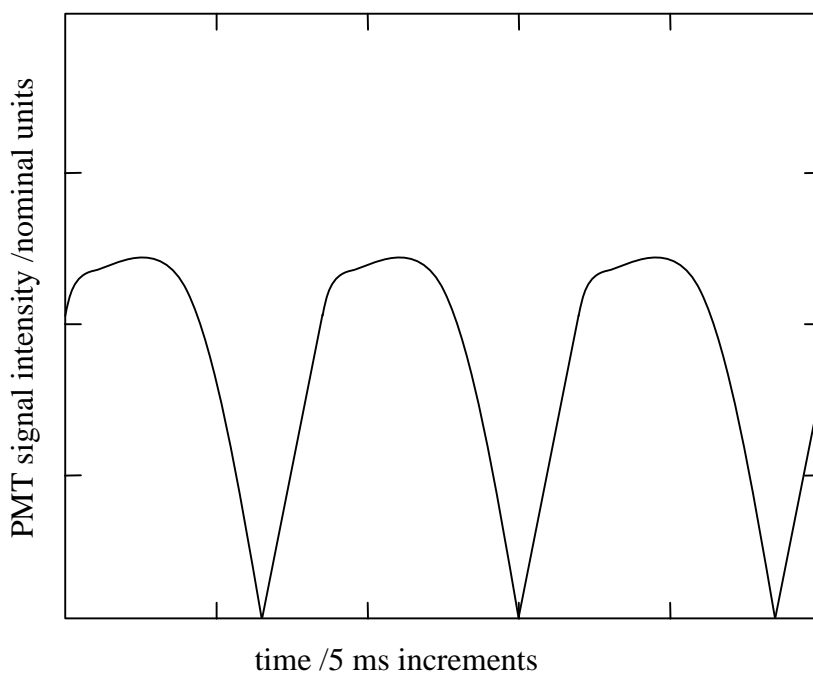


Figure 7.10 Signal from PMT exposed to mercury pen ray lamp powered by AC current supply (Oriel LSP060, after data sheet from LOT-Oriel). A similar signal was observed in the lab on an oscilloscope (see text)

7.2.2.2.5 Humidity generation

Zero air was passed through two mass flow controllers (10 slpm maximum flow) one directly through a water bubbler, the other in bypass. Total flow was kept typically at 6 slpm with 1.5 slpm going to a chilled mirror dew point hygrometer (General Easton 1131DR). Flow to the flow tube was therefore 4.5 slpm. The water reservoir was held at a constant temperature of 25°C to aid the reproducibility of air flow settings in maintaining a dew point.

7.2.3 Comparison of HO₂ source and CH₃O₂ source

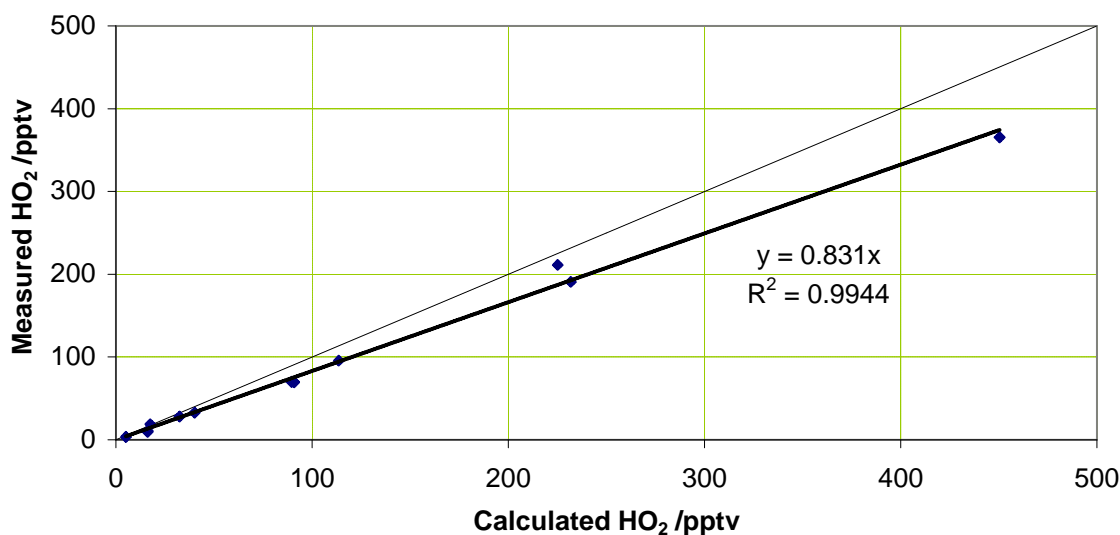


Figure 7.11 Calibration using both HO₂ source and CH₃O₂ source (18th July 2005)

This comparison takes into account self-losses occurring in the region between the point of photolysis and the reaction zone of the PERCA inlet. As this is proportional to the square of HO₂ mixing ratios, it is more significant at higher mixing ratios, i.e. 12% at 500 pptv compared to 2.4% at 100 pptv. The chain length used in the measured HO₂ has been corrected for humidity as the radicals were generated at dew points of -10°C, -20°C, -30°C. [Ashbourn, *et al.*, 1998] found a similar instrument (in fact a predecessor of the instrument

used in this work, using a similar inlet design) detected CH₃O₂ preferentially to HO₂ in a ratio of 1.13 : 1. This was explained by greater wall losses of HO₂ compared to losses of CH₃O₂ in the pre-inlet region and the side-arm joining the radical source to the pre-inlet. Taking this into account brings the measured to 93% of calculated instead of 83%, which is well within experimental error of 35%. [Ashbourn, *et al.*, 1998] also noted an increase in detection of HO₂ when increasing relative humidity from 0 to 20% explained by preferential adsorption of H₂O on the pyrex inlet. This seems to contradict other work [Salisbury, *et al.*, 2002], [Mihele and Hastie, 1998], that register a decrease in radical detection with increasing humidity.

7.3 Determination of loss rates for HO₂ and CH₃O₂

7.3.1 Inlet extension

The chosen method of separation of HO₂ from organic peroxy radicals was removal of HO₂ from the air sample by extending the length of the pre-inlet by 30 cm (Figure 7.12). Taking the loss rate of HO₂ through PFA tubing as 2.8 s⁻¹, it would be expected that 99.32 % of HO₂ to be lost in the extended pre-inlet,

$$\text{volume of pre-inlet} = 60 \text{ cm}^3, \text{ inlet flow} = 33 \text{ cm}^3 \text{ s}^{-1}$$

$$\Rightarrow \text{transit time, } t \approx 1.78 \text{ s. } k_{\text{loss}} = 2.8 = \ln([\text{HO}_2]_{\text{in}}/[\text{HO}_2]_{\text{out}})/t$$

$$\Rightarrow [\text{HO}_2]_{\text{in}}/[\text{HO}_2]_{\text{out}} = 146, [\text{HO}_2]_{\text{out}} = 0.0068[\text{HO}_2]_{\text{in}}$$

assuming that the loss rate through the tubing is the same as that through the glass inlet extension.

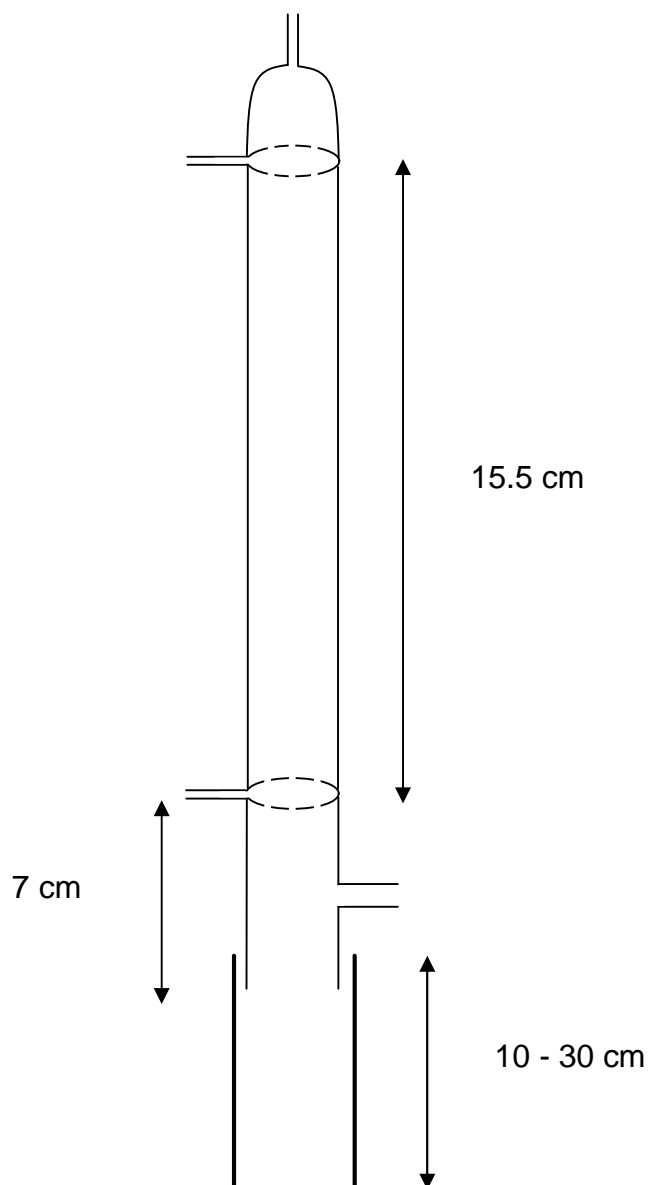


Figure 7.12 Inlet extension (see text)

7.3.2 Loss rates through glass extensions

This compares to 0.74 s^{-1} for $k_{loss}(\text{HO}_2)$ on glass. Experiments to deduce $k_{loss}(\text{CH}_3\text{O}_2)$ for glass were inconclusive.

7.3.3 Loss rates through metal extensions

A similar experiment was carried out replacing the glass extension with one of steel, the only other difference being a diameter of 2.1 cm instead of 1.6 cm. Three mixing ratios of CH₃O₂ and three of HO₂ were flowed through metal extensions of length 10, 20 and 30 cm and with no extension. Rate losses for each extension length at each radical mixing ratio are summarised in Tables 7.2 and 7.3. For both HO₂ and CH₃O₂ it was found that the 20 cm and 30 cm extensions average k_{losses} were within 5% of each other. For the 10 cm extension for HO₂ k_{loss} was negative and CH₃O₂ k_{loss} was over 20% more than for the longer extensions. The 10cm extension could affect the flow characteristics of the inlet. Taking the values from the 20 cm and 30 cm extensions, $k_{loss}(\text{HO}_2)$ and $k_{loss}(\text{CH}_3\text{O}_2)$ are $0.63 \pm 0.03 \text{ s}^{-1}$ and $0.096 \pm 0.021 \text{ s}^{-1}$ respectively. This compares to 0.74 s^{-1} for $k_{loss}(\text{HO}_2)$ on glass. Experiments to deduce $k_{loss}(\text{CH}_3\text{O}_2)$ for glass were inconclusive.

Extension	$k_{\text{loss}} \text{ s}^{-1}$			Average	
	for three HO ₂ mixing ratios			s ⁻¹	σ
	390 pptv	110 pptv	30 pptv		
10 cm	0.825991	1.089528	0.563906	0.83	0.262867
20 cm	0.621962	0.674096	0.63115	0.64	0.027835
30 cm	0.582274	0.638918	0.615529	0.61	0.028471

Table 7.2 k_{loss} steel HO₂ at dew point = 0°C

Extension	$k_{\text{loss}} \text{ s}^{-1}$			Average	
	for three CH ₃ O ₂ mixing ratios			s ⁻¹	σ
	120 pptv	90 pptv	60 pptv		
10 cm	-0.12939	-0.00235	0.104332	-0.0091	0.117
20 cm	0.081695	0.09971	0.107632	0.096	0.013
30 cm	0.060642	0.106146	0.118164	0.095	0.030

Table 7.3 k_{loss} steel CH₃O₂ in dry air

7.3.4 Modifications to extension

In order to increase the effectiveness of the extension to denude HO₂, varying numbers of lengths of PFA tubing (1/4" OD, 1/8" ID) were added to the inlet. Each piece of tubing of length approximately 30 cm adds 88 cm² surface area to the denuder whilst at the same time removing 7 cm³ from the volume of the extension thus decreasing the residence time.

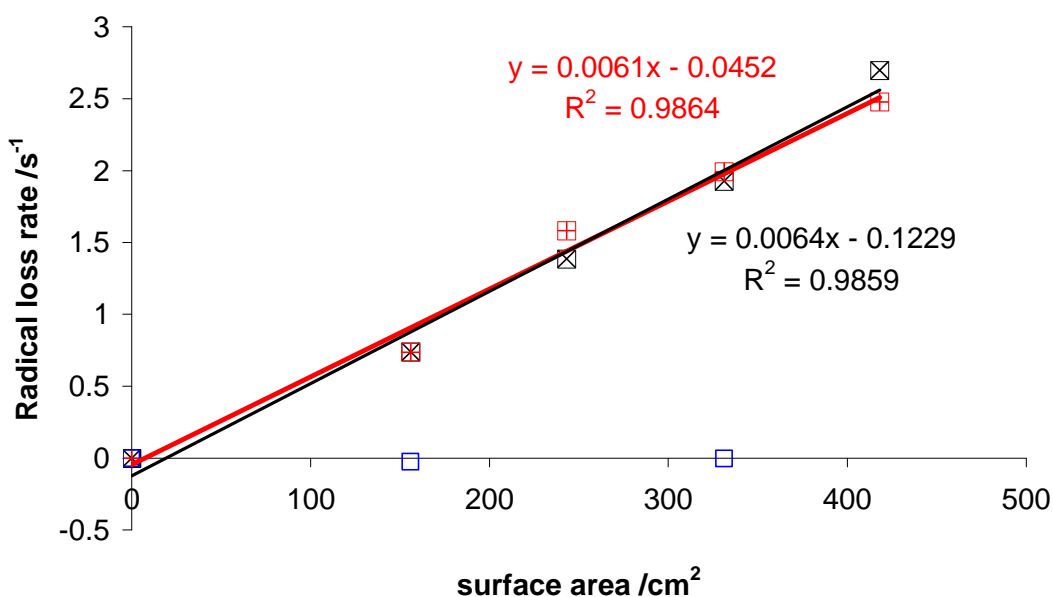


Figure 7.13 Effect of internal surface area of of 30cm glass denuder on HO₂ and CH₃O₂ loss rat. Blue squares are k_{loss} for CH₃O₂, red plus signs are k_{loss} for HO₂ on 14th July 2005 and black crosses k_{loss} for HO₂ on 15th July 2005.

7.4 An attempt to measure both HO₂ and RO₂ in ambient air

An inlet with a glass extension of 30cm was deployed in the TORCH 1 field campaign in Writtle, Essex, 25 miles north-east of central London (see Chapter 3). For the first eight days that PERCA was running, the inlet with extension was operating in amplification mode only. The intention was to calculate the background from a combination of the original two inlets. This, however, proved difficult as the background signal is typically two orders of magnitude greater than the signal from the peroxy radicals. On the ninth day, the instrument control program was modified to switch the reagent gases, CO and N₂ (see Chapter 2) in phase with inlet 2 and out of phase with inlet 1. This offers the possibility of combining inlet 3 with inlet 1 to have a dual inlet peroxy radical measurement. Data can also be worked up in single inlet mode, i.e. two channels measuring HO₂ + ? R_iO₂ and the other measuring ? R_iO₂ only. Data from 13th to 30th August 2003 were analysed using both the single channel and the dual channel work up. The mixing ratios for the inlet with the extension were if anything systematically higher than those with no extension, i.e. a negative HO₂ mixing ratio, which is clearly not right.

7.4.1 Calculation of HO₂

Two approaches can be taken to calculate HO₂ mixing ratio from the three inlets:

- (i) The big difference is that inlet 1 is measuring HO₂ + SR_iO₂ whereas inlet 3 is measuring (1-m)HO₂ + (1-n)SR_iO₂

m = fraction of HO₂ lost in extra length of third inlet, 0 = m = 1

n = fraction of SR_iO₂ lost in extra length of third inlet, 0 = n = 1

$$[\text{RO}_x] = [\text{HO}_2] + [\text{RO}_2] + [\text{OH}] + [\text{RO}] \sim [\text{HO}_2] + [\text{RO}_2]$$

since [HO₂] + [RO₂] >> [OH] + [RO]

$$[\text{RO}_x] = \text{inlets (1,2)}$$

$$[\text{HO}_2] = \{\text{inlets (1,2)} - \text{inlets (1,3)}\} * 2$$

$$[\text{RO}_2] = [\text{RO}_x] - [\text{HO}_2]$$

$$= \text{inlets (1,2)} - \{\text{inlets (1,2)} - \text{inlets (1,3)}\} * 2$$

Characterisation experiments using the HO₂ source will determine values for m and n.

Why did the denuder not work in the field?

- (i) mixing ratios of HO₂ are much lower than those of RO₂
- (ii) ambient conditions affect the ability of the inlet extension to denude, e.g.:
 - a. humidity
 - b. temperature
 - c. HO₂ formation in the inlet extension
- (iii) Systematic differences in the three channels are large enough to mask the differences between totals peroxy radical concentration and SR_iO₂.

7.5 Chapter 7 summary

This chapter discusses the history and usefulness of separate measurements of HO₂ and SR_iO₂. It presents results of laboratory experiments to modify a chemical amplifier in order to make separate but simultaneous measurements of HO₂ and SR_iO₂ as well as presenting details of the HO₂ source constructed to carry out the experiments and used for field calibration of the PERCA instrument. The method chosen in order to separate the inorganic and sum of organic radicals is to preferentially denude HO₂ from the sampled air using a glass or metal inlet extension, thus leaving SR_iO₂ to be measured. Another channel measures total peroxy radical mixing ratio so individual mixing ratios of HO₂ and SR_iO₂ can be calculated.

First order rate constants for the denuding of HO₂ and CH₃O₂ were determined: $k_{\text{metal}}(\text{HO}_2)$ and $k_{\text{metal}}(\text{CH}_3\text{O}_2)$ were 0.63 s⁻¹ and 0.096 s⁻¹ respectively and $k_{\text{glass}}(\text{HO}_2)$ 0.74 s⁻¹ while experiments to deduce $k_{\text{glass}}(\text{CH}_3\text{O}_2)$ were inconclusive, i.e. losses were too small to be measured with the equipment available. Increasing the surface area of the glass denuder by inserting up to four lengths of PFA tubing led to loss rates for HO₂ of up to 2.8 s⁻¹. Loss rate was proportional to surface area for the first three additions of tubing, after which it decreased, possibly owing to flow characteristics of the denuder.

As expected, the loss rate for HO₂ was significantly greater than that for CH₃O₂, supporting the possibility of using this method in the field. However, analysis of data from deployment of the system at the TORCH campaign in summer 2003 was inconclusive. Unlike in the laboratory, ambient conditions are highly variable in temperature, humidity and chemical composition, all of which potentially affect the denuding rates of both HO₂ and SR_iO₂.

8 Conclusions and Further Research

Measurements of a peroxy radicals and a range of other compounds and meteorological parameters were made in a semi-rural location in the vicinity of London in August 2003. This coincided with a heat wave across much of Europe including the UK with temperatures exceeding 38°C in the South of England. Average afternoon peroxy radical mixing ratios during the period of high temperatures were 80 pptv, a factor of two greater than outside it. The highest value recorded was 120 pptv on the afternoon of August 6th. Concentrations of ozone as well as of other secondary photochemical products were also higher during the heat wave. The significance of the peroxy radical mixing ratios with respect to high ozone levels will be discussed as will the context and consequences of the high ozone levels.

A photostationary steady state analysis was carried out also predicting enhanced peroxy radical mixing ratios during the heat wave.

An investigation of the sources and sinks of ROx was carried out and suggested that during the heat wave PAN thermolysis was a greater source of ROX than primary production via photolysis of ozone and subsequent reaction with water. A correlation of isoprene and PAN production suggests isoprene as a source for PAN and therefore also for peroxy radicals and ultimately ozone.

A comparison of P(O₃) with hour on hour actual change in ozone mixing ratio also seems to correlate rather well for the heat wave period.

During the TORCH II campaign at Weybourne, on the Norfolk coast of the East of England in the evening of the 10th May there was an unusual event during which peroxy radical concentration suddenly rose to values in excess of 50 pptv. At about 20:00 GMT, with photochemical radical production negligible, this amounted to four times the midday maximum. The event was correlated with enhanced CO, acetaldehyde and HCHO (increases of 5.8, 14.6, and 7.1 ppbv respectively) and a drop in ozone of 13.52 ppbv (all values are hourly averages). At the same time the alkene loading rose to 144 ppbv, mostly owing to propene exceeding values of 143 ppbv. The rise in propene is indicative of Weybourne being influenced by emissions from the oil and natural gas industries in the North Sea. The increase in CO and carbonyl compounds and the decrease in ozone provides dramatic evidence for the potential of ozone-alkene reactions to produce peroxy radicals and initiate oxidation in the atmosphere.

This chapter discusses the history and usefulness of separate measurements of HO₂ and SR_iO₂. It presents results of laboratory experiments to modify a chemical amplifier in order to make separate but simultaneous measurements of HO₂ and SR_iO₂ as well as presenting details of the HO₂ source constructed to carry out the experiments and used for field calibration of the PERCA instrument. The method chosen in order to separate the inorganic and sum of organic radicals is to preferentially denude HO₂ from the sampled air using a glass or metal inlet extension, thus leaving SR_iO₂ to be measured. Another channel measures total peroxy radical mixing ratio so individual mixing ratios of HO₂ and SR_iO₂ can be calculated.

First order rate constants for the denuding of HO₂ and CH₃O₂ were determined: $k_{\text{metal}}(\text{HO}_2)$ and (CH_3O_2) were 0.63 s⁻¹ and 0.096 s⁻¹ respectively and $k_{\text{glass}}(\text{HO}_2)$ 0.74 s⁻¹ while experiments to deduce $k_{\text{glass}}(\text{CH}_3\text{O}_2)$ were inconclusive, i.e. losses were too small to be measured with the equipment available. Increasing the surface area of the glass denuder by

inserting up to four lengths of PFA tubing led to loss rates for HO₂ of up to 2.8 s⁻¹. Loss rate was proportional to surface area for the first three additions of tubing, after which it decreased, possibly owing to flow characteristics of the denuder.

As expected, the loss rate for HO₂ was significantly greater than that for CH₃O₂, supporting the possibility of using this method in the field. However, analysis of data from deployment of the system at the TORCH campaign in summer 2003 was inconclusive. Unlike in the laboratory, ambient conditions are highly variable in temperature, humidity and chemical composition, all of which potentially affect the denuding rates of both HO₂ and SR_iO₂.

Abram, J. P., et al. (2000), Hydroxyl radical and ozone measurements in England during the solar eclipse of 11 August 1999, *Geophysical Research Letters*, 27, 3437-3440.

Alicke, B., et al. (2003), OH formation by HONO photolysis during the BERLIOZ experiment, *Journal of Geophysical Research-Atmospheres*, 108, art. no.-8247.

Arias, M. C., and D. R. Hastie (1996), Radical chemistry at the SONTOS site in rural Ontario, *Atmospheric Environment*, 30, 2167-2175.

Ashbourn, S. F. M., et al. (1998), Laboratory studies of the response of a peroxy radical chemical amplifier to HO₂ and a series of organic peroxy radicals, *Journal of Atmospheric Chemistry*, 29, 233-266.

Bird, R. B., Stewart, W.E., Lightfoot, E.N. (1960), *Transport Phenomena*, John Wiley & Sons, New York.

Black, E., Blackburn, M., Harrison, G., Hoskins, B., Methven, J. (2004), Factors contributing to the summer 2003 European heatwave, *Weather*, 59, 217 - 223.

Brune, W. H., et al. (1998), Airborne in-situ OH and HO₂ observations in the cloud-free troposphere and lower stratosphere during SUCCESS, *Geophysical Research Letters*, 25, 1701-1704.

Brune, W. H., et al. (1999), OH and HO₂ chemistry in the North Atlantic free troposphere, *Geophysical Research Letters*, 26, 3077-3080.

Calvert, J. G. (1976), Test of Theory of Ozone Generation in Los-Angeles Atmosphere, *Environmental Science & Technology*, 10, 248-256.

Cantrell, C. A., et al. (1992), Peroxy-Radicals in the Rose Experiment - Measurement and Theory, *Journal of Geophysical Research-Atmospheres*, 97, 20671-20686.

Cantrell, C. A., et al. (2003), Steady state free radical budgets and ozone photochemistry during TOPSE, *Journal of Geophysical Research-Atmospheres*, 108, art. no.-8361.

Cantrell, C. A., et al. (1996a), Peroxy radical chemistry during FIELDVOC 1993 in Brittany, France, *Atmospheric Environment*, 30, 3947-3957.

Cantrell, C. A., et al. (1995), Comparison of Peroxy Radical Concentrations at Several Contrasting Sites, *J. Atmos. Sci.*, 52, 3408-3412.

Cantrell, C. A., et al. (1996b), Dual-inlet chemical amplifier for atmospheric peroxy radical measurements, *Anal. Chem.*, 68, 4194-4199.

Cantrell, C. A., et al. (1997a), Some considerations of the origin of nighttime peroxy radicals observed in MLOPEX 2c, *Journal of Geophysical Research-Atmospheres*, 102, 15899-15913.

Cantrell, C. A., et al. (1997b), Peroxy radicals from photostationary state deviations and steady state calculations during the Tropospheric OH Photochemistry Experiment at Idaho Hill, Colorado, 1993, *Journal of Geophysical Research-Atmospheres*, 102, 6369-6378.

Cantrell, C. A., et al. (1996c), Peroxy radicals measured during Mauna Loa observatory photochemistry experiment 2: The data and first analysis, *Journal of Geophysical Research-Atmospheres*, 101, 14643-14652.

Cantrell, C. A., et al. (1996d), Peroxy radical concentrations measured and calculated from trace gas measurements in the Mauna Loa observatory photochemistry experiment 2, *Journal of Geophysical Research-Atmospheres*, 101, 14653-14664.

Cantrell, C. A., et al. (1993a), An Improved Chemical Amplifier Technique for Peroxy Radical Measurements, *Journal of Geophysical Research-Atmospheres*, 98, 2897-2909.

Cantrell, C. A., et al. (1993b), Measurement Methods for Peroxy-Radicals in the Atmosphere, *Advances in Chemistry Series*, 291-322.

Cantrell, C. A., et al. (1984), Measurement of Atmospheric Peroxy-Radicals by Chemical Amplification, *Anal. Chem.*, 56, 1496-1502.

Cantrell, C. A., et al. (1997c), Absorption cross sections for water vapor from 183 to 193 nm, *Geophysical Research Letters*, 24, 2195-2198.

Carpenter, L. J. (1996), Measurements of Peroxy Radicals in the Remote Marine Boundary Layer, PhD thesis, University of East Anglia, Norwich.

- Carpenter, L. J., et al. (1998), Investigation and evaluation of the NO_x/O₃ photochemical steady state, *Atmospheric Environment*, 32, 3353-3365.
- Carpenter, L. J., et al. (1997), A study of peroxy radicals and ozone photochemistry at coastal sites in the northern and southern hemispheres, *Journal of Geophysical Research-Atmospheres*, 102, 25417-25427.
- Carslaw, N., et al. (2000), A detailed case study of isoprene chemistry during the EASE96 Mace Head campaign, *Atmospheric Environment*, 34, 2827-2836.
- Carslaw, N., et al. (1997), Simultaneous observations of nitrate and peroxy radicals in the marine boundary layer, *Journal of Geophysical Research-Atmospheres*, 102, 18917-18933.
- Carslaw, N., et al. (2002), Eastern Atlantic Spring Experiment 1997 (EASE97) - 2. Comparisons of model concentrations of OH, HO₂, and RO₂ with measurements, *Journal of Geophysical Research-Atmospheres*, 107, art. no.-4190.
- Carslaw, N., et al. (1999a), Modeling OH, HO₂, and RO₂ radicals in the marine boundary layer - 1. Model construction and comparison with field measurements, *Journal of Geophysical Research-Atmospheres*, 104, 30241-30255.
- Carslaw, N., et al. (1999b), Modeling OH, HO₂, and RO₂ radicals in the marine boundary layer 2. Mechanism reduction and uncertainty analysis, *Journal of Geophysical Research-Atmospheres*, 104, 30257-30273.
- Chameides, W. L., et al. (1990), Observed and Model-Calculated NO₂/NO Ratios in Tropospheric Air Sampled During the Nasa Gte/Cite-2 Field-Study, *Journal of Geophysical Research-Atmospheres*, 95, 10235-10247.
- Chameides, W. L., et al. (1988), The Role of Biogenic Hydrocarbons in Urban Photochemical Smog - Atlanta as a Case-Study, *Science*, 241, 1473-1475.
- Clemetshaw, K. C., et al. (1997), A calibrated peroxy radical chemical amplifier for ground-based tropospheric measurements, *Journal of Geophysical Research-Atmospheres*, 102, 25405-25416.
- Clemetshaw, K. C., Penkett, S.A. (1994), TOR Station number 7: The Weybourne Atmospheric Observatory, in *The TOR Network. A description of TOR measurement Stations*, edited by T. Cvitas, Kley, D., pp. 59 - 63, EUROTRAC International Scientific Secretariat, Garmisch Partenkirchen.
- Coll, I., et al. (2005), 3D analysis of high ozone production rates observed during the ESCOMPTE campaign, *Atmospheric Research*, 74, 477-505.
- COMEAP (1998), Quantification of the Effects of Air Pollution on Health in the United Kingdom, Department of Health Committee on the Medical Effects of Air Pollutants, London.
- Creasey, D. J., et al. (1997), Implementation and initial deployment of a field instrument for measurement of OH and HO₂ in the troposphere by laser-induced fluorescence, *Journal of the Chemical Society-Faraday Transactions*, 93, 2907-2913.
- Creasey, D. J., et al. (2000), Absorption cross-section measurements of water vapour and oxygen at 185 nm. Implications for the calibration of field instruments to measure OH, HO₂ and RO₂ radicals, *Geophysical Research Letters*, 27, 1651-1654.
- Creasey, D. J., et al. (2002), Eastern Atlantic Spring Experiment 1997 (EASE97) 1. Measurements of OH and HO₂ concentrations at Mace Head, Ireland, *Journal of Geophysical Research-Atmospheres*, 107.
- Derwent, R. G., et al. (2003), Photochemical ozone formation in north west Europe and its control, *Atmospheric Environment*, 37, 1983-1991.
- Edwards, G. D., et al. (2003), Chemical ionization mass spectrometer instrument for the measurement of tropospheric HO₂ and RO₂, *Anal. Chem.*, 75, 5317-5327.
- Eisele, F. L., and D. J. Tanner (1991), Ion-Assisted Tropospheric Oh Measurements, *Journal of Geophysical Research-Atmospheres*, 96, 9295-9308.

Emmerson, K. M., et al. (2005a), Urban atmospheric chemistry during the PUMA campaign 1: Comparison of modelled OH and HO₂ concentrations with measurements, *Journal of Atmospheric Chemistry*, 52, 143-164.

Emmerson, K. M., et al. (2006), Free Radical Modelling during the UK TORCH Campaign in Summer 2003, *Atmospheric Chemistry and Physics Discussions*, submitted.

Emmerson, K. M., et al. (2005b), Urban atmospheric chemistry during the PUMA campaign 2: Radical budgets for OH, HO₂ and RO₂, *Journal of Atmospheric Chemistry*, 52, 165-183.

Faloon, I., et al. (2000), Observations of HO_x and its relationship with NO_x in the upper troposphere during SONEX, *Journal of Geophysical Research-Atmospheres*, 105, 3771-3783.

Fleming, Z. L. (2005), The Measurement of Peroxy Radicals in the Marine Boundary Layer using the PERCA Technique, University of Leicester, Leicester.

Fleming, Z. L., et al. (2006), Peroxy radical chemistry and the control of ozone photochemistry at Mace Head, Ireland during the summer of 2002, *Atmospheric Chemistry and Physics*, 6, 2193-2214.

Fowler, D. (1997), Ozone in the United Kingdom, Fourth Report of the Photochemical Oxidants Review Group.

George, L. A., et al. (1999), Measurement of free radicals OH and HO₂ in Los Angeles smog, *Journal of Geophysical Research-Atmospheres*, 104, 11643-11655.

Geyer, A., et al. (1999), Comparison of tropospheric NO₃ radical measurements by differential optical absorption spectroscopy and matrix isolation electron spin resonance, *Journal of Geophysical Research-Atmospheres*, 104, 26097-26105.

Geyer, A., and J. Stutz (2004), The vertical structure of OH-HO₂-RO₂ chemistry in the nocturnal boundary layer: A one-dimensional model study, *Journal of Geophysical Research-Atmospheres*, 109.

Green, T. J., et al. (2003), Airborne measurements of peroxy radicals using the PERCA technique, *Journal of Environmental Monitoring*, 5, 75-83.

Green, T. J., et al. (2006), An improved dual channel PERCA instrument for atmospheric measurements of peroxy radicals, *Journal of Environmental Monitoring*, 8, 530-536.

Guenther, A., et al. (1995), A Global-Model of Natural Volatile Organic-Compound Emissions, *Journal of Geophysical Research-Atmospheres*, 100, 8873-8892.

Haggerstone, A. L., et al. (2005), Improved model predictions of HO₂ with gas to particle mass transfer rates calculated using aerosol number size distributions, *Journal of Geophysical Research-Atmospheres*, 110.

Hard, T. M., et al. (1992), Diurnal HO₂ Cycles at Clean-Air and Urban Sites in the Troposphere, *Journal of Geophysical Research-Atmospheres*, 97, 9785-9794.

Hard, T. M., et al. (2002), An absolute calibration for gas-phase hydroxyl measurements, *Environmental Science & Technology*, 36, 1783-1790.

Harris, G. W., et al. (1982), Observations of Nitrous-Acid in the Los-Angeles Atmosphere and Implications for Predictions of Ozone Precursor Relationships, *Environmental Science & Technology*, 16, 414-419.

Hastie, D. R., et al. (1991), Calibrated Chemical Amplifier for Atmospheric RO_x Measurements, *Anal. Chem.*, 63, 2048-2057.

Hauglustaine, D. A., et al. (1999), Photochemistry and budget of ozone during the Mauna Loa Observatory Photochemistry Experiment (MLOPEX 2), *Journal of Geophysical Research-Atmospheres*, 104, 30275-30307.

Hauglustaine, D. A., et al. (1996), Observed and model-calculated photostationary state at Mauna Loa observatory during MLOPEX 2, *Journal of Geophysical Research-Atmospheres*, 101, 14681-14696.

Hofzumahaus, A., et al. (1997), The measurement of tropospheric OH radicals by laser-induced fluorescence spectroscopy during the POPCORN field campaign and Intercomparison of tropospheric OH radical measurements by multiple folded long-path laser

absorption and laser induced fluorescence - Reply, *Geophysical Research Letters*, 24, 3039-3040.

Hu, J., and D. H. Stedman (1995), Atmospheric Ro(X) Radicals at an Urban Site - Comparison to a Simple Theoretical-Model, *Environmental Science & Technology*, 29, 1655-1659.

Jaegle, L., et al. (2000), Photochemistry of HOx in the upper troposphere at northern midlatitudes, *Journal of Geophysical Research-Atmospheres*, 105, 3877-3892.

Jaegle, L., et al. (1999), Ozone production in the upper troposphere and the influence of aircraft during SONEX: Approach of NOx-saturated conditions, *Geophysical Research Letters*, 26, 3081-3084.

Jaegle, L., et al. (1998), Sources of HOx and production of ozone in the upper troposphere over the United States, *Geophysical Research Letters*, 25, 1709-1712.

Jaegle, L., et al. (1997), Observed OH and HO2 in the upper troposphere suggest a major source from convective injection of peroxides, *Geophysical Research Letters*, 24, 3181-3184.

Jenkin, M. E., et al. (2003), Protocol for the development of the Master Chemical Mechanism, MCM v3 (Part B): tropospheric degradation of aromatic volatile organic compounds, *Atmospheric Chemistry and Physics*, 3, 181-193.

Kanaya, Y., et al. (1999), Nighttime observation of the HO2 radical by an LIF instrument at Oki island, Japan, and its possible origins, *Geophysical Research Letters*, 26, 2179-2182.

Kleinman, L. I., et al. (2005), A comparative study of ozone production in five U.S. metropolitan areas, *Journal of Geophysical Research-Atmospheres*, 110.

Koppmann, R., J. Kesselmeier, F. X. Meixner, M. Schatzmann, B. Leitl, T. Hoffmann, R. Dlugi, M. Zelger, J. Kleffmann, A. Neftel, J. Dommen, C. Thomas, T. Trautmann, B. Neininger (2004), Emission und chemische Umwandlung biogener flüchtiger organischer Verbindungen Untersuchungen in und über einem Mischwaldbestand (ECHO), Forschungszentrum Jülich.

Lee, J. D., et al. (2006), Ozone Photochemistry and the Relationship to Isoprene in the UK Heatwave of August 2003, *Atmospheric Environment, In press*.

Leighton, P. A. (1961), *Photochemistry of Air Pollution*, Academic Press.

Levy, H. (1971), Normal Atmosphere - Large Radical and Formaldehyde Concentrations Predicted, *Science*, 173, 141-&.

Lightfoot, P. D., et al. (1992), Organic Peroxy-Radicals - Kinetics, Spectroscopy and Tropospheric Chemistry, *Atmospheric Environment Part a-General Topics*, 26, 1805-1961.

Mather, J. H., et al. (1997), OH and HO2 measurements using laser-induced fluorescence, *Journal of Geophysical Research-Atmospheres*, 102, 6427-6436.

Matsumoto, J., et al. (2006), Examination on photostationary state of NOx in the urban atmosphere in Japan, *Atmospheric Environment*, 40, 3230-3239.

McKeen, S. A., et al. (1997), The photochemistry of acetone in the upper troposphere: A source of odd-hydrogen radicals, *Geophysical Research Letters*, 24, 3177-3180.

Mihelcic, D., et al. (2003), Peroxy radicals during BERLIOZ at Pabstthum: Measurements, radical budgets and ozone production, *Journal of Geophysical Research-Atmospheres*, 108.

Mihelcic, D., et al. (1993), Simultaneous Measurements of Peroxy and Nitrate Radicals at Schauinsland, *Journal of Atmospheric Chemistry*, 16, 313-335.

Mihelcic, D., et al. (1985), An Improved Method of Measuring Tropospheric No2 and Ro2 by Matrix-Isolation and Electron-Spin-Resonance, *Journal of Atmospheric Chemistry*, 3, 341-361.

Mihele, C. M., and D. R. Hastie (1998), The sensitivity of the radical amplifier to ambient water vapour, *Geophysical Research Letters*, 25, 1911-1913.

Mihele, C. M., and D. R. Hastie (2003), Radical chemistry at a forested continental site: Results from the PROPHET 1997 campaign, *Journal of Geophysical Research-Atmospheres*, 108, art. no.-4450.

Mihele, C. M., et al. (1999), Radical loss in a chain reaction of CO and NO in the presence of water: Implications for the radical amplifier and atmospheric chemistry, *International Journal of Chemical Kinetics*, *31*, 145-152.

Monks, P. S. (2005), Gas-phase radical chemistry in the troposphere, *Chemical Society Reviews*, *34*, 376-395.

Monks, P. S., et al. (1996), Night-time peroxy radical chemistry in the remote marine boundary layer over the Southern ocean, *Geophysical Research Letters*, *23*, 535-538.

Monks, P. S., et al. (1998), Fundamental ozone photochemistry in the remote marine boundary layer: The SOAPEX experiment, measurement and theory, *Atmospheric Environment*, *32*, 3647-3664.

Monks, P. S., et al. (2000), A seasonal comparison of ozone photochemistry in the remote marine boundary layer, *Atmospheric Environment*, *34*, 2547-2561.

Oke, T. R. (1987), *Boundary Layer Climates*, Second ed., Methuen, London.

Parrish, D. D., et al. (1986), Measurements of the Nox-O₃ Photostationary State at Niwot Ridge, Colorado, *Journal of Geophysical Research-Atmospheres*, *91*, 5361-5370.

Penkett, S. A., et al. (1999), Studies of oxidant production at the Weybourne Atmospheric Observatory in summer and winter conditions, *Journal of Atmospheric Chemistry*, *33*, 111-128.

Penkett, S. A., et al. (1997), Relationships between ozone photolysis rates and peroxy radical concentrations in clean marine air over the Southern Ocean, *Journal of Geophysical Research-Atmospheres*, *102*, 12805-12817.

Pierce, T., et al. (1998), Influence of increased isoprene emissions on regional ozone modeling, *Journal of Geophysical Research-Atmospheres*, *103*, 25611-25629.

PORG (1997), Ozone in the United Kingdom 1997. Fourth Report of the United Kingdom Photochemical Oxidants Review Group, Department of the Environment, London.

Reichert, L., et al. (2003), Investigation of the effect of water complexes in the determination of peroxy radical ambient concentrations: Implications for the atmosphere, *Journal of Geophysical Research-Atmospheres*, *108*.

Reiner, T., et al. (1997), Atmospheric peroxy radical measurements by ion molecule reaction mass spectrometry: A novel analytical method using amplifying chemical conversion to sulfuric acid, *Journal of Geophysical Research-Atmospheres*, *102*, 1311-1326.

Reiner, T., et al. (1999), Aircraft-borne measurements of peroxy radicals by chemical conversion/ion molecule reaction mass spectrometry: Calibration, diagnostics, and results, *Journal of Geophysical Research-Atmospheres*, *104*, 18647-18659.

Roselle, S. J., et al. (1991), The Sensitivity of Regional Ozone Modeling to Biogenic Hydrocarbons, *Journal of Geophysical Research-Atmospheres*, *96*, 7371-7394.

Sadanaga, Y., et al. (2004), Development of a measurement system of peroxy radicals using a chemical amplification/laser-induced fluorescence technique, *Review of Scientific Instruments*, *75*, 864-872.

Salisbury, G. (2001), Measurements of Peroxy Radicals in the marine boundary layer, University of Leicester, Leicester.

Salisbury, G., et al. (2002), A seasonal comparison of the ozone photochemistry in clean and polluted air masses at Mace Head, Ireland, *Journal of Atmospheric Chemistry*, *41*, 163-187.

Salisbury, G., et al. (2001), Production of peroxy radicals at night via reactions of ozone and the nitrate radical in the marine boundary layer, *Journal of Geophysical Research-Atmospheres*, *106*, 12669-12687.

Saunders, S. M., et al. (2003), Protocol for the development of the Master Chemical Mechanism, MCM v3 (Part A): tropospheric degradation of non-aromatic volatile organic compounds, *Atmospheric Chemistry and Physics*, *3*, 161-180.

Savage, N. H., et al. (2001), Steady-state modelling of hydroxyl radical concentrations at Mace Head during the EASE '97 campaign, May 1997, *Atmospheric Environment*, 35, 515-524.

Schar, C., et al. (2004), The role of increasing temperature variability in European summer heatwaves, *Nature*, 427, 332-336.

Schultz, M., et al. (1995), Calibration Source for Peroxy-Radicals with Built-in Actinometry Using H₂O and O₂ Photolysis at 185 Nm, *Journal of Geophysical Research-Atmospheres*, 100, 18811-18816.

Shetter, R. E., et al. (1983), The NO/NO₂/O₃ Photostationary State in Claremont, California, *Journal of the Air Pollution Control Association*, 33, 212-214.

Skjølsvik, K. O. (2001), VOC Emission from Offshore Crude Oil Loading and Storage, *Martinek Review*.

Smith, S. C., et al. (2006), Concentrations of OH and HO₂ radicals during NAMBLEX: measurements and steady state analysis, *Atmospheric Chemistry and Physics*, 6, 1435-1453.

Sommariva, R., et al. (2004), OH and HO₂ chemistry in clean marine air during SOAPEX-2, *Atmospheric Chemistry and Physics*, 4, 839-856.

Stedman, J. R. (2004), The predicted number of air pollution related deaths in the UK during the August 2003 heatwave, *Atmospheric Environment*, 38, 1087-1090.

Stevens, P. S., et al. (1997), HO₂/OH and RO(2)/HO₂ ratios during the Tropospheric OH Photochemistry Experiment: Measurement and theory, *Journal of Geophysical Research-Atmospheres*, 102, 6379-6391.

Stöbener, D. (1999), Weiterentwicklung einer Peroxyradikalquelle für die Kalibration von RO₂-Messungen in Außenluft, MSc thesis, Universität Bremen.

Stott, P. A., et al. (2004), Human contribution to the European heatwave of 2003, *Nature*, 432, 610-614.

Viswanath, R. S., van Sandt, J.H. (1989), Oil Field Emissions of Volatile Organic Compounds, Office of Air Quality Planning and Standards, U. S. Environmental Protection Agency, North Carolina.

Watanabe, K., and M. Zelickoff (1953), Absorption Coefficients of Water Vapor in the Vacuum Ultraviolet, *Journal of the Optical Society of America*, 43, 753-755.

Wennberg, P. O., et al. (1998), Hydrogen radicals, nitrogen radicals, and the production of O₃ in the upper troposphere, *Science*, 279, 49-53.

Yoshino, K., et al. (1983), High-Resolution Absorption Cross-Section Measurements and Band Oscillator-Strengths of the (1,0)-(12,0) Schumann-Runge Bands of O₂, *Planetary and Space Science*, 31, 339-353.

Zanis, P., et al. (2003), Seasonal variation of peroxy radicals in the lower free troposphere based on observations from the FREE Tropospheric EXperiments in the Swiss Alps, *Geophysical Research Letters*, 30, art. no.-1497.

Zanis, P., et al. (2000a), In situ ozone production under free tropospheric conditions during FREETEX '98 in the Swiss Alps, *Journal of Geophysical Research-Atmospheres*, 105, 24223-24234.

Zanis, P., et al. (1999), On the relationship of HO₂+RO₂ with j((OD)-D-1) during the Free Tropospheric Experiment (FREETEX '96) at the Jungfraujoch Observatory (3580 m above sea level) in the Swiss Alps, *Journal of Geophysical Research-Atmospheres*, 104, 26913-26925.

Zanis, P., et al. (2000b), The role of in situ photochemistry in the control of ozone during spring at the Jungfraujoch (3,580 m asl) - Comparison of model results with measurements, *Journal of Atmospheric Chemistry*, 37, 1-27.

Zenker, T., et al. (1998), Intercomparison of NO, NO₂, NO_y, O₃, and RO_x measurements during the oxidizing capacity of the tropospheric atmosphere (OCTA) campaign 1993 at Izana, *Journal of Geophysical Research-Atmospheres*, 103, 13615-13634.

9 Postgraduate Record of Activities

1st year research proposal presentation 26th March 2003
1st year research committee meeting 24th October 2002

9.1 Presentations

9th February 2004 TORCH progress meeting *Peroxy Radical Measurements at TORCH 1*

3rd December 2003 Young Atmospheric Scientists Network VIP presentation to the UK Minister for Science, Lord Sainsbury of Turville, and the Swiss Secretary of State for Science, Dr Charles Kleiber, EPFL, Lausanne, Switzerland: *The European Summer Heatwave of 2003*

26th September 2003 Molecular Properties group meeting – topic presentation
The Science behind the TORCH experiment

21st March 2003 Molecular Properties group meeting – paper presentation:
Bloss et al (Environmental Monitoring and Assessment 2003) Application of a compact all solid-state laser system to the in situ detection of atmospheric OH, HO₂, NO and IO by laser-induced fluorescence

8th November 2002 Molecular Properties group meeting paper presentation:
Lewis et al (Nature 2000) A larger pool of ozone forming carbon compounds in urban atmospheres

9.2 Posters

Measurements of peroxy radicals in the boundary layer using PERCA
ERCA 2003, Grenoble, France 13th January 2003

9.3 Field Campaigns

TORCH 1 (Tropospheric Organic Chemistry Experiment)

July/August 2003 Writtle, Essex – responsible for running PERCA instrument and data collection of radiometers

9.3.1.1.1 TORCH 2

April/May 2004 Weybourne, Norfolk – responsible for running PERCA instrument and data collection of radiometers

ITOP (Intercontinental Transport of Ozone and Precursors)

July 12th to August 2nd 2004 – Operation of PERCA instrument on three science flights over Atlantic and general running of instrument

9.3.1.1.1.2 PERCA/FAGE comparison

August 18th – September 2nd 2004 Leeds – responsible for running PERCA

9.4 Demonstrating

Level 2 physical chemistry practicals Spring Semester 2003

63 contact hours – 12 afternoon sessions (11:30 – 16:45)

7 preparation hours

10 assessment hours

9.5 Meetings

9.5.1 International

Network for Young Atmospheric Scientists Institut Universitaire Kurt Bosch, Sion, Switzerland, 1st – 3rd December 2003

9.5.2 UK

Atmospheric Chemistry Special Interest Group of the Royal Meteorological Society Annual Meeting, University of Leicester, 1st April 2004

The 2003 Heatwave – joint DEFRA/Polluted Troposphere meeting Novartis Foundation, London, 12th February 2004

TORCH progress meeting, UEA, 9th – 10th February 2004

DIAC Launch Meeting, University of London, 27th January 2004

Aircraft PERCA instrument rack inspection and inlet design meeting BAE Systems, Woodford, Manchester, 15th December 2003

ITOP planning meeting University of York, 30th – 31st October 2003

NERC Polluted Troposphere modelling workshop University of Leicester, 14th October 2003

ITOP (International Transport of Ozone and Precursors) initial planning meeting University of Leicester, 16th June 2003

Aircraft PERCA Inlet design meeting BAE Systems, Woodford, Manchester, 9th April 2003

Royal Meteorological Society Atmospheric Chemistry Study Group annual meeting Atmospheric chemistry and climate University of Oxford, 27th March 2003

Aircraft PERCA Inlet design meeting BAE Systems, Woodford, Manchester, 20th February 2003

UEA-Leicester joint group meeting University of East Anglia, 29th November 2002

TORCH (Tropospheric Organic Chemistry Experiment) start-up meeting University of Leeds, 12th November 2002

Aircraft PERCA Instrument rack design assessment meeting BAE Systems, Woodford, Manchester, 6th November 2002

9.6 Academic Courses

9.6.1 International

ERCA 2003 (European Research Course on Atmospheres)
Université Joseph Fourier, Grenoble, France
6th January 2003 – 6th February 2003

Intensive four weeks of lectures given by leading international researchers in various fields of atmospheric science. Fifth week spent at OHP (Observatoire de Haute-Provence), St Martin l'Observatoire, France.

9.6.2 University of Leicester Lecture Courses

Atmospheric Chemistry – CH4008

Convenor: Dr Paul Monks

Summary: Exploration of fundamental physical and chemical processes that control atmospheric composition

Assessment: Oral examination

Earth Observation Science – PA361/3 Opt 3653

Convenor: Dr Sean Lawrence

Summary: Introduction to physical properties and circulation of the earth's oceans and atmosphere and methods by which they are studied from space

Assessment: Written examination

Physics of the Natural Environment – PA442 Opt 4425

Convenor: Dr Sean Lawrence

Summary: Introduction to dynamical meteorology

Assessment: None

9.7 Training Courses

Lecturing large groups	17 th December 2003
Applications of 'Endnote'	25 th June 2003
Developing skills for a future career	22 nd March 2003
Powerful presentations	20 th March 2003
Reading and note making skills	10 th March 2003
Effective time management	3 rd March 2003
Writing skills	12 th February 2003
Personal skills portfolio	4 th December 2002
Introduction to chemical information databases	30 th October 2002
Demonstrating/small group teaching (part 2)	23 rd October 2002
Demonstrating/small group teaching (part 1)	2 nd October 2002
Departmental procedures and fire safety	2 nd October 2002
Faculty induction	26 th September 2002
Graduate school induction	25 th September 2002

9.8 Seminars Attended

Connectivity of Functionalised Nanoparticles and Their Arrays Prof. David Schiffrin (University. of Liverpool) 15th March 2004

Applications of ESR Spectroscopy to Biological Problems Dr. Chris Kay (Free University, Berlin) 8th March 2004

Radiative and Climate Impact of Aerosols (Space Research Centre) Dr. Eleanor Highwood (University. of Reading) 9th March 2004

Accelerated Discovery of Electrochemical Materials Dr. John Owen (University. of Southampton) 16th February 2004

Scalable parallel quantum chemistry: the course grained approach (Mathematical Modelling Seminar) Prof Peter Taylor (University of Warwick) 12th December 2003

Bird navigation: a photochemical magnetic compass Prof Peter Hore (University of Oxford) 8th December 2003

9.8.1.1.1 Richard Anschutz, Archibald Scott Couper, Josef Loschmidt: A detective at work

Dr Alfred Bader (Founder of Aldrich Chemical Company) 20th November 2003

UK Space Science Policy (Space Research Centre) Dr David Hall (British National Space Centre) 18th November 2003

Building high-performance magnetic materials by assembling nanoclusters Prof Chris Binns (University of Leicester) 17th November 2003

Green solvents for catalysis – from molecular understanding to process design Prof Dr Walter Leitner (Max Planck Institute, Mühlheim) 14th November 2003

Controlling electrons and molecules using light Prof Helen Fielding (University College London) 3rd November 2003

Climate change: fact or fiction (Space Research Centre) Dr Sean Lawrence (University of Leicester) 28th October 2003

NMR and Proteins (2nd Tim Norwood memorial lecture) Prof Iain Campbell, FRS (University of Oxford) 8th October 2003

Against nature: unnatural products in the service of humanity (inaugural lecture) Prof Jonathan Percy (University of Leicester) 3rd June 2003

Using Meteosat data to evaluate the diurnal cycle in the Hadley Centre Climate Model (Space Research Centre) Prof Tony Slingo (Environmental Systems Science Centre, University of Reading) 3rd June 2003

Green Chemistry (Lunchtime seminar, Institute for Environment and Health, Leicester) Prof James Clark (University of York) 10th April 2003

First principles computation of electronic structure: from atoms to biomolecules (Mathematical modelling seminar) Prof Peter Knowles (University of Birmingham) 15th November 2002

Finding your way downhill – interactive least-squares fitting with examples from intermolecular forces (Mathematical modelling seminar) Prof Jeremy Hutson (University of Durham) 1st November 2002

Theoretical and experimental studies of NO-containing complexes Dr Timothy Wright (University of Sussex) 16th October 2002